PSEUDOPOTENTIAL TREATMENT OF TWO BODY INTERACTIONS

By

KRITTIKA KANJILAL

A dissertation submitted in partial fulfillment of
the requirements for the degree of

DOCTOR OF PHILOSOPHY

WASHINGTON STATE UNIVERSITY
Department of Physics and Astronomy

MAY 2009

To the Faculty of Washington State University:

The members of the Committee appointed to examine the dissertation of KRITTIKA KANJILAL find it satisfactory and recommend that it be accepted.

Doerte Blume, Ph.D., Chair

Peter Engels, Ph.D.

Chuanwei Zhang, Ph.D.

ACKNOWLEDGEMENT

I would like to start by thanking my adviser Doerte Blume without whom this thesis would not have been possible. Her patience, involvement and encouragement made it possible for me to develop as a researcher at my own pace. She has always shown great confidence in me, which I greatly appreciate. She has also taught me to tackle complex ideas by starting with simple ideas that I clearly understand and then building up step by step from a firm foundation.

I want to thank the members of my research group, past and present, as well as the attendees of the "Journal Club", specially Peter Engels and Chuanwei Zhang for all the insightful discussions I have had with them.

I want to thank our collaborator John Bohn for providing us with a set of scattering data during the initial stage of our two-dipole studies.

I also want to thank the many professors I have taken classes from at Washington State University. Many things I learned in these classes have been useful in my research. Also the classes were enjoyable and thought provoking and contributed to making my graduate student life fun.

I would not have been in graduate school doing physics without the encouragement from my two undergraduate mentors Mr. Ajay Patwardhan and Dr. Bhanu Pratap Das. They kindled the love for physics in me and I am very grateful to them.

I want to thank my family for always supporting me, believing in my abilities and encouraging me to push my boundaries. It is this attitude that has enabled me to get through all the frustrating times.

I want to thank my husband Kovid Goyal for all the heated physics arguments we have had, the help he has given me with LaTeX and Mathematica and the emotional support he has provided me with for the last six years.

Finally, I want to thank the National Science Foundation for funding my research as a graduate student.

PSEUDOPONTENTIAL TREATMENT OF TWO BODY

INTERACTIONS

Abstract

by Krittika Kanjilal, Ph. D.
Washington State University
May 2009

Chair: Doerte Blume

Ultracold atomic gases have been of great theoretical and experimental interest in the last two decades. In these systems, the de Broglie wavelength of the particles is much greater than the two body van der Waals length. As a result, the details of the two body interaction potential are irrelevant for a large number of applications and the realistic two body interaction potential can be replaced by a simple finite range or zero range model potential that reproduces the scattering quantities of the full interaction potential. This thesis develops zero range pseudopotentials and applies them to trapped two-particle systems.

Ultracold gases loaded into optical lattices can be used to realize two particle systems under approximately harmonic confinement. We use pseudopotentials to obtain the eigenspectrum of two particles under external harmonic confinement semi-

analytically.

Advancements in trapping technology have resulted in the realization of low dimensional systems. We develop pseudopotentials to treat two body interactions in one and two dimensions. We also elaborate on the physics that is unique to one and two dimensional systems.

Feshbach resonances allow for the tunability of the effective two body interaction strength in the presence of a magnetic field. To model Feshbach resonances in two and three dimensions we develop coupled two channel zero range potentials.

Dipole-dipole interactions in Chromium and polar molecules have been the subject of a lot of recent research. Unlike the interactions between two alkali atoms, these interactions are long range and anisotropic. We explore the scattering properties of two aligned dipoles using a simple shape dependent model potential. To understand a system two aligned dipoles under confinement, we develop a pseudopotential treatment for cylindrically symmetric interaction potentials under cylindrically symmetric harmonic confinement. This pseudopotential can be used to model any cylindrically symmetric interaction potential. Our zero range treatment describes many features of two aligned dipoles under spherically symmetric harmonic confinement accurately but breaks down when applied to two aligned dipoles under cylindrically symmetric harmonic confinement. The breakdown is unique to the long range nature of the dipole-

dipole interaction and expected to be absent for short range interactions.

Contents

List of Figures

List of Tables

Chapter 1

Introduction

The goal of this thesis is to investigate two body interactions at very low temperatures, with a view towards understanding the behavior of degenerate quantum gases. Our models accurately reproduce the wavefunction of two interacting particles at large interparticle distances. They also enable us to analytically obtain the eigenenergies of the two particle system under external harmonic confinement.

Due to the advancement in trapping technology it is possible to obtain effectively low dimensional systems. We explore the effects of reduced dimensionality on two body interactions and develop zero range potentials to model them in strictly one and two dimensions.

Section 1.1 introduces quantum degenerate gases. The need to obtain a better understanding of some interesting systems, listed in Sec. 1.2, motivates the techniques and ideas developed in this thesis. Section 1.3 discusses two body interactions and Feshbach resonances. Section 1.4 deals with confining potentials and systems with reduced dimensionality. Section 1.5 introduces zero range pseudopotentials and Sec. 1.6 gives an overview of the thesis.

1.1 Quantum degenerate gases

Recent reviews of quantum degenerate gases can be found in [1, 2, 3, 4]. The discussion here follows [1, 5]. Consider a gas of non-interacting identical particles in a box. The relevant length scales of this system are the average interparticle spacing d_{int} ($d_{\text{int}} = n^{-\frac{1}{3}}$, where n is the average number density of the gas), the length of the box L and the de Broglie wavelength λ_{dB} of the particles. We assume that the box is very large, i. e., $L \gg d_{\text{int}}$ and $L \gg \lambda_{\text{dB}}$. In the regime where $d_{\text{int}} \gg \lambda_{\text{dB}}$, the atoms or molecules of the gas behave like point particles, Maxwell-Boltzmann statistics is valid, and the gas can be treated classically. However, for $d_{\text{int}} \lesssim \lambda_{\text{dB}}$, the gas is in the quantum degenerate regime, the atoms or molecules of the gas behave like extended wave packets that overlap with each other, and the gas has to be treated quantum mechanically.

In a classical gas the particles are treated as identical but distinguishable, while in a quantum gas they are treated as identical and indistinguishable. The particles in classical gases follow Maxwell-Boltzmann statistics. In a quantum gas the statistics followed by the particles depends upon their spin. Gases of particles with integer spin (bosons) follow Bose-Einstein statistics. For a Bose gas at temperature T, the mean occupation number $\overline{n}_B(E)$ of a state with energy E is given by [5]

$$\overline{n}_B(E) = \frac{1}{e^{\frac{E-\mu_B}{k_B T}} - 1}, \tag{1.1}$$

where μ_B is the chemical potential of the Bose gas and k_B is Boltzmann's constant. A gas is considered to approach quantum degeneracy if the occupation number corresponding to some energy state approaches one or exceeds it. A dilute gas of bosonic atoms undergoes Bose-Einstein condensation, a phenomenon in which, below a certain critical temperature, the bosons macroscopically occupy the single particle ground state

(if the single particle picture is applicable). This corresponds to quantum degeneracy, since the mean occupation number of the ground state is one or greater.

In contrast, gases of particles with half integer spin (fermions) follow Fermi-Dirac statistics. For a Fermi gas at temperature T, the mean occupation number $\overline{n}_F(E)$ of a state with energy E is given by [5]

$$\overline{n}_F(E) = \frac{1}{e^{\frac{E-\mu_F}{k_B T}} + 1}, \tag{1.2}$$

where μ_F is the chemical potential of the Fermi gas. At very low temperatures the mean occupation number of a gas of fermionic atoms at energies $E < \mu$ approaches one indicating quantum degeneracy. The experimental realization of Bose-Einstein condensates [6, 7] and degenerate Fermi gases [8] has led to a lot of research in cold atom physics.

1.2 Motivation

Quantum degenerate gases exhibit interesting behavior in many different ways. They can be loaded into periodic potentials called optical lattices (see Sec. 1.4.2 and for a review see, e. g., Ref. [9]). This set up is reminiscent of an ionic lattice with an electron gas in a crystal. Hence optical lattices loaded with degenerate ultracold gases can be used as condensed matter analogs. These systems allow for an unprecedented degree of control. Optical lattices with exactly n (n is an integer) atoms per lattice site can be created [10] and, unlike real crystals, these systems have essentially no defects. Optical lattices loaded with ultracold degenerate gases have been created in one, two and three dimensions [11, 12, 13]. Pairwise two body interactions dominate the behavior of these gases, while three body (and higher order) interactions can generally be neglected. In

order to gain insight into these systems, it is important to first understand the interaction between just two particles. The two particle system itself is interesting and can be realized in an optical lattice with exactly two atoms per lattice site, negligible interactions between atoms in neighboring lattice sites and negligible tunneling between lattice sites [14]. Chapters 2 to 4 treat two interacting particles in a harmonic trap in one, two and three dimensions.

In addition to many alkali atoms like Rubidium (Rb) [6], Sodium (Na) [7], Potassium (K) [15], Lithium (Li) [16, 17] and Cesium (Cs) [18], recently Chromium (Cr) [19] was Bose condensed. Compared to alkali atoms, Cr has a large magnetic moment of 6 Bohr magneton. This relatively large magnetic moment leads to a dipole-dipole interaction between the Cr atoms, which has been observed to affect the cloud shape during expansion [20]. In addition there has been a lot of interest in the creation of ground state polar molecules [21, 22, 23, 24, 25, 26]. These molecules can have a large induced electric dipole moment of the order of a few Debye, which can be tuned by varying an electric field [27, 26]. Polar molecules are a candidate for qubits in quantum computing [28] and may be used in high precision measurements that aim at placing yet stricter limits on the electric dipole moment of the electron [29]. Unlike the interaction between alkali atoms, the dipole-dipole interaction is long-range and anisotropic [30]. In Ch. 5, we develop a zero range treatment for two aligned dipoles under harmonic confinement. Since the dipole-dipole interaction potential is anisotropic, the nature of the interactions (attractive or repulsive) depends on the relative orientation of the dipoles. This results in the stability of a dipolar gas being dependent on the trapping geometry [31, 32]. In the case of cylindrical traps, e. g., it depends on the aspect ratio. In addition, dipolar gases in pancake shaped traps are expected to show interesting structures like biconcave condensates [33]. Chapter 5 also explores the complications that arise when applying the anisotropic pseudopotential to systems confined in non-spherically sym-

metric traps.

1.3 Two body interactions

So far, quantum degeneracy has been achieved in gases of alkali atoms [6, 7, 15, 18], Cr [19], metastable helium (He) [34] and Ytterbium (Yb) [35]. Alkali atoms have one outer s electron and much of their energy level structure is similar to that of hydrogenic atoms [36]. For simplicity, this section considers the energy level structure of hydrogenic atoms as opposed to alkali atoms or Cr. The atomic energy level structure becomes important when the atoms in the cloud have large interparticle distances.

The non-relativistic Schrödinger equation for hydrogenic atoms without electron or nuclear spin results in quantized energy levels E_n (labeled by the principal quantum number n) [36],

$$E_n = -\frac{e^2}{8\pi\epsilon_0 a_0}\frac{\mu}{m}\frac{Z^2}{n^2}, \tag{1.3}$$

where a_0 is the Bohr radius, ϵ_0 is the permittivity of free space, μ is the reduced mass of the electron and the nucleus, m is the mass of the electron, Z is the atomic number and "$-e$" is the charge on the electron. Each of these levels has a degeneracy of n^2 corresponding to different l (orbital angular momentum quantum number) and m_l (magnetic quantum number) and the level spacing between the lowest adjacent levels is of the order of a few eV (electron Volts). Accounting for the two possible orientations of the electron spin ($m_s = \pm\frac{1}{2}$), changes the degeneracy of hydrogenic energy levels E_n from n^2 to $2n^2$.

Using the relativistic Schrödinger equation partially breaks the degeneracy in l and reveals the fine structure [36]. The total electronic angular momentum $\vec{J}$ is given by

$\vec{J} = \vec{L} + \vec{S}$, where $\vec{L}$ denotes the electronic orbital angular momentum and $\vec{S}$ the electronic spin. The quantum numbers corresponding to the operators $\vec{J}$, $\vec{L}$ and $\vec{S}$ are given by j, l and s, respectively. The total electronic angular momentum is conserved and the relativistic energy levels depend on n and j, i. e., levels with the same principal quantum number n and the same total electronic angular momentum quantum number j (but possibly different l) have the same energy. The fine structure splitting is of the order of $10^{-5} eV$. Including the Lamb shift (radiative corrections that take into account the interaction of the electron with a quantized electromagnetic field) lifts the partial degeneracy in l and leads to a level splitting of the order of a few μeV.

The nuclear spin $\vec{I}$ (corresponding quantum number denoted by i) and the finite size of the nucleus introduce energy shifts of the order of a few μeVs, which are referred to as the hyperfine structure [36]. The total angular momentum of the atom $\vec{F}$ including the nuclear spin is given by $\vec{F} = \vec{J} + \vec{I}$. The quantum number corresponding to $\vec{F}$ is given by f. Each hyperfine level corresponds to a particular value of f. Each of these levels is $2f+1$ fold degenerate with each of the degenerate levels corresponding to a different m_f (projection of total angular momentum) quantum number ranging from $-f$ to f in steps of one. This degeneracy is broken in the presence of an external magnetic field; this is referred to as the Zeeman effect. For magnetic fields of a few hundred Gauss the energy splitting is almost linear [37], i. e., the energy shift due to the magnetic field $\vec{B}$ is approximately given by

$$\Delta E_{m_f} = \vec{\mu}_{m_f} \cdot \vec{B}, \tag{1.4}$$

where $\vec{\mu}_{m_f}$ is the magnetic dipole moment of the state with quantum number m_f.

Figure 1.1 shows the $n = 1$ and $n = 2$ energy levels of the hydrogen atom with the level splittings introduced by the relativistic corrections, the radiative corrections and the inclusion of the nuclear spin. This leaves us with $\vec{F} = \vec{S} + \vec{I}$. In Fig. 1.1 each hyperfine

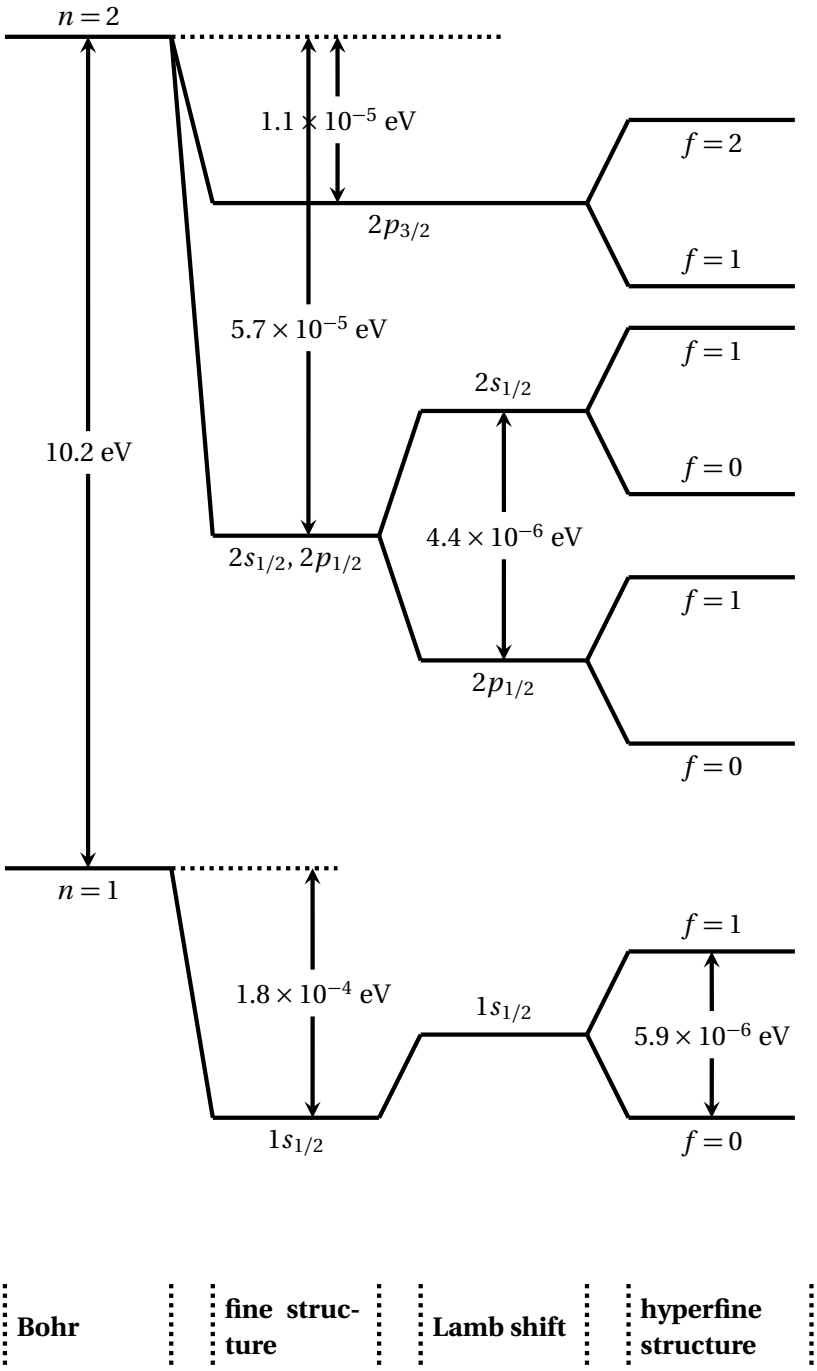

Figure 1.1: Fine structure and hyperfine structure splitting of the lowest two electronic levels of the hydrogen atom. The energy levels are labeled using the spectroscopic notation nl_j. Figure is not to scale. Data taken from Ref. [38].

level is labeled by its f quantum number. The Zeeman splitting of the hyperfine levels in the presence of an external magnetic field is not shown. Having obtained the detailed spectrum of a single atom we now look at interactions between two atoms.

In general, the interaction between two neutral atoms is quite complicated. For reviews of two body interactions at low temperatures see Refs. [39, 40]. The interaction potential between two neutral atoms, labeled A and B, with atomic numbers Z_A and Z_B, respectively, is given by [41]

$$V_{\rm int} = \frac{Z_A Z_B e^2}{4\pi\epsilon_0|\vec{R}_A - \vec{R}_B|} - \sum_{i=1}^{Z_A+Z_B} \frac{e^2}{4\pi\epsilon_0|\vec{r}_i - \vec{R}_B|} - \sum_{i=1}^{Z_A+Z_B} \frac{e^2}{4\pi\epsilon_0|\vec{R}_A - \vec{r}_i|} + \sum_{i=1}^{Z_A+Z_B}\sum_{j=1}^{i-1} \frac{e^2}{4\pi\epsilon_0|\vec{r}_i - \vec{r}_j|}, \tag{1.5}$$

where $\vec{R}_A$ and $\vec{R}_B$ are the position vectors of the nuclei of atoms A and B, respectively, and $\vec{r}_i$ is the position vector of the $i^{\rm th}$ electron. The first term in Eq. (1.5) corresponds to the repulsive Coulomb interaction between the two nuclei, the second and third terms to the attractive interactions between the electrons and the nuclei, and the forth term to the repulsive interactions between the electrons. The Schrödinger equation for two interacting atoms in the relative coordinate is

$$H\Psi = E\Psi, \tag{1.6}$$

where

$$H = T_N + T_e + V_{\rm int} \tag{1.7}$$

with

$$T_N = -\frac{\hbar^2}{2M_N}\left[\frac{1}{r^2}\frac{\partial}{\partial r}\left(r^2\frac{\partial}{\partial r}\right) + \frac{1}{r^2\sin\theta}\frac{\partial}{\partial\theta}\left(\sin\theta\frac{\partial}{\partial\theta}\right) + \frac{1}{r^2\sin^2\theta}\frac{\partial^2}{\partial\phi^2}\right] \tag{1.8}$$

and

$$T_e = \sum_{i=1}^{Z_A+Z_B} \left(\frac{-\hbar^2}{2m} \nabla^2_{\vec{r}_i} \right). \tag{1.9}$$

M_N is the reduced mass of the two nuclei and $\vec{r} = \vec{R}_B - \vec{R}_A$ is the relative vector between the two nuclei with spherical polar coordinates given by r, θ and ϕ.

Since the nuclei are heavy and move much slower than the electrons, the Born-Oppenheimer approximation assumes a fixed internuclear distance r [41]. Under this assumption, Eq. (1.6) can be numerically solved for different values of r to obtain the eigenenergies $E(r)$. As an example, consider the adiabatic Born-Oppenheimer curves $E(r)$ for the hydrogen molecule ($Z_A = Z_B = 1$). The large r Born-Oppenheimer energies are in this case given by $E_{n_A} + E_{n_B}$, where E_{n_A} and E_{n_B} denote, respectively, the electronic energies of the first and second hydrogen atom. The Born-Oppenheimer energies depend on the electronic spin through the requirement that the electronic wavefunction has to be antisymmetric under exchange of the two electrons. To illustrate this point, let us as before, consider the hydrogen molecule. If $\vec{S}_A$ and $\vec{S}_B$ denote the electronic spin of the first and second hydrogen atom, the quantum number s corresponding to the total electron spin $\vec{S}$, $\vec{S} = \vec{S}_A + \vec{S}_B$, can take the values 0 and 1. If $s = 0$, the spatial part of the electronic wavefunction has to be symmetric; if $s = 1$, the spatial part of the electronic wavefunction has to be antisymmetric. Consequently, there exist two Born-Oppenheimer potential curves (a singlet and a triplet curve), which asymptotically approach the same threshold energy. It is convenient to label the Born-Oppenheimer potential curves $E_s(r)$ by the electron spin s. In Sec. 1.3.1 we choose our energy scale such that the energetically lowest lying Born-Oppenheimer potential curve approaches zero as $r \to \infty$.

The adiabatic potential curves for neutral diatomic molecules vary to leading order as $-C_6/r^6$ for $r \to \infty$, where C_6 [38] denotes the positive van der Waals coefficient.

Hence these are short range interaction potential curves in the relative coordinate. The van der Waals length l_{vdW} [39], determined using the classical turning point of a bound state, is given by

$$l_{\mathrm{vdW}} = \frac{1}{2}\left(\frac{2M_N C_6}{\hbar^2}\right)^{1/4}, \tag{1.10}$$

is typically of the order of $100a_0$.

1.3.1 Feshbach resonances

The Born-Oppenheimer adiabatic potential curves do not include relativistic corrections or the nuclear spin. To account for these effects, the full effective potential of two atoms A and B in the presence of an external magnetic field $\vec{B}$, $\vec{B} = B\hat{z}$, can be schematically written as [42]

$$V_{\mathrm{tot}}(r) = E(r) + H_A^{\mathrm{M}} + H_A^{\mathrm{HF}} + H_B^{\mathrm{M}} + H_B^{\mathrm{HF}}, \tag{1.11}$$

where H_α^{HF} ($\alpha = A, B$) is the hyperfine Hamiltonian of the atom α,

$$H_\alpha^{\mathrm{HF}} = C(\vec{F}_\alpha^2 - \vec{S}_\alpha^2 - \vec{I}_\alpha^2), \tag{1.12}$$

and H_α^{M} is the Zeeman Hamiltonian of the atom α,

$$H_\alpha^{\mathrm{M}} = -B[g_e\mu_e S_z^\alpha + g_N^\alpha \mu_N^\alpha I_z^\alpha]. \tag{1.13}$$

Here, μ_N and μ_e refer to the magnetic moments of the nucleus and the electron, respectively, and g_e and g_N are the g-factors for the electron and the nucleus, respectively. F_z^α, S_z^α and I_z^α are the z projections of $\vec{F}_\alpha$, $\vec{S}_\alpha$ and $\vec{I}_\alpha$, respectively. Finally, C is a constant that depends on the hyperfine energy splitting and the nuclear spin. Equation (1.11) as-

sumes s-wave scattering, i. e., $l = 0$. For $l > 0$, additional corrections, to be discussed later, occur.

It is convenient to consider the effective potentials in two different regions [43]. For small internuclear distances r the overlap of the electron clouds of the two atoms is large and the system is most conveniently treated in the molecular basis. For large internuclear distances, in contrast, a basis of the eigenstates of two non-interacting atoms is more suitable as can be seen from Eq. (1.11). For alkali atoms, the separation of these two regions occurs at $r \sim 20a_0$, where the overlap between the electronic clouds becomes exponentially small.

For two scattering atoms, the initial and final states are labeled by the atomic quantum numbers corresponding to the atomic basis. The atomic basis consists of a direct product of the eigenstates of the individual atoms and is labeled by $|f_A, m_{f_A}\rangle \otimes |f_B, m_{f_B}\rangle \equiv |f_A, m_{f_A}, f_B, m_{f_B}\rangle$, where f_A and m_{f_A} are the hyperfine quantum numbers of the eigenstate of atom A and f_B and m_{f_B} are the hyperfine quantum numbers of the eigenstate of atom B [42]. In the large r limit, the full effective potential curves $V_{\text{tot}}(r)$ are labeled by $|f_A, m_{f_A}, f_B, m_{f_B}\rangle$. The thresholds (which is the potential in the large r limit) with different f values are separated by energies of the order of $10\mu eV$. A magnetic field of a few hundred Gauss shifts the thresholds corresponding to fixed f_A and f_B but different m_{f_A} and m_{f_B}, e.g., in ^{85}Rb the states $|3,-2,2,-2\rangle$ and $|3,-3,2,-1\rangle$ are separated by an energy of approximately $3\mu eV$ in a magnetic field of $600G$ [43] [see Eq. (1.4)].

During the scattering process, the atoms closely approach each other. Since $E(r)$ is not diagonal in the atomic basis, coupling between different atomic hyperfine states arises during the collision. The molecular basis consists of states labeled by $|s, m_s, i, m_i\rangle$ [42], where $\vec{I} = \vec{I}_A + \vec{I}_B$ is the total nuclear spin, i denotes the quantum number corresponding to $\vec{I}$, and m_s and m_i are the electronic and nuclear spin projection quantum num-

bers, respectively. The matrix elements of $E(r)$ in the atomic basis are given by [42],

$$\begin{aligned}\langle f'_A, m'_{f_A}, f'_B, m'_{f_B}|E(r)|f_A, m_{f_A}, f_B, m_{f_B}\rangle = \\ \sum_{s,s',i,i',m_s,m'_s,m_i,m'_i} \langle f'_A, m'_{f_A}, f'_B, m'_{f_B}|s', m'_s, i', m'_i\rangle \times \\ \langle s', m'_s, i', m'_i|E(r)|s, m_s, i, m_i\rangle \times \\ \langle s, m_s, i, m_i|f_A, m_{f_A}, f_B, m_{f_B}\rangle. \qquad (1.14)\end{aligned}$$

Using that $E(r)$ is diagonal in the molecular basis, we obtain

$$\begin{aligned}&\langle f'_A, m'_{f_A}, f'_B, m'_{f_B}|E(r)|f_A, m_{f_A}, f_B, m_{f_B}\rangle = \\ &\sum_s E_s(r)\langle f'_A, m'_{f_A}, f'_B, m'_{f_B}|s, m_s, i, m_i\rangle\langle s, m_s, i, M_i|f_A, m_{f_A}, f_B, m_{f_B}\rangle, \qquad (1.15)\end{aligned}$$

where $E_s(r)$ denotes the Born-Oppenheimer potential curve corresponding to a particular s value, e. g., $E_0(r)$ is the singlet potential curve and $E_1(r)$ is the triplet potential curve. Equation (1.15) shows that $E(r)$ [the effective short range interaction potential] leads to a coupling between the different hyperfine states. Equation (1.15) also shows that $m'_{f_A} + m'_{f_B} = m_s + m_i = m_{f_A} + m_{f_B}$, i.e., coupling occurs only between those channels for which the total m_f quantum number is conserved. Physically this makes sense since the Hamiltonian has cylindrical symmetry.

As an example, we consider the scattering between two neutral ^{85}Rb atoms [44] in a magnetic field $\vec{B}$. We assume that both atoms are initially in the hyperfine state $|f, m_f\rangle = |2,-2\rangle$, i. e., $|f_A, m_{f_A}, f_B, m_{f_B}\rangle = |2,-2,2,-2\rangle$. This hyperfine state has nonzero coupling to four other hyperfine states with $m_f = 4$, $|3,-3,2,-1\rangle$, $|3,-2,2,-2\rangle$, $|3,-3,3,-1\rangle$ and $|3,-2,3,-2\rangle$. These states $|3,-3,2,-1\rangle$, $|3,-2,2,-2\rangle$, $|3,-3,3,-1\rangle$ and $|3,-2,3,-2\rangle$ have energies in ascending order in the presence of a magnetic field in the

range of zero to a thousand Gauss, and are energetically higher lying than the initial state [43]. For the scattering of two ^{85}Rb atoms at an energy larger than the threshold of the $|2,-2,2,-2\rangle$ state but lower than the threshold of the $|3,-3,2,-1\rangle$ state, the adiabatic potential curve corresponding to state $|2,-2,2,-2\rangle$ constitutes an open channel while the adiabatic potential curves corresponding to the states $|3,-3,2,-1\rangle$, $|3,-2,2,-2\rangle$, $|3,-3,3,-1\rangle$ and $|3,-2,3,-2\rangle$ constitute closed channels. For sufficiently low scattering energy, this multichannel set up leads to a Feshbach resonance at $B = 155.2G$ [45, 46]. It turns out that the scattering length near this Feshbach resonance can be modeled using just two effective channels, one open and one closed.

Figure 1.2 gives a schematic picture of the two adiabatic potential curves corresponding to the two effective channels as a function of the relative coordinate. The lower curve is labeled channel one and corresponds to the effective open channel, and the upper curve is labeled channel two and corresponds to the effective closed channel. Let $\vec{\mu}_1$ and $\vec{\mu}_2$ be the magnetic moments of the atoms in the states corresponding to channels one and two, respectively. If channel one has a threshold at zero energy, then channel two has a threshold at an energy of ε, where $\varepsilon = |(\vec{\mu}_1 - \vec{\mu}_2) \cdot \vec{B}|$. For an ultracold atomic gas the relative scattering energy E of the atoms is small. We assume that the channel two supports a bound state. Since the difference ε in thresholds can be adjusted by varying the magnetic field $\vec{B}$, the value of the bound state can be varied. When the relative scattering energy E of the two atoms corresponds to the bound state energy E_b of the coupled channel system a Feshbach resonance occurs. The two body scattering length diverges at the resonance. By varying the magnetic field around the resonance value, the scattering length can be tuned to essentially any desired value. In Sec. 3.2, we develop coupled two channel treatments using zero range and finite range square well potentials [47, 48] and apply them to the ^{85}Rb resonance at $B = 155.2G$. As we will see in Chs. 2 to 5, the effective interaction strength of two interacting atoms is

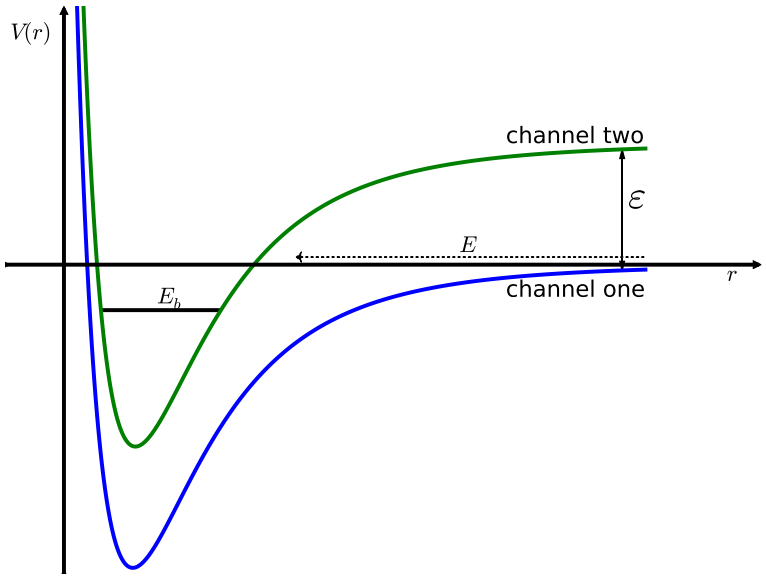

Figure 1.2: Adiabatic potential curves corresponding to two different hyperfine states. The lower curve is labeled as channel one (effectively open channel) and the upper curve as channel two (effectively closed channel). E is the relative scattering energy and E_b is the bound state energy of the coupled channel system. ϵ is the difference in threshold energies of the two channels.

determined by their scattering lengths. A Feshbach resonance thus provides a powerful tool to tune the effective interaction strength between two particles to any desired value.

So far, the effective potentials considered in Eq. (1.11) do not account for the dipole-dipole interaction that arises due to the magnetic dipole moments of the electrons. For s-wave scattering ($l = 0$), this term does not change the energy spectrum because the dipole-dipole interactions average to zero for spherically symmetric $l = 0$ wavefunctions. For higher partial waves, however, the dipole-dipole interaction has a nonzero contribution and introduces a splitting of energy levels with different m_l quantum numbers. The dipole-dipole interaction is given by [49]

$$H_{ss} = -\alpha^2 \frac{3(\hat{R}\cdot\hat{S}_A)(\hat{R}\cdot\hat{S}_B) - \hat{S}_A\cdot\hat{S}_B}{R^3}, \tag{1.16}$$

where α is the fine structure constant, R is the distance between the two electrons and $\hat{R}$ is the unit vector pointing from electron A to electron B. The Hamiltonian H_{ss} can be simplified to isolate the spin and partial wave operators [43, 49, 50],

$$-\frac{2\sqrt{6\pi}}{5R^3}\sum_{q=-2}^{2}(-1)^q Y_{2q}(\Theta,\Phi)(S_A\otimes S_B)^2_{-q}, \tag{1.17}$$

where Θ is the angle between $\hat{R}$ and the z-axis (direction of the magnetic field vector), Φ is the azimuthal angle of $\hat{R}$, and $Y_{2q}(\Theta,\Phi)$ is a spherical harmonic. The matrix elements of this term in the atomic basis are

$$-\frac{2\sqrt{6\pi}}{5R^3}\sum_{q=-2}^{2}(-1)^q\langle l', m_l'|Y_{2q}(\Theta,\Phi)|l, m_l\rangle\langle f_A', m_{f_A}', f_B', m_{f_B}'|(S_A\otimes S_B)^2_{-q}|f_A, m_{f_A}, f_B, m_{f_B}\rangle. \tag{1.18}$$

For elastic s-wave scattering the term $\langle 0,0|Y_{2q}(\Theta,\Phi)|0,0\rangle$ vanishes (see above). For elas-

tic ($q = 0$) p-wave scattering, however, the $\langle 1, m_1' | Y_{2q}(\Theta, \Phi) | 1, m_1 \rangle$ term is non-zero and depends on m_1 ($m_1 = m_1'$). It follows that the bound state energy E_b is slightly different for $m_1 = m_1' = 0$ and for $m_1 = m_1' = \pm 1$ [49]. Consequently two closely spaced p-wave Feshbach resonances can occur. Reference [49] shows, for the ^{40}K resonance at 198.5G, that the spacing between the splitting of the resonance is larger than the width of the resonances. As a result the $m_1 = 0$ and $m_1 = \pm 1$ resonances can be modeled separately.

1.4 Confining potentials and reduced dimensionality

So far we have introduced two body interactions in free space. However any experiment on degenerate quantum gases confines the atoms. Most commonly used trapping potentials are harmonic or nearly harmonic. Section 1.4.1 introduces the harmonic trapping potential and shows that for two particles in a harmonic trap, the center of mass motion and the relative motion separate. Section 1.4.1 also introduces quasi-one and quasi-two dimensional systems and Sec. 1.4.2 discusses optical lattices.

1.4.1 Harmonic traps

As explained in Sec. 1.3, each hyperfine state with a particular value of m_F has a magnetic dipole moment μ_{m_f} corresponding to it. Since the energy of an atomic state depends on the external magnetic field, an inhomogeneous magnetic field can be used to trap atoms. Magnetic traps like the time averaged orbiting potential (TOP) trap [51] and the Ioffe-Pritchard [52] trap have an approximately quadratic spatial dependence (for magnetic fields of the order of a few hundred Gauss) with a local minimum and are therefore approximately harmonic [1]. In the case of the TOP trap, the magnetic field is always linear , but averaging over the fast period of the bias field rotation makes it

effectively quadratic for the atoms. A harmonic potential has the form $\frac{1}{2}m\left(\omega_x^2x^2+\omega_y^2y^2+\omega_z^2z^2\right)$, where m is the mass of the trapped particle, ω_x, ω_y and ω_z are the angular trapping frequencies along the x, y and z axes, respectively, and (x,y,z) denotes the position of the particle in cartesian coordinates with respect to the center of the trap.

Separability of center of mass coordinate

Consider a one dimensional system of two particles with masses m_1 and m_2 and positions z_1 and z_2 under harmonic confinement. We assume that the trapping frequency ω_z experienced by the two particles is the same. The classical Hamiltonian of the system is

$$H=\frac{p_{z1}^2}{2m_1}+\frac{p_{z2}^2}{2m_2}+V_{\text{int}}(z)+\frac{1}{2}m_1\omega_z^2z_1^2+\frac{1}{2}m_2\omega_z^2z_2^2, \tag{1.19}$$

where $z=z_1-z_2$, $V_{\text{int}}(z)$ denotes the interaction potential, and p_{zi} is the momentum of the i^{th} particle.

The center of mass coordinate Z is given by

$$Z=\frac{m_1z_1+m_2z_2}{M}, \tag{1.20}$$

where the total mass M is given by

$$M=m_1+m_2. \tag{1.21}$$

Expressing z_1 and z_2 in terms of the center of mass and relative coordinates, we have

$$z_1=Z+\frac{m_2}{M}z \tag{1.22}$$

and

$$z_2 = Z - \frac{m_1}{M} z. \tag{1.23}$$

Using the center of mass and relative coordinates, the potential energy term in Eq. (1.19) can be rewritten,

$$\frac{1}{2} m_1 \omega_z^2 z_1^2 + \frac{1}{2} m_2 \omega_z^2 z_2^2 = \frac{1}{2} M \omega_z^2 Z^2 + \frac{1}{2} \mu \omega_z^2 z^2, \tag{1.24}$$

where the reduced mass μ is given by

$$\mu = \frac{m_1 m_2}{M}. \tag{1.25}$$

Classically, p_{zi} is given by $m_i \dot{z}_i$, where $\dot{z}_i$ is the first time derivative of z_i. Consequently, the kinetic energy term of H can also be rewritten in terms of the center of mass and relative coordinates,

$$\frac{p_{z1}^2}{2m_1} + \frac{p_{z2}^2}{2m_2} = \frac{p_z^2}{2\mu} + \frac{P_Z^2}{2M}, \tag{1.26}$$

where $p_z = \mu \dot{z}$ is the relative momentum and $P_Z = M\dot{Z}$ is the center of mass momentum. Putting Eqs. (1.26) and (1.24) into Eq. (1.19), we obtain

$$H = \left[\frac{p_z^2}{2\mu} + V_{\text{int}}(z) + \frac{1}{2} \mu \omega_z^2 z^2 \right] + \left[\frac{P_Z^2}{2M} + \frac{1}{2} M \omega_z^2 Z^2 \right]. \tag{1.27}$$

The quantum mechanical operator for the center of mass momentum P_Z is $P_Z = -\imath\hbar\frac{\partial}{\partial Z}$ and the relative momentum p_z is $p_z = -\imath\hbar\frac{\partial}{\partial z}$, where $\imath = \sqrt{-1}$. Plugging this into Eq. (1.27), we obtain

$$H = H_{\text{rel}} + H_{\text{com}}, \tag{1.28}$$

where

$$H_{\text{rel}} = \left[-\frac{\hbar^2}{2\mu}\frac{\partial^2}{\partial z^2} + V_{\text{int}}(z) + \frac{1}{2}\mu\omega_z^2 z^2 \right] \tag{1.29}$$

and

$$H_{\text{com}} = \left[-\frac{\hbar^2}{2M}\frac{\partial^2}{\partial Z^2} + \frac{1}{2}M\omega_z^2 Z^2 \right]. \tag{1.30}$$

This shows that the center of mass and relative coordinates separate. The separation of relative and center of mass Hamiltonians in the absence of an external trapping potential simply follows by setting $\omega_z = 0$. Further on, whenever we consider a system of two particles in a harmonic trap or in the absence of an external confining potential, we only consider the relative Hamiltonian H_{rel}. The solution to the center of mass Hamiltonian is well known, and can be multiplied by the solution obtained for H_{rel} to yield the full solution.

Low dimensional systems

It is possible to have harmonic traps with different trapping frequencies ω_x, ω_y and ω_z. Here we consider cylindrically symmetric systems with $\omega_x = \omega_y = \omega_\perp$ different from ω_z. The trapping potential is thus characterized by two different length scales, the oscillator length $a_\perp$ in the xy-plane (or ρ direction) and the oscillator length a_z in the z-direction,

$$a_\perp = \sqrt{\frac{\hbar}{\mu\omega_\perp}} \tag{1.31}$$

and

$$a_z = \sqrt{\frac{\hbar}{\mu\omega_z}}. \tag{1.32}$$

Cigar shaped traps are characterized by $\omega_\perp > \omega_z$ or $a_\perp < a_z$ and pancake shaped traps are characterized by $\omega_\perp < \omega_z$ or $a_\perp > a_z$. In the following, we are interested in

traps geometrized with very large and very small aspect ratios η, where

$$\eta = \frac{\omega_\perp}{\omega_z}. \tag{1.33}$$

Experimentally, quasi-one and quasi-two dimensional Bose and Fermi gases have been realized [53, 54].

Consider a degenerate Bose gas consisting of N mass m particles under cylindrically symmetric harmonic confinement. The chemical potential μ_e^B is defined as the amount of energy required to add a boson to the system. In the Thomas Fermi approximation, the chemical potential is given by [55]

$$\mu^B = \frac{1}{2}\left(15\hbar^2 N a m^{1/2}\omega_z\omega_\perp^2\right)^{2/5}, \tag{1.34}$$

where a is the scattering length. For the system to be quasi low dimensional, we must have

$$\mu^B \ll \hbar\omega_t, \tag{1.35}$$

where ω_t is the trapping frequency in the tight confining direction [53]. For cigar shaped systems, we have $\omega_t = \omega_\perp$; if Eq. (1.35) is fulfilled, then excitations along the ρ direction are effectively frozen out and the system is quasi one dimensional. For pancake shaped systems, we have $\omega_t = \omega_z$; if Eq. (1.35) is fulfilled, then excitations along the z direction are effectively frozen out and the system is quasi two dimensional.

Similarly, for a degenerate Fermi gas under cylindrically symmetric harmonic confinement, the system is considered quasi low dimensional if [3]

$$\epsilon_F \ll \hbar\omega_t, \tag{1.36}$$

where ϵ_F is the Fermi energy of the system.

For a quasi one dimensional system, one might naively assume that the effective one dimensional interaction potential $V_{1D}(\vec{z})$ can be calculated from the s-wave three dimensional zero range potential $V_{3D}(\vec{r})$ by assuming that the wavefunction in ρ and ϕ is given by the two dimensional harmonic oscillator wavefunction $\psi_0^{2D}(\rho,\phi)$,

$$V_{1D}(\vec{z}) = \int \left(\psi_0^{2D}(\rho,\phi)\right)^* V_{3D}(\vec{r})\psi_0^{2D}(\rho,\phi)\rho\, d\rho\, d\phi. \tag{1.37}$$

This treatment is only approximate and discussed in more detail in Sec. 2.3. Similarly, one might naively expect that the quasi two dimensional zero range potential can be obtained from the three dimensional zero range potential by freezing out the motion along the z direction and integrating over z. This naive picture only holds for weak interactions and is discussed in more detail in Sec. 4.1.4.

1.4.2 Optical lattices

An optical lattice is a periodic intensity pattern that can be created e. g., by interfering two counter-propagating lasers. The resulting potential can be used to trap neutral atoms [13]. The optical lattice potential in the special case of a cubic lattice has the form

$$V(x,y,z) = V_0[\sin^2(kx)+\sin^2(ky)+\sin^2(kz)], \tag{1.38}$$

where $\vec{k}$ is the wave vector of the laser light ($k = |\vec{k}|$ with $k = \frac{2\pi}{\lambda}$, where λ is the wavelength of the laser) and V_0 is determined by the laser intensity and the detuning from the atomic resonance. The above potential has local minima at $x = \frac{n_x\pi}{k}, y = \frac{n_y\pi}{k}$ and $z = \frac{n_z\pi}{k}$, where n_x, n_y and n_z are integers. Consider one such local minimum at $x = x_0, y = y_0$

and $z = z_0$. For small displacements from this local minimum, i. e., for $k(x - x_0)$, $k(y - y_0)$ and $k(z - z_0) \ll 1$, $V(x, y, z)$ can be Taylor expanded about $x = x_0, y = y_0$ and $z = z_0$, yielding to lowest order

$$V(x, y, z) \approx V_0 k^2 [(x - x_0)^2 + (y - y_0)^2 + (z - z_0)^2]. \tag{1.39}$$

Hence to lowest order, each optical lattice site can be considered to be a harmonic trap. Optical lattices have been created in one, two and three dimensions [14, 12, 11].

It is possible to load an optical lattice with exactly two atoms per lattice site [56, 57, 10]. If the optical lattice is set up such that the tunneling between neighboring sites can be neglected then each site acts as an approximately harmonic trap with two interacting atoms [14]. This provides a good testing ground for the results obtained in Chs. 2 to 5.

1.5 Introduction to pseudopotentials

For ultracold quantum degenerate gases, the de Broglie wavelength λ_{dB} is typically of the order of $10^5 a_0$ [39], and thus much larger than the van der Waals length l_{vdW} [see Eq. (1.10)]. To investigate physical systems we need to use probes. The resolution of information we gain depends on the size of the probe we use. For example, if we use light to measure the position of a spherical object then the uncertainty in the position of the object is of the order of the wavelength λ of the light used. Ideally, we would want this uncertainty to be much smaller than the diameter D of the object. To accurately measure the position of the sphere, we must require, $\lambda \ll D$. An equivalent analysis can be done in terms of energy scales. Any length scale corresponds to an energy scale. For example, light of wavelength λ has an energy E, $E = (hc)/\lambda$, where h is Planck's constant and c is the velocity of light. The discussion presented to measure the position of the

object translates straight forwardly to cold atomic gases, with D replaced by the typical length scale of the atom-atom potential and λ replaced by the de Broglie wavelength λ_{dB}. Since $\lambda_{\mathrm{dB}} \gg l_{\mathrm{vdW}}$, the atoms are unable to probe the details of the atom-atom interaction potential. Hence the complicated atom-atom interaction potential can be replaced by simple model potentials, including zero range model potentials, that are designed to reproduce the eigenfunctions of the two atom system at large r but fail to reproduce the small r details of the eigenfunctions.

For ultracold systems, unless there is a resonance in a channel corresponding to one of the higher partial waves, the scattering processes are usually dominated by the lowest partial wave. Hence for a system of bosons, the scattering processes and some many-body properties are s-wave dominated and can be described by a single atomic physics parameter, the s-wave scattering length a. In many cases, a zero range pseudopotential that depends only on the s-wave scattering length [58, 59, 60] can be used to model a system of bosons. s-wave pseudopotentials have been extensively used to describe both two-body and many-body systems of identical bosons. The mean field Gross-Pitaevskii equation [61, 62, 63] that describes a gas of identical bosons can, e. g., be derived with in a Hartree Fock framework that utilizes an s-wave pseudopotential.

In a system of identical fermions, s-wave scattering is forbidden by symmetry and at low temperatures p-wave scattering dominates. A pseudopotential description of spin polarized fermions [64] must thus account for the p-wave scattering length and possibly also for other relevant length scales of the problem. If the p-wave scattering length is the only parameter, it becomes important to include the energy dependence of the scattering length in the strength of the pseudopotential to obtain an accurate description of the system.

The scattering of higher partial waves may be important if there is a resonance in a channel corresponding to one of them. A pseudopotential has been developed to de-

scribe the scattering between two particles for all partial waves [65]. The pseudopotential (or equivalently, boundary condition) has proven extremely useful in solving few-body problems [66]. Due to the advances in trapping technology quasi one and two dimensional systems have been obtained. Pseudopotentials that describe atom-atom interactions in low dimensional systems have been developed in Refs. [64, 67].

In the above examples, the interaction potential has been assumed to be spherically symmetric. This assumption is usually justified for pseudopotentials that are designed to describe scattering processes in ultracold alkali gases like Rb, K or Cs. In the case of Cr atoms and in case of polar molecules, however, the interactions are long ranged and anisotropic. Although the anisotropic interactions are long ranged (the leading behavior at large r goes as $1/r^3$), a zero range pseudopotential that reproduces the K-matrix of the true atom-atom or molecule-molecule potential for aligned particles has been suggested in Refs. [68, 69]. This pseudopotential was used, e.g., to obtain an analytical expression for the eigenenergies of two interacting aligned dipoles under external spherically symmetric harmonic confinement [70, 71]. This application and extensions thereof to cylindrically symmetric traps, which turns out to be non-trivial, is discussed in Ch. 5.

1.6 Thesis overview

Chapter 2 deals with two body interactions in one dimension and develops zero range pseudopotentials to model two body interaction potentials in one dimension. It compares the different pseudopotential representations and obtains the eigenenergies of two interacting particles in a harmonic trap in one dimension. It also discusses the bound state spectrum of two interacting particles. The chapter relates the two body scattering length in one dimension to its three dimensional counterpart.

Chapter 3 discusses two body interactions in three dimensions using both single channel and coupled channel model potentials. It obtains the eigenenergies of two interacting particles under harmonic confinement in three dimensions using a single channel model interaction potential. It uses a coupled two channel model to obtain a description of a Feshbach resonance in three dimensions.

Chapter 4 treats two body interactions in two dimensions using zero range and finite range single and coupled channel models. It obtains the eigenenergies of two particles in a harmonic trap in two dimensions for any partial wave. It also uses a zero range coupled channel model to describe a Feshbach resonance in two dimensions and studies the effect of varying the coupling strength on the energy levels and the molecular fraction. The chapter also relates the two dimensional s-wave scattering length to its three dimensional counterpart.

Chapter 5 deals with anisotropic interactions under spherically symmetric and cylindrically symmetric harmonic confinement. One example of an anisotropic interaction is the interaction between two aligned dipoles. The chapter has a detailed discussion on the scattering between two aligned dipoles. Although the dipole-dipole interaction is long ranged, Ch. 5 successfully uses a zero range pseudopotential to obtain the eigenenergies of two aligned dipoles under spherically symmetric harmonic confinement. The pseudopotential treatment breaks down in treating two aligned dipoles under cylindrically symmetric harmonic confinement, due to the long ranged nature of the dipole-dipole interaction. However, Ch. 5 obtains an eigenequation to treat two particles interacting via a short range anisotropic interaction potentials under cylindrically symmetric harmonic confinement.

Chapter 6 summarizes the thesis and points out some interesting extensions of the research done here.

Chapter 2

Two body systems in one dimension

We start with the simplest case of two interacting particles in one dimension. In this chapter all Hamiltonian, potentials, wavefunctions, phase shifts and scattering lengths are one dimensional. Since we are using relative coordinates in one dimension and, as shown later, model interaction potentials with well defined symmetries, the wavefunctions have either even or odd parity. The even (denoted by subscript "+") and odd (denoted by subscript "-") parity wavefunctions belong to orthogonal Hilbert spaces. For two identical bosons only even parity solutions are allowed (as the wavefunction describing two identical bosons must be symmetric under exchange), while for two identical fermions only odd parity solutions are allowed (as the wavefunction describing two identical fermions must be antisymmetric under exchange). For non-identical particles both even and odd parity solutions are allowed as there are no symmetry constraints. In three dimensions a system with even angular momentum l quantum number has even parity and can be mapped onto the even parity one dimensional system, while a system with odd l quantum number has odd parity and can be mapped onto the odd parity one dimensional system.

Section 2.1 defines the even and odd parity phase shifts and corresponding scattering lengths and Sec. 2.1.1 derives expressions for the phase shifts and scattering lengths

for two particles interacting through a square well potential. Section 2.1.2 develops zero range pseudopotentials that reproduce the scattering properties of the square well potential. Section 2.1.3 derives boundary conditions, which are alternative, equivalent representations of the zero range pseudopotentials, and then uses these boundary conditions to derive the so-called Fermi-Bose duality. Section 2.2 compares the even and odd parity eigenenergies for two particles in a harmonic trap interacting through square well and zero range potentials. The excellent agreement between the two sets of eigenenergies verifies the validity of the pseudopotential treatment.

2.1 Scattering in one dimension

The one dimensional Schrödinger equation for the relative coordinate z of two particles interacting through the potential $V_{\text{int}}(z)$ is given by

$$H^{\text{free}}\Psi^{\text{free}}(z) = E\Psi^{\text{free}}(z), \tag{2.1}$$

where

$$H^{\text{free}} = -\frac{\hbar^2}{2\mu}\frac{\partial^2}{\partial z^2} + V_{\text{int}}(z). \tag{2.2}$$

Here, E denotes the positive relative scattering energy of the two particles, and the superscript "free" corresponds to the absence of an external trapping potential. The potential $V_{\text{int}}(z)$ is assumed to be short range, i. e., it is assumed to fall off faster than $1/z$ as $z \to \infty$. In this case, there exists a distance z_0 such that the potential $V_{\text{int}}(z)$ can be neglected for all $|z| > z_0$, i. e., $V_{\text{int}}(z) = 0$ for $|z| > z_0$. We denote the two linearly independent solutions of the second order differential equation Eq. (2.1) with $V_{\text{int}}(z) = 0$ by $f_{\pm}(z)$ (the regular solution) and $g_{\pm}(z)$ (the irregular solution), where $f_{+}^{\text{free}}(z) = \frac{z}{|z|}\sin(kz)$, $f_{-}^{\text{free}}(z) = \sin(kz)$, $g_{+}^{\text{free}}(z) = \cos(kz)$ and $g_{-}^{\text{free}}(z) = \frac{z}{|z|}\cos(kz)$. The relative wavefunc-

tion in the outer region ($|z| > z_0$) can then be written as

$$\Psi_{\pm}^{\text{free}(>)}(z) = \aleph_{\pm}(k)\left(f_{\pm}^{\text{free}}(z) + \tan\delta_{\pm}(k) g_{\pm}^{\text{free}}(z)\right). \tag{2.3}$$

In Eq. (2.3), $\aleph_{\pm}(k)$ is the normalization constant and $\delta_{\pm}(k)$ is the energy dependent phase-shift accumulated due to the interaction potential for $|z| < z_0$, where

$$k = \sqrt{(2\mu E)/\hbar^2}. \tag{2.4}$$

Since the potential is neglected for $|z| > z_0$, no further phase is accumulated beyond $|z| = z_0$. The solution $\Psi_{\pm}^{\text{free}(<)}(z)$ for $|z| < z_0$ (this region is represented using the superscript "<") depends on the details of the interaction potential and has to be determined explicitly for each interaction potential provided the interaction potential is finite for $|z| \leq z_0$. The phase shifts $\delta_{\pm}(k)$ can be determined by imposing the following two continuity conditions at $z = z_0$ (or at $z = -z_0$, which yields identical results),

$$\Psi_{\pm}^{\text{free}(<)}(z_0) = \Psi_{\pm}^{\text{free}(>)}(z_0) \tag{2.5}$$

and

$$\left(\frac{\partial \Psi_{\pm}^{\text{free}(<)}(z)}{\partial z}\right)_{z=z_0} = \left(\frac{\partial \Psi_{\pm}^{\text{free}(>)}(z)}{\partial z}\right)_{z=z_0}. \tag{2.6}$$

The even and odd parity phase shifts define the energy dependent scattering lengths $a_{\pm}(k)$,

$$a_{\pm}(k) = -\frac{\tan\delta_{\pm}(k)}{k}, \tag{2.7}$$

and the energy independent scattering lengths $a_{\pm}$,

$$a_{\pm} = \lim_{k\to 0} a_{\pm}(k). \tag{2.8}$$

Since the details of the atom-atom interaction are in general unimportant to describe two body scattering in quantum degenerate gases, the next section uses a simple shape dependent model potential, a square well potential, to represent the interaction between the atoms. Section 2.2 confirms the validity of the zero range pseudopotentials developed in Sec. 2.1.2 by comparing their eigenenergies with those for the square well potential.

2.1.1 Finite range square well potential

We consider the scattering of two particles interacting through the square well potential $V_{\rm SW}(z)$, where

$$V_{\rm SW}(z) = \begin{cases} -V_0 & \text{for} \quad |z| < z_0 \\ 0 & \text{for} \quad |z| > z_0, \end{cases} \tag{2.9}$$

with $V_0 > 0$. Since $V_{\rm SW}(z) = 0$ for $|z| > z_0$, the solution to Eq. (2.1) with $V_{\rm int}(z) = V_{\rm SW}(z)$ is given by $\Psi_{\pm}^{\rm free(>)}(z)$ [Eq. (2.3)]. For $|z| < z_0$, the even parity solution is given by

$$\Psi_{+}^{\rm free(<)}(z) = A_{+}(k)\cos(k_{\rm in} z), \tag{2.10}$$

where $A_{+}(k)$ is a constant that can be determined from the continuity condition given in Eq. (2.5) and

$$k_{\rm in} = \sqrt{\frac{2\mu(E+V_0)}{\hbar^2}}. \tag{2.11}$$

Imposing the continuity conditions given in Eqs. (2.5) and (2.6), we get

$$\tan\delta_{+}(k) = \frac{1 + \frac{k_{\rm in}}{k}\tan(k_{\rm in} z_0)\tan(k z_0)}{-\frac{k_{\rm in}}{k}\tan(k_{\rm in} z_0) + \tan(k z_0)}. \tag{2.12}$$

Plugging Eq. (2.12) into Eq. (2.8), the even parity energy independent scattering length for the square well interaction potential becomes

$$a_+ = z_0 + \frac{1}{\overline{k}_{\text{in}}}\cot(\overline{k}_{\text{in}} z_0), \tag{2.13}$$

where

$$\overline{k}_{\text{in}} = \sqrt{\frac{2\mu V_0}{\hbar^2}}. \tag{2.14}$$

The odd parity solution to Eq. (2.1) with $V_{\text{int}} = -V_0$ is given by

$$\Psi_-^{\text{free}(<)}(z) = A_-(k)\sin(k_{\text{in}} z), \tag{2.15}$$

where $A_-(k)$ is a constant that can be determined using the continuity condition given in Eq. (2.5). Following the same procedure as for the even parity case yields the one dimensional odd parity energy independent scattering length a_-,

$$a_- = z_0 - \frac{\tan(\overline{k}_{\text{in}} z_0)}{\overline{k}_{\text{in}}}. \tag{2.16}$$

Figure 2.1(a) shows the dimensionless even parity energy independent scattering length a_+/z_0 [Eq. (2.13)] as a function of the dimensionless quantity $\overline{k}_{\text{in}} z_0$. For vanishing V_0, a_+ is infinitely large. a_+ decreases till $\overline{k}_{\text{in}} z_0 = \pi$, where a_+ diverges. Past this divergence, a_+ is again infinitely large and the cycle is repeated. In general, a_+ diverges when $\overline{k}_{\text{in}} z_0 = n\pi$ ($n = 0, 1, 2\ldots$). We have adopted a definition of the scattering length such that the divergence of a_+ coincides with the presence of a zero-energy even parity bound state. The even parity eigenenergies ($E < 0$ for a bound state) of the square well

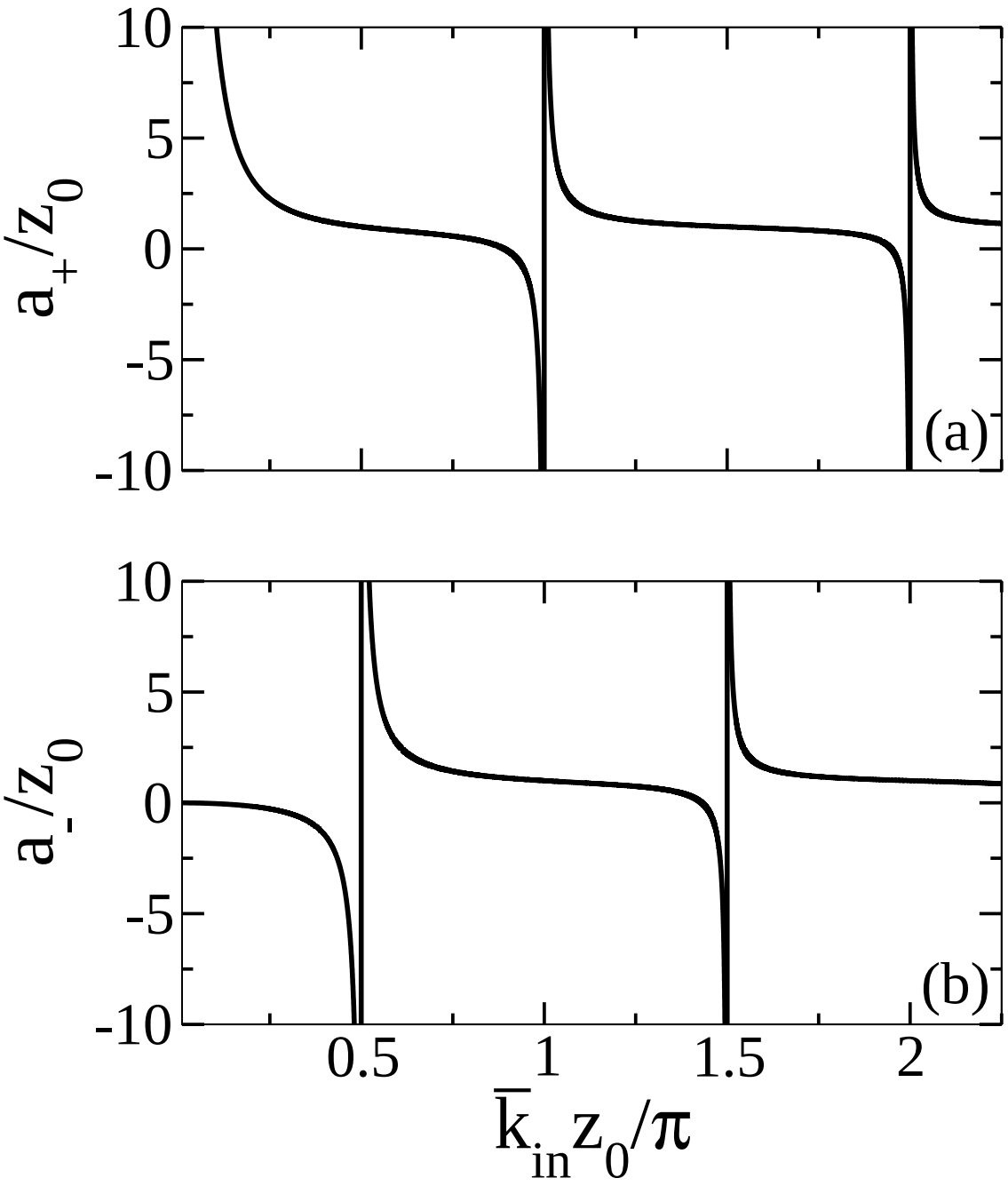

Figure 2.1: Panel (a) shows the even parity scattering length a_+ [Eq. (2.13)] as a function of $\overline{k}_{\rm in}z_0/\pi$, while panel (b) shows the odd parity scattering length a_- [Eq. (2.16)] as a function of $\overline{k}_{\rm in}z_0/\pi$.

potential are given by the solutions to the eigenequation [72]

$$k_{\text{in}} \tan(k_{\text{in}} z_0) = -\imath k. \tag{2.17}$$

Equation (2.17) shows that the square well potential supports a zero energy bound state if $\overline{k}_{\text{in}} z_0 = n\pi$ ($n = 0, 1, 2\ldots$); this condition agrees with that given above for a diverging a_+. In particular, the square well potential supports a bound state for an infinitesimally small well depth V_0, i. e., no minimum threshold value of V_0 is required to support a bound state . This can be explained by the fact that in the $k \to 0$ limit, when $V_0 = 0$, the wavefunction extends to infinity and has zero slope everywhere. Consequently, the expectation value of the kinetic energy, which is given by the slope of the wavefunction, vanishes. The infinitesimally small V_0 value in turn, results in an attractive potential energy that leads to formation of a bound state.

Figure 2.1(b) shows the dimensionless odd parity scattering length a_-/z_0 [Eq. (2.16)] as a function of the dimensionless quantity $\overline{k}_{\text{in}} z_0$. The scattering length a_- vanishes in the absence of a potential ($V_0 = 0$). As $\overline{k}_{\text{in}} z_0$ increases, a_- decreases from zero to minus infinity at $\overline{k}_{\text{in}} z_0 = \pi/2$. Past this divergence, a_- is infinitely large and then decreases till it reaches zero at $\tan(k_{\text{in}} z_0) = 1.4303\pi$. As $\overline{k}_{\text{in}} z_0$ increases further, the cycle is repeated. In general, a^- diverges when $\overline{k}_{\text{in}} z_0 = n\pi/2$ ($n = 1, 3, 5\ldots$). Similarly to the even parity case, we have adopted a definition of the odd parity scattering length such that the divergence of a_- coincides with the presence of a zero energy odd parity bound state. The odd parity eigenenergies for the square well potential are given by the solutions to the eigenequation [72]

$$k_{\text{in}} z_0 \cot(k_{\text{in}} z_0) = \imath k z_0. \tag{2.18}$$

Equation (2.18) shows that the square well supports a zero-energy odd parity bound

state if $\overline{k}_{\rm in} z_0 = (n\pi)/2$ ($n = 1,3,5\ldots$). Unlike the even parity wavefunction, the odd parity wavefunction has a finite slope near $z = 0$, and the kinetic energy increases faster than the absolute value of the potential energy for small $\overline{k}_{\rm in} z_0$. For a bound state the sum of the expectation values of kinetic and potential energies must be negative. As a result, unlike in the even parity case, a_- does not diverge at $\overline{k}_{\rm in} z_0 = 0$ ($V_0 = 0$).

2.1.2 Derivation of one dimensional delta function potentials

Realistic atom-atom interaction potentials are complicated and, in general, cannot be treated analytically. However, since they are short range potentials, their outside wavefunctions ($|z| > z_0$) are given by Eq. (2.3). The outside wavefunction is characterized by a single atomic physics parameter, the phase shift. The goal here is to design a zero range pseudopotential that reproduces a given phase shift. The advantage of such a zero range potential is that certain calculations can be performed analytically. Furthermore, the pseudopotential depends on a single parameter that has a clear physical interpretation. We will see later that the one dimensional even parity pseudopotential has a very simple form. Although the algebra is quite simple and the result well known, we present the details of the derivation to highlight the procedure. The procedure is general and is later used to derive pseudopotentials for more complicated systems.

Using the idea of δ-shell interactions [65], we write the interaction potential $V_{\rm int}(z)$ in one dimension as

$$V_{\rm ps}^{\pm}(z) = \lim_{z_0 \to 0} \left[\delta(z+z_0) + \delta(z-z_0)\right] \hat{O}^{\pm}(z), \tag{2.19}$$

where $\hat{O}^{\pm}(z)$ denotes an operator. The goal in the following is to determine $\hat{O}^{\pm}(z)$ such that the even and odd parity pseudopotentials $V_{\rm ps}^{+}(z)$ and $V_{\rm ps}^{-}(z)$ produce the scattering phase shifts $\delta^{+}(k)$ and $\delta^{-}(k)$, respectively. The potentials $V_{\rm ps}^{\pm}(z)$ are represented by a δ-

shell of radius z_0, which in one dimension reduces to two δ-functions centered at $z = z_0$ and $z = -z_0$. This implies that the potentials are infinitely large at those two points and zero everywhere else, and that all the phase is accumulated at two isolated points corresponding to $z = z_0$ and $z = -z_0$. The eigenfunctions of the Schrödinger equation for $V_{\rm int}(z) = V_{\rm ps}^{\pm}(z)$ are continuous but have discontinuous derivatives at $z = \pm z_0$ (z_0 is non-zero and finite). In the following, we first determine the operator $\hat{O}^{\pm}(z)$ for a finite z_0, and then take the limit $z_0 \to 0$. In the even parity case, the operator $\hat{O}^{+}(z)$ turns out to be a constant. The corresponding eigenfunctions are, in the limit $z_0 \to 0$, continuous at $z = 0$, but have discontinuous first derivatives. In the odd parity case, the operator $\hat{O}^{-}(z)$ contains a derivative with respect to z. The corresponding eigenfunctions are, in the limit $z_0 \to 0$, discontinuous but have continuous first derivatives.

Since $V_{\rm ps}^{\pm}$ vanishes for $|z| > z_0$, the solution to Eq. (2.1) is given by $\Psi_{\pm}^{\rm free(>)}(z)$, Eq. (2.3). The Schrödinger equation for $|z| < z_0$ is given by Eqs. (2.1) and (2.2) with $V_{\rm int}(z) = 0$. The even parity solution to this Schrödinger equation is given by

$$\Psi_{+}^{\rm free(<)}(z) = \alpha_{+}(k)\cos(kz), \tag{2.20}$$

where $\alpha_{+}(k)$ is a constant that can be determined by imposing the continuity of the wavefunction at $z = |z_0|$ [see Eq. (2.5)],

$$\alpha_{+}(k) = \aleph_{+}(k)[\tan(kz_0) + \tan\delta_{+}(k)]. \tag{2.21}$$

Since we are considering an infinite δ-function potential, the derivative of the wavefunction is not continuous at $z = z_0$. In fact, the difference in the derivatives of the wavefunction for $z \to z_0^{+}$ and $z \to z_0^{-}$ can be obtained by integrating Eq. (2.1), with $V_{\rm int}(z) = V_{\rm ps}^{+}(z)$, from $z_0 - \epsilon$ to $z_0 + \epsilon$ and taking the $\epsilon \to 0$ limit,

$$\lim_{z_0\to 0}\left\{-\frac{\hbar^2}{2\mu}\left[\left(\frac{\partial\Psi_+^{\text{free}(>)}(z)}{\partial z}\right)_{z\to z_0}-\left(\frac{\partial\Psi_+^{\text{free}(<)}(z)}{\partial z}\right)_{z\to z_0}\right]+\hat{O}^+(z_0)\Psi_+^{\text{free}(>)}(z_0)\right\}=0. \quad (2.22)$$

Inserting the expressions for $\Psi_+^{\text{free}(>)}(z)$ and $\Psi_+^{\text{free}(<)}(z)$ from Eqs. (2.3) and (2.20) into Eq. (2.22) and using Eq. (2.21), we obtain

$$\lim_{z_0\to 0}\left\{\hat{O}^+(z_0)[\sin(kz_0)+\tan\delta_+(k)\cos(kz_0)]\right\}=\lim_{z_0\to 0}\left\{\frac{\hbar^2 k}{2\mu}[\tan(kz_0)\sin(kz_0)+\cos(kz_0)]\right\}. \quad (2.23)$$

Lastly, taking the limit $z_0\to 0$, Eq. (2.23) becomes

$$\hat{O}^+=\frac{\hbar^2 k}{2\mu\tan\delta_+(k)}, \quad (2.24)$$

which, using Eq. (2.7), can be re-expressed in terms of the scattering length,

$$\hat{O}^+=-\frac{\hbar^2}{2\mu a_+(k)}. \quad (2.25)$$

Our derivation shows that $\hat{O}^+$ is independent of z and therefore the same for all z. Plugging Eq. (2.25) into Eq. (2.19), the δ-shell pseudopotential becomes

$$V_{\text{ps}}^+(z)=\frac{\hbar^2 g_{1D}^+(E)}{2\mu}\lim_{z_0\to 0}[\delta(z+z_0)+\delta(z-z_0)], \quad (2.26)$$

or taking the $z_0\to 0$ limit explicitly,

$$V_{\text{ps}}^+(z)=\frac{\hbar^2}{\mu}g_{1D}^+(E)\delta(z), \quad (2.27)$$

where

$$g_{1D}^{+}(E) = -\frac{1}{a_{+}(k)}. \tag{2.28}$$

The coupling strength $g_{1D}^{+}(E)$ of the even parity pseudopotential indicates the strength of the interaction, i. e., the stronger the interaction, the greater the value of $\left|g_{1D}^{+}(E)\right|$. The non interacting system has $g_{1D}^{+}(E) = 0$, which corresponds to $\delta_{+}(k) = \pi/2$. A weakly interacting system corresponds to $\delta_{+}(k) = (\pi/2) + \Delta\delta_{+}(k)$, where $|\Delta\delta_{+}(k)| \ll 1$. Hence, for a weakly interacting system, we have

$$g_{1D}^{+}(k) \approx -k\Delta\delta^{+}(k). \tag{2.29}$$

Figure 2.2(a) shows that the wavefunction with positive $\Delta\delta_{+}(k)$ (dashed line) is shifted to smaller $|z|$ compared to the wavefunction for vanishing interaction potential (solid line). Thus, a negative interaction strength g_{1D}^{+} implies an effectively attractive interaction. Similarly, the wavefunction with negative $\Delta\delta_{+}(k)$ (dotted line) is shifted to larger $|z|$ compared to the wavefunction for vanishing interaction potential. Thus, a positive interaction strength g_{1D}^{+} implies an effectively repulsive interaction.

We now determine the operator $\hat{O}^{-}$ of the odd parity δ-shell pseudopotential. In the odd parity case, the solution to Eq. (2.1), with $V_{\text{int}}(z) = V_{\text{ps}}^{-}(z) = 0$ for $|z| < z_0$, is given by

$$\Psi_{-}^{\text{free}(<)}(z) = \alpha_{-}(k)\sin(kz), \tag{2.30}$$

where $\alpha_{-}(k)$ is a normalization constant. Following the same procedure as in the even parity case, we obtain

$$V_{\text{ps}}^{-}(z) = \frac{\hbar^2 g_{1D}^{-}(E)}{2\mu} \lim_{z_0 \to 0} [\delta(z+z_0) + \delta(z-z_0)] \frac{1}{z}\frac{\partial}{\partial z}, \tag{2.31}$$

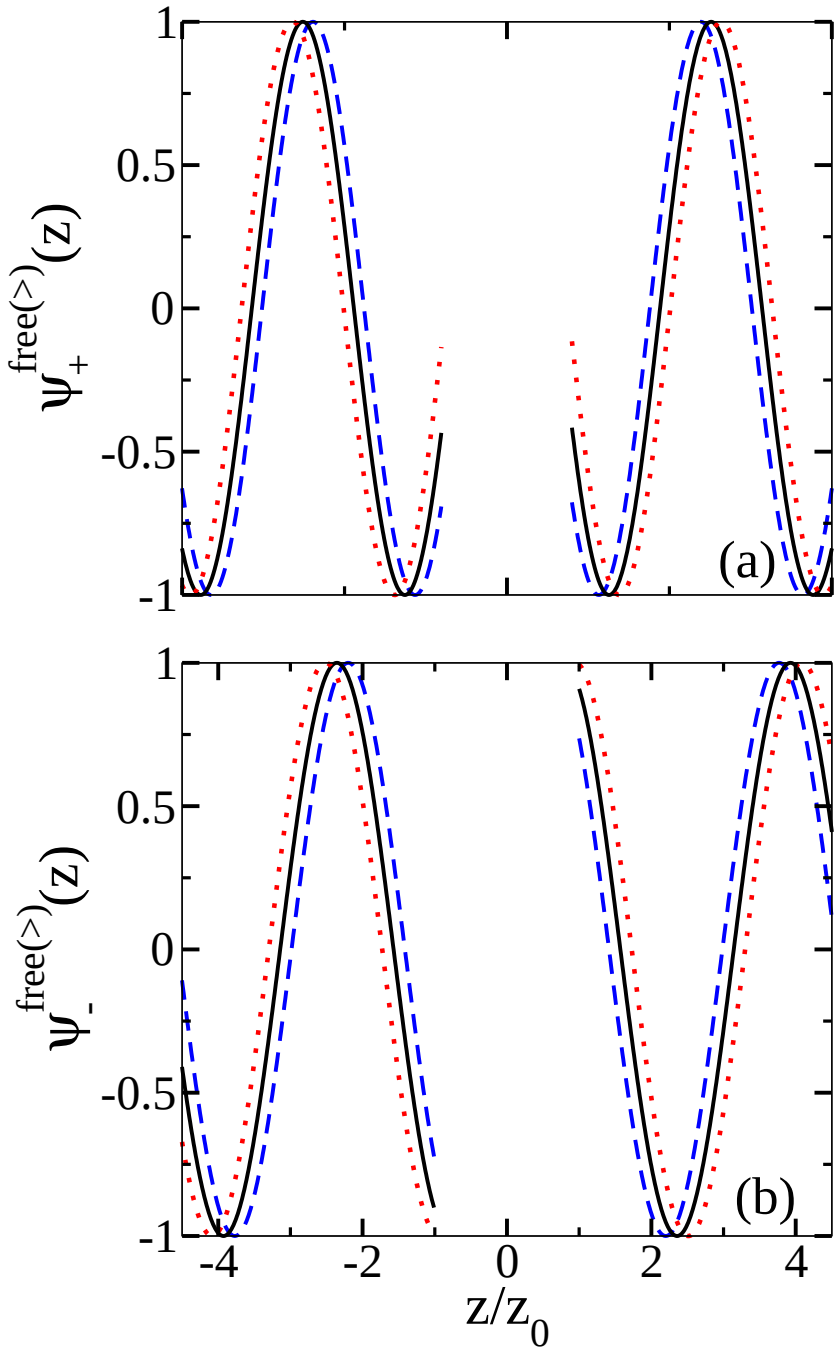

Figure 2.2: Panels (a) and (b) show the even and odd parity wavefunctions $\Psi_\pm^{\text{free}(>)}$ for $z > |z_0|$. Solid lines show the free particle wavefunctions ($\Delta\delta_\pm = 0$). Dashed lines show the outside wavefunctions for $\Delta\delta_\pm = \pi/10$, while dotted lines show outside wavefunctions for $\Delta\delta_\pm = -\pi/10$. Panels (a) and (b) have the same x-scale and label.

or taking the $z_0 \to 0$ limit explicitly,

$$V_{\mathrm{ps}}^{-}(z) = \frac{\hbar^2}{\mu} g_{1D}^{-}(E)\delta(z)\frac{1}{z}\frac{\partial}{\partial z}, \tag{2.32}$$

where

$$g_{1D}^{-}(E) = a_{-}(k) \tag{2.33}$$

denotes the coupling strength of the odd parity zero range pseudopotential.

The non interacting system has $g_{1D}^{-}(E) = 0$, which corresponds to $\delta_{-}(k) = 0$. A weakly interacting system corresponds to $\delta_{-}(k) = \Delta\delta_{-}(k)$, where $|\Delta\delta_{-}(k)| \ll 1$. In this case, the coupling strength becomes

$$g_{1D}^{-} \approx -\frac{\Delta\delta_{-}(k)}{k}. \tag{2.34}$$

Figure 2.2(b) shows that the wavefunction with positive $\Delta\delta_{-}(k)$ (dashed line) is shifted to smaller $|z|$ compared to the wavefunction for vanishing interaction potential (solid line). This indicates that a negative interaction strength g_{1D}^{-} implies an effectively attractive interaction. Similarly, the wavefunction with negative $\Delta\delta_{-}(k)$ (dotted line) is shifted to larger $|z|$ compared to the wavefunction for vanishing interaction potential. This indicates that a positive interaction strength implies an effectively repulsive interaction.

The pseudopotential in Eq. (2.32) can be equivalently represented by the following differential operator [64],

$$V_{\mathrm{ps}}^{-}(z) = \frac{\hbar^2}{\mu} g_{1D}^{-}(E)\frac{\overleftarrow{d}}{dz}\delta(z)\frac{\overrightarrow{d}}{dz}. \tag{2.35}$$

In Eq. (2.35), the first derivative acts to the left and the second to the right,

$$\int_{-\infty}^{\infty} \phi^*(z) V_{\rm ps}^-(z) \chi(z) dz = \frac{\hbar^2}{\mu} g_{1D}^-(E) \left(\frac{d\phi^*(z)}{dz} \right)_{z\to 0} \left(\frac{d\chi(z)}{dz} \right)_{z\to 0}. \tag{2.36}$$

The pseudopotential $V_{\rm ps}^-(z)$ in both representations [Eqs. (2.32) and (2.35)] leads to discontinuous eigenfunctions with continuous first derivatives at $z=0$.

We now determine the bound state or negative eigenenergies of $V_{\rm ps}^+$ and $V_{\rm ps}^-$ by analytic continuation. For a negative energy state, the wavefunction $\Psi_\pm^{\rm free(>)}(z)$ in Eq. (2.3) must decay exponentially for $|z|\to\infty$. The corresponding wavevector k is imaginary and can be written as

$$k = \imath\kappa, \tag{2.37}$$

where κ is a positive, real number,

$$\kappa = \sqrt{\frac{-2\mu E}{\hbar^2}}. \tag{2.38}$$

Using analytic continuation, we can rewrite the wavefunction $\Psi_\pm^{\rm free(>)}(z)$ in Eq. (2.3) for negative energies in terms of exponentials,

$$\Psi_+^{\rm free(>)}(z) = \frac{\aleph_+(k)}{2} \left[\left(\tan\delta_+(\imath\kappa) + \imath \frac{z}{|z|} \right) e^{\kappa z} + \left(\tan\delta_+(\imath\kappa) - \imath \frac{z}{|z|} \right) e^{-\kappa z} \right] \tag{2.39}$$

and

$$\Psi_-^{\rm free(>)}(z) = \frac{\aleph_-(k)}{2} \left[\left(\frac{z}{|z|} \tan\delta_-(\imath\kappa) + \imath \right) e^{\kappa z} + \left(\frac{z}{|z|} \tan\delta_-(\imath\kappa) - \imath \right) e^{-\kappa z} \right]. \tag{2.40}$$

Since $\Psi_\pm^{\rm free(>)}(z)$ must decay exponentially in the $|z|\to\infty$ limit, we require that the pref-

	positive	negative
$a_+(k)$	bound state exists	bound state does *not* exist
$g^+_{1D}(E)$	bound state does *not* exist	bound state exists
$a_-(k)$	bound state exists	bound state does *not* exist
$g^-_{1D}(E)$	bound state exists	bound state does *not* exist

Table 2.1: Conditions on one dimensional scattering lengths and scattering strengths for the existence of a free-space bound state.

actor of the growing exponentials in Eqs. (2.39) and (2.40) vanishes; this implies

$$\tan\delta_\pm(\imath\kappa) = -\imath. \tag{2.41}$$

From Eqs. (2.7) and (2.41), we get $a_\pm(k) = 1/\kappa$. The conditions for the existence of a bound state are summarized in Table 2.1. Since κ is positive by definition [see Eq. (2.38)], this indicates that a bound state exists only for $a_\pm(k) \geq 0$.

Combining Eqs. (2.7) and (2.41), the bound state energy E for $V^\pm_{\rm ps}$ can be expressed in terms of the scattering lengths $a_\pm(k)$,

$$E = -\frac{\hbar^2}{2\mu[a_\pm(k)]^2}. \tag{2.42}$$

Equation (2.42) is an implicit eigenequation with energy dependence on both the left hand side and the right hand side. Hence, the solution to Eq. (2.42) must be obtained self-consistently. Realistic atom-atom interaction potentials generally support multiple bound states for positive and negative values of the energy independent scattering length. If the energy dependence of $a_\pm$ is known, Eq. (2.42) can be used to accurately obtain the eigenenergies of all bound states (highest lying as well as deeply bound). However, the eigenfunctions of deeply bound states cannot be described using the zero range pseudopotential.

If we neglect the energy dependence of the scattering lengths in Eq. (2.42) and approximate $a_{\pm}(k)$ by $a_{\pm}$, then the zero range pseudopotentials V_{+} and V_{-} support a single bound state for all positive $a_{\pm}$. Since the zero range pseudopotentials are designed to reproduce the outside wavefunction ($|z| > z_0$) of a given state, they accurately describe wavefunctions which have most of their amplitude in the region $|z| > z_0$. Bound state wavefunctions decay for $|z| > z_0$. If λ is the size of the bound state, then the zero range pseudopotential describes eigenfunctions with size $\lambda \gg z_0$ accurately, and correspondingly eigenenergies with $|E| \ll \hbar^2/(\mu z_0^2)$. By design, the zero range pseudopotential reproduces the eigenfunctions of weakly bound states accurately, but not of deeply bound states.

2.1.3 Fermi-Bose duality

The zero range pseudopotentials derived in the Sec. 2.1.2 [Eqs. (2.27), (2.32) and (2.35)], can be equivalently represented by a boundary condition for the wavefunction at $z = 0$. Taking the first derivative of the even parity solution $\Psi_{+}^{\text{free}(>)}(z)$ with respect to z, we find the boundary condition at $z = 0$,

$$\left(\frac{\frac{\partial \Psi_{+}^{\text{free}(>)}(z)}{\partial z}}{\Psi_{+}^{\text{free}(>)}(z)} \right)_{z \to 0} = g_{1D}^{+}(E). \tag{2.43}$$

Similarly, the boundary condition for the odd parity case reads

$$\left(\frac{\frac{\partial \Psi_{-}^{\text{free}(>)}(z)}{\partial z}}{\Psi_{-}^{\text{free}(>)}(z)} \right)_{z \to 0} = -\frac{1}{g_{1D}^{-}(E)}. \tag{2.44}$$

A system of two identical bosons can be characterized by the even parity boundary condition [Eq. (2.43)], while a system of two identical fermions can be characterized by

the odd parity boundary condition [Eq. (2.44)]. Equations (2.43) and (2.44) imply that the even and odd parity systems obey the same boundary condition, if we require

$$g_{1D}^{+} = -\frac{1}{g_{1D}^{-}}. \tag{2.45}$$

If g_{1D}^{+} and g_{1D}^{-} are chosen so that Eq. (2.45) is fulfilled, then the outside solutions of the even and odd parity systems agree to within a factor of ± 1 [see Eq. (2.65) and Fig. 2.8 for the trapped system]. Since the energy spectrum is determined by the square of the wavefunctions, the even and odd parity systems have the same energy spectrum if Eq. (2.45) is fulfilled. In particular, the energy spectrum of two strongly interacting identical bosons (large $|g_{1D}^{+}|$) coincides with that of a pair of weakly interacting identical fermions (small $|g_{1D}^{-}|$), and vice-versa. Note that the sign is also reversed, i. e., a strongly *attractive* two-boson system corresponds to a weakly *repulsive* two-fermion system. Equation (2.45) together with the sgn() function, where

$$\mathrm{sgn}(z) = \frac{z}{|z|}, \tag{2.46}$$

provides a rule for mapping a system of two interacting bosons onto a system of two interacting fermions, and vice-versa.

The mapping derived here for the two-particle system generalizes to many-body systems in one dimension and is referred to as Fermi-Bose duality [73, 74, 75, 76, 77]. The many body wavefunction $\psi_B(z_1, z_2, \ldots, z_N)$, where z_i denotes the position of the i^{th} boson, of a system of infinitely strongly interacting N bosons (strongly interacting Bose gas) is given by [78, 79]

$$\psi_B(z_1, z_2, \ldots, z_N) = A(z_1, z_2, \ldots, z_N)\psi_F(z_1, z_2, \ldots, z_N), \tag{2.47}$$

where $\psi_F(z_1, z_2, \ldots, z_N)$ is the wavefunction of a fictitious system of N non interacting spinless fermions and

$$A(z_1, z_2, \ldots, z_N) = \prod_{j>i} \mathrm{sgn}(z_j - z_i). \tag{2.48}$$

The many body wavefunction of the Bose gas is still symmetric under exchange of any two bosons while that of the Fermi gas is antisymmetric under the exchange of any two fermions.

The implications of this mapping for a many-body system is that local observables, like the energy, are the same for bosonic and fermionic systems related by Eq. (2.45). In particular, the amount of energy required to add a boson to a strongly interacting Bose gas, is the same as that required to add a fermion to a non interacting Fermi gas with the same chemical potential. However, nonlocal observables such as the momentum distribution are *not* the same for bosonic and fermionic systems related by Eq. (2.45)[80, 81].

The Fermi-Bose duality has practical implications: Although it may be difficult to treat a strongly interacting system of bosons (fermions), one might be able to treat the corresponding weakly interacting system of fermions (bosons) quite easily using techniques such as perturbation theory, which are not applicable in the case of strong interactions.

2.2 Atoms in a harmonic trap

While Sec. 2.1 considered two particle systems in one dimension without an external trapping potential, this section considers two particle systems in one dimension under

external harmonic confinement. The Schrödinger equation of this system is given by

$$H\Psi(z) = E\Psi(z), \tag{2.49}$$

where

$$H = H^{\text{free}} + \frac{1}{2}\mu\omega_z^2 z^2, \tag{2.50}$$

and H^{free} is given in Eq. (2.2). For a constant $V_{\text{int}}(z)$, the linearly independent solutions to Eq. (2.49) are given in terms of the confluent hypergeometric functions M and U [82]: M is well behaved at the origin and diverges for large z, and U diverges at the origin and decays for large z. As in Sec. 2.1, we consider short range interaction potentials so that $V_{\text{int}}(z)$ can be neglected for $|z| > z_0$. The even parity solution to Eq. (2.49) for $|z| > z_0$ is given by

$$\Psi_+^{(>)}(z) = N_+(k)\exp\left(-\frac{z^2}{2a_z^2}\right) U\left(-\frac{E}{2\hbar\omega_z} + \frac{1}{4}, \frac{1}{2}, \frac{z^2}{a_z^2}\right), \tag{2.51}$$

while the odd parity solution is given by

$$\Psi_-^{(>)}(z) = N_-(k)\exp\left(-\frac{z^2}{2a_z^2}\right) U\left(-\frac{E}{2\hbar\omega_z} + \frac{3}{4}, \frac{3}{2}, \frac{z^2}{a_z^2}\right), \tag{2.52}$$

where $N_\pm(k)$ denote normalization constants.

Now consider two particles interacting through the square well potential $V_{\text{int}}(z)$. The solution to Eq. (2.49) for $|z| < z_0$ has to be well behaved at $z = 0$. This implies

$$\Psi_+^{(<)}(z) = B^+(k)\exp\left(-\frac{z^2}{2a_z^2}\right) M\left(-\frac{E+V_0}{2\hbar\omega_z} + \frac{1}{4}, \frac{1}{2}, \frac{z^2}{a_z^2}\right) \tag{2.53}$$

and

$$\Psi_-^{(<)}(z) = B^-(k)\exp\left(-\frac{z^2}{2a_z^2}\right) M\left(-\frac{E+V_0}{2\hbar\omega_z} + \frac{3}{4}, \frac{3}{2}, \frac{z^2}{a_z^2}\right), \tag{2.54}$$

where $B^{\pm}(k)$ can be determined using the continuity condition given in Eq. (2.5). Enforcing continuity of the wavefunction and its derivative at $|z| = z_0$, we obtain an implicit quantization condition,

$$\frac{\left(\frac{\partial \Psi_{\pm}^{(<)}(z)}{\partial z}\right)_{z=z_0}}{\Psi_{\pm}^{(<)}(z_0)} - \frac{\left(\frac{\partial \Psi_{\pm}^{(>)}(z)}{\partial z}\right)_{z=z_0}}{\Psi_{\pm}^{(>)}(z_0)} = 0. \tag{2.55}$$

Equation (2.55) can be solved straightforwardly for the even and odd parity eigenenergies for a given V_0 and z_0. In particular, we can determine the eigenenergies for square well potentials characterized by the same scattering length but different z_0. Pluses in Figs. 2.3(a) and (b) show the even and odd parity eigenenergies of two trapped particles interacting through the square well potential as a function of the range z_0. The pluses in Fig. 2.3(a) are calculated for an energy independent even parity scattering length of $a_+ = 0.2a_z$ and V_0 is adjusted so that $V_{\rm SW}$ supports two even parity bound states in free space. The pluses in Fig. 2.3(b) are calculated for an energy independent odd parity scattering length of $a^- = -5a_z$ and V_0 is adjusted so that $V_{\rm SW}$ supports one odd parity bound state in free space.

Figure 2.3 shows that the eigenenergies for the square well potential vary nearly linearly with z_0 for $z_0 \lesssim 0.05a_z$. This implies that the $z_0 \to 0$ limit can be extrapolated through a linear fit. Hence, it is always possible to find a small enough z_0, $z_0 \neq 0$, so that the difference between observables calculated for the zero range and finite range potentials, is much smaller than the observable itself. In the rest of this chapter we fix z_0, $z_0 = 0.01a_z$; for this range, the difference between the eigenenergy for the zero range and the finite range potentials is very small ($\approx 0.005\hbar\omega_z$ in Fig. 2.3).

Equations (2.28) and (2.33) define the interaction strengths $g_{1D}^{\pm}$ for the one dimensional even and odd parity pseudopotentials. To compare the eigenspectrum for differ-

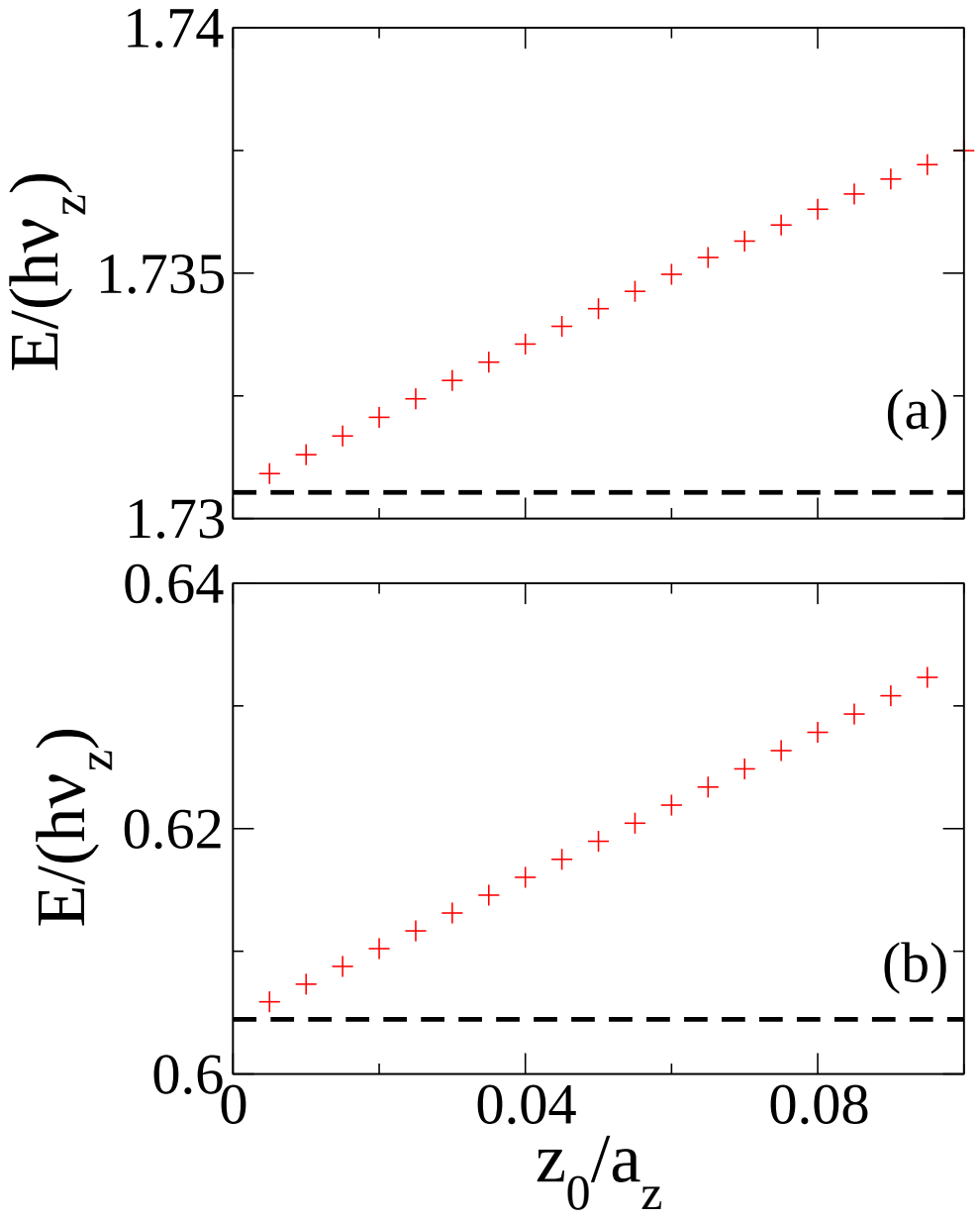

Figure 2.3: Pluses in panels (a) and (b) show the even and odd parity eigenenergies of two particles under harmonic confinement interacting through $V_{\rm SW}$ as a function of the range z_0. The depths V_0 of $V_{\rm SW}$ are chosen so that the even and odd parity energy independent scattering lengths are $a_+ = 0.2a_z$ and $a_- = -5a_z$, respectively, and so that the free-space square well supports two even and one odd parity bound states. The dashed lines indicate the corresponding eigenenergy for two particles under external harmonic confinement interacting through the energy independent zero range pseudopotentials $V_{\rm ps}^{\pm}$ [Eq. (2.60) and Eq. (2.61)].

ent interaction potentials, we define the interaction strengths $g_{1D}^{\pm}$ for finite range potentials through their scattering lengths via Eqs. (2.13) and (2.13). Hence, the eigenenergies obtained from Eq. (2.55) for different V_0 and fixed z_0 can be plotted as a function of the interaction strength $g_{1D}^{\pm}$ (see Figs. 2.5 and 2.6). Later in this section, we discuss these figures in detail.

Next, we consider two atoms under external harmonic confinement interacting through the δ-shell pseudopotentials $V_{\rm ps}^{\pm}$ [Eqs. (2.27) and (2.32)]. In the even parity case, the solution to Eq. (2.49) for $|z|<z_0$ is given by

$$\Psi_{+}^{(<)}(z)=\beta^{+}(k)\exp\left(-\frac{z^2}{2a_z^2}\right)M\left(-\frac{E}{2\hbar\omega_z}+\frac{1}{4},\frac{1}{2},\frac{z^2}{a_z^2}\right). \tag{2.56}$$

Enforcing continuity of the wavefunction at $z=z_0$, we obtain a relationship between $N^{+}(k)$ and $\beta_{+}(k)$,

$$\beta_{+}(k)=N_{+}(k)\left(\frac{U\left(-\frac{E}{2\hbar\omega_z}+\frac{1}{4},\frac{1}{2},\frac{z_0^2}{a_z^2}\right)}{M\left(-\frac{E}{2\hbar\omega_z}+\frac{1}{4},\frac{1}{2},\frac{z_0^2}{a_z^2}\right)}\right). \tag{2.57}$$

As discussed in Sec. 2.1.2, the δ-shell interaction potential implies a discontinuity of the derivative of the wavefunction at $z=z_0$. Integrating Eq. (2.49), with $V_{\rm int}(z)=V_{\rm ps}^{+}(z)$, over z/a_z from $(z/a_z)=(z_0/a_z)-\epsilon$ to $(z/a_z)=(z_0/a_z)+\epsilon$ with $\epsilon\to 0$, yields

$$\lim_{z_0\to 0}\left\{-\frac{1}{2}\left[\left(\frac{\partial\Psi_{+}^{(>)}(z)}{\partial(z/a_z)}\right)_{z\to z_0}-\left(\frac{\partial\Psi_{+}^{(<)}(z)}{\partial(z/a_z)}\right)_{z\to z_0}\right]-\frac{a_z}{2a_{1D}^{+}}\Psi_{+}^{(>)}(z_0)\right\}=0. \tag{2.58}$$

Inserting the expressions for $\Psi_{+}^{(<)}(z)$ and $\Psi_{+}^{(>)}(z)$ from Eqs. (2.56) and (2.51) into Eq. (2.58) and using Eq. (2.57), we obtain

$$\lim_{z_0\to 0}\left\{-\frac{1}{2}\left(\frac{\partial\left(\exp\left(-\frac{z^2}{2a_z^2}\right)U\left(-\frac{E}{2\hbar\omega_z}+\frac{1}{4},\frac{1}{2},\frac{z^2}{a_z^2}\right)\right)}{\partial(z/a_z)}\right)_{z\to z_0}\right\}$$

$$+\lim_{z_0\to 0}\left\{\frac{1}{2}\frac{\partial}{\partial(z/a_z)}\left(\frac{U\left(-\frac{E}{2\hbar\omega_z}+\frac{1}{4},\frac{1}{2},\frac{z_0^2}{a_z^2}\right)}{M\left(-\frac{E}{2\hbar\omega_z}+\frac{1}{4},\frac{1}{2},\frac{z_0^2}{a_z^2}\right)}\exp\left(-\frac{z^2}{2a_z^2}\right)M\left(-\frac{E}{2\hbar\omega_z}+\frac{1}{4},\frac{1}{2},\frac{z^2}{a_z^2}\right)\right)_{z\to z_0}\right\}$$

$$=\lim_{z_0\to 0}\left\{\frac{a_z}{2a_{1D}^+}\exp\left(-\frac{z_0^2}{2a_z^2}\right)U\left(-\frac{E}{2\hbar\omega_z}+\frac{1}{4},\frac{1}{2},\frac{z_0^2}{a_z^2}\right)\right\}. \tag{2.59}$$

Using the power series expansions of the confluent hypergeometric functions M and U (see Ref. [83]) and taking the limit $z_0\to 0$, we get

$$\frac{a_+(k)}{a_z}=\frac{\Gamma\left(-\frac{E}{2\hbar\omega_z}+\frac{1}{4}\right)}{2\Gamma\left(-\frac{E}{2\hbar\omega_z}+\frac{3}{4}\right)}. \tag{2.60}$$

The eigenequation derived here for the δ-shell potential with $z_0\to 0$ agrees with the eigenequation derived in Ref. [60] for the interaction potential given in Eq. (2.27) by means of a basis set expansion approach.

Following the same procedure, the odd parity eigenenergies for two particles interacting through $V_{\rm ps}^-$ are determined by

$$\frac{a_-(k)}{a_z}=\frac{\Gamma\left(-\frac{E}{2\hbar\omega_z}+\frac{1}{4}\right)}{2\Gamma\left(-\frac{E}{2\hbar\omega_z}+\frac{3}{4}\right)}. \tag{2.61}$$

This eigenequation is in agreement with that obtained in Ref. [64] by an alternative approach. Reference [64] expands the eigenfunction $\Psi_-^{(>)}(z)$ in terms of the odd parity eigenfunctions of two non-interacting particles under harmonic confinement. It

then plugs this expansion into the Schrödinger equation [Eq. (2.49) with $V_{\rm int}(z) = V_{\rm ps}^{-}(z)$, where $V_{\rm ps}^{-}(z)$ is given by Eq. (2.35)], performs the required infinite sums analytically and obtains the implicit equation for the eigenenergy given in Eq. (2.61).

Figures 2.4(a) and (b) show the even and odd parity energy dependent scattering lengths as a function of energy over the energy range $-10\hbar\omega_z \leq E \leq 10\hbar\omega_z$ for $a_\pm = 0.2a_z$ and $z_0 = 0.01a_z$ ($V_0 \approx 49872\hbar\omega_z$ in the even parity case and $V_0 \approx 111558\hbar\omega_z$ in the odd parity case). Over the range of energies shown in Figs. 2.4(a) and (b), the even and odd parity energy dependent scattering lengths vary by less than $0.01a_z$. Since this variation is small, over the chosen energy range, the energy dependent scattering lengths and interaction strengths can be replaced by the corresponding energy independent ones.

The dashed lines in Fig. 2.3(a) and (b) show the eigenenergies of two particles interacting through the energy independent zero range even and odd parity pseudopotentials, with $g_{1D}^{\pm} = -5a_z$. In Figs. 2.3(a) and (b), the extrapolation of the eigenenergies estimated for the square well interaction to $z_0 = 0$ closely matches the eigenenergies obtained using the zero range pseudopotentials. The square well potential with $z_0 \to 0$ and V_0 adjusted so that the corresponding $a_\pm$ has some constant value has infact been used as an alternative representation of the zero range pseudopotential [76, 84].

Figures 2.5 and 2.6 show the even and odd parity eigenenergies for two particles in a harmonic trap as a function of the interaction strength $g_{1D}^{\pm}$. Solid curves correspond to the eigenenergies of two particles interacting through $V_{\rm ps}^{\pm}(z)$ with $g_{1D}^{\pm}(E)$. The solid lines in Figs. 2.5 and 2.6 are obtained by solving Eqs. (2.60) and (2.61), respectively. For $g_{1D}^{\pm} = 0$, the system is effectively non-interacting and the eigenenergies correspond to those of two non-interacting particles with even and odd parity (solid lines in Figs. 2.5 and 2.6). Positive and negative $g_{1D}^{\pm}$ correspond to effectively repulsive and effectively attractive systems, respectively. Correspondingly, the energies are shifted up compared to the

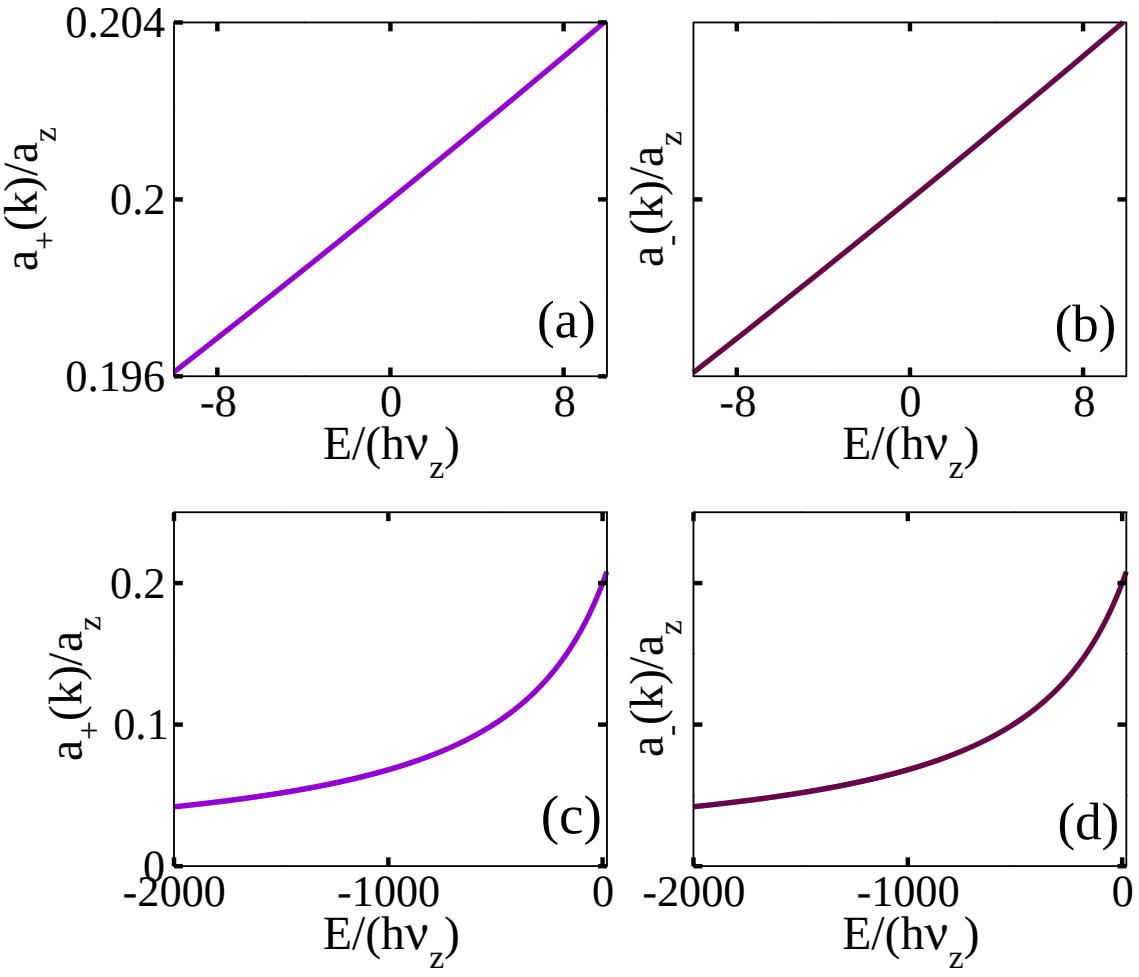

Figure 2.4: Panels (a) and (c) show the even parity energy dependent scattering length $a_+(k)$ over the energy ranges $-10\hbar\omega_z \leq E \leq 10\hbar\omega_z$ and $-2000\hbar\omega_z \leq E \leq 10\hbar\omega_z$, respectively, for $V_0 = 49872.91172171189\hbar\omega_z$. Panels (b) and (d) show the odd parity energy dependent scattering length $a_-(k)$ over the energy ranges $-10\hbar\omega_z \leq E \leq 10\hbar\omega_z$ and $-2000\hbar\omega_z \leq E \leq 10\hbar\omega_z$, respectively, for $V_0 = 111558.73382438572\hbar\omega_z$. Panels (a) and (b) have the same y-scale and so do panels (c) and (d). The range z_0 is fixed at $0.01a_{\text{ho}}$ in all panels

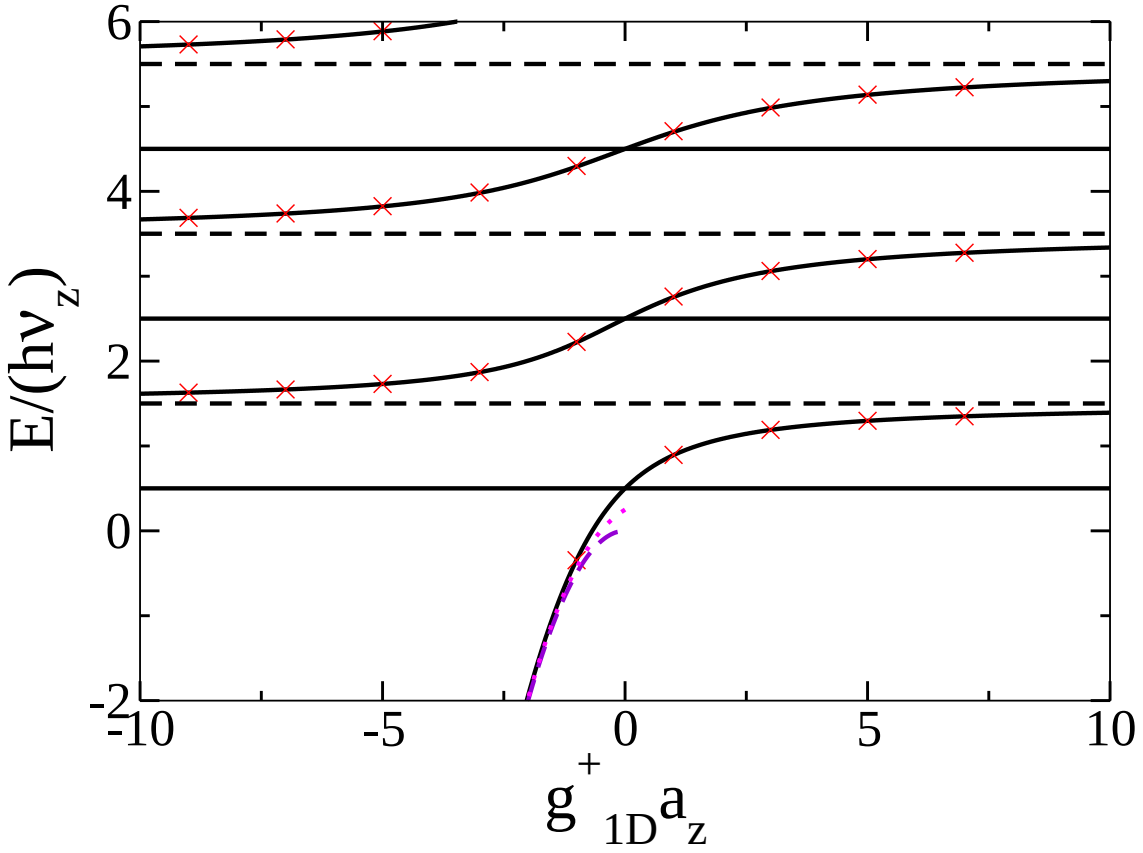

Figure 2.5: Even parity eigenenergies E for two one dimensional particles under harmonic confinement as a function of the interaction strength g^{+}_{1D}. Solid lines correspond to the eigenenergies for particles interacting through the energy independent zero range interaction potential $V^{+}_{\rm ps}(z)$ [Eq.(2.60)], while crosses correspond to the eigenenergies for particles interacting through the square well interaction potential $V_{\rm SW}(z)$. Horizontal solid lines correspond to the even parity eigenenergies of two non-interacting particles in a harmonic trap and horizontal dashed lines correspond to the odd parity eigenenergies of two non-interacting particles in a harmonic trap. The dashed curve for negative g^{+}_{1D} shows the free-space binding energy of two particles interacting through $V^{+}_{\rm ps}(z)$ [see Eqs. (2.42) and (2.62)]. The dotted curve includes the next order correction [see Eq. (3.17)].

non-interacting values for $g_{1D}^{\pm} > 0$ and shifted down compared to the non-interacting values for $g_{1D}^{\pm} < 0$. For $|g_{1D}^{\pm} a_z| \ll 1$, the energy shifts away from the non-interacting values can be calculated using first order perturbation theory. For $|g_{1D}^{\pm} a_z| \to \infty$, the shift is $\hbar\omega_z$. As already pointed out in Sec. 2.1.3, the even parity eigenenergies for $g_{1D}^{+} \to \infty$ coincide with the odd parity eigenenergies of the non-interacting system and the odd parity eigenenergies for $g_{1D}^{-} \to \infty$ coincide with the even parity eigenenergies of the non-interacting system.

The dashed curves in Figs. 2.5 and 2.6 indicate the binding energy in the absence of an external trapping potential [Eq. (2.42) with $a_{\pm}(k) = a_{\pm}$]. These free-space energies lie below the eigenenergies of the trapped system since the trap pushes the energies up. For comparison, Figs. 2.5 and 2.6 also show the eigenenergies for two particles interacting through a square well potential with $z_0 = 0.01 a_z$ that supports two bound states. To obtain the eigenenergies, we adjust V_0 to obtain the desired $a_{\pm}$ (or equivalently $g_{1D}^{\pm}$). The excellent agreement between the eigenenergies for the square well and pseudopotentials indicates that the zero range model, though simple, reproduces the eigenenergies well. This agreement is encouraging.

The dashed curves in Figs. 2.5 and 2.6 can also be obtained from Eqs. (2.60) and (2.61), respectively, by considering a very weak trap, i. e., by considering the limit $|E/(\hbar\omega_z)| \to \infty$. A first order expansion of the right hand sides of Eqs. (2.60) and (2.61) for large $|E/(\hbar\omega_z)|$ gives

$$\frac{E}{\hbar\omega_z} = -\frac{a_z^2}{2(a_{\pm}(k))^2}. \tag{2.62}$$

Equation (2.62) is identical to Eq.(2.42) obtained for the free system. This can be explained by the fact that the wavefunction of the state with large negative energy extends out to about z_0 and is thus approximately zero when the trapping potential becomes appreciable. The dotted curves in Figs. 2.5 and 2.6 are obtained by considering the next

order term in the expansion of the right hand sides of Eqs. (2.60) and (2.61) for large negative energies, i. e., by solving the approximate eigenequations

$$g_{1D}^{+} a_z = -2\sqrt{-\frac{E}{2\hbar\omega_z}+\frac{1}{4}} + \frac{1}{4\sqrt{-\frac{E}{2\hbar\omega_z}+\frac{1}{4}}} \tag{2.63}$$

and

$$\frac{g_{1D}^{-}}{a_z} = \frac{1}{2\sqrt{-\frac{E}{2\hbar\omega_z}+\frac{1}{4}}\left(1-\frac{1}{8\left(-\frac{E}{2\hbar\omega_z}+\frac{1}{4}\right)}\right)}, \tag{2.64}$$

respectively.

Figures 2.7(a) and (b) show the even and odd parity negative eigenenergies for two particles in a harmonic trap as a function of the interaction strengths $g_{1D}^{\pm}$. The solid line corresponds to $V_{\rm int} = V_{\rm SW}$. The dashed line corresponds to $V_{\rm ps}^{\pm}$ with $g_{1D}^{\pm}(E) = g_{1D}^{\pm}$. For small energies [$|E| \lesssim 10\hbar\omega_z$; see also Figs. 2.4(a) and (b)], the agreement between the eigenenergies calculated using the energy independent zero range pseudopotential and those calculated using the square well interaction potential is quite good. This can also be seen from Figs. 2.5 and 2.6. However, for large negative energies, Figs. 2.7(a) and (b) show significant deviations between the two sets of eigenenergies (dashed and solid lines). This is expected because there exists a significant difference between the energy dependent and energy independent scattering lengths for large negative energies [see Figs. 2.4(c) and (d)]. The pluses in Fig. 2.7(a) and (b) show the eigenenergies for two particles interacting through the energy dependent zero range even and odd parity pseudopotentials, respectively. The agreement between the eigenenergies calculated using the energy dependent zero range pseudopotential and those calculated using the square well interaction potential is very good over the entire range of energies considered.

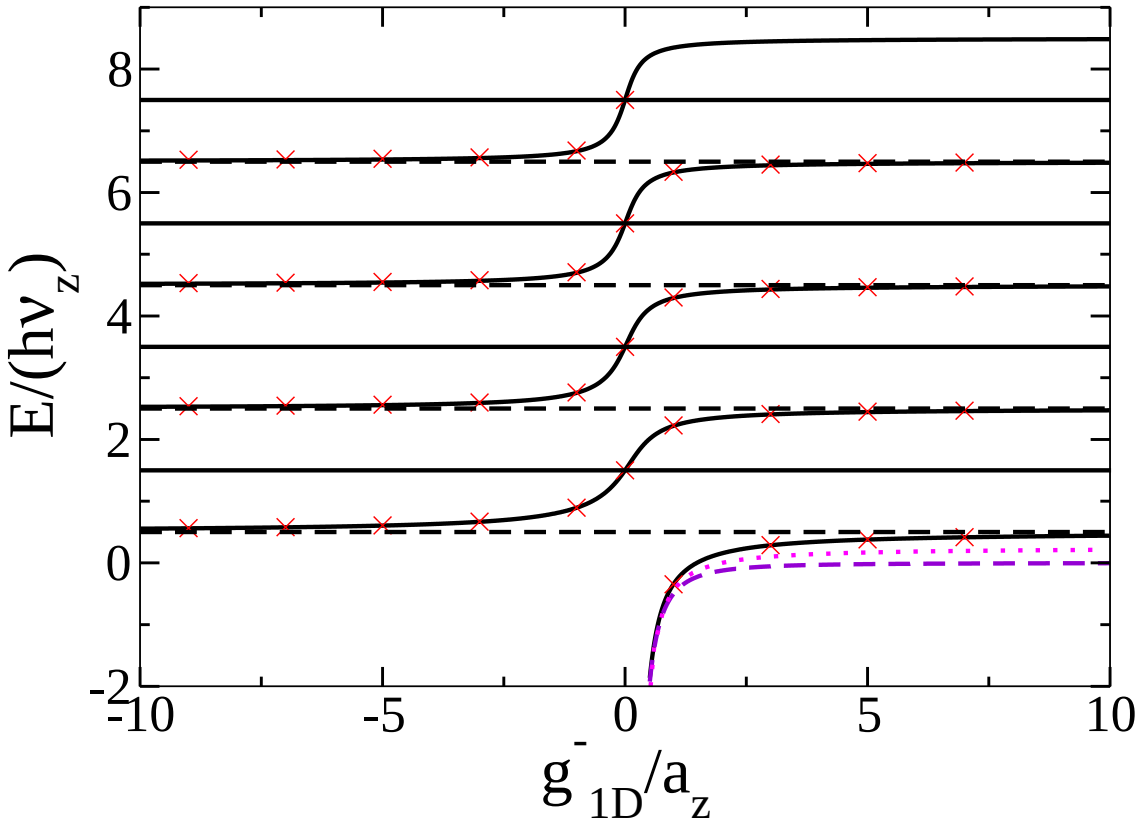

Figure 2.6: Odd parity eigenenergies E for two particles under harmonic confinement as a function of the interaction strength g^{-}_{1D}. Solid lines correspond to the eigenenergies for particles interacting through the energy independent zero range interaction potential $V^{-}_{\rm ps}(z)$ [Eq.(2.61)], while crosses correspond to the eigenenergies for particles interacting through the square well interaction potential $V_{\rm SW}(z)$. Horizontal solid lines correspond to the odd parity eigenenergies of two non-interacting particles in a harmonic trap and horizontal dashed lines correspond to the even parity eigenenergies of two non-interacting identical particles in a harmonic trap. The dashed curve for positive g^{-}_{1D} shows the free-space binding energy of two particles interacting through $V^{-}_{\rm ps}(z)$ [see Eqs. (2.42) and (2.62)]. The dotted curve includes the next order correction [see Eq. (2.64)].

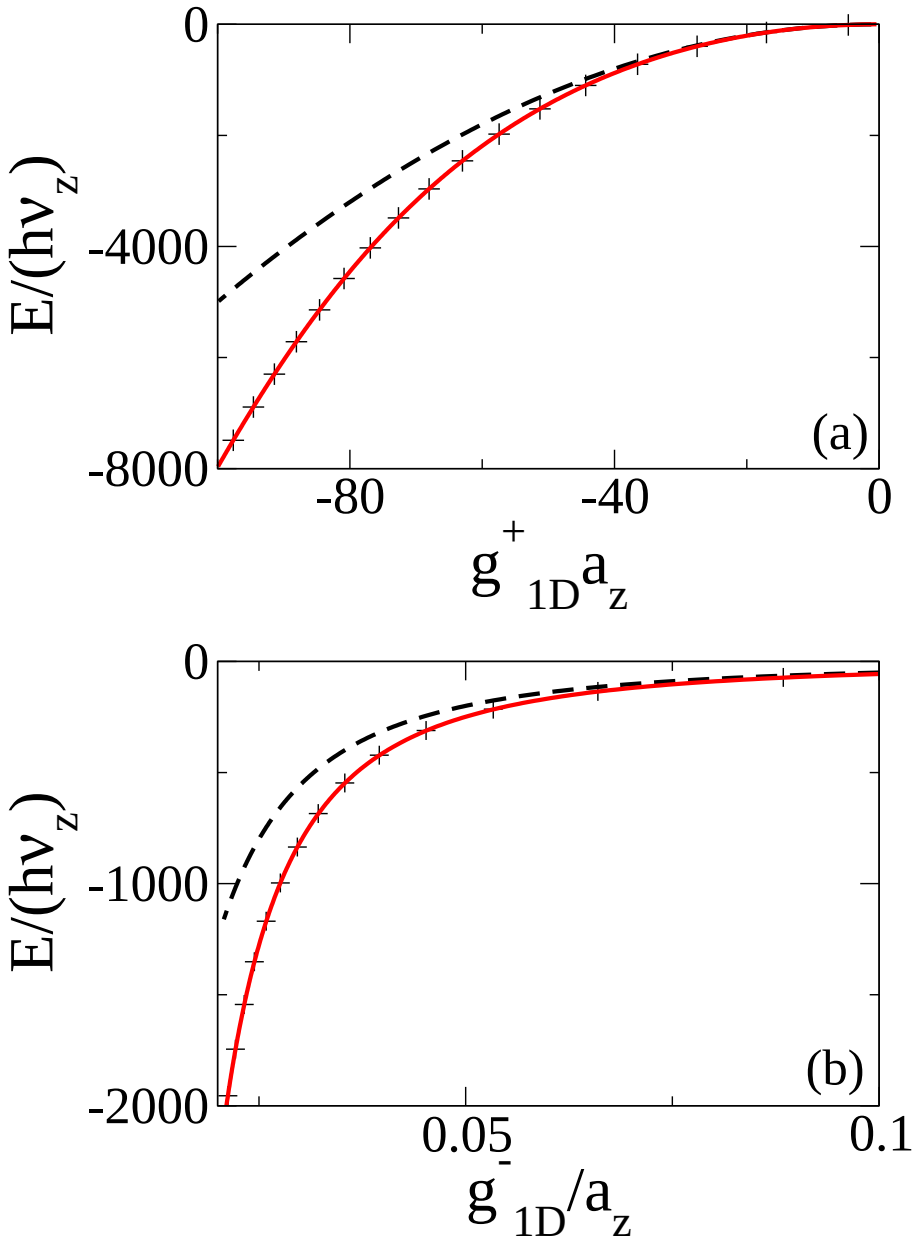

Figure 2.7: Panels (a) and (b) show the negative even and odd parity eigenenergies of two particles in a harmonic trap as a function of the interaction strengths g^{+}_{1D} and g^{-}_{1D}, respectively. The solid line corresponds to $V_{\rm int} = V_{\rm SW}$ with $z_0 = 0.01 a_z$ and V_0 chosen so that $V_{\rm SW}$ supports one bound state. The dashed line in panel (a) [panel (b)] shows the eigenenergies for two particles interacting through the energy independent zero range even [odd] parity pseudopotential, while the pluses in panel (a) [panel(b)] show the eigenenergies for two particles interacting through the energy dependent zero range even [odd] parity pseudopotential.

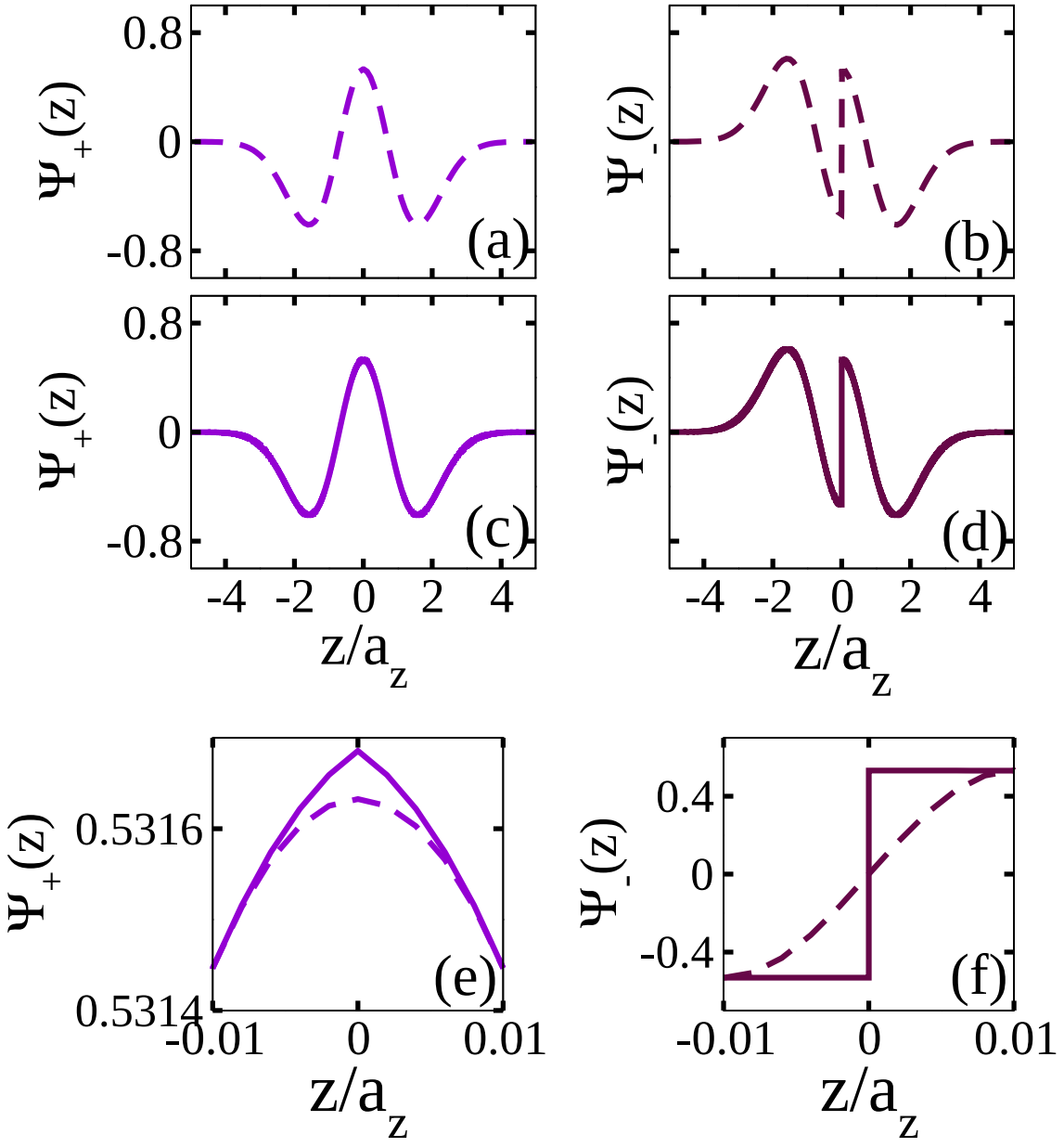

Figure 2.8: Panels (a) and (c) show the normalized even parity wavefunctions $\Psi_+(z)$ of the first excited state as a function of z for two particles in a harmonic trap interacting through $V_{\rm SW}(z)$ and $V_{\rm ps}^+(z)$, respectively, with interaction strength $g_{1D}^+ = -0.0199972/a_z$ ($V_0 = 1\hbar\omega_z$). Panels (b) and (d) show the normalized odd parity wavefunction $\Psi_-(z)$ of the first excited state as a function of z for two particles in a harmonic trap interacting through $V_{\rm SW}$ and $V_{\rm ps}^+(z)$, respectively, with interaction strength $g_{1D}^- = -1/(g_{1D}^+) = (1/0.0199972)a_z$. Panel (e) shows a blow up of panels (a) and (c) around $z = 0$, while panel (f) shows a blow up of panels (b) and (d) around $z = 0$. Panels (a) and (b) have the same y-scale and so do panels (c) and (d). Panels (a) and (c) have the same x-scale and label and so do panels (b) and (d).

So far, we have examined the Fermi-Bose duality in terms of the boundary conditions implied by the zero range pseudopotentials and the eigenequations for the trapped two-particle system. Next, we examine the eigenfunctions $\Psi_{\pm}^{(>)}(z)$ for two trapped particles interacting through the square well and pseudopotentials. For $|z| > z_0$, the wavefunction $\Psi_{+}^{(>)}(z)$ for two identical bosons in a harmonic trap with interaction strength g_{1D}^{+} can be mapped to the wavefunction $\Psi_{-}^{(>)}(z)$ for two identical fermions with interaction strength g_{1D}^{-}, if the interaction strengths are related through Eq. (2.45),

$$\Psi_{+}^{(>)}(z) = \mathrm{sgn}(z)\Psi_{-}^{(>)}(z). \tag{2.65}$$

The first four panels in Fig. 2.8 illustrate this mapping. A weak attractive even parity interaction strength is chosen, $g_{1D}^{+} = -0.0199972/a_z$. The wavefunction of this system maps onto that for two identical fermions with a strongly repulsive odd parity interaction strength given by $g_{1D}^{-} = (1/0.0199972)a_z = 50.075a_z$. The last two panels in Fig. 2.8 point out that, while for finite range interaction potentials the wavefunctions and their derivatives are continuous, in the case of zero range pseudopotentials either the wavefunction or its derivative is discontinuous at $z = 0$.

Figure 2.8(a) shows the even parity wavefunction $\Psi_{+}(z)$ for two identical bosons interacting through $V_{\mathrm{SW}}(z)$ with $g_{1D}^{+} = -0.0199972/a_z$ in a harmonic trap. Since the wavefunction has even parity, the wavefunction for positive and negative z values is the same. Also since the interaction strength $|g_{1D}^{+}|$ is small, the wavefunction is similar to the wavefunction of the first excited state of two non-interacting bosons in a harmonic trap.

For comparison, Fig. 2.8(b) shows the odd parity wavefunction $\Psi_{-}(z)$ for two identical fermions interacting through $V_{\mathrm{SW}}(z)$ in a harmonic trap with $g_{1D}^{-} = (1/0.0199972)a_z = 50.075a_z$. The chosen value of $|g_{1D}^{-}|$ is large indicating strong interactions. This is visi-

ble from the wavefunction in Fig. 2.8(b), which is very different from the wavefunction of non-interacting fermions. From Figs. 2.8(a) and (b), it can be seen that the mapping rule in Eq. (2.65) is followed for $|z| > z_0$ (here, $z_0 = 0.01 a_z$).

Figures 2.8(c) and (d) show the wavefunctions for the zero range pseudopotentials $V_{\rm ps}^{+}$ and $V_{\rm ps}^{-}$ with the same $g_{1D}^{\pm}$ as in Figs. 2.8(a) and (b). It can be seen that the mapping rule [Eq. (2.65)] is followed for all $z \neq 0$. Also note that, by construction, the wavefunctions in Figs. 2.8(a) and (c), as well as in Figs. 2.8(b) and (d) are identical for $|z| > 0.01 a_z$.

Figure 2.8(e) compares the wavefunctions shown in Figs. 2.8(a) and (c) near $z = 0$. While the wavefunction obtained for the square well potential and its derivative are continuous at $z = 0$, the derivative of the wavefunction obtained for the zero range pseudopotential is discontinuous at $z = 0$. The wavefunction itself, however, is continuous. Similarly, Fig. 2.8(f) compares the wavefunctions shown in Figs. 2.8(b) and (d). While the wavefunction obtained for the square well potential and its derivative are continuous at $z = 0$, the wavefunction obtained for the zero range pseudopotential is discontinuous at $z = 0$. The derivative of the wavefunction, however, is continuous. This has been discussed already in Sec. 2.1.2.

2.3 Quasi one dimensional systems

Although the real world is three dimensional, this chapter has so far considered strictly one dimensional systems. As discussed in Ch. 1, advancements in trapping technology have led to the realization of quasi one dimensional systems [53], where excitations along ρ are frozen out. We now relate the one dimensional scattering strengths to the three dimensional scattering quantities.

Just like in the one dimensional case, a zero range pseudopotential can be used to model atom atom interactions in three dimensions. The three dimensional energy

independent s-wave zero range pseudopotential $V_{\rm ps}^{l=0}(\vec{r})$ is given in Sec. 3.1.2. For a system of two bosons or nonidentical particles in a quasi one dimensional harmonic trap we would naively assume that the motion in the ρ direction is frozen in the lowest oscillator mode $\psi_0^{2D}(\rho)$,

$$\psi_0^{2D}(\rho) = \frac{1}{a_\perp\sqrt{\pi}} e^{-\frac{\rho^2}{2a_\perp^2}}. \tag{2.66}$$

Integrating over ρ and ϕ, we obtain the following one dimensional even parity pseudopotential $V^+(z)$,

$$V_+(z) = \int \psi_0^{2D}(\rho) V_{\rm ps}^{l=0}(\vec{r}) \psi_0^{2D}(\rho) \rho\, d\rho\, d\phi = \frac{2\hbar^2 a_s(k)}{\mu a_\perp^2}\delta(z). \tag{2.67}$$

Comparing this with the energy independent even parity one dimensional pseudopotential in Eq. (2.27), we obtain a relationship between the one dimensional and the three dimensional energy independent scattering lengths,

$$a^+ = -\frac{a_\perp^2}{2a_s}. \tag{2.68}$$

The naive derivation outlined here holds approximately for weak interactions. For stronger interactions, however, coupling between the motion in z- and ρ- directions have to be accounted for. A full treatment of the problem results in [80]

$$a_+ = -\frac{a_\perp^2}{2a_s}\left(1 - \zeta(1/2)\frac{a_s}{a_\perp}\right), \tag{2.69}$$

where $\zeta(.)$ denotes the Riemann zeta function and $\zeta(1/2) \approx 1.4603$. The term in the round brackets on the right hand side of Eq. (2.69) can be interpreted as a renormalization due to virtual excitations or the strong transverse confinement.

Figure 2.9(a) shows the interaction strength g_{1D}^+ in a quasi one dimensional system

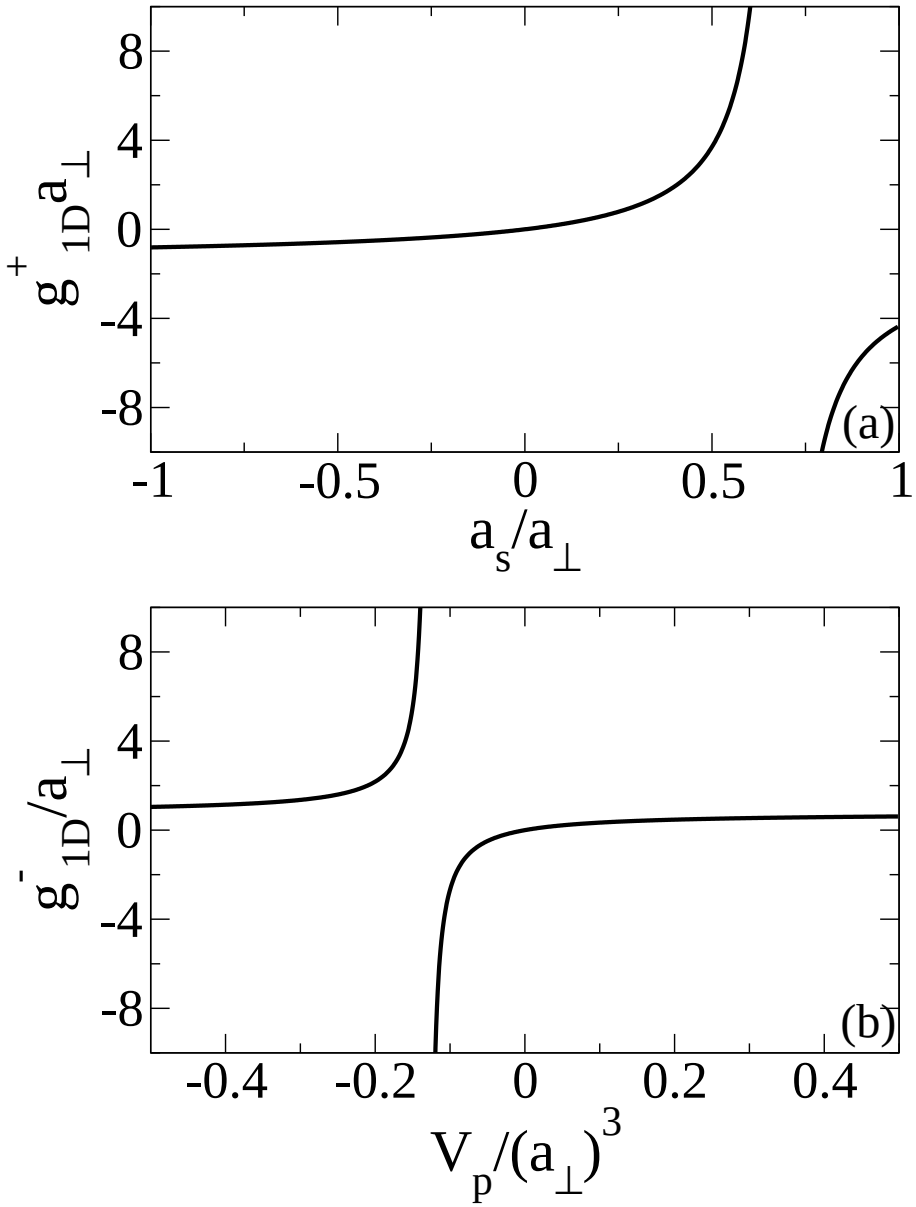

Figure 2.9: (a) One dimensional even parity interaction strength g^{+}_{1D} in a quasi one dimensional system as a function of the three dimensional scattering length a_s [see Eq. (2.69)]. (b) One dimensional odd parity interaction strength g^{-}_{1D} in a quasi one dimensional system as a function of the three dimensional scattering volume V_p [see Eq. (2.69)]

as a function of the three dimensional scattering length a_s obtained from Eq. (2.69). g_{1D}^{+} diverges for a finite value of a_s indicating that the quasi one dimensional system can have infinitely strong interactions even though the corresponding three dimensional system has a finite interaction strength. Such a resonance is called a confinement induced resonance.

The relationship between the energy independent odd parity one dimensional scattering length a_- and the three dimensional p-wave scattering volume V_p has been obtained in Ref. [75],

$$a_- = \frac{6V_p}{a_\perp^2}\left[1 - 12\frac{V_p}{a_\perp^3}\zeta_H\left(-\frac{1}{2},\frac{3}{2}\right)\right]^{-1}, \tag{2.70}$$

where $\zeta_H(.,.)$ denotes the Hurwitz zeta function. Figure 2.9(b) shows the interaction strength g_{1D}^{-} in a quasi one dimensional system as a function of the three dimensional scattering volume V_p obtained from Eq. (2.70). This system exhibits a confinement induced resonance for negative V_p.

2.4 Conclusions

Short range interaction potentials can be modeled by zero range pseudopotentials in one dimension. While the eigenequations for particles interacting through the even parity zero range pseudopotential under harmonic confinement in one dimension have been obtained in Ref. [60], we [64] were the first to do this for the odd parity case. Although most of the energy spectrum can be accurately reproduced using the energy independent interaction strengths, for regimes where $|E|$ is comparable to $\frac{\hbar^2}{\mu z_0^2}$ it is extremely important to include the energy dependence. Boundary conditions and wavefunctions for two identical particles interacting through zero range pseudopotentials in a harmonic trap can be used to demonstrate Fermi-Bose duality.

Chapter 3

Spherically symmetric two body systems in three dimensions

In this chapter all Hamiltonian, potentials, wavefunctions and phase shifts are three dimensional. Section 3.1 introduces spherically symmetric three dimensional model interaction potentials and Sec. 3.1.1 obtains the three dimensional single channel scattering length for any partial wave. Section 3.1.2 considers two interacting particles under spherically symmetric three dimensional harmonic confinement and obtains the eigenenergies of two particles interacting through a single channel s-wave model potential, while Sec. 3.1.3 does the equivalent for p-wave interactions. Section 3.2 introduces spherically symmetric three dimensional model interaction potentials with two coupled channels, having two distinct thresholds. Section 3.2.1 outlines the procedure to obtain the coupled channel scattering length for any partial wave. Using this procedure, Sec. 3.2.2 obtains the expression for the coupled channel s-wave scattering length for two coupled square well potentials. Section 3.2.2 applies the results of Sec. 3.2.1 to the ^{85}Rb s-wave Feshbach resonance at $155.2G$ [45, 46]. Section 3.2.3 considers coupled two channel zero range model interaction potentials.

3.1 Single channel treatment

In this section all Hamiltonian, potentials and wavefunctions are for single channel model interaction potentials.

3.1.1 Single channel scattering

The relative Schrödinger equation for two particles in three dimensions in free space is given by

$$H^{\text{free}}\Psi^{\text{free}}(\vec{r}) = E\Psi^{\text{free}}(\vec{r}), \tag{3.1}$$

where

$$H^{\text{free}} = -\frac{\hbar^2}{2\mu}\nabla^2_{\vec{r}} + V_{\text{int}}(r). \tag{3.2}$$

Here, E denotes the relative scattering energy of the two particles in three dimensions. We assume that the interaction potential $V_{\text{int}}(r)$ is spherically symmetric and short range, i. e., that it falls off faster than $1/r^3$. In general, an interaction potential in d dimensional space that depends on the relative distance r is short range if it falls off faster than $1/r^d$. There exists a distance r_0 such that $V_{\text{int}}(r)$ can be neglected for $r > r_0$, i. e., $V_{\text{int}}(r) = 0$ for $r > r_0$. A discussion on scattering by short range spherically symmetric interaction potentials can be found in Ref [85]. The wavefunction $\Psi^{\text{free}}(\vec{r})$ can be expressed as a product of a radial wavefunction, denoted by $R_l(r)$, and the angular part given by the spherical harmonics $Y_{l,m}(\theta,\phi)$,

$$\Psi^{\text{free}}(\vec{r}) = \sum_{l'=0}^{\infty}\sum_{m'=-l'}^{l'} R^{\text{free}}_{l'}(r)Y_{l',m'}(\theta,\phi), \tag{3.3}$$

where θ and ϕ denote the polar and the azimuthal angle, respectively. Putting Eq. (3.3) into Eq. (3.1), multiplying by $Y^*_{l,m}(\theta,\phi)$ and performing the angular integrations, we

obtain the radial Schrödinger equation

$$\left[-\frac{\hbar^2}{2\mu}\left(\frac{\partial^2}{\partial r^2}+\frac{2}{r}\frac{\partial}{\partial r}-\frac{l(l+1)}{r^2}\right)+V_{\rm int}(r)\right]R_l^{\rm free}(r)=ER_l^{\rm free}(r). \tag{3.4}$$

For $r > r_0$ (or $V_{\rm int}=0$), the two linearly independent solutions to the second order differential equation [Eq. (3.4)] are given by the regular spherical Bessel function $j_l(kr)$, which is well behaved at $r=0$, and the irregular spherical Neumann function $n_l(kr)$, which diverges at $r=0$. The outer radial solution can be written as

$$R_l^{\rm free(>)}(r)=\aleph_l(k)\left[j_l(kr)-\tan\delta_l(k)n_l(kr)\right], \tag{3.5}$$

where $\aleph_l(k)$ denotes the normalization constant and $\delta_l(k)$ the energy dependent phase-shift accumulated in the region $r < r_0$. Since the potential is neglected for $r > r_0$, no further phase is accumulated beyond $r=r_0$. The phase shifts $\delta_l(k)$ can be determined by imposing the following two continuity conditions at $r=r_0$,

$$R_l^{\rm free(<)}(r_0)=R_l^{\rm free(>)}(r_0) \tag{3.6}$$

and

$$\left(\frac{\partial R_l^{\rm free(<)}(r)}{\partial r}\right)_{r=r_0}=\left(\frac{\partial R_l^{\rm free(>)}(r)}{\partial r}\right)_{r=r_0}. \tag{3.7}$$

The inner solutions $R_l^{\rm free(<)}(r)$ depend upon $V_{\rm int}$. The phase shifts define the energy dependent generalized scattering lengths $a_l(k)$,

$$a_l(k)=-\frac{\tan\delta_l(k)}{k^{2l+1}}. \tag{3.8}$$

The energy independent generalized scattering lengths a_l are defined through

$$a_l = \lim_{k\to 0} a_l(k). \tag{3.9}$$

The generalized scattering lengths a_l have units of (length)$^{2l+1}$.

For ultracold atomic gases, the scattering processes are dominated by the lowest partial wave allowed by symmetry unless there is a resonance in a higher partial wave channel. This implies that the scattering between two identical bosons or two non-identical particles is s-wave dominated, and that the scattering between two identical fermions is p-wave dominated.

3.1.2 s- wave interacting atoms under harmonic confinement

We now consider two interacting particles under spherically symmetric harmonic confinement. The three dimensional harmonic oscillator Hamiltonian $H^{\rm osc}$ is given by

$$H^{\rm osc} = -\frac{\hbar^2}{2\mu}\nabla^2_{\vec{r}} + \frac{1}{2}\mu\omega^2_{\rm ho}\vec{r}^2, \tag{3.10}$$

where $\omega_{\rm ho}$ denotes the angular trapping frequency. The corresponding Schrödinger equation for the relative coordinate reads

$$H\Psi(\vec{r}) = E\Psi(\vec{r}), \tag{3.11}$$

where

$$H = H^{\rm osc} + V_{\rm int}(\vec{r}). \tag{3.12}$$

This section briefly reviews Fermi Huang's regularized s-wave pseudopotential, while Sec. 3.1.3 solves Eq. (3.11) for a regularized p-wave zero-range potential analytically. To illustrate the applicability of this p-wave pseudopotential, Section 3.1.3 also compares the resulting relative eigenenergies E for two particles under harmonic confinement with those obtained numerically for a shape-dependent short range model potential and discusses the importance of including the energy dependence of the p-wave scattering volume in the zero range model potential.

Using Fermi-Huang's regularized s-wave ($l=0$) pseudopotential $V_{\rm ps}^{l=0}(\vec{r})$ [58, 59],

$$V_{\rm ps}^{l=0}(\vec{r}) = \frac{2\pi\hbar^2}{\mu} a_s(k)\delta(\vec{r})\frac{\partial}{\partial r}r, \tag{3.13}$$

where $\delta(\vec{r})$ denotes the radial component of the three dimensional δ-function,

$$\delta(\vec{r}) = \frac{1}{4\pi r^2}\delta(r), \tag{3.14}$$

and $a_s(k)$ the three dimensional energy dependent s-wave scattering length [$a_s(k) = a_0(k)$], Busch *et al.* [60] derive a transcendental equation for the relative three dimensional eigenenergies E for the Schrödinger equation given in Eq. (3.11),

$$\frac{a_s(k)}{a_{\rm ho}} = \frac{\Gamma(-\frac{E}{2\hbar\omega_{\rm ho}}+\frac{1}{4})}{2\Gamma(-\frac{E}{2\hbar\omega_{\rm ho}}+\frac{3}{4})}. \tag{3.15}$$

Here, $a_{\rm ho}$ denotes the oscillator length, $a_{\rm ho} = \sqrt{\hbar/(\mu\omega_{\rm ho})}$. Solid lines in Fig. 3.1(a) show the s-wave energies E [the solution to Eq. (3.15) using a_s instead of $a_s(k)$] as a function of a_s. For large and negative E (and hence positive a_s), an expansion of Eq. (3.15) to

lowest order results in

$$E = -\frac{\hbar^2}{2\mu(a_s(k))^2}, \tag{3.16}$$

which corresponds to the binding energy of $V_{\rm ps}^{l=0}(\vec{r})$ without the confining potential. A dashed line in Fig. 3.1(a) shows the energy given by Eq. (3.16) [with $a_s(k)$ replaced by a_s], while a dash-dotted line shows the expansion of Eq. (3.15) including the next higher order term, i. e., the solution to the equation

$$\frac{a_{\rm ho}}{a_s} = -2\sqrt{-\frac{E}{2\hbar\omega_{\rm ho}}+\frac{3}{4}} + \frac{1}{4\sqrt{-\frac{E}{2\hbar\omega_{\rm ho}}+\frac{3}{4}}}. \tag{3.17}$$

Since only s-wave wavefunctions have a non-vanishing amplitude at $r = 0$, Fermi-Huang's regularized pseudopotential leads exclusively to s-wave scattering (no other partial waves are scattered). Equation (3.15) hence applies to two ultracold bosons or two non identical particles under external confinement for which higher even partial waves, such as d- or g-waves, are negligible [for d- or g-wave scattering, see Eq. (3.50)].

The irregular $l = 0$ solution $n_0(kr)$ diverges as r^{-1}. The so-called regularization operator $\frac{\partial}{\partial r}r$ of the pseudopotential $V_{\rm ps}^{l=0}(\vec{r})$, Eq. (3.13), cures this divergence. The solutions $\Psi(\vec{r})$ of two particles interacting through $V_{\rm ps}^{l=0}(\vec{r})$ under external confinement or in free space obey the boundary condition

$$\left[\frac{\frac{\partial}{\partial r}(r\Psi(\vec{r}))}{r\Psi(\vec{r})}\right]_{r\to 0} = -\frac{1}{a_s(k)}; \tag{3.18}$$

this boundary condition is an alternative representation of $V_{\rm ps}^{l=0}(\vec{r})$.

3.1.3 p-wave interacting atoms under harmonic confinement

The importance of angle-dependent p-wave interactions has been demonstrated experimentally for two potassium atoms in the vicinity of a magnetic field-dependent p-wave Feshbach resonance [49]. Here, we use an isotropic p-wave pseudopotential to model the in general anisotropic atom-atom interaction. As discussed in Sec. 1.3.1, the anisotropy arises due to the magnetic dipole dipole interactions between the electrons of the two atoms. This leads to a splitting of the Feshbach resonance and two separate Feshbach resonances, corresponding to $m_l = 0$ and $m_l = \pm 1$. For ^{40}K, e. g., the splitting is about $0.5G$. Since these Feshbach resonances are well resolved, they, in a first attempt, can be treated separately. The scattering volume, which enters into the pseudopotential (see below), can be calculated for each partial wave channel.

We use the following p-wave pseudopotential $V_{\rm ps}^{l=1}(\vec{r})$,

$$V_{\rm ps}^{l=1}(\vec{r}) = g_1(E)\overleftarrow{\nabla}_{\vec{r}}\delta^{(3)}(\vec{r})\overrightarrow{\nabla}_{\vec{r}}\frac{1}{2}\frac{\partial^2}{\partial r^2}r^2, \tag{3.19}$$

where the coupling strength $g_1(E)$ "summarizes" the scattering properties of the original shape-dependent atom-atom interaction potential [86, 87],

$$g_1(E) = \frac{6\pi\hbar^2}{\mu}V_p(k) \tag{3.20}$$

[$V_p(k) = a_1(k)$, see Eqs. (3.8) and (3.9)]. The pseudopotential written in this way can be conveniently used only for spherically symmetric external harmonic confinement and the treatment that follows applies only to spherically symmetric harmonic traps. The case of cylindrically symmetric external harmonic confinement is treated in Ch. 5. The gradient $\overleftarrow{\nabla}_{\vec{r}}$ with respect to the relative vector $\vec{r}$ acts to the left, while the gradient $\overrightarrow{\nabla}_{\vec{r}}$

acts to the right,

$$\int \phi^*(\vec{r}) V_{\rm ps}^{l=1}(\vec{r}) \chi(\vec{r}) d^3\vec{r} = g_1(E) \int \left[\vec{\nabla}_{\vec{r}} \phi^*(\vec{r})\right] \delta^{(3)}(\vec{r}) \left[\vec{\nabla}_{\vec{r}} \left\{ \frac{1}{2} \frac{\partial^2}{\partial r^2} \left(r^2 \chi(\vec{r}) \right) \right\}\right] d^3\vec{r}. \quad (3.21)$$

Just as the s-wave pseudopotential $V_{\rm ps}^{l=0}(\vec{r})$ does not couple to partial waves with $l \neq 0$, the p-wave pseudopotential $V_{\rm ps}^{l=1}(\vec{r})$ does not couple to partial waves with $l \neq 1$ [88]. Pseudopotentials of the form $g_1(E) \overleftarrow{\nabla}_{\vec{r}} \delta^{(3)}(\vec{r}) \overrightarrow{\nabla}_{\vec{r}}$ have been used by a number of researchers before [86, 88, 87, 89]; discrepancies regarding the proper value of the coefficient $g_1(E)$, however, exist (see, e.g., Ref. [88]). In the Born approximation, we get

$$\int_0^\infty j_1(kr) V_{\rm ps}^{l=1}(\vec{r}) j_1(kr) r^2 dr = \tan\delta_1(k), \quad (3.22)$$

indicating that our pseudopotential has the correct strength. Equation (3.19) introduces the regularization operator $\frac{1}{2}\frac{\partial^2}{\partial r^2} r^2$, which eliminates divergences that would arise otherwise from the irregular p-wave solution (which diverges as r^{-2}). A similar regularization operator has been proposed by Huang and Yang in 1957 [59]; they, however, use it in conjunction with a coupling parameter g_1 different from that given by Eq. (3.20). By comparing with numerical results for a shape-dependent model potential, we show that the pseudopotential $V_{\rm ps}^{l=1}(\vec{r})$ describes the scattering behaviors of two spin-aligned three dimensional fermions properly.

To determine the relative eigenenergies E of two spin-polarized three dimensional fermions under harmonic confinement analytically, we expand the three dimensional wave function $\Psi(\vec{r})$ for fixed angular momentum, $l = 1$, in *continuous* harmonic oscillator eigenfunctions $\phi_{nlm}(\vec{r})$,

$$\Psi(\vec{r}) = \sum_{nm} c_{nm} \Phi_{nlm}(\vec{r}), \quad (3.23)$$

where the c_{nm} denote expansion coefficients.

The $\Phi_{nlm}(\vec{r})$ depend on the principal quantum number n, the angular momentum quantum number l, and the projection quantum number m,

$$H_{3D}^{\rm osc}\Phi_{nlm}(\vec{r}) = E_{nl}^{\rm osc}\Phi_{nlm}(\vec{r}) \tag{3.24}$$

and

$$E_{nl}^{\rm osc} = \left(2n + l + \frac{3}{2}\right)\hbar\omega_{\rm ho}, \tag{3.25}$$

where $n = 0, 1, \cdots$; $l = 0, 1, \cdots, n-1$; and $m = 0, \pm 1, \cdots, \pm l$. The $\Phi_{nlm}(\vec{r})$ can be written in spherical coordinates $[\vec{r} = (r, \theta, \phi)]$,

$$\Phi_{nlm}(\vec{r}) = R_{nl}(r)\, Y_{lm}(\theta, \phi), \tag{3.26}$$

where the $R_{nl}(r)$ are given by

$$R_{nl}(r) = \sqrt{\frac{2^{l+2}\pi}{(2l+1)!!\,\sqrt{\pi^3}\, L_n^{(l+1/2)}(0) a_{ho}^3}} \times \left(\frac{r}{a_{ho}}\right)^l \exp\left(-\frac{r^2}{2a_{ho}^2}\right) L_n^{(l+1/2)}\left(\frac{r^2}{a_{ho}^2}\right), \tag{3.27}$$

with

$$(2l+1)!! = 1 \cdot 3 \cdot \cdots \cdot (2l+1). \tag{3.28}$$

The normalizations of $R_{nl}(r)$ and $Y_{lm}(\theta, \phi)$ are chosen as

$$\int_0^{2\pi}\int_0^{\pi} |Y_{lm}(\theta, \phi)|^2 \sin\theta\, d\theta\, d\phi = 1 \tag{3.29}$$

and

$$\int_0^\infty |R_{nl}(r)|^2\, r^2 dr = 1. \tag{3.30}$$

If we plug expansion (3.23) into Eq. (3.11) [with H given by Eq. (3.12) with $V_{\rm int}(\vec{r}) = V_{\rm ps}^{l=1}(\vec{r})$], multiply from the left with $\Phi^*_{n'lm'}(\vec{r})$ [with $l=1$], and integrate over $\vec{r}$, we obtain an expression for the coefficients $c_{n'm'}$,

$$c_{n'm'}(E^{\rm osc}_{n'l} - E) = -\frac{g_1(E)}{4\pi}\left[\vec{\nabla}_{\vec{r}} R^*_{n'l}(0)\right] \cdot \left[\vec{\nabla}_{\vec{r}}\left\{\frac{1}{2}\frac{\partial^2}{\partial r^2}\left(r^2 \sum_{n=0}^{\infty} c_{nm'} R_{nl}(r)\right)\right\}\right]_{r\to 0}, \tag{3.31}$$

where

$$\vec{\nabla}_{\vec{r}} R^*_{nl}(0) = \left[\vec{\nabla}_{\vec{r}} R^*_{nl}(r)\right]_{r=0}. \tag{3.32}$$

In deriving Eq. (3.31), we use that

$$\vec{\nabla}_{\vec{r}}\left[R_{nl}(r) Y_{lm}(\theta,\phi)\right] = \left[\vec{\nabla}_{\vec{r}} R_{nl}(r)\right] Y_{lm}(\theta,\phi) + R_{nl}(r)\left[\vec{\nabla}_{\vec{r}} Y_{lm}(\theta,\phi)\right], \tag{3.33}$$

where the second term on the right-hand side goes to zero in the $r \to 0$ limit. Since the gradients $\vec{\nabla}_{\vec{r}}$ in Eq. (3.31) act on arguments that depend solely on r, we can replace them by $\hat{e}_r \frac{\partial}{\partial r}$ (where $\hat{e}_r$ denotes the unit vector in the r-direction),

$$c_{n'm'}(E^{\rm osc}_{n'l} - E) = -\frac{g_1(E)}{4\pi}\frac{\partial R^*_{n'l}(0)}{\partial r}\left[\frac{1}{2}\frac{\partial^3}{\partial r^3}\left(r^2 \sum_{n=0}^{\infty} c_{nm'} R_{nl}(r)\right)\right]_{r\to 0}. \tag{3.34}$$

Equation (3.34) implies that the coefficients $c_{n'm'}$ are of the form

$$c_{n'm'} = A \, \frac{\frac{\partial R^*_{n'l}(0)}{\partial r}}{E^{\rm osc}_{n'l} - E}, \tag{3.35}$$

where A is a constant independent of n'. Plugging Eq. (3.35) into Eq. (3.34) results in an implicit expression for the three dimensional energies E,

$$\left[\frac{1}{2} \frac{\partial^3}{\partial r^3} \left(r^2 \sum_{n=0}^{\infty} \frac{\frac{\partial R^*_{nl}(0)}{\partial r} R_{nl}(r)}{E^{\rm osc}_{nl} - E} \right) \right]_{r \to 0} = -\frac{4\pi}{g_1(E)}. \tag{3.36}$$

To simplify the infinite sum over n, we use expression (3.27) for the $R_{nl}(r)$, and introduce a non-integer quantum number ν,

$$E = \left(2\nu + l + \frac{3}{2} \right) \hbar \omega_{\rm ho}. \tag{3.37}$$

For $l = 1$, we obtain

$$\frac{1}{3\sqrt{\pi^3}} \left[\frac{1}{2} \frac{\partial^3}{\partial r^3} \left(\exp\left(-\frac{r^2}{2a_{ho}^2} \right) r^3 \sum_{n=0}^{\infty} \frac{L_n^{(3/2)}(r^2/a_{ho}^2)}{n-\nu} \right) \right]_{r \to 0} = -\frac{\hbar \omega_{\rm ho} \, a_{ho}^5}{g_1(E)}. \tag{3.38}$$

Using the identity

$$\sum_{n=0}^{\infty} \frac{L_n^{(3/2)}\left(r^2/a_{ho}^2\right)}{n-\nu} = \Gamma(-\nu) \, U\left(-\nu, \frac{5}{2}, \frac{r^2}{a_{ho}^2} \right), \tag{3.39}$$

the infinite sum in Eq. (3.38) can be rewritten,

$$\frac{\Gamma(-\nu)}{3\sqrt{\pi^3}} \left[\frac{1}{2} \frac{\partial^3}{\partial r^3} \left(\exp\left(-\frac{r^2}{2a_{ho}} \right) r^3 \; U\left(-\nu, \frac{5}{2}, \frac{r^2}{a_{ho}^2} \right) \right) \right]_{r \to 0} = -\frac{\hbar \omega_{\rm ho} \, a_{ho}^5}{g_1(E)}, \tag{3.40}$$

where the $r \to 0$ limit is well behaved, as discussed above, due to the regularization operator of $V_{\rm ps}^{l=1}(\vec{r})$. Expression (3.40) can be evaluated using the known small r behavior of the hypergeometric function $U(-\nu, \frac{5}{2}, \frac{r^2}{a_{ho}^2})$ [82],

$$\frac{1}{\pi}\Gamma(-\nu)\, U\left(-\nu, \frac{5}{2}, \frac{r^2}{a_{ho}^2}\right) \approx -\left(\frac{r}{a_{ho}}\right)^{-3} \frac{1}{\Gamma(-\frac{1}{2})} - \left(\frac{r}{a_{ho}}\right)^{-1} \frac{(2\nu+3)}{\Gamma(-\frac{1}{2})} + \frac{\Gamma(-\nu)}{\Gamma(-\nu-\frac{3}{2})\Gamma(\frac{5}{2})} + \mathcal{O}(r). \tag{3.41}$$

If we insert expansion (3.41) into Eq. (3.40), evaluate the derivatives, and take the $r \to 0$ limit, we find

$$-\frac{\hbar\omega_{\rm ho}\, a_{ho}^5}{g_1(E)} = \frac{1}{\sqrt{\pi}} \frac{\Gamma(-\nu)}{\Gamma(-\nu-\frac{3}{2})\Gamma(\frac{5}{2})}. \tag{3.42}$$

Using Eqs. (3.20) and (3.37), we obtain our final expression for the relative eigenenergies E for $l = 1$,

$$\frac{V_p(k)}{a_{ho}^3} = -\frac{\Gamma(-\frac{E}{2\hbar\omega_{\rm ho}} - \frac{1}{4})}{8\Gamma(-\frac{E}{2\hbar\omega_{\rm ho}} + \frac{5}{4})}. \tag{3.43}$$

The above approach expresses the relative eigenfunction of the system in terms of single particle harmonic oscillator eigenfunctions. Infinite sums are performed to obtain the eigenenergies. This an alternative but equivalent approach to that used in Sec. 2.2 for the one dimensional pseudopotential, where we started with a δ-shell of radius z_0, used boundary conditions to relate the inside and outside wavefunctions and then took the limit $z_0 \to 0$.

Solid lines in Fig. 2.1(b) show the relative three dimensional eigenenergies E (solution to Eq. (3.43) with $V_p(k)$ replaced by V_p) for two spin-polarized fermions under ex-

ternal harmonic confinement interacting through the energy independent zero-range pseudopotential $V_{\rm ps}^{l=1}(\vec{r})$ as a function of the energy independent three dimensional scattering volume V_p. For vanishing coupling strength g_1 (or equivalently, for $V_p = 0$), E coincides with the $l = 1$ harmonic oscillator eigenenergy. As V_p increases [decreases], E increases [decreases].

Expansion of Eq. (3.43) for a negative and large in absolute value eigenenergy (and hence negative V_p), results in

$$E = -\frac{\hbar^2}{2\mu(V_p(k))^{2/3}}, \tag{3.44}$$

which agrees with the binding energy of $V_{\rm ps}^{l=1}(\vec{r})$ without the confinement potential. A dashed line in Fig. 2.1(b) shows this binding energy (with $V_p(k)$ replaced by V_p), while a dash-dotted line shows the expansion of Eq. (3.43) including the next higher order, i. e., the solution to the equation

$$-\frac{a_{\rm ho}^3}{V_p} = 8\left(-\frac{E}{2\hbar\omega_{\rm ho}} - \frac{1}{4}\right)^{3/2} + 3\left(-\frac{E}{2\hbar\omega_{\rm ho}} - \frac{1}{4}\right)^{1/2}. \tag{3.45}$$

Compared to the eigenenergy of the system without confinement, Eq. (3.44), the lowest eigenenergy given by Eq. (3.43) is downshifted. This downshift is somewhat counterintuitive, and contrary to the s-wave case. This difference is explained later in the context of Fig. 3.3.

In addition to the eigenergies E of two atoms with $l = 1$ under harmonic confinement, we determine the corresponding eigenfunctions $\Psi(\vec{r})$,

$$\Psi(\vec{r}) \propto \frac{\Gamma(-\nu)}{(a_{ho})^{3/2}} \frac{r}{a_{ho}} \exp\left(-\frac{r^2}{2a_{ho}^2}\right) U\left(-\nu, \frac{5}{2}, \frac{r^2}{a_{ho}^2}\right), \tag{3.46}$$

which lead to the well-behaved boundary condition

$$\left[\frac{\frac{\partial^3}{\partial r^3}\left(\frac{1}{2}r^2\Psi(\vec{r})\right)}{r^2\Psi(\vec{r})}\right]_{r\to 0} = -\frac{1}{V_p(k)}. \tag{3.47}$$

This boundary condition is an alternative representation of the pseudopotential $V_{\rm ps}^{l=1}(\vec{r})$, and depends on only one parameter, that is, the scattering volume $V_p(k)$. This is in contrast to earlier work [90, 91], which treated a boundary condition similar to Eq. (3.47) but evaluated the left hand side at a finite value of r, i.e., at $r = r_e$. The boundary condition containing the finite parameter r_e is not equivalent to a zero-range pseudopotential. References [92, 93, 94] discuss alternative derivations and representations of the boundary condition given in Eq. (3.47).

To benchmark our p-wave pseudopotential treatment of two spin-polarized three dimensional fermions under harmonic confinement, we solve the three dimensional Schrödinger equation, Eq. (3.11), for the Hamiltonian given by Eq. (3.12) numerically for the shape-dependent Morse potential $V_{\rm morse}(r)$,

$$V_{\rm morse}(z) = d\, e^{-\alpha(r-r_0)}\left[e^{-\alpha(r-r_0)} - 2\right]. \tag{3.48}$$

Our numerical calculations are performed for $r_0 = 11.65$a.u., $\alpha = 0.35$a.u., $\omega_{\rm ho} = 10^{-9}$a.u. ($2\pi\nu_{\rm ho} = \omega_{\rm ho}$), and $m = m(^{87}{\rm Rb})$. The well depth d is chosen such that the three dimensional Morse potential supports between zero and two $l = 1$ bound states. Solid lines in Fig. 3.2 show the resulting three dimensional eigenenergies E with $l = 1$ obtained numerically as a function of the depth d.

To compare the $l = 1$ eigenenergies obtained numerically for the Morse potential $V_{\rm morse}(r)$ with those obtained for the p-wave pseudopotential $V_{\rm ps}^{l=1}(\vec{r})$, we first determine the energy-dependent free-space scattering volume $V_p(k)$ for the three dimen-

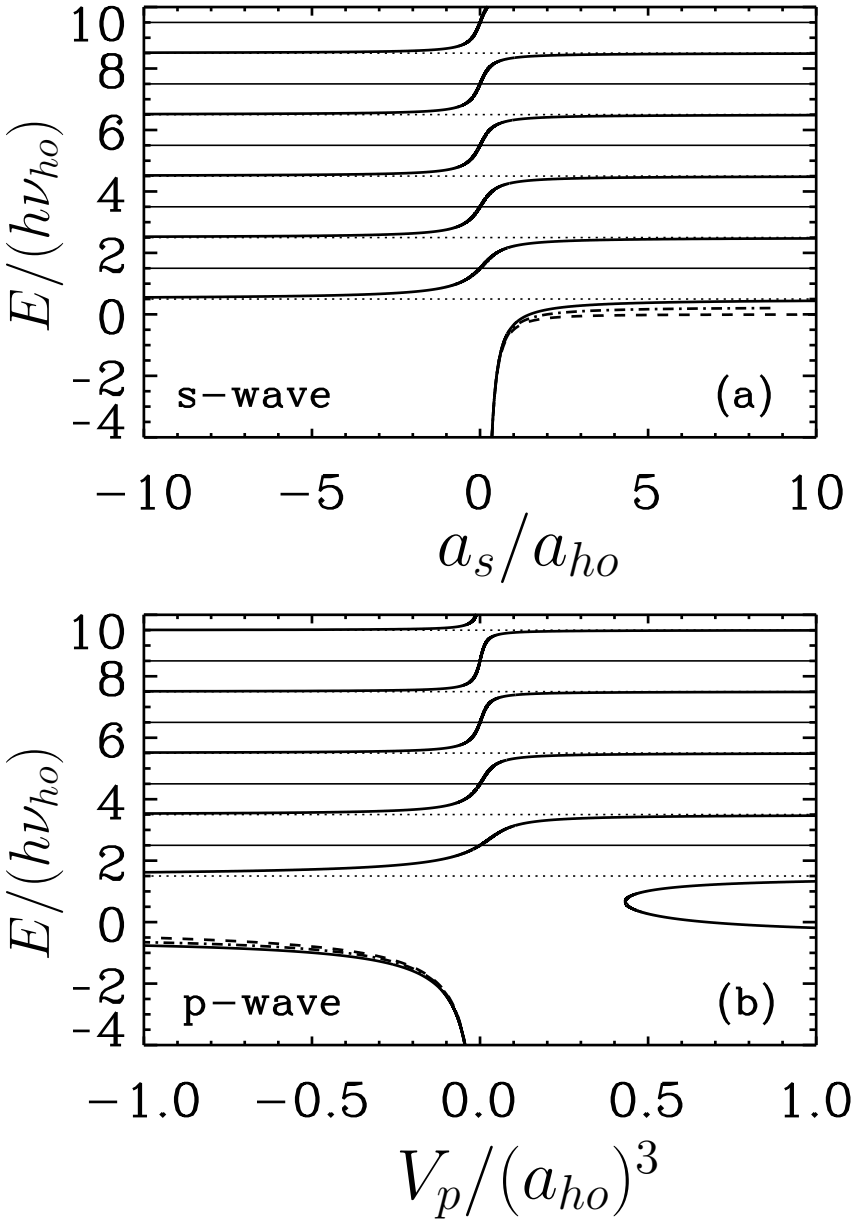

Figure 3.1: Solid lines in panel (a) show the relative s-wave energies E [Eq. (3.15)] calculated using the pseudopotential $V_{\rm ps}^{l=0}(\vec{r})$ as a function of the scattering length a_s. Solid lines in panel (b) show the relative p-wave energies E [Eq. (3.43)] calculated using the pseudopotential $V_{\rm ps}^{l=1}(\vec{r})$ as a function of the scattering volume V_p. Horizontal solid lines indicate the harmonic oscillator eigenenergies [for $l=0$ in panel (a), and for $l=1$ in panel (b)]. Horizontal dotted lines indicate the asymptotic eigenenergies E [for $a_s \to \pm\infty$ in panel (a), and for $V_p \to \pm\infty$ in panel (b)]. Dashed lines show the binding energies, Eq. (3.16) in panel (a) and Eq. (3.44) in panel (b), of the pseudopotentials $V_{\rm ps}^{l=0}(\vec{r})$ and $V_{\rm ps}^{l=1}(\vec{r})$, respectively, without confinement. Dash-dotted lines show the expansion of Eq. (3.15) [panel (a)] and Eq. (3.43) [panel (b)] including the next order term.

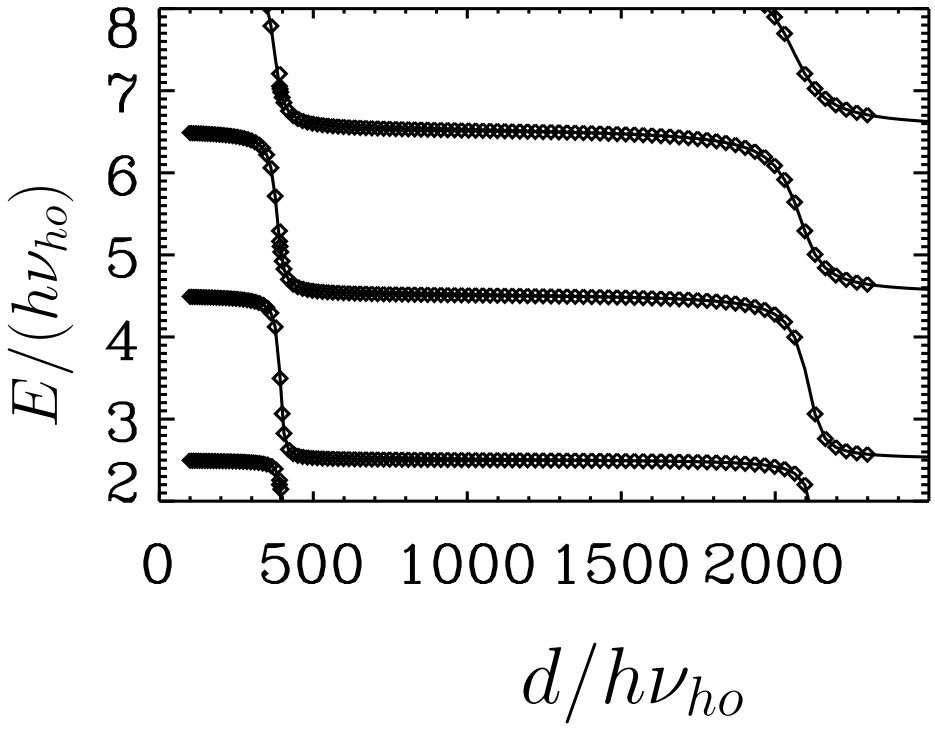

Figure 3.2: Relative three dimensional eigenenergies E with $l = 1$ for two spin-polarized fermions under three dimensional harmonic confinement as a function of the well depth d. Solid lines show the eigenenergies obtained by solving the three dimensional Schrödinger equation, Eq. (3.11), for the Hamiltonian given in Eq. (3.12) numerically for the Morse potential, Eq. (3.48). Symbols show the eigenenergies obtained for the pseudopotential $V_{\rm ps}^{l=1}(\vec{r})$, taking the energy-dependence of the three dimensional scattering volume V_p into account, $V_p = V_p(E)$ (see text). This figure is taken from Ref. [64].

sional Morse potential as a function of the relative scattering energy E for various well depths d. We then solve the transcendental equation (3.43) self-consistently for E. Diamonds in Fig. 3.2 show the resulting $l = 1$ eigenenergies E for two three dimensional particles under harmonic confinement interacting through the $l = 1$ pseudopotential $V_{\rm ps}^{l=1}(\vec{r})$. Excellent agreement between these eigenenergies and those obtained for the Morse potential (solid lines) is visible for all well depths d. We emphasize that this agreement depends crucially on the usage of *energy-dependent* three dimensional scattering volumes. Figure 3.2 illustrates that the p-wave pseudopotential $V_{\rm ps}^{l=1}(\vec{r})$ describes p-wave scattering processes properly.

In obtaining the excellent agreement between the energies calculated using the shape dependent and zero range potentials in Fig. 3.2 we used the energy dependent p-wave scattering volume $V_p(k)$ in the zero range pseudopotential. We now elaborate on the importance of the energy dependence of the scattering volume. Figure 3.3(a) shows the eigenenergies for two interacting particles with $l = 1$ under harmonic confinement as a function of the energy independent scattering volume V_p. The solid lines show the eigenenergies for a square well potential with depth V_0 and range r_0 and crosses show the eigenenergies for the energy dependent zero range p-wave pseudopotential. The range r_0 of the square well potential is chosen to be much smaller than the oscillator length ($r_0 = 0.01 a_{\rm ho}$); finite range effects are not visible on the scale chosen in Fig. 3.3(a).

The dashed lines show the eigenenergies for the energy independent zero range p-wave pseudopotential. Figure 3.3(a) illustrates that the eigenenergies for the square well potential and the energy dependent pseudopotentials agree very well. The energies obtained for the energy independent pseudopotential, in contrast, differ significantly from those obtained for the square well. For $E < 1.5\hbar\omega_{\rm ho}$, the energies for the square well and the energy independent pseudopotentials differ even qualitatively. Thus, for three dimensional p-wave interacting systems, it is extremely important to

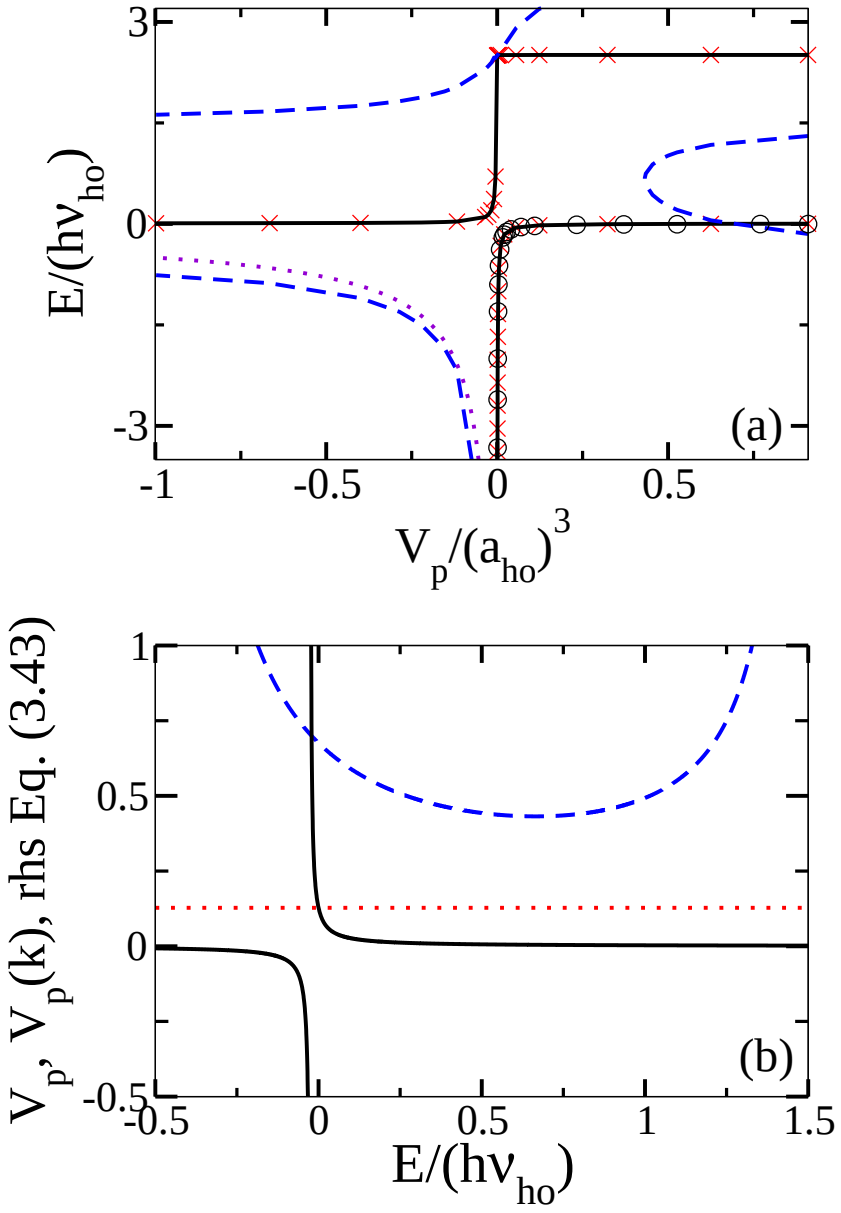

Figure 3.3: (a) Eigenenergies for two interacting particles with $l = 1$ under harmonic confinement as a function of the energy independent scattering volume V_p. The solid lines and crosses show the eigenenergies obtained by solving the Schrödinger equation, Eq. (3.11), for the Hamiltonian given in Eq. (3.12) for the square well potential and the energy dependent zero range p-wave pseudopotential, respectively. The dashed lines show the eigenenergies obtained for the energy independent zero range p-wave pseudopotential. The circles show the energies obtained by solving Eq. (3.44) including the energy dependence of V_p, while the dotted curve is obtained by considering the energy independent V_p. (b) The solid curve shows the energy dependent scattering length as a function of energy for $V_0 = 49348.1\hbar\omega_{\rm ho}$. The dashed curve shows the right hand side of Eq. (3.43), while the dotted line shows the energy independent scattering length for $V_0 = 49348.1\hbar\omega_{\rm ho}$.

include the energy dependence of the generalized scattering length. This is in contrast to the one dimensional square well potential where the energy dependence becomes important only for large values of $|E|/\hbar\omega_z$. It can be shown that any pseudopotential treatment of higher partial wave scattering ($l > 0$) has to account for the energy dependence of the generalized scattering lengths. The dotted curve and circles are obtained using the free-space bound state energy expression for $V_{\rm ps}^{l=1}$, Eq. (3.44), with the energy independent scattering volume V_p and the energy dependent scattering volume $V_p(k)$, respectively. The circles lie slightly below the solid line and crosses (this cannot be seen on the scale of Fig. 3.3), in agreement with the fact that the energy gets pushed up by the trap [see also Fig. 3.1(a)].

Focussing on a particular value of V_p, Fig. 3.3(b) illustrates that the energy independent p-wave pseudopotential results in a qualitatively incorrect eigenspectrum. The solid and dashed curves in Fig. 3.3(b) show the right hand side and the left hand side of Eq. (3.43) as a function of energy. If the curves cross, a solution exists. If the curves do not cross, Eq. (3.43) has no solution in the chosen energy range. The dotted curve shows the energy independent scattering volume V_p, $V_p = 0.123465 a_{\rm ho}^3$ [energy independent left hand side of Eq. (3.43)], of the square well potential. Since the dotted line does not intersect the dashed curve in the range $-0.5\hbar\omega_{\rm ho} < E < 1.5\hbar\omega_{\rm ho}$, Eq. (3.43) with the energy independent generalized scattering length does not have a root in this energy range (see dashed curves in Fig. 3.3(a)). The solid curve, however, intersects the dashed curve at $E = -0.0212335\hbar\omega_{\rm ho}$. Hence, Eq. (3.43) with the energy dependent generalized scattering length has a root at $E = -0.0212335\hbar\omega_{\rm ho}$ (see crosses in Fig. 3.3(a)). Due to the strong energy dependence of the scattering length the eigenenergies obtained using the energy independent generalized scattering length gives us a misleading picture of the energy spectrum. If we do not include the energy dependence, there appears to be a diving weakly bound state only for negative values of V_p (effectively attractive in-

teractions). The square well potential, however, supports, a weakly bound state only for positive V_p (effectively repulsive interactions).

Following the δ-shell method described in Sec. 2.1.2, spherically symmetric pseudopotentials for different l have been derived [65],

$$V_{\rm ps}^{l}(r) = -\lim_{r_0\to 0} \frac{\hbar^2}{2\mu}\frac{(2l+1)!!}{(2l)!!}\frac{\tan\delta_l(k)}{k^{2l+1}}\frac{\delta(r-r_0)}{r_0^{l+2}}\frac{\partial^{2l+1}}{\partial r^{2l+1}}r^{l+1}. \tag{3.49}$$

The pseudopotential given in Eq. (3.19) is equivalent to that in Eq. (3.49) with l=1: This can be seen e. g., by comparing the expectation value of the $l = 1$ pseudopotentials for a radial function with $l = 1$. The eigenequation for two particles in a spherically symmetric harmonic trap interacting through $V_{\rm ps}^{l}(r)$ is given by [65]

$$\frac{\Gamma(\frac{-E}{2\hbar\omega_{\rm ho}}+\frac{1}{4}-\frac{l}{2})}{2^{2l+1}\Gamma(\frac{-E}{2\hbar\omega_{\rm ho}}+\frac{3}{4}+\frac{l}{2})} = (-1)^l\frac{a_l}{a_{ho}^{2l+1}}. \tag{3.50}$$

3.2 Coupled channel treatment

In this section all Hamiltonian, potentials and wavefunctions are for coupled two channel interaction potentials.

3.2.1 Coupled channel scattering length

So far we have considered only single channel models for the interaction potential $V_{\rm int}(r)$. We treat two channels with two distinct thresholds that differ in energy by ε ($\varepsilon > 0$). For two atoms in the presence of an external magnetic field, the two channels correspond to two non-degenerate hyperfine levels (see Sec. 1.3). The energy difference ε, $\varepsilon = \vec{B}\cdot(\vec{\mu_2}-\vec{\mu_1})$, where $\vec{\mu_1}$ and $\vec{\mu_1}$ are the magnetic moments of the atom in hyperfine

levels corresponding to channels one and two, respectively, can be tuned by changing the magnetic field. For the remainder of this chapter, subscript "(1)" corresponds to channel one, while subscript "(2)" corresponds to channel two.

Assuming the coupled channel interaction potential $\boldsymbol{V}_{\text{int}}$ depends on r only,

$$\boldsymbol{V}_{\text{int}}(r) = \begin{pmatrix} V_{(1)}(r) & V_{(12)}(r) \\ V_{(12)}(r) & V_{(2)}(r) \end{pmatrix}, \tag{3.51}$$

the radial Schrödinger equation for two particles in three dimensions reads

$$\boldsymbol{H}_{\text{rad}}^{\text{free}} \boldsymbol{\Psi}_{l}^{\text{free}}(r) = \boldsymbol{E} \boldsymbol{\Psi}_{l}^{\text{free}}(r), \tag{3.52}$$

where

$$\boldsymbol{H}_{\text{rad}}^{\text{free}} = -\frac{\hbar^2}{2\mu} \boldsymbol{I} \left(\frac{\partial^2}{\partial r^2} + \frac{2}{r} \frac{\partial}{\partial r} - \frac{l(l+1)}{r^2} \right) + \boldsymbol{V}_{\text{int}}(r), \tag{3.53}$$

$$\boldsymbol{E} = E \boldsymbol{I} \tag{3.54}$$

and

$$\boldsymbol{\Psi}_{l}^{\text{free}}(r) = \begin{pmatrix} \Psi_{l(1)}^{\text{free}}(r) \\ \Psi_{l(2)}^{\text{free}}(r) \end{pmatrix}. \tag{3.55}$$

Above, $\boldsymbol{I}$ denotes the 2×2 identity matrix,

$$\boldsymbol{I} = \begin{pmatrix} 1 & 0 \\ 0 & 1 \end{pmatrix}. \tag{3.56}$$

To define the coupled channel scattering length a_l^{cc}, we require that $V_{(1)}(r)$, $V_{(2)}(r)$ and $V_{(12)}(r)$ are all short range potentials. Furthermore, the large r thresholds are given by 0, ε and 0 for $V_{(1)}(r)$, $V_{(2)}(r)$ and $V_{(12)}(r)$, respectively.

If the relative scattering energy E lies between 0 and ε, then channel (1) is an open

channel and channel (2) is a closed channel. The solution to Eq. (3.52) for $r > r_0$ is in this case given by

$$\Psi_l^{\text{free}(>)}(r) = A_{\text{cc}}(k) \begin{pmatrix} j_l(kr) - \tan\delta_l^{\text{cc}}(k) n_l(kr) \\ B_{\text{cc}}(k)\tilde{k}_l(qr), \end{pmatrix}, \tag{3.57}$$

where $A_{\text{cc}}(k)$ is a normalization constant, $B_{\text{cc}}(k)$ a proportionality constant, and $\delta_l^{\text{cc}}(k)$ the coupled channel phase shift. The solution $\tilde{k}_l$ in channel (2) is the spherical modified Bessel function of the second kind, which depends on q,

$$q = \sqrt{\frac{2\mu(\varepsilon - E)}{\hbar^2}}, \tag{3.58}$$

and decays exponentially.

The solution to Eq. (3.52) for $r < r_0$, denoted by $\Psi_l^{\text{free}(<)}(\vec{r})$, depends on the details of the interaction potential and has to be determined explicitly for each interaction potential. To determine the coupled channel phase shift $\delta_l^{\text{cc}}(k)$, we impose the following two continuity conditions at $r = r_0$,

$$\Psi_l^{\text{free}(<)}(r_0) = \Psi_l^{\text{free}(>)}(r_0) \tag{3.59}$$

and

$$\left(\frac{\partial \Psi_l^{\text{free}(<)}(r)}{\partial r}\right)_{r=r_0} = \left(\frac{\partial \Psi_l^{\text{free}(>)}(r)}{\partial r}\right)_{r=r_0}. \tag{3.60}$$

The phase shift defines the energy dependent coupled channel scattering length $a_l^{\text{cc}}(k)$,

$$a_l^{\text{cc}}(k) = -\frac{\tan\delta_l^{\text{cc}}(k)}{k^{2l+1}}, \tag{3.61}$$

and the energy independent coupled channel scattering length $a_l^{\rm cc}$,

$$a_l^{\rm cc} = \lim_{k\to 0} a_l^{\rm cc}(k). \tag{3.62}$$

3.2.2 Coupled channel square well model: s-wave scattering

The coupled two channel square well potential has been successfully used to model a Feshbach resonance in Refs. [47, 48]. This section determines the s-wave coupled channel scattering length for the lowest partial wave ($l = 0$) for a coupled channel square well potential following Ref. [95]. The potential $\boldsymbol{V}_{\rm SW}^{\rm cc}(r)$ is parametrized by V_1, V_2 and V_{12},

$$\boldsymbol{V}_{\rm SW}^{\rm cc}(r) = \begin{pmatrix} -V_1\Theta(r_0-r) & V_{12}\Theta(r_0-r) \\ V_{12}\Theta(r_0-r) & -V_2\Theta(r_0-r)+\varepsilon\Theta(r-r_0) \end{pmatrix}, \tag{3.63}$$

where V_1 and V_2 are positive constants and $\Theta(x)$ denotes the step function ($\Theta(x) = 0$ for $x < 0$ and $\Theta(x) = 1$ for $x > 0$). In this section we consider $l = 0$ and omit the subscript "l". For $r > r_0$, the solution to Eq. (3.52) with $\boldsymbol{V}_{\rm int}(r) = \boldsymbol{V}_{\rm SW}^{\rm cc}(r)$ is given by $\boldsymbol{\Psi}^{\rm free(>)}(r)$, Eq. (3.57). We now illustrate the procedure to obtain the solution to Eq. (3.52) for $r < r_0$. For $r < r_0$, we rescale $\boldsymbol{\Psi}^{\rm free(<)}(r)$,

$$\boldsymbol{\Psi}^{\rm free(<)}(r) = \frac{1}{r}\boldsymbol{u}^{\rm free(<)}(r). \tag{3.64}$$

Equation (3.52) then becomes

$$-\frac{\hbar^2}{2\mu}\frac{d^2}{dr^2}\boldsymbol{u}^{\rm free(<)}(r) + \boldsymbol{W}\boldsymbol{u}^{\rm free(<)}(r) = 0, \tag{3.65}$$

where $\boldsymbol{W}$ is given by

$$\boldsymbol{W} = \boldsymbol{V}_{\rm SW}^{\rm cc}(r) - \boldsymbol{E}. \tag{3.66}$$

Equation (3.65) represents two coupled second order differential equations with four independent solutions. Imposing that $\boldsymbol{u}^{\text{free}(<)}(r)$ vanishes at $r = 0$, leaves us with just two independent solutions. $\boldsymbol{W}$ is a 2×2 matrix, whose eigenvalues and eigenvectors can be easily obtained. We denote the two eigenvalues of the matrix $\boldsymbol{W}$ by w_α^2 ($\alpha = 1, 2$) and the corresponding eigenvectors (2×1 matrices) by $\boldsymbol{X}_\alpha$,

$$\boldsymbol{W}\boldsymbol{X}_{\boldsymbol{\alpha}} = w_\alpha^2 \boldsymbol{X}_{\boldsymbol{\alpha}}. \tag{3.67}$$

We define a 2×2 matrix $\boldsymbol{X}$ that consists of the eigenvectors $\boldsymbol{X}_\alpha$,

$$\boldsymbol{X} = \begin{pmatrix} \boldsymbol{X}_1 & \boldsymbol{X}_2 \end{pmatrix}. \tag{3.68}$$

To diagonalize $\boldsymbol{W}$, we multiply Eq. (3.65) by $\boldsymbol{X}^T$, where $\boldsymbol{X}^T$ is the transpose of $\boldsymbol{X}$. The resulting uncoupled single channel second order differential equations read

$$\frac{d^2 \boldsymbol{y}_\alpha}{d r^2} + w_\alpha^2 \boldsymbol{y}_\alpha = 0, \tag{3.69}$$

where

$$\boldsymbol{y}_\alpha(r) = \boldsymbol{X}^T \boldsymbol{u}^{\text{free}(<)}(r) \tag{3.70}$$

is a 2×1 eigenvector matrix. The regular solutions $\boldsymbol{y}_\alpha$ ($\alpha = 1$ and 2) to Eq. (3.69) are given by

$$\boldsymbol{y}_1(r) = \begin{pmatrix} \sin(w_1 r) \\ 0 \end{pmatrix} \tag{3.71}$$

and

$$\boldsymbol{y}_2(r) = \begin{pmatrix} 0 \\ \sin(w_2 r) \end{pmatrix}. \tag{3.72}$$

Neither of the two short range solutions $\boldsymbol{y}_\alpha$ lead to a $\boldsymbol{\Psi}^{\text{free}(<)}(r)$ that can be smoothly matched to $\boldsymbol{\Psi}^{\text{free}(>)}(r)$. Hence, we must use a linear combination of the two solutions given by $\boldsymbol{y}(r)\boldsymbol{z}$. Here, $\boldsymbol{y}(r)$ is a 2×2 matrix that consists of the eigenvectors $\boldsymbol{y}_1$ and $\boldsymbol{y}_2$,

$$\boldsymbol{y}(r)=\begin{pmatrix}\boldsymbol{y}_1(r) & \boldsymbol{y}_2(r)\end{pmatrix}, \tag{3.73}$$

and $\boldsymbol{z}$ is a 2×1 matrix,

$$\boldsymbol{z}=\begin{pmatrix}z_1(k)\\ z_2(k)\end{pmatrix}, \tag{3.74}$$

where $z_1(k)$ and $z_2(k)$ are energy dependent constants. Using Eq. (3.70) and replacing $\boldsymbol{y}(r)$ by $\boldsymbol{y}(r)\boldsymbol{z}$, the inner solution is given by

$$\boldsymbol{u}^{\text{free}(<)}(r)=\boldsymbol{X}\boldsymbol{y}(r)\boldsymbol{z}. \tag{3.75}$$

Equations (3.64) and (3.75) can be combined to obtain $\boldsymbol{\Psi}^{\text{free}(<)}(r)$. Having obtained $\boldsymbol{\Psi}^{\text{free}(<)}(r)$, we proceed to find an expression for the energy independent coupled channel scattering length.

Applying the two continuity conditions in Eqs. (3.59) and (3.60) (this eliminates $\boldsymbol{z}$, and $A_{\text{cc}}(k)$ can be used to determine $B_{\text{cc}}(k)$), we get the following expression for the coupled channel s-wave phase shift,

$$\tan\delta^{\text{cc}}(k)=-\frac{(R_{22}(E)+q)(-R_{11}(E)\sin(kr_0)+k\cos(kr_0))+R_{12}^2(E)\sin(kr_0)}{(R_{22}(E)+q)(R_{11}(E)\cos(kr_0)+k\sin(kr_0))-R_{12}(E)^2\cos(kr_0)}, \tag{3.76}$$

where

$$\boldsymbol{R}=\begin{pmatrix}R_{11}(E) & R_{12}(E)\\ R_{12}(E) & R_{22}(E)\end{pmatrix}=\left\{\boldsymbol{X}\frac{d\boldsymbol{y}}{dr}\boldsymbol{y}^{-1}\boldsymbol{X}^T\right\}_{r=r_0}. \tag{3.77}$$

Using Eqs. (3.62) and (3.76) the energy independent coupled channel scattering

length for the coupled channel square well potential becomes

$$a^{\rm cc} = r_0 - \frac{R_{22}+\overline{q}}{(R_{22}+\overline{q})R_{11}-R_{12}^2}, \tag{3.78}$$

where

$$\overline{q} = \sqrt{\frac{2\mu\varepsilon}{\hbar^2}} \tag{3.79}$$

and the energy independent $\boldsymbol{R}$ matrix elements are given by

$$R_{ij} = \lim_{E\to 0} R_{ij}(E). \tag{3.80}$$

The energy independent $\boldsymbol{R}$ matrix elements are given in Eqs. (B.2) to (B.4) in terms of the parameters of the square well potential. The scattering length $a^{\rm cc}$ in Eq. (3.78) has a resonance for $\overline{q} = q_0$, where

$$q_0 = \frac{R_{12}^2}{R_{11}} - R_{22}. \tag{3.81}$$

The magnetic field B at which this resonance occurs is given by $B = B_0$. Close to resonance, we Taylor expand ε in about $B = B_0$. To first order in $B - B_0$, we obtain

$$\varepsilon(B) = \varepsilon(B_0) + \gamma_M(B - B_0), \tag{3.82}$$

where γ_M,

$$\gamma_M = \left(\frac{\partial\,\varepsilon(B)}{\partial\,B}\right)_{B=B_0}, \tag{3.83}$$

is the difference between magnetic moments of the atoms in the open and closed channels. Expressing ε in terms of $\overline{q}$, we find

$$\overline{q}(B) = q_0 + \frac{\gamma_M}{\frac{R_{12}^2}{R_{11}-R_{22}}}(B - B_0). \tag{3.84}$$

Since the resonance occurs at $B = B_0$, we have $q_0 = \overline{q}(B_0)$. Using Eqs. (3.81) and (3.84), Eq. (3.78) can be written as

$$a^{\rm cc} = r_0 - \frac{1}{R_{11}} - \frac{R_{12}^2\left(\frac{R_{12}^2}{R_{11}-R_{22}}\right)}{R_{11}^2\mu\gamma_M(B-B_0)} \tag{3.85}$$

or Equation 3.85 can be written in the form

$$a^{\rm cc} = a_{\rm bg}\left(1 - \frac{\Delta}{B-B_0}\right), \tag{3.86}$$

where $a_{\rm bg} = r_0 - \frac{1}{R_{11}}$ and $\Delta = \frac{R_{12}^2}{\gamma_M R_{11}}\frac{R_{12}^2}{(r_0R_{11}-1)(R_{11}-R_{22})}$. $a_{\rm bg}$ can be interpreted as the almost unchanging value of the coupled channel scattering length away from resonance and Δ as the width of the resonance.

The observed scattering length of ^{85}Rb near an s-wave Feshbach resonance ($B_0 \approx$ 155G, see Sec. 1.3.1 [45, 46]) has been fit to the functional form in Eq. (3.86) [37] by treating $a_{\rm bg}$, Δ and B_0 as three independent fitting parameters. The solid curve in Fig. 3.4 shows the scattering length of ^{85}Rb for $a_{\rm bg} = -380a_0$, $\Delta = 10$G and $B_0 = 155.2$G [96], as a function of the magnetic field B near resonance. The crosses show the coupled channel scattering length for the square well potential, for $\gamma_M = -3.5$MHz/G (experimentally determined for ^{85}Rb at $B \approx 155G$), with R_{11}, R_{12} and R_{22} adjusted so as to reproduce the solid curve in Fig. 3.4. For $r_0 = 100a_0$, we find $R_{11} = 0.0023/a_0$, $R_{12} = 0.0005/a_0$ and $R_{22} = -3.4/a_0$. These $\boldsymbol{R}$ matrix elements impose a boundary condition on the outside wavefunction, which in turn can be fulfilled by adjusting the three parameters V_1, V_2 and V_{12} of the square well potential. The coupled channel scattering length for the square well potential agrees well with the solid curve obtained by fitting to experimental data. This agreement shows that the coupled channel square well model captures much of the key physics near an s-wave Feshbach resonance.

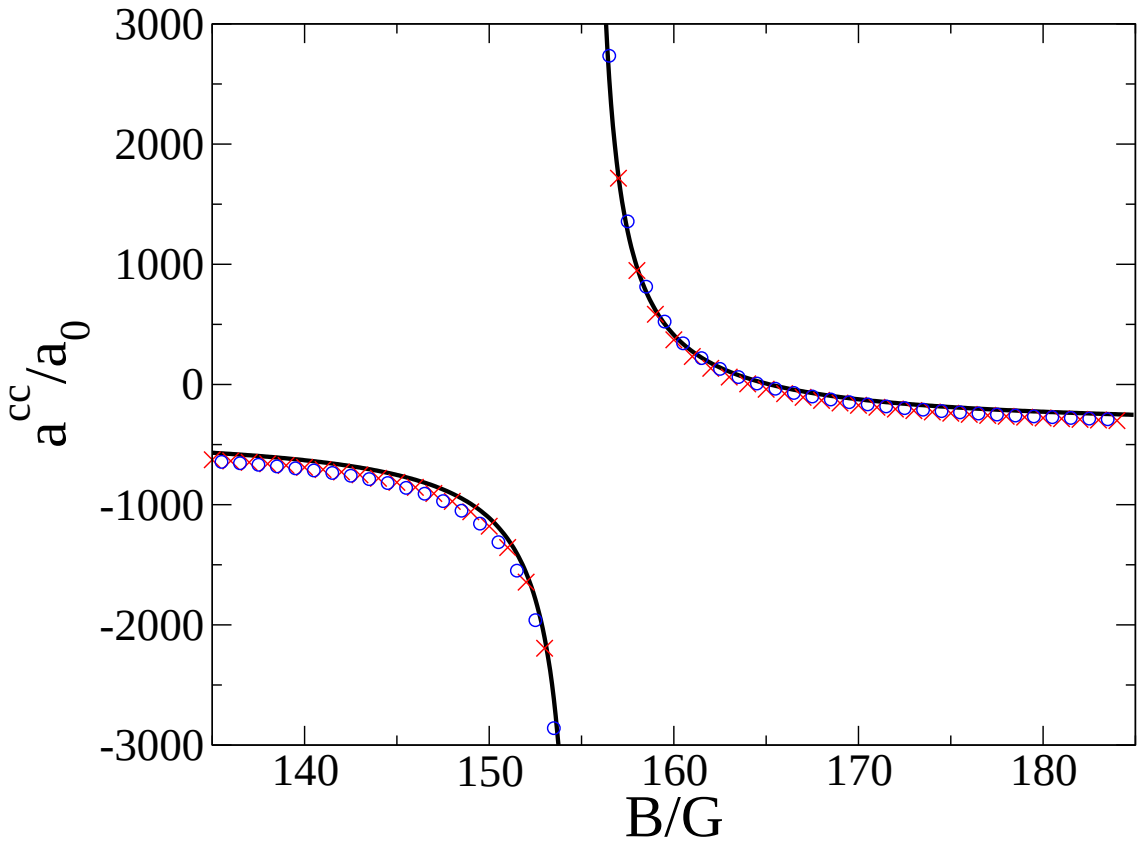

Figure 3.4: Energy independent coupled channel scattering length as a function of the magnetic field B. The solid curve shows a fit of Eq. (3.86) to experimental data; the parameters of the fit are $a_{\rm bg} = -380a_0$, $\Delta = 10$G and $B_0 = 155.2$G. The crosses are obtained by using Eq. (3.85) with $R_{11} = 0.0023/a_0$, $R_{12} = 0.0005/a_0$, $R_{22} = -3.4/a_0$ and $r_0 = 100a_0$. Circles are obtained using Eq. (3.91) with $a_1 = -435a_0$, $a_2 = 1.49a_0$ and $\beta = 0.00116/a_0$.

3.2.3 Coupled channel zero range model

Section 3.1.2 obtained the boundary condition for two particles interacting through the zero range s-wave pseudopotential in three dimensions [see Eq. (3.18)]. This section uses the boundary condition to develop a three parameter description of the coupled channel s-wave scattering length. The discussion in this section follows Ref. [96]. The radial Schrödinger equation for this system is given by Eq. (3.52) with $\boldsymbol{V}_{\rm int}(r) = \boldsymbol{0}$ for $r > 0$. The boundary condition in Eq. (3.18) determines the diagonal elements,

$$\left[\frac{d}{dr}\left(\boldsymbol{\Psi}^{\rm free(>)}(r)\right)\right]_{r\to 0} = \begin{pmatrix} -\frac{1}{a_1} & \beta \\ \beta & -\frac{1}{a_2} \end{pmatrix} \left(\boldsymbol{\Psi}^{\rm free(>)}(r)\right)_{r\to 0}, \tag{3.87}$$

where a_1 and a_2 are the single channel scattering lengths in the open and closed channels, and β is a constant coupling between the two channels. For $r > 0$, the two channels are uncoupled. Since $\boldsymbol{V}_{\rm int}(r) = \boldsymbol{0}$ for $r > 0$, the wavefunction matrix $\boldsymbol{\Psi}^{\rm free(>)}(r)$ is given by Eq. (3.57). Forcing $\boldsymbol{\Psi}^{\rm free(>)}(r)$ to obey the boundary condition given in Eq. (3.87) determines the energy dependent coupled channel scattering length $a^{\rm cc}(k)$,

$$a^{\rm cc}(k) = \left[\frac{1}{a_1} + \frac{\beta^2}{\sqrt{\frac{2\mu(\varepsilon - E)}{\hbar^2}} - (1/a_2)}\right]^{-1}, \tag{3.88}$$

and the energy independent coupled channel scattering length $a^{\rm cc}$,

$$a^{\rm cc} = \left[\frac{1}{a_1} + \frac{\beta^2}{\sqrt{(2\mu\varepsilon)/\hbar^2} - (1/a_2)}\right]^{-1}. \tag{3.89}$$

The solid curves in Figs. 3.5(a) and (b) show the energy independent coupled channel scattering length [see Eq. (3.89)] and the coupled channel bound state energy, respectively, as a function of ε. Just below resonance, the coupled channel scattering

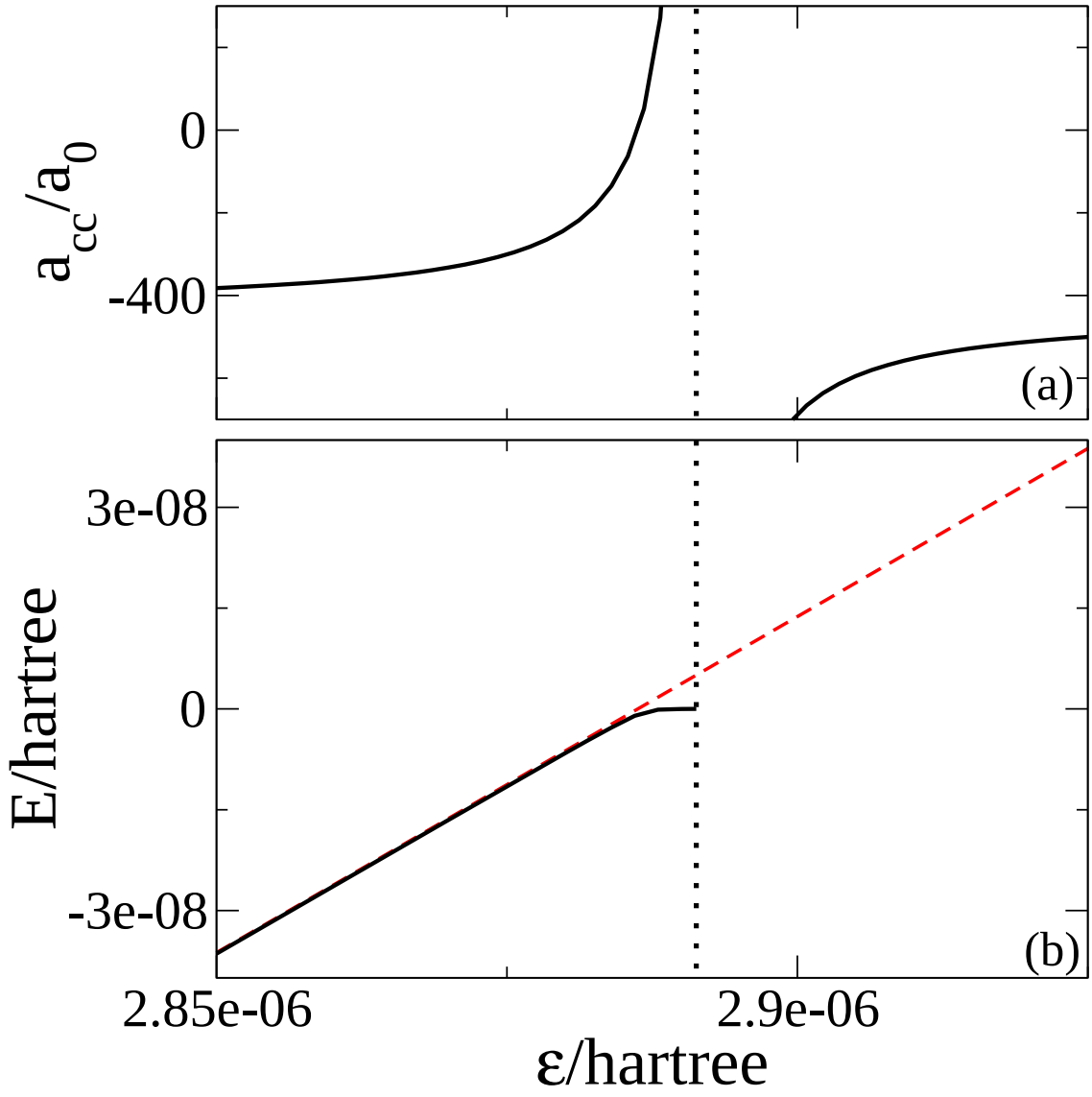

Figure 3.5: Results for zero range coupled channel model with parameters $a_1 = -435a_0$, $a_2 = 1.49a_0$ and $\beta = 0.00116/a_0$. The solid curves in (a) and (b) show the coupled channel scattering length and the coupled channel bound state energy, respectively, as a function of ε. The dotted line in (a) and (b) indicates the resonance value of ε, which is 2.8913×10^{-6} hartree. For comparison, the dashed line in (b) shows the bound state energy of the closed channel as a function of ε. The x-axis label and scale are the same in (a) and (b).

length is large and positive indicating the presence of a weakly bound state. Just above resonance, the coupled channel scattering length is large and negative and the coupled channel system does not support a bound state. For comparison, the dashed line in Fig. 3.5(b) shows the bound state energy for the bare closed channel as a function of ε. For small ε, the bound state energy of the closed channel closely agrees with the coupled channel bound state energy. This indicates that the wavefunction of the coupled channel system is dominated by the closed channel. Near resonance, deviations appear between the closed channel and coupled channel bound state energies indicating that there is a significant contribution from the open channel to the coupled channel wavefunction. Above resonance, the bound state in the closed channel has a positive energy with respect to the threshold of the open channel and no coupled channel bound state exists. This shows that the wavefunction of the coupled channel system is dominated by the open channel.

On resonance ($B = B_0$), the coupled channel scattering length diverges and

$$\varepsilon(B_0) = \frac{1}{2\mu}\left(\frac{1}{a_2} - a_1\beta^2\right)^2. \tag{3.90}$$

Plugging Eqs. (3.82) and (3.90) into Eq. (3.89) and neglecting terms that are quadratic or higher order in $B - B_0$, we get

$$a^{\mathrm{cc}} = a_1\left(1 - \frac{a_1\beta^2\left(\frac{1}{a_2} - a_1\beta^2\right)}{\mu\gamma_M(B - B_0)}\right). \tag{3.91}$$

Equation (3.91) can be written in the form of Eq. (3.86), where $a_{\mathrm{bg}} = a_1$ and $\Delta = \frac{a_1\beta^2}{\mu\gamma_M}\left(\frac{1}{a_2} - a_1\beta^2\right)$. Circles in Fig. 3.4 show Eq. (3.91) for $a_1 = -435a_0$, $a_2 = 1.49a_0$ and $\beta = 0.00116/a_0$ [96]. The agreement between the coupled channel scattering length obtained by fitting to experimental data and from the coupled channel zero range model

is very good.

3.3 Conclusions

In this chapter we discussed scattering by three dimensional spherically symmetric interaction potentials. Due to the spherical symmetry of the interactions, the angular momentum is conserved and each partial wave can be treated separately. Zero range pseudopotentials exist for all partials waves. For most purposes, however, s- and p-wave pseudopotentials suffice. The first p-wave regularized zero range pseudopotential was proposed by us in Ref. [64].

A coupled two channel potential can be used to model a Feshbach resonance in three dimensions. The model depends on three parameters and can be set up in different ways using finite range or zero range coupled two channel potentials. In this chapter we have adjusted the three parameters in the coupled two channel model potentials to reproduce the s-wave Feshbach resonance in ^{85}Rb.

Chapter 4

Azimuthally symmetric two body systems in two dimensions

This chapter considers two dimensional systems, for which the motion in the tight confining direction, the z-direction, is frozen out [97, 98]. The equation of state then depends on the generalized two dimensional scattering length. A thorough understanding of the two-particle physics in two dimensions for any partial wave might aid studies of the two dimensional many-body problem. Toward this end, Sec. 4.1 derives two dimensional zero range pseudopotentials for any partial wave m and Sec. 4.2 develops a coupled channel model applicable to two particles with $m = 0$ across a Feshbach resonance.

Experiments on ultracold gases routinely utilize Feshbach resonances, which allow the interaction strength between two particles to be tuned to essentially any value through application of an external magnetic field. Confinement induced resonances in two dimensions have been predicted [97, 99] and observed for p-wave interactions [100], thus allowing the effective two dimensional coupling constant to be tuned to essentially any value including zero and infinity. Assuming a strictly two dimensional geometry, Sec. 4.2 proposes a coupled channel model for the lowest partial wave, i.e., $m = 0$, with

three parameters, the scattering lengths b_1 and b_2 of the "open" and "closed" channel and the coupling strength β. The detuning is given by ϵ. While b_1, b_2 and β are fixed for a given system, varying the detuning ϵ corresponds to changing the strength of an external magnetic field.

The model predicts that the dependence of the effective two dimensional scattering length on the external control parameter is distinctly different than that of the effective three dimensional scattering length (see Ch. 3), thus highlighting the non-intuitive behavior of systems with reduced dimensionality. Section 4.2.2 determines the binding energy and the occupation of the open and closed channel across a two dimensional resonance. These observables have been measured across a three dimensional resonance [14, 101] but not yet across a two dimensional resonance; however, we expect measurements on quasi-two dimensional systems to be performed in the near future.

In this chapter all Hamiltonian, potentials, wavefunctions and phase shifts are two dimensional.

4.1 Single channel treatment

4.1.1 Two dimensional scattering length

The Schrödinger equation for two identical particles in two dimensions in the relative vector $\vec{\rho}$ is given by

$$H^{\text{free}}\Psi^{\text{free}}(\vec{\rho}) = E\Psi^{\text{free}}(\vec{\rho}), \tag{4.1}$$

where

$$H^{\text{free}} = -\frac{\hbar^2}{2\mu}\nabla^2_{\vec{\rho}} + V_{\text{int}}(\rho). \tag{4.2}$$

Here, $\nabla^2_{\vec{\rho}}$ is the two dimensional Laplacian operator,

$$\nabla^2_{\vec{\rho}} = \frac{\partial^2}{\partial \rho^2} + \frac{1}{\rho}\frac{\partial}{\partial \rho} + \frac{1}{\rho^2}\frac{\partial^2}{\partial \phi^2}, \tag{4.3}$$

and ρ and ϕ denote the length and polar angle of $\vec{\rho}$. We assume that the interaction potential $V_{\text{int}}(\rho)$ is radially symmetric and short range, i. e., it falls off faster than $1/\rho^2$. There exists a distance ρ_0 such that $V_{\text{int}}(\rho)$ can be neglected for $\rho > \rho_0$, i. e., $V_{\text{int}}(\rho) = 0$ for $\rho > \rho_0$. The wavefunction $\Psi(\vec{\rho})$ can be expressed as a product of a radial wavefunction, denoted by $R_{m'}(\rho)$, and the angular part given by $e^{\imath m'\phi}$,

$$\Psi^{\text{free}}(\vec{\rho}) = \sum_{m'=-\infty}^{\infty} R^{\text{free}}_{m'}(\rho) e^{\imath m'\phi}, \tag{4.4}$$

where m' denotes the orbital quantum number. Wavefunctions with even m' only have even parity while those with odd m' only have odd parity. As in the three dimensions, the even and odd parity sub spaces are completely decoupled from each other and can be treated separately. $m = 0$ applies to scattering between two, two dimensional identical bosons or two non-identical particles, $m = 1$ to that between spin-polarized fermions, and so on. Putting Eq. (4.4) into Eq. (4.1), multiplying by $e^{-\imath m\phi}$ and doing the angular integral over ϕ, we obtain the radial Schrödinger equation

$$\left[-\frac{\hbar^2}{2\mu}\left(\frac{\partial^2}{\partial \rho^2} + \frac{1}{\rho}\frac{\partial}{\partial \rho} - \frac{m^2}{\rho^2}\right) + V_{\text{int}}(\rho)\right] R^{\text{free}}_m(\rho) = E R^{\text{free}}_m(\rho). \tag{4.5}$$

For $\rho > \rho_0$ (or $V_{\text{int}} = 0$), the two linearly independent solutions to the second order differential equation [Eq. (4.5)] are given by the regular cylindrical Bessel function $J_m(k\rho)$, which is well behaved at $\rho = 0$, and the irregular cylindrical Neumann function $N_m(k\rho)$,

which diverges at $r = 0$. The outer radial solution can be written as

$$R_m^{\text{free}(>)}(\rho) = A_m(J_m(k\rho) - \tan\delta_m(k) N_m(k\rho)), \tag{4.6}$$

where $A_m(k)$ denotes the normalization constant and $\delta_m(k)$ the energy dependent phase-shift accumulated in the region $\rho < \rho_0$.

Since the potential is neglected for $\rho > \rho_0$, no further phase is accumulated beyond $\rho = \rho_0$. The phase shifts $\delta_m(k)$ can be determined by imposing the following two continuity conditions at $\rho = \rho_0$,

$$R_m^{\text{free}(<)}(\rho_0) = R_m^{\text{free}(>)}(\rho_0) \tag{4.7}$$

and

$$\left(\frac{\partial R_m^{\text{free}(<)}(\rho)}{\partial \rho}\right)_{\rho=\rho_0} = \left(\frac{\partial R_m^{\text{free}(>)}(\rho)}{\partial \rho}\right)_{\rho=\rho_0}. \tag{4.8}$$

The inner solutions $R_m^{\text{free}(<)}(\rho)$ depend on V_{int}. For two dimensional s-wave scattering ($m = 0$), the phase shift $\delta_0(k)$ determines the two dimensional energy-dependent scattering length $a_0(k)$ [102],

$$a_0(k) = \frac{2}{k}\exp\left[\frac{\pi}{2}\cot\delta_0(k) - \gamma\right], \tag{4.9}$$

where γ denotes Euler's constant. The energy-dependent scattering length $a_0(k)$, which is always greater or equal to zero, is defined such that the scattering wave function has a node at $\rho = a_0(k)$. The unusual functional form of $a_0(k)$, i.e., the exponential dependence on the phase shift, is a direct consequence of the logarithmic dependence of $N_m(k\rho)$ on $k\rho$,

$$N_0(k\rho) \approx \frac{2}{\pi}[\ln(k\rho/2) + \gamma] \tag{4.10}$$

for $k\rho \to 0$. For higher partial waves, we define generalized energy-dependent scattering lengths $a_m(k)$ [67], which have dimensions of (length)^{2m}, as

$$a_m(k) = -\frac{\tan(\delta_m(k))}{k^{2m}} \frac{\Gamma(m)\Gamma(m+1)2^{2m}}{\pi}. \tag{4.11}$$

Since $a_1(k)$ has dimensions of (length)^2, we refer to it as scattering area. Energy-independent generalized scattering lengths a_m are readily defined through

$$a_m = \lim_{k\to 0} a_m(k). \tag{4.12}$$

4.1.2 Derivation of pseudopotential

To derive two dimensional zero range potentials, we assume that the atom-atom potential $V_{\rm int}(\rho)$ depends only on the distance ρ between the two atoms, that is, we neglect any angular dependence that may arise from spin-dependent interactions. The radial Schrödinger equation in the relative coordinate is then given by Eq. (4.5). We now derive m-dependent two dimensional zero range pseudopotentials, $V_{\rm int}(\rho) = V_m^{\rm ps}(\rho)$, which reproduce the low-energy observables of a shape-dependent short-range potential.

We follow the δ-shell procedure illustrated in detail for the one dimensional case. We write the pseudopotential $V_m^{\rm ps}(\rho)$ in terms of a δ-shell of radius ρ_0 and a yet to be determined operator $\hat{O}_m(\rho)$ [65],

$$V_m^{\rm ps}(\rho) = \{\delta(\rho-\rho_0)\hat{O}_m(\rho)\}_{\rho_0\to 0}. \tag{4.13}$$

The solutions to Eq. (4.5) for $V_{\rm int}(\rho) = V_m^{\rm ps}(\rho)$ can be written in terms of the cylindrical Bessel functions $J_m(k\rho)$ and $N_m(k\rho)$. For $\rho < \rho_0$, only J_m, which is regular at the origin,

contributes,

$$R_m^{\text{free}(<)}(\rho) = B_m J_m(k\rho). \tag{4.14}$$

Since $V_{\text{int}}(\rho) = V_m^{\text{ps}}(\rho) = 0$ for $\rho > \rho_0$, the wave function is given by Eq.(4.6) [as in the one dimensional case, the δ-shell introduces a phase shift $\delta_m(k)$ of the m^{th} partial]. In Eq. (4.14), B_m denotes a constant to be determined below.

Imposing continuity of the wave function $R_m^{\text{free}}(\rho)$ at $\rho = \rho_0$, that is, requiring $R_m^{\text{free}(>)}(\rho_0) = R_m^{\text{free}(<)}(\rho_0)$, allows B_m to be expressed in terms of A_m. Integrating the Schrödinger equation from $\rho = \rho_0 - \epsilon$ to $\rho_0 + \epsilon$ and then taking the limit $\epsilon \to 0$, results in

$$\frac{\hbar^2}{2\mu}\left[\frac{\partial}{\partial\rho}R_m^{\text{free}(>)}(\rho) - \frac{\partial}{\partial\rho}R_m^{\text{free}(<)}(\rho)\right]_{\rho=\rho_0} = \hat{O}_m(\rho_0)R_m^{\text{free}(>)}(\rho_0). \tag{4.15}$$

As in the one dimensional case, the derivative of the wavefunction is discontinuous at $\rho = \rho_0$ since the interaction potential $V_m^{\text{ps}}(\rho)$ is infinite at $\rho = \rho_0$. The discontinuity of the derivative is given by Eq. (4.15). Plugging Eqs. (4.14) and (4.6) into Eq. (4.15) and taking $k\rho_0 \ll 1$ determines the operator $\hat{O}_m(\rho_0)$, and hence the pseudopotential $V_m^{\text{ps}}(\rho)$. For $m = 0$, we find [67]

$$V_0^{\text{ps}}(\rho) = \left\{ \frac{-\frac{\hbar^2}{\mu}\tan(\delta_0(k))}{\left(1 - \frac{2\tan(\delta_0(k))}{\pi} f_0(k,\rho)\right)\pi\rho} \frac{\partial}{\partial\rho}\rho\,\delta(\rho - \rho_0) \right\}_{\rho_0 \to 0}, \tag{4.16}$$

where $f_0(k,\rho) = 1 + \gamma + \ln(k\rho/2)$. The explicit k dependence of the $m = 0$ zero range

potential drops out when $V_0^{\rm ps}(\rho)$ is written in terms $a_0(k)$,

$$V_0^{\rm ps}(\rho)=\left\{\frac{\hbar^2}{2\mu\left(\ln\left(\frac{\rho}{a_0(k)}\right)+1\right)\rho}\frac{\partial}{\partial\rho}\rho\,\delta(\rho-\rho_0)\right\}_{\rho_0\to 0}, \tag{4.17}$$

where the energy dependence enters only through the energy dependent scattering length $a_0(k)$. The prefactor in the pseudopotential contains $\ln a_0(k)$ [recall $a_0(k)>0$], and can take both positive and negative values. The pseudopotential can thus be either effectively repulsive or effectively attractive. Our s-wave pseudopotential agrees with the Λ potential derived in Ref. [103] if one sets Λ equal to k (see also Ref. [104]). The boundary condition at $\rho=0$ corresponding to the pseudopotential $V_0^{\rm ps}(\rho)$ is

$$\left[\frac{\rho\frac{\partial R_0^{\rm free(>)}(\rho)}{\partial\rho}}{R_0^{\rm free(>)}(\rho)-\rho\frac{\partial R_0^{\rm free(>)}(\rho)}{\partial\rho}\left[f_0(k,\rho)-1\right]}\right]_{\rho\to 0}=\frac{-1}{\gamma+\ln(\frac{ka_0(k)}{2})}, \tag{4.18}$$

which simplifies to

$$\left[\frac{\rho\ln(\frac{\rho}{a_0(k)})\frac{\partial R_0^{\rm free(>)}(\rho)}{\partial\rho}}{R_0^{\rm free(>)}(\rho)}\right]_{\rho\to 0}=1. \tag{4.19}$$

As expected there is no explicit k dependence in the boundary condition. In Sec. 4.2, we use Eq. (4.19) to develop a coupled channel zero range model for two dimensional scattering.

For $m > 0$, a straightforward yet somewhat tedious calculation gives [67]

$$V_m^{\mathrm{ps}}(\rho,k) = \left\{ \frac{-\frac{\hbar^2[\Gamma(m+1)]^2\tan(\delta_m(k))}{\mu(2m)!\pi}\left(\frac{2}{k}\right)^{2m}\frac{\partial^{2m}}{\partial\rho^{2m}}\rho^m\delta(\rho-s)}{(1+\frac{\tan(\delta_m(k))}{\pi}f_m(k,\rho))\rho^{m+1}} \right\}_{s\to 0}, \tag{4.20}$$

where

$$f_m(k,\rho) = \bar{\psi}(m) - 2\ln\left(\frac{k\rho}{2}\right) - \sum_{r=0}^{r=2m-1}\frac{2}{2m-r}. \tag{4.21}$$

Here, $\bar{\psi}(m) = \psi(1)+\psi(m+1)$, where ψ denotes the digamma function.

As written in Eq. (4.20), the $m > 0$ pseudopotential leads, despite the regularization operator, to divergences at $\rho \to 0$ if the energy-dependent coefficients C_m and D_m of the ρ^{-m} and $\rho^m\ln(\rho)$ terms in the expansion of the eigenfunction sought differ from the corresponding coefficients c_m and d_m of the expansion of the irregular free particle solution $N_m(k\rho)$. To cure this divergence, the right hand side of Eq. (4.20) has to be multiplied by $d_m C_m/(c_m D_m)$, resulting in a pseudopotential that has to be determined self-consistently.

For example, the ratio C_m/D_m for the harmonic oscillator eigenfunctions with non integer quantum number χ [see Eq. (4.30)] is given by

$$\frac{C_m}{D_m} = (-1)^{m+1}\frac{1}{2}\frac{\Gamma(m)\Gamma(m+1)\Gamma(-\chi-m)}{2\Gamma(-\chi)}. \tag{4.22}$$

The ratio c_m/d_m for the free particle Neumann function $N_m(k\rho)$, in contrast, is given by

$$\frac{c_m}{d_m} = \frac{1}{2}\left(\frac{2}{k}\right)^{2m}\Gamma(m)\Gamma(m+1). \tag{4.23}$$

Combining Eqs. (4.22) and (4.23), we obtain

$$\frac{C_m d_m}{D_m c_m} = (-1)^{m+1} \left(\frac{k}{2}\right)^{2m} \frac{\Gamma(-\chi - m)}{2\Gamma(-\chi)}. \tag{4.24}$$

Hence the pseudopotential corresponding to the m^{th} partial wave ($m > 0$) for two interacting particles in two dimensions under radially symmetric external harmonic confinement is given by

$$V_m^{\text{ps}}(\rho, k) = (-1)^{m+1} \left(\frac{k}{2}\right)^{2m} \frac{\Gamma(-\chi - m)}{2\Gamma(-\chi)} \times \left\{ \frac{-\frac{\hbar^2[\Gamma(m+1)]^2 \tan(\delta_m(k))}{\mu(2m)!\pi} \left(\frac{2}{k}\right)^{2m}}{(1 + \frac{\tan(\delta_m(k))}{\pi} f_m(k,\rho))\rho^{m+1}} \frac{\partial^{2m}}{\partial \rho^{2m}} \rho^m \delta(\rho - \rho_0) \right\}_{\rho_0 \to 0}. \tag{4.25}$$

Interestingly, such a self-consistency condition is not needed for systems with odd dimensionality.

The bound state energies E of the pseudopotentials $V_m^{\text{ps}}(\rho)$ can be determined through analytic continuation [65]. For $m = 0$, we recover the well known expression for the zero range binding energy E [105],

$$E = \frac{-\hbar^2}{2\mu(a_0(k))^2} 4\exp(-2\gamma). \tag{4.26}$$

For $m > 0$, the binding energies E are given by

$$E = \frac{-2\hbar^2}{\mu[-\imath(-1)^m a_m(k)]^{1/m}} \left(\frac{\Gamma(m)\Gamma(m+1)}{\pi}\right)^{1/m}. \tag{4.27}$$

The occurrence of an "$\imath$" in Eq. (4.27) appears odd at first sight. This puzzle is resolved by noting that the two dimensional generalized energy-dependent scattering

lengths $a_m(k)$ with $m > 0$ are, in contrast to the one dimensional and three dimensional counterparts, complex. Consequently, the binding energies E are determined by those $a_m(k)$ [106, 107] for which the real part vanishes.

We now illustrate for a square well potential $V_{\rm SW}$ with range ρ_0 and depth V_0 that Eq. (4.27) predicts the binding energy E of the two dimensional dimer accurately. First, we determine the generalized scattering area $a_1(k)$ analytically [see Eq. (C.1) for $m = 1$]. Dashed lines in Fig. 4.1(b) show the real part of $a_1(k)$, $\Re(a_1(k))$, while solid lines show the imaginary part of $a_1(k)$, $\Im(a_1(k))$, as a function of E for a square well potential with $V_0 = 9E_0$, where $E_0 = \hbar^2/(\mu\rho_0^2)$. $\Im(a_1(k))$ vanishes for positive energies, and is non-zero for negative E. $\Re(a_1(k))$ changes from negative to positive values at $E \approx -4.38E_0$. The corresponding imaginary part of $a_1(k)$ at this energy value determines the binding energy E, Eq. (4.27), in the zero range approximation. Asterisks in Fig. 4.1(a) show the resulting E for various well depths V_0. For comparison, a solid line shows the $m = 1$ binding energy for $V_{\rm SW}(\rho)$. The energy for $V_{\rm SW}(\rho)$ (solid line) and that determined from the energy-dependent scattering area via Eq. (4.27) (asterisks) agree, by construction, to many digits.

4.1.3 Atoms in a harmonic trap

We now use the proposed pseudopotentials to determine the eigenspectrum of two atoms in two dimensions under external harmonic confinement. The radial Schrödinger equation for this system is given by

$$\left[-\frac{\hbar^2}{2\mu}\left(\frac{\partial^2}{\partial\rho^2}+\frac{1}{\rho}\frac{\partial}{\partial\rho}-\frac{m^2}{\rho^2}\right)+V_{\rm int}(\rho)+V_{\rm ext}(\rho)\right]R_m(\rho)=ER_m(\rho), \tag{4.28}$$

where $V_{\rm ext}(\rho)=\mu\omega^2\rho^2/2$ is the external two dimensional harmonic trapping potential. The solutions for $\rho < \rho_0$ and $\rho > \rho_0$ are proportional to the confluent hypergeometric

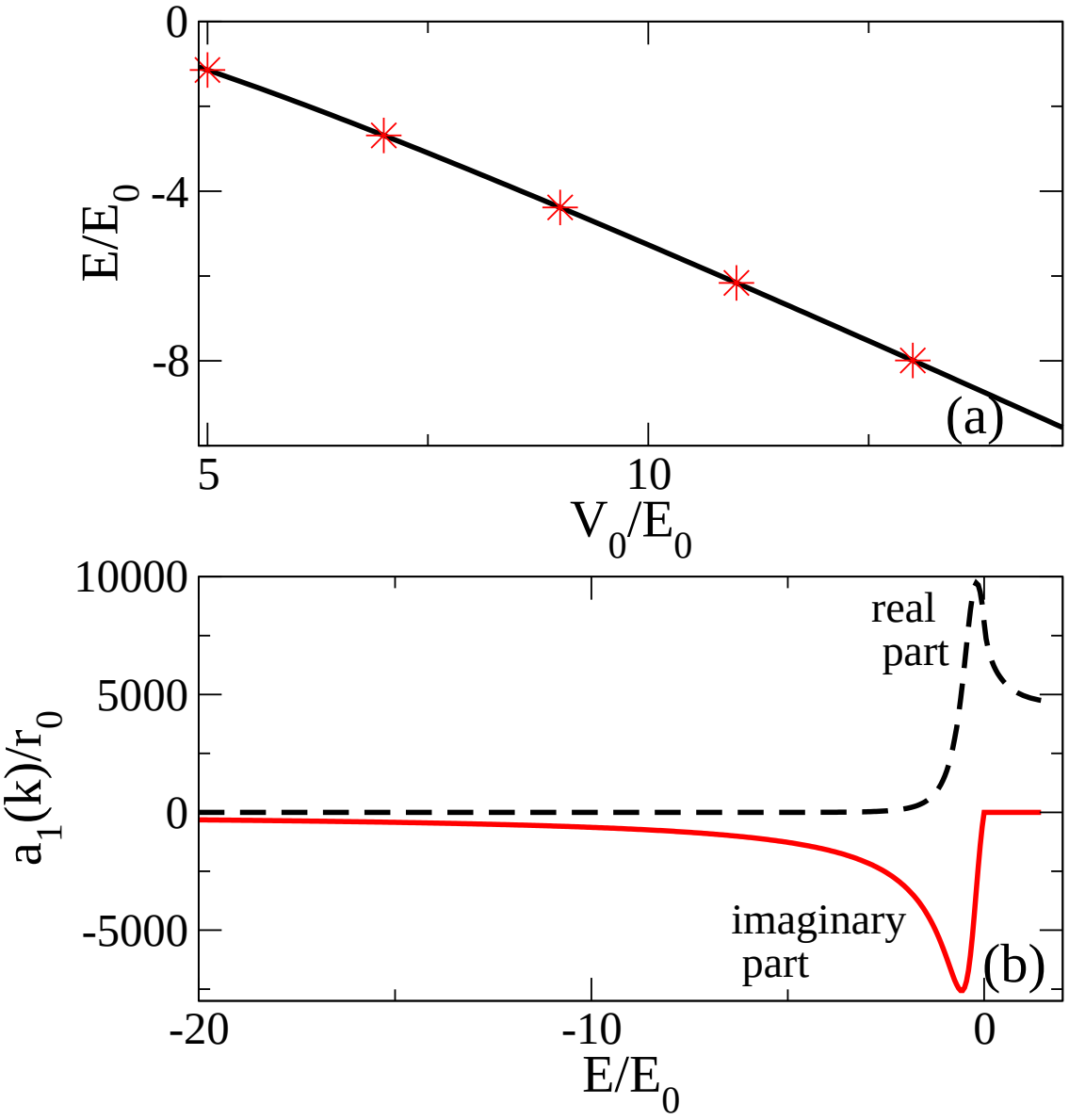

Figure 4.1: (a) Binding energy E for $m = 1$ as a function of V_0/E_0, where $E_0 = \frac{\hbar^2}{\mu\rho_0^2}$. Asterisks show E predicted by the zero range potential, Eq. (4.27), and evaluated self-consistently for $V_{\rm SW}$ with $\rho_0 = 1$. The solid line shows E for two particles interacting through $V_{\rm SW}$ with $\rho_0 = 1$. (b) Real (dashed line) and imaginary (solid line) parts of $a_1(k)$ as a function of E/E_0 for $V_0 = 9E_0$.

functions M and U, i.e.,

$$R_m^{(<)}(\rho) \propto \rho^m \exp\left(-\frac{\rho^2}{2a_{\rm ho}^2}\right) M\left(-\chi, m+1, \frac{\rho^2}{a_{\rm ho}^2}\right) \tag{4.29}$$

and

$$R_m^{(>)}(\rho) \propto \rho^m \exp\left(-\frac{\rho^2}{2a_{\rm ho}^2}\right) U\left(-\chi, m+1, \frac{\rho^2}{a_{\rm ho}^2}\right), \tag{4.30}$$

where χ denotes a non-integer quantum number, $E_{m\chi} = (2\chi + 1 + m)\hbar\omega$. Following steps similar to those detailed in Sec. 2.2, we derive an implicit eigenequation for the eigenenergies $E_{m\chi}$,

$$\begin{aligned} &(-1)^{m+1}\frac{\Gamma(-\chi-m)}{\Gamma(-\chi)}\sum_{r=0}^{m-1}\frac{(-\chi-m)_r(-1)^{m-r}}{(1-m)_r r!(2m-2r)!!} \\ &= \frac{\ln\left(\chi+\frac{m+1}{2}\right)-\psi(-\chi)}{\Gamma(m)\Gamma(m+1)} + \frac{a_{\rm ho}^{2m}}{a_m(k_{m\chi})}\frac{1}{\left(\chi+\frac{m+1}{2}\right)^m}, \end{aligned} \tag{4.31}$$

where $k_{m\chi} = \sqrt{2\mu E_{m\chi}}/\hbar$ and $(x)_r = x(x+1)\cdots(x+r-1)$ with $(x)_0 = 1$. Equation (4.31) contains the generalized *energy-dependent* two dimensional scattering length $a_m(k)$ evaluated at $k = k_{m\chi}$ and is valid for $m > 0$; for $m = 0$, the eigenenergies are given by

$$\ln\left(\frac{a_0(k_{0\chi})}{a_{\rm ho}}\right) + \frac{1}{2}\psi\left(\frac{1}{2} - \frac{E_{0\chi}}{2\hbar\omega}\right) - \psi(1) = 0. \tag{4.32}$$

Asterisks in Fig. 2.6 show the $m = 1$ eigenenergies for two particles interacting through the proposed zero range potential, Eq. (4.31), under harmonic confinement over a large range of zero-energy scattering areas a_1. For comparison, solid lines show the exact eigenenergies, determined semi-analytically, for two particles under harmonic confinement interacting through a square well potential with range $\rho_0 = 0.01a_{\rm ho}$. Figure 4.2 illustrates excellent agreement between the eigenenergies for two two dimensional par-

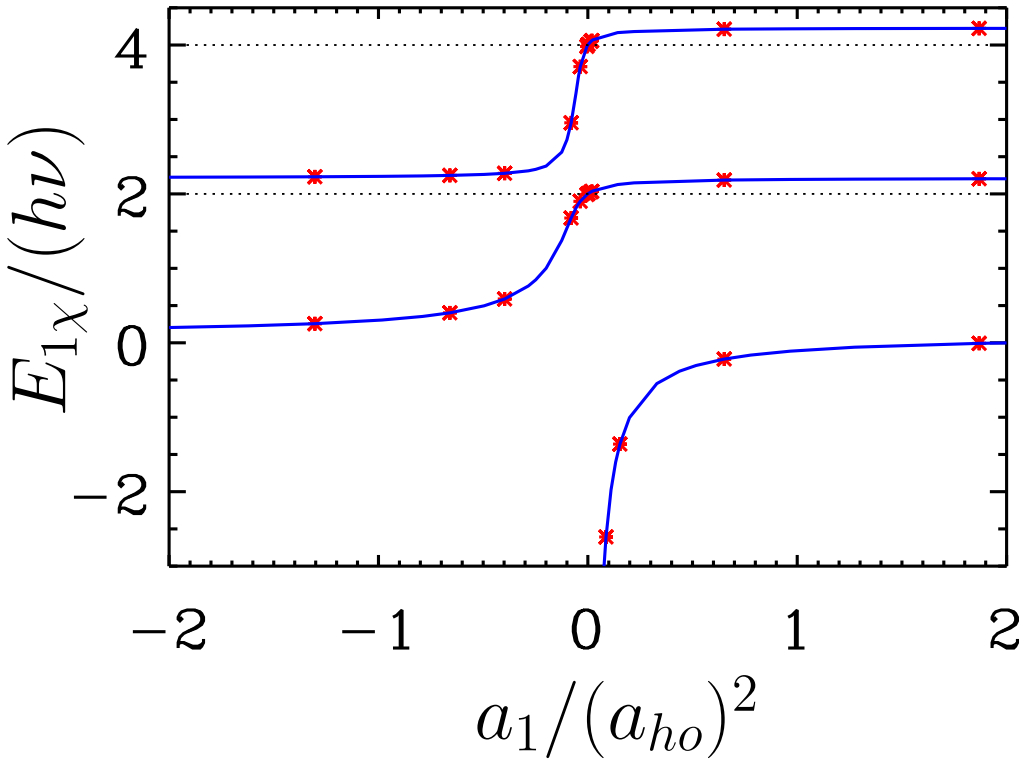

Figure 4.2: $E_{1\chi}$ as a function of the energy independent generalized scattering length a_1 for $m=1$ ($\omega=2\pi\nu$). Asterisks show $E_{1\chi}$, Eq. (4.31), for the energy-dependent pseudopotential $V_1^{\rm ps}(\rho)$ and solid lines show $E_{1\chi}$ for $V_{\rm SW}$ with $\rho_0=0.01a_{\rm ho}$. For comparison, horizontal dotted lines indicate the energy levels for $a_1=0$.

ticles interacting through the pseudopotential and those interacting through the square well potential. We find similar behaviors for higher partial waves.

4.1.4 Quasi two dimensional systems

So far in this section we have considered strictly two dimensional single channel potentials. As discussed in Ch. 1, advancements in trapping technology have led to the realization of quasi two dimensional systems [53]. In quasi two dimensional systems excitations along z are frozen out. The s-wave ($m = 0$) scattering wavefunction of a strictly two dimensional system can be written as [108, 109]

$$\psi_0^{2D}(\rho) = J_0(k\rho) - \overline{f}(k,\phi) H_0^{(1)}(k\rho), \tag{4.33}$$

where $H_0^{(1)}$ is the Hankel function of the first kind and $\overline{f}(k,\phi)$ is the scattering amplitude,

$$\overline{f}(k,\phi) = -\frac{\imath\pi/2}{\ln\left(\frac{k a_0^{2D}}{2}\right) + \gamma - \frac{\imath\pi}{2}}. \tag{4.34}$$

In this section we use the superscript $2D$ to distinguish the two and three dimensional wavefunctions and scattering lengths. The s-wave scattering wavefunction in a quasi two dimensional system can be written as [108]

$$\psi_0(\rho) = Q_n(z) J_0(k\rho) - \sum_{n'} Q_{n'}(z) \overline{f}_{nn'}(k_{n'},\phi) H_0^{(1)}(k_{n'}\rho), \tag{4.35}$$

where $Q_n(z)$ denote the one dimensional harmonic oscillator functions. If we naively assume that the system occupies the lowest harmonic oscillator orbital in the z-direction,

then in Eq. (4.35) we have $n = n' = 0$ and

$$\psi_0(\rho) = Q_0(z)J_0(k\rho) - Q_0(z)\overline{f}_{00}(k_0,\phi)H_0^{(1)}(k_0\rho), \tag{4.36}$$

where [108]

$$|\overline{f}_{00}|^2 = \frac{2\pi}{\pi^2 + \left(\sqrt{2\pi}\frac{a_z}{a_s} + \ln\left(\frac{B}{\pi k^2 a_z^2}\right)\right)^2} \tag{4.37}$$

and $B \approx 0.915$. Comparing $|\overline{f}_{00}|^2$ from Eq. (4.37) and $|\overline{f}(k,\phi)|^2$ from Eq. (4.34), we get a relationship between the two and three dimensional scattering lengths,

$$\frac{a_0^{2D}}{a_z} = \frac{2\sqrt{\pi}e^{-\gamma/2}}{\sqrt{B}} e^{-\sqrt{\frac{\pi}{2}}\frac{a_z}{a_s}}. \tag{4.38}$$

This expression does not account for the virtual excitations and is only approximate. A more accurate expression for a_0^{2D} in terms of a_s is given by [97, 110]

$$\frac{a_0^{2D}}{a_z} = \frac{1}{\sqrt{2}} \exp\left(\frac{\Phi(0)}{2} - \frac{\sqrt{\pi}a_z}{2a_s}\right), \tag{4.39}$$

where

$$\Phi(x) = 2 - \ln(1+x) + 2\sum_{k=1}^{\infty} \frac{(2k)!}{(2^k k!)^2}\left[\left(k+\frac{1}{2}\right)\ln\frac{x+k}{x+k+1} + 1\right] \tag{4.40}$$

and $\Phi(0) = 1.938$.

Figure 4.3 shows the two dimensional scattering length a_0^{2D} for a quasi two dimensional system as a function of the three dimensional scattering length a_s. Although a_s takes both positive and negative values, a_0^{2D} is always positive. The interaction strength for the two dimensional potential g_{2D} [108, 109, 97] that is used in the two dimensional

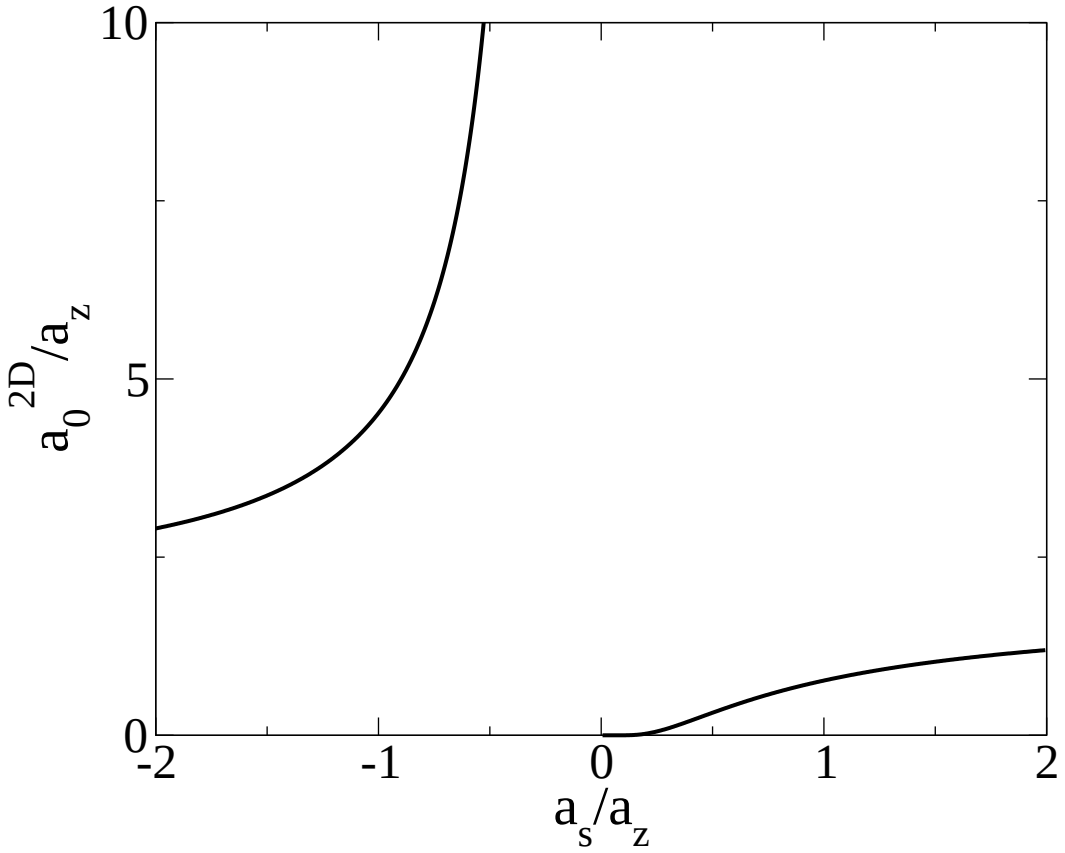

Figure 4.3: Two dimensional $m = 0$ scattering length a_0^{2D} in a quasi two dimensional system as a function of the three dimensional scattering length a_s [see Eq. (4.39)].

mean-field Gross-Pitaevskii equation is given by

$$g_{2D} = -\frac{\pi\hbar^2}{\mu \ln(k a_0^{2D})}. \tag{4.41}$$

Since the interaction strength contains $\ln(a_0^{2D})$, it can take both positive and negative values, allowing for both effectively attractive and effectively repulsive interactions.

4.2 Coupled channel treatment

4.2.1 Coupled channel scattering length

To describe the two-body physics across a two dimensional Feshbach resonance for two bosons or for two fermions with opposite spin, we develop a coupled channel zero range model for $m = 0$. The procedure is similar to that outlined in Ch. 3 for a three dimensional s-wave Feshbach resonance. In this section we consider $m = 0$ and omit the subscript "m". For $\rho > 0$, the wave function with components $R_{(1)}^{\text{free}}(\rho)$ and $R_{(2)}^{\text{free}}(\rho)$ satisfies the free particle Schrödinger equation in the relative coordinate,

$$\begin{pmatrix} \left[\frac{\hbar^2}{2\mu}(\frac{\partial^2}{\partial\rho^2} + \frac{1}{\rho}\frac{\partial}{\partial\rho}) + E\right] R_{(1)}^{\text{free}}(\rho) \\ \left[\frac{\hbar^2}{2\mu}(\frac{\partial^2}{\partial\rho^2} + \frac{1}{\rho}\frac{\partial}{\partial\rho}) + E - \epsilon\right] R_{(2)}^{\text{free}}(\rho) \end{pmatrix} = 0, \tag{4.42}$$

where ϵ denotes a detuning ($\epsilon \geq 0$), which can be changed, e.g., by varying the strength of an external magnetic field and subscripts "(1)" and "(2)" indicate channels one and two respectively. Since $R_{(1)}^{\text{free}}(\rho)$ satisfies the free particle Schrödinger equation it is given by [see Eq. (4.6)]

$$R_{(1)}^{\text{free}}(\rho) = A_m(J_m(k\rho) - \tan\delta_m(k) N_m(k\rho)). \tag{4.43}$$

We are interested in energies E in the range $0 < E < \epsilon$. Since E is less than the threshold energy ϵ of the closed channel (2), the wavefunction in channel two is given by

$$R^{\text{free}}_{(2)}(\rho) = F_m K_m(k\rho), \tag{4.44}$$

where F_m is a constant that can be determined through boundary conditions at $\rho = 0$ [see Eq. (4.45) below] and $K_m(k\rho)$ is the modified cylindrical Bessel function of the second kind. The two dimensional pseudopotential $V_0^{\text{ps}}(\rho)$ imposes a boundary condition at $\rho = 0$, which we parametrize as

$$\left[\begin{pmatrix} \ln(\rho/b_1) & \beta \\ \beta & \ln(\rho/b_2) \end{pmatrix} \begin{pmatrix} \rho \frac{\partial}{\partial \rho} R^{\text{free}}_{(1)}(\rho) \\ \rho \frac{\partial}{\partial \rho} R^{\text{free}}_{(2)}(\rho) \end{pmatrix} \right]_{\rho \to 0} = \begin{pmatrix} R^{\text{free}}_{(1)}(\rho) \\ R^{\text{free}}_{(2)}(\rho) \end{pmatrix}_{\rho \to 0}. \tag{4.45}$$

The coupling between the two channels is characterized by the dimensionless parameter β. To ensure a divergence-free treatment, Eq. (4.45) takes this coupling parameter to be proportional to the *derivative* of the wave function components, and not, as done in three dimensions [96], to be proportional to the wave function components themselves. In the absence of coupling ($\beta = 0$), Eq. (4.45) reduces to the single channel boundary conditions given in Eq. (4.19). The scattering length $a^{CC}(E,\epsilon)$ predicted by Eqs. (4.42) and (4.45) is

$$a^{CC}(E,\epsilon) = b_1 \exp\left\{ -\beta^2 / \left[\gamma + \frac{1}{2} \ln\left(\frac{\mu b_2^2}{2\hbar^2}(\epsilon - E) \right) \right] \right\}. \tag{4.46}$$

To determine the behavior of the scattering length $a^{CC}(E,\epsilon)$ in the vicinity of the resonance as a function of the magnetic field strength B, we Taylor-expand $a^{CC}(E,\epsilon)$ about the resonance position ϵ_R, which is given by the binding energy E of the strongly closed molecular channel, $\epsilon_R = 2\exp(-2\gamma)\hbar^2/(\mu b_2^2)$. We find a simple functional form

for $a^{CC}(E=0,B)$ in terms of the background scattering length A_{bg}, the resonance width Δ and the resonance position B_R,

$$a^{CC}(E=0,B)=A_{bg}\exp\left(-\frac{\Delta}{B-B_R}\right), \tag{4.47}$$

where $A_{bg}=b_1$, $B_R=\epsilon_R/\gamma$ and $\Delta=2\beta^2\epsilon_R/\gamma_M$ (γ_M denotes the difference in magnetic moment between atoms in the open and closed channel). The functional dependence of the two dimensional coupled channel scattering length a^{CC} on B near a resonance is distinctly different from that of the three dimensional counterpart. In principle, the parameters b_1, b_2 and β can be determined by comparing Eq. (4.47) with experimental data for a specific two dimensional Feshbach resonance. Since no such data exist to date, the inset of Fig. 4.4 illustrates the behavior of a^{CC} as a function of ϵ for $E=0$, $a_1=0.5a_{\rm ho}$, $a_2=0.05a_{\rm ho}$ and $\beta=0.1$. The scattering length a^{CC} changes from infinity to zero at the resonance value ϵ_R, which is indicated by a vertical dotted line.

4.2.2 Coupled channel system under confinement

We now consider two particles interacting through the two dimensional coupled channel $m=0$ zero range pseudopotential under radially symmetric external harmonic confinement. For $\rho>0$, the wave function with components $R_{(1)}(\rho)$ and $R_{(2)}(\rho)$ satisfies the harmonic oscillator Schrödinger equation in the relative coordinate,

$$\begin{pmatrix} \left[\frac{\hbar^2}{2\mu}(\frac{\partial^2}{\partial\rho^2}+\frac{1}{\rho}\frac{\partial}{\partial\rho})-\frac{1}{2}\mu\omega^2\rho^2+E\right]R_{(1)}(\rho) \\ \left[\frac{\hbar^2}{2\mu}(\frac{\partial^2}{\partial\rho^2}+\frac{1}{\rho}\frac{\partial}{\partial\rho})-\frac{1}{2}\mu\omega^2\rho^2+E-\epsilon\right]R_{(2)}(\rho) \end{pmatrix}=0. \tag{4.48}$$

The boundary condition at $\rho=0$ is given by Eq. (4.45) without the superscript "free", since this is for the trapped system. We find an implicit eigenequation [67] for the

eigenenergies E_n, $E_n < \epsilon$, of the coupled channel zero range model for two particles under harmonic confinement with $m = 0$,

$$\beta^2 \left\{ \ln\left(\frac{b_1}{a_{\rm ho}}\right) + \frac{1}{2}\psi\left(\frac{1}{2} - \frac{E_n}{2\hbar\omega}\right) - \psi(1) \right\}^{-1} = \left\{ \ln\left(\frac{b_2}{a_{\rm ho}}\right) + \frac{1}{2}\psi\left(\frac{1}{2} - \frac{E_n - \epsilon}{2\hbar\omega}\right) - \psi(1) \right\}. \tag{4.49}$$

Figure 4.5 shows the eigenenergies E_n as a function of ϵ for $b_1 = 0.5a_{\rm ho}$, $b_2 = 0.05a_{\rm ho}$ and three different values of β, i.e., $\beta = 0.03$ (solid lines), 0.1 (dotted lines) and $\beta = 0.3$ (dashed lines). The non-vanishing coupling leads to a series of energy level crossings at $\epsilon \approx \epsilon_R$, which become narrower as the coupling β decreases. For higher-lying states, i.e., for larger E_n, the resonance of the energy-dependent scattering length $a^{CC}(\epsilon, E)$, Eq. (4.46), moves to larger ϵ values. This explains why the energy level crossings move to larger ϵ for higher n. The energy of the state $n = 1$ for $\epsilon < \epsilon_R$ corresponds to the binding energy of the open channel, i.e., of channel (1). A two dimensional coupled channel square-well system (see Ref. [95] for the three dimensional analog) reproduces the results obtained for our proposed coupled channel zero range system.

Our coupled channel model leads to a mixing of the strongly closed molecular channel $R_{(2)n}(\rho)$ and the open channel $R_{(1)n}(\rho)$. To quantify the admixture of the strongly closed molecular level across the resonance, we define the molecular fraction P_n [95],

$$P_n = \int |R_{(2)n}|^2 \rho\, d\rho \Big/ \left[\int \left(|R_{(1)n}|^2 + |R_{(2)n}|^2 \right) \rho\, d\rho \right]. \tag{4.50}$$

The main part of Fig. 4.4 shows P_n for $b_1 = 0.5a_{\rm ho}$, $b_2 = 0.05a_{\rm ho}$ and different β values as a function of ϵ; a solid line shows P_0 for $\beta = 0.1$, and dotted lines show P_1 for $\beta = 0.03$, 0.1 and 0.3. The molecular fraction P_0 is close to one for small ϵ, and drops to zero as ϵ is swept across the resonance. This indicates that the character of the $n = 0$ state

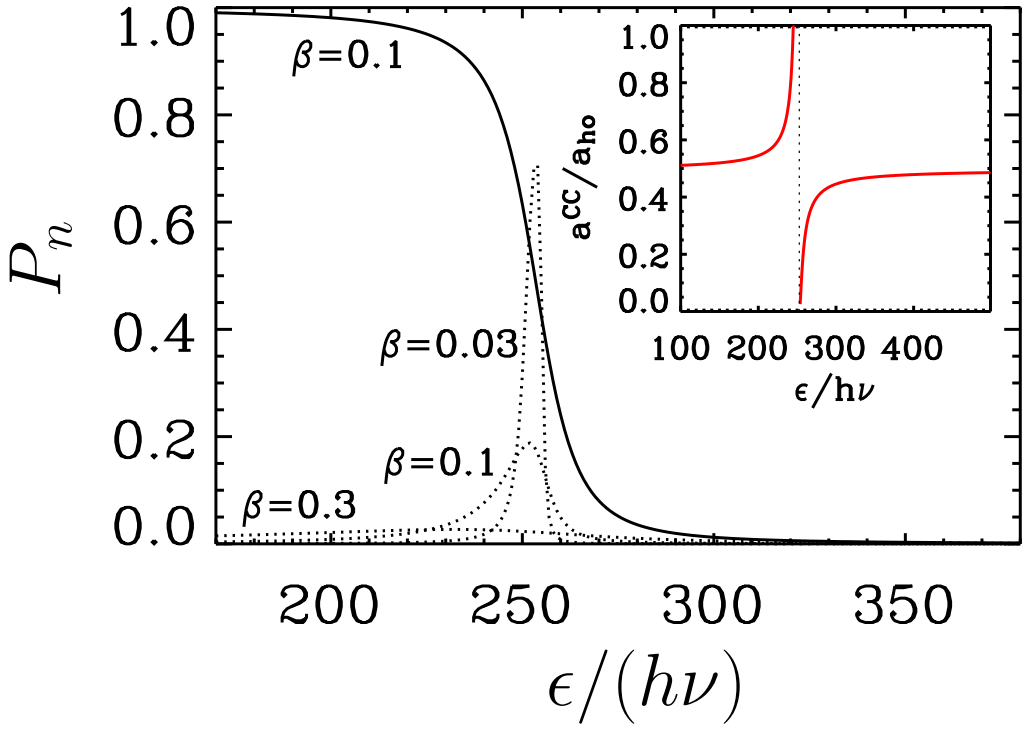

Figure 4.4: Molecular fractions P_0 (solid line) and P_1 (dotted lines), Eq. (4.50), for $b_1 = 0.5a_{\rm ho}$, $b_2 = 0.05a_{\rm ho}$ and different coupling constants β as a function of ϵ. Inset: 2D scattering length $a^{CC}(E,\epsilon)$ as a function of ϵ for $E = 0$, $b_1 = 0.5a_{\rm ho}$, $b_2 = 0.05a_{\rm ho}$ and $\beta = 0.1$.

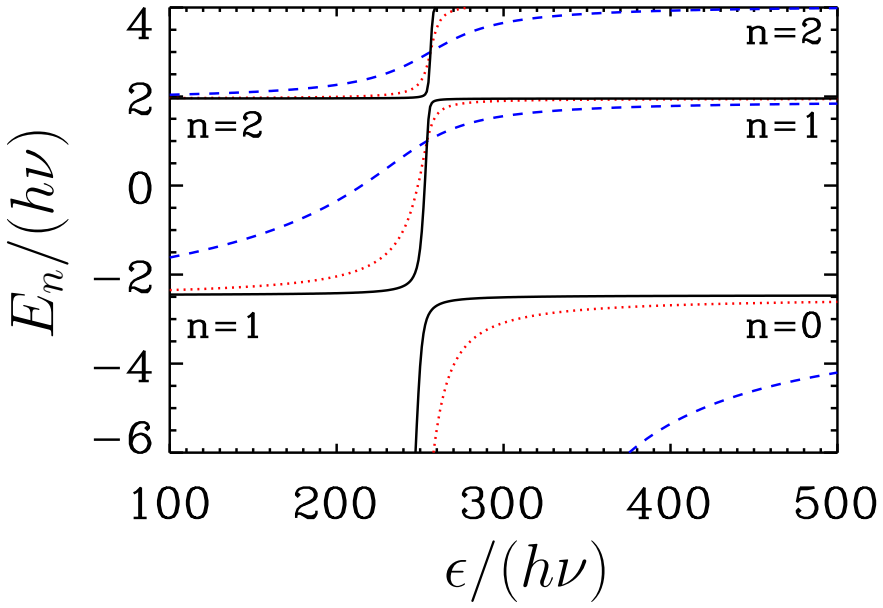

Figure 4.5: Eigenenergies E_n, Eq. (4.49), for $b_1 = 0.5a_{\rm ho}$, $b_2 = 0.05a_{\rm ho}$ and three different values of β, i.e., $\beta = 0.03$ (solid lines), 0.1 (dotted lines) and 0.3 (dashed lines) as a function of ϵ.

changes from "strongly closed molecular" to "weakly closed molecular" as ϵ changes from $\epsilon < \epsilon_R$ to $\epsilon > \epsilon_R$. The molecular fraction of the $n = 1$ state is close to zero away from resonance for all coupling strengths considered. Near resonance, however, P_1 depends on β. For weak coupling, P_1 approaches one on resonance. For strong coupling, in contrast, P_1 is comparatively small as shown in Fig. 4.4 for $\beta = 0.3$. This suggests that the two dimensional analog of the BEC-BCS crossover can be best studied utilizing two dimensional Feshbach resonances with strong coupling for which the admixture of the strongly closed molecular channel is small. Similar behavior is found for three dimensional systems [111].

4.3 Conclusions

This chapter derives a series of two dimensional zero range pseudopotentials, which describe the low-energy scattering of two particles with partial wave m. The boundary condition implied by the $m = 0$ pseudopotential is then used to develop an analytically solvable coupled channel model, which describes the physics across a two dimensional Feshbach resonance. The predicted dependence of the effective two dimensional scattering length a^{CC} on the strength B of the external magnetic field, Eq. (4.47), may prove useful in analyzing experimental data for quasi-two dimensional Bose gases or two-component Fermi gases. We also determine the binding energy of two dimensional dimers, which can be measured with present-day technology by utilizing optical lattices with doubly-occupied lattice sites in the no-tunneling regime [14], across a Feshbach resonance.

Chapter 5

Anisotropic two body systems in three dimensions

In this chapter we treat anisotropic interactions. All Hamiltonian, potentials, wavefunctions and phase shifts are three dimensional. Section 5.1 obtains the coupled channel energy dependent K-matrix elements $K_{lm}^{l'm'}(k)$. Section 5.2 provides a detailed description of two aligned dipoles interacting through a shape dependent finite range model potential in free space and under harmonic confinement. Section 5.3 presents a zero range pseudopotential treatment. Section 5.3.1 introduces the pseudopotential, Sec. 5.3.2 derives the eigenequation for the two-dipole system under confinement and Sec. 5.3.3 discusses the eigenspectrum. Section 5.4 develops a zero range pseudopotential treatment for anisotropic interaction potentials applicable to cylindrically symmetric harmonic confinement: Section 5.4.1 derives the pseudopotential, Sec. 5.4.2 derives the eigenequation, and Secs 5.4.3 and 5.4.4 discuss the eigenspectrum.

5.1 Scattering for coupled channel partial waves

Chapter 3 considered spherically symmetric model interaction potentials, while this chapter considers scattering by anisotropic interaction potentials [112]. Unlike the spherically symmetric interaction potentials that depend only on the distance between the two particles, anisotropic potentials have an angle dependence, i.e., the interaction potential between the two particles depends on the angle between the relative distance vector and some symmetry breaking axis. For two dipoles aligned along the z axis, e. g., the interaction potential depends on the angle between the relative distance vector and the z-axis.

The Schrödinger equation for two particles in three dimensions in the relative coordinate $\vec{r}$ is given by Eq. (3.1). For an anisotropic interaction potential, the solution to Eq. (3.1) can be decomposed into different partial waves,

$$\Psi^{\text{free}}(\vec{r}) = \sum_{l'=0}^{\infty} \sum_{m'=-l'}^{l'} c_{l'm'} R^{\text{free}}_{l'm'}(r) Y_{l'm'}(\theta,\phi), \tag{5.1}$$

where $R^{\text{free}}_{l'm'}(r)$ is a function of r only. Putting Eq. (5.1) into Eq. (3.1), multiplying by $Y^*_{lm}(\theta,\phi)$ and performing the angular integral yields

$$\left[-\frac{\hbar^2}{2\mu}\left(\frac{\partial^2}{\partial r^2}+\frac{2}{r}\frac{\partial}{\partial r}-\frac{l(l+1)}{r^2}\right)-E\right] c_{lm} R^{\text{free}}_{lm}(r) = \sum_{l'=0}^{\infty} \sum_{m'=-l'}^{l'} c_{l'm'} V^{l'm'}_{lm}(r) R^{\text{free}}_{l'm'}(r), \tag{5.2}$$

where

$$V^{l'm'}_{lm}(r) = \int Y^*_{lm}(\theta,\phi) V_{\text{int}}(\vec{r}) Y_{l'm'}(\theta,\phi) d\Omega. \tag{5.3}$$

Due to the angle dependence of the interaction potential, the angular momentum is not conserved during the scattering process. This results in a coupling of different partial waves and consequently non-vanishing matrix elements $V^{l'm'}_{lm}$ for $lm \neq l'm'$. We

assume that there exists a distance r_0 such that the interaction potential $V_{\rm int}(\vec{r})$ can be neglected for all $r > r_0$. The solution to Eq. (5.2) for $r > r_0$ is then given by

$$R_{lm}^{\rm free(>)}(r) = \aleph(k) \left[j_l(kr) - \sum_{l',m'} K_{lm}^{l'm'}(k) n_l(kr) \right], \tag{5.4}$$

where $\aleph(k)$ denotes the normalization constant and the K-matrix elements $K_{lm}^{l'm'}(k)$ are determined by the energy dependent phase shifts $\delta_{lm}^{l'm'}(k)$, i. e., $K_{lm}^{l'm'}(k) = \tan\delta_{lm}^{l'm'}(k)$ [112, 113]. As in the single channel case, the phase shifts are determined by requiring that the wavefunction and its first derivative are continuous at $r = r_0$. The K-matrix is symmetric, i. e.,

$$K_{lm}^{l'm'}(k) = K_{l'm'}^{lm}(k). \tag{5.5}$$

For potentials that have even parity, like the interaction potential between two aligned dipoles, the K-matrix is block diagonal and each block can be treated separately. Even partial waves are scattered only into even partial waves and odd partial waves are scattered only into odd partial waves.

5.2 Dipole-dipole interaction: Finite range shape dependent potential

This section determines the scattering properties of two aligned dipoles, either identical bosons or identical fermions, as functions of the dipole moment and the scattering energy. Sequences of scattering resonances are found. The first types of resonances (termed B_1 and F_1 for identical bosons and fermions, respectively) are associated with the pulling in of a bound state in the lowest adiabatic potential curve, while the second types (termed B_2 and F_2 for identical bosons and fermions, respectively) are associ-

ated with the manifold of excited adiabatic potential curves. The resonances of type B_1 have previously, due to the absence of a barrier in the lowest adiabatic potential curve, been termed potential resonances, while those of type B_2 have been termed shape resonances [114]. Following this nomenclature, resonances of types F_1 and F_2 are shape resonances. The behavior of identical fermions differs, in certain respects, distinctly from that of identical bosons. Contrary to our finding, Ref. [27] reported the absence of scattering resonances for identical fermions. The resonance positions are correlated with the appearance of bound states in free-space and trapped systems. The nature of the resonances is further elucidated by analyzing the bound state wavefunctions.

Neglecting hyperfine interactions and treating each dipole as a point particle, the interaction potential between two dipoles aligned along the z-axis is for large interparticle distances r given by $V_{\rm dd}$,

$$V_{\rm dd}(\vec{r}) = d^2 \frac{(1-3\cos^2\theta)}{r^3}, \tag{5.6}$$

where d denotes the dipole moment. We model the short-range interaction $V_{\rm sr}$ between the dipoles by a simplistic hardwall potential,

$$V_{\rm sr}(\vec{r}) = \begin{cases} \infty & \text{for} \quad r < r_c \\ 0 & \text{for} \quad r > r_c, \end{cases} \tag{5.7}$$

so that the full model potential is given by

$$V_{\rm model}(\vec{r}) = \begin{cases} V_{\rm sr}(\vec{r}) & \text{for} \quad r < r_c \\ V_{\rm dd}(\vec{r}) & \text{for} \quad r > r_c. \end{cases} \tag{5.8}$$

The boundary condition imposed at r_c can be thought of as introducing a short-range K-matrix. Beyond r_c, the interaction is purely dipolar; this long-range interaction modifies the short-range K-matrix [27]. The characteristic length scale of $V_{\rm sr}$ is given by the hardcore radius r_c and that of $V_{\rm dd}$ by the dipole length D_*, $D_* = \mu d^2/\hbar^2$. The corresponding natural energy scales are given by E_{r_c} and E_{D_*}, respectively [$E_{r_c} = \hbar^2/(\mu r_c^2)$ and $E_{D_*} = \hbar^2/(\mu D_*^2)$]. A straightforward scaling of the relative Schrödinger equation shows that D_* and r_c are not independent but that the properties of the system depend only on the ratio D_*/r_c [115, 116], which can be tuned experimentally through the application of an electric field [27].

To obtain the K-matrix elements $K_{lm}^{l',m'}$ we solve the relative Schrödinger equation [Eq. (3.1)], with $V_{\rm int}(\vec{r}) = V_{\rm model}(\vec{r})$, for a fixed scattering energy E numerically. The azimuthal symmetry conserves the projection quantum number, and throughout we restrict our analysis to $m = 0$ (hence we omit the m label). The radial Schrödinger equation [Eq.(5.2)] is propagated using the Johnson algorithm with adaptive step size [117]. The K-matrix elements $K_{l0}^{l'0}(k) = \tan\delta_{ll'}(k)$ are found by matching the log-derivative to the free-space solutions [Eq. (5.4)] at sufficiently large r. Since the long-range part of $V_{\rm model}(\vec{r})$ is proportional to the spherical harmonic $Y_{20}(\theta,\phi)$, the phase shifts $\delta_{ll'}(k)$ are only non-zero if $|l-l'| \leq 2$.

To illustrate the convergence of K-matrix elements with increasing matching point r_0, crosses in Figs. 5.1(a), (b) and (c) show the zero-energy K-matrix elements K_{00}^{00}, K_{20}^{00} and K_{20}^{20}, respectively, as a function of r_0 for $D_* = 9.7329 r_c$. Figure 5.1 shows that the K-matrix elements converge with increasing r_0. As can be seen from Fig. 5.1(a), K_{00}^{00} converges quickly (to an accuracy of about 0.5% of its converged value) near $r_0 = 100 r_c$. K_{20}^{00} converges more slowly ($r_0 = 1000 r_c$) and K_{20}^{20} converges yet more slowly ($r_0 = 10000 r_c$). The convergence depends on the functional form of the effective potential, which contains the sum of $V_{l0}^{l'0}(r)$ and the angular momentum term $-\frac{\hbar^2 l(l+1)}{2\mu r^2}\delta_{ll'}$. For (l,l') given

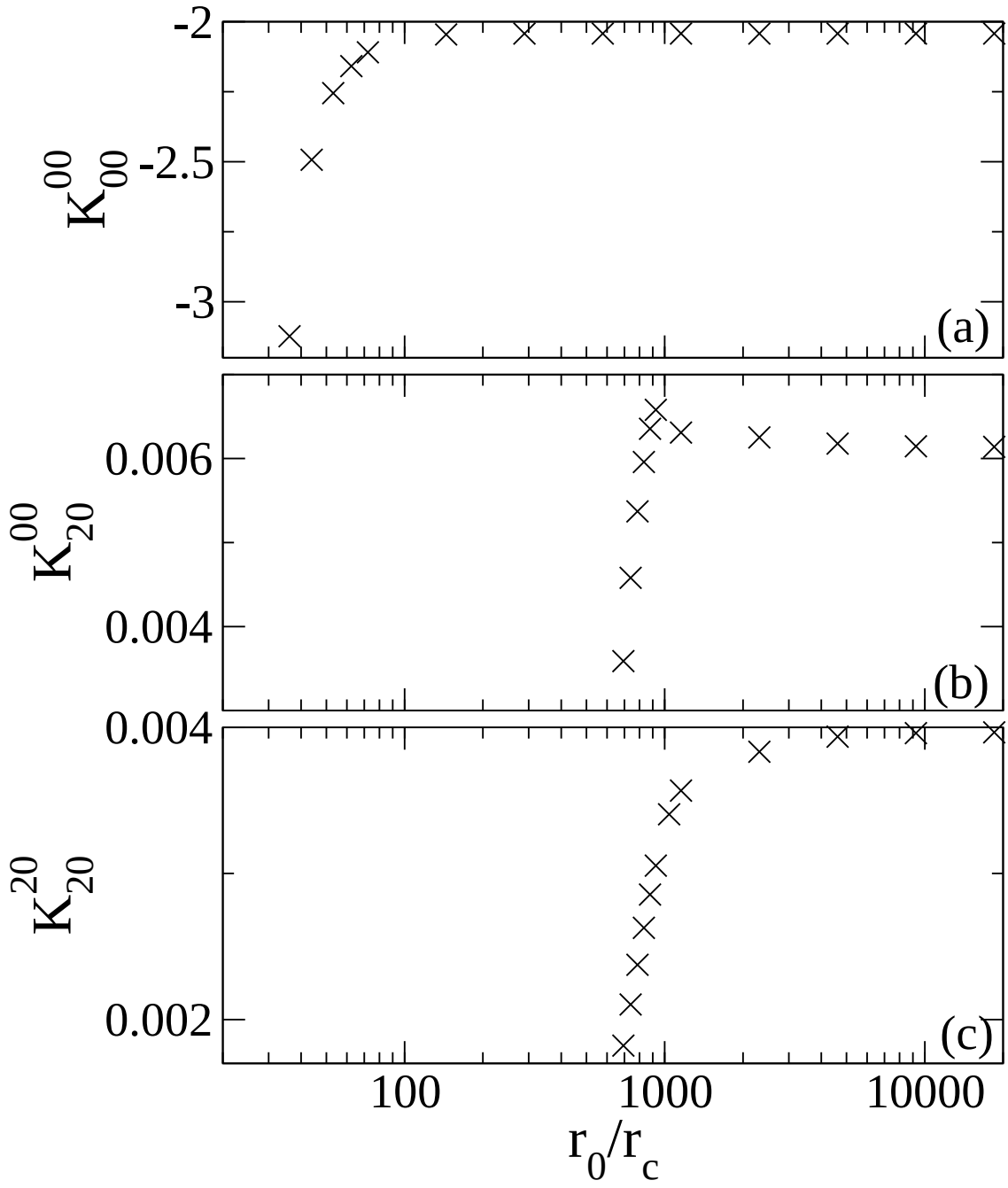

Figure 5.1: Panels (a), (b) and (c) show the zero-energy K-matrix elements K_{00}^{00}, K_{20}^{00} and K_{20}^{20}, respectively, as a function of r_0 on a logarithmic scale for $D_* = 9.7329 r_c$. Panels (a), (b) and (c) all have the same x-axis label and scale.

by $(0,0)$, the effective potential has no long range part and K_{00}^{00} converges quickly. For $(2,0)$, the effective potential varies to leading order as $1/r^3$ for large r, which makes it long range. Consequently, K_{20}^{00} converges more slowly. For $(2,2)$, the effective potential varies to leading order as $1/r^2$ for large r, which makes it more long range than the effective potential for $(2,0)$. Consequently, K_{20}^{20} converges slower than K_{20}^{00}.

The energy dependent generalized scattering lengths $a_{ll'}(k)$ for the dipole-dipole interaction potential (this definition applies only to the dipole-dipole interaction potential), are defined through the K-matrix elements [112],

$$a_{ll'}(k) = -\frac{K_{l0}^{l'0}(k)}{k}, \tag{5.9}$$

so that the $a_{ll'}(k)$ approach a constant as $k \to 0$ [39, 32]. The energy independent generalized scattering lengths are given by

$$a_{ll'} = \lim_{k\to 0} a_{ll'}(k). \tag{5.10}$$

It has been shown that the K-matrix elements (except for K_{00}^{00}) for realistic potentials, such as for the Rb-Rb potential in a strong electric field [118] or an OH-OH model potential [115], away from resonances, are approximated with high accuracy by the K-matrix elements for the dipolar potential only, calculated in the first Born approximation. Applying the Born approximation to $V_{\rm dd}(\vec{r})$, we find for $m = 0$ and $l = l'$ ($l \geq 1$)

$$a_{ll} = -\frac{2D_*}{(2l-1)(2l+3)}, \tag{5.11}$$

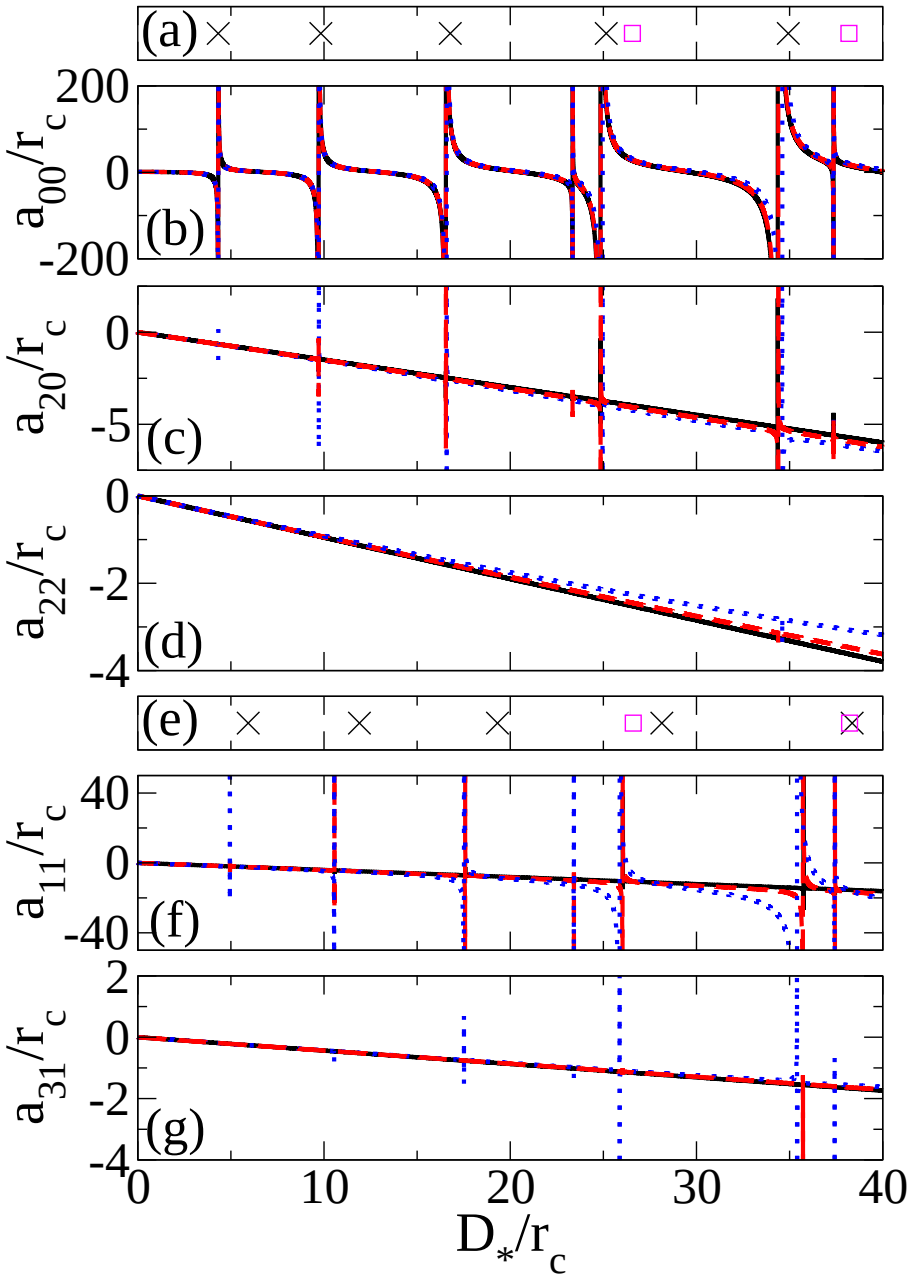

Figure 5.2: Scattering data [(a)-(d) for identical bosons and (e)-(g) for identical fermions]: Scaled scattering lengths (b) a_{00}/r_c, (c) a_{20}/r_c, (d) a_{22}/r_c, (f) a_{11}/r_c, and (g) a_{31}/r_c as a function of the scaled dipole length D_*/r_c for two dipoles interacting through V_{model} for three different scattering energies: $E = 9.36\times10^{-8}E_{r_c}$ (solid line), $E = 9.36\times10^{-6}E_{r_c}$ (dashed line) and $E = 9.36\times10^{-5}E_{r_c}$ (dotted line). In (a), crosses and squares indicate the positions of B_1 and B_2 resonances, respectively. In (e), crosses and squares indicate the positions of F_1 and F_2 resonances, respectively. The resonance positions are obtained by analyzing the WKB phase of the adiabatic potential curves (see text).

and for $m = 0$ and $l = l' + 2$

$$a_{ll-2} = -\frac{D_*}{(2l-1)\sqrt{(2l+1)(2l-3)}}. \tag{5.12}$$

For $l' = 2$ and $l = 0$, e.g., Eq. (5.12) reduces to $a_{20} = -D_*/(3\sqrt{5})$, in agreement with Ref. [68]. The scattering lengths $a_{l-2,l}$ are equal to a_{ll-2}, and all other generalized scattering lengths are zero. All non-zero scattering lengths $a_{ll'}$, in the Born approximation, are negative, depend on l and l', and are directly proportional to D_*. Furthermore, for fixed D_*, the absolute value of the non-zero $a_{ll'}$ decreases with increasing angular momentum quantum number l, indicating that the coupling between different angular momentum channels decreases with increasing l.

Figure 5.2 shows the generalized scattering lengths $a_{ll'}$ for two identical bosons and two identical fermions for three different scattering energies E as a function of the dipole length D_*. The generalized scattering lengths have units of length. The largest D_*/r_c value considered in Fig. 5.2 is 40. If we choose $r_c \approx 100a_0$, then the largest dipole length considered in Fig. 5.2 is $D_*^{\max} \approx 4000a_0$, implying a minimum dipole energy $E_{D_*}^{\min}$ of 1.27×10^{-6} K. For the polar molecule OH, this corresponds to a maximum dipole moment of 1.29 Debye, a value that should be attainable experimentally. The scattering energies in Fig. 5.2 range from $9.36 \times 10^{-8} E_{r_c}$ to $9.36 \times 10^{-5} E_{r_c}$, or, using as before $r_c = 100a_0$, from 1.91×10^{-10} K to 1.91×10^{-7} K. Thus, the largest E/E_{D_*} value considered in Fig. 5.2 is 0.15. This places the present study in the regime where the minimum value of the cross section has been predicted to behave universally [119, 120], but where the parameters of the two-body potential and the s-wave scattering length it results in, especially near resonance, are important [121]. Although the resonance positions depend on the details of the short-range physics, the type of physics discussed here for $V_{\text{model}}(\vec{r})$ in the vicinity and away from resonance should be to a large degree generic. In prin-

ciple the K-matrix has infinite entries with l and l' taking values from zero to infinity resulting in infinite generalized scattering lengths $a_{ll'}$. In practice, the $a_{ll'}$ progressively decrease with increasing $l+l'$ in case of the dipole-dipole interaction potential for the above energies and we cut it off at some large value of l ($l = l' = l_{\max}$).

Figure 5.2(b) shows the scattering length a_{00} as a function of D_* for two identical bosons interacting through $V_{\text{model}}(\vec{r})$. Five B_1 and two B_2 resonances (located at $D_* \approx 23 r_c$ and $37 r_c$) are clearly visible. Figures 5.2(c) and 5.2(d) show the generalized scattering lengths a_{20} and a_{22}, respectively. In the Born approximation for V_{dd}, both a_{20} and a_{22} vary linearly with D_* [see Eqs.(5.11) and (5.12)] [32, 70].

a_{20} and a_{22} obtained from the full coupled channel calculation show deviations from the Born approximation for certain D_* values. The positions of the "spikes" coincide with the resonance positions of a_{00}. Notably, the widths of the spikes decrease with increasing $l+l'$.

For a given D_*, the adiabatic potential curves $V^{(i)}(D_*, r)$ are obtained by diagonalizing the matrix, whose elements are the sum of $V_{l0}^{l'0}(r)$ and the angular momentum term $-\frac{\hbar^2 l(l+1)}{2\mu r^2}\delta_{ll'}$, for different r values [114]. Solid and dashed curves in Fig. 5.3 show the adiabatic potential curves $V^{(i)}(D_*, r)$ for $i = 0$ and $i = 1$, respectively, for $D_* = 13.064 r_c$ and even l. $i = 0$ labels the energetically lowest lying adiabatic potential curve, $i = 1$ labels the energetically next higher lying adiabatic potential curve and so on. $V^{(0)}(D_*, r)$ is purely attractive for $r > r_c$. $V^{(1)}(D_*, r)$, in contrast, has a repulsive barrier, which stems from the angular momentum barrier for $l = 2$.

The WKB phases $\phi^{(i)}_{\text{WKB}}(D_*)$, are calculated by integrating over the adiabatic potential curves $V^{(i)}(D_*, r)$ between the inner and outer classical turning points $r_{\min}$ and $r_{\max}$, respectively,

$$\phi^{(i)}_{\text{WKB}}(D_*) = \int_{r_{\min}}^{r_{\max}} \sqrt{-\frac{2\mu V^{(i)}(D_*, r)}{\hbar^2}}\, dr. \tag{5.13}$$

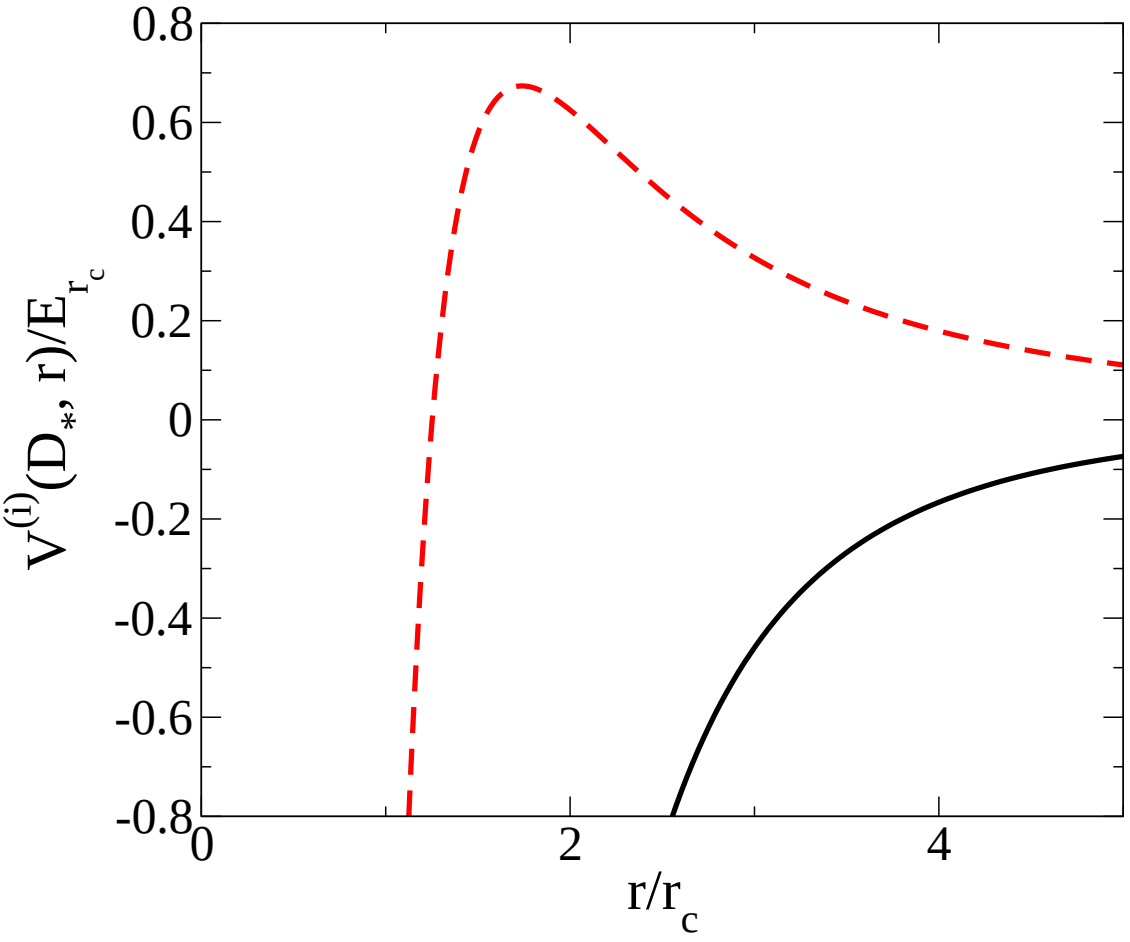

Figure 5.3: Adiabatic potential curves $V^{(i)}(D_*, r)$ as a function of r, for $D_* = 13.064 r_c$: The solid curve shows the lowest adiabatic potential curve ($i = 0$) and the dashed curve shows the energetically next higher lying adiabatic potential curve ($i = 1$).

For the interaction potential $V_{\rm model}$, the inner classical turning point of all the adiabatic potential curves is given by r_c. In the even l case, $V^{(0)}(D_*, r)$ is attractive for $r > r_c$ and the outer turning point is given by $r_{\rm max} = \infty$. For adiabatic potential curves with $i > 0$, the outer classical turning point $r_{\rm max}$ is given by the the r value at which $V^{(1)}(D_*, r)$ first crosses zero. Hence the WKB phase is obtained from Eq. (5.13), by integrating over the range of r values for which the adiabatic potential curves are negative. When the WKB phase is an integral multiple of π a new bound state is pulled in. This corresponds to a resonance in the scattering lengths $a_{ll'}$.

Figure 5.2(a) shows the resonance positions as predicted by the WKB phase accumulated in different adiabatic potential curves [114]. Crosses indicate the D_* values at which $\phi^{(0)}_{\rm WKB}(D_*)$ is an integral multiple of π and resonances occurring at approximately these D_* values are classified as B_1 resonances. Squares indicate the D_* values at which $\sum_{i=1}^{\infty} \phi^{(i)}_{\rm WKB}(D_*)$ is an integral multiple of π and resonances occurring at approximately these D_* values are classified as B_2 resonances.

Figures 5.2(f) and 5.2(g) show the generalized scattering lengths a_{11} and a_{31} for two aligned identical fermions interacting through $V_{\rm model}(\vec{r})$ as a function of D_*. Away from resonance, a_{11} and a_{31} vary approximately linearly with D_* [see Eqs. (5.11) and (5.12)]. The spikes in Figs. 5.2(f) and 5.2(g) correspond to F_1 and F_2 resonances. Figures 5.2(f) and 5.2(g) show five F_1 and two F_2 resonances (located at $D_* \approx 23.5 r_c$ and $37.5 r_c$). A key difference between dipole scattering of identical bosons and identical fermions is that the lowest non-vanishing scattering length for bosons (i.e., a_{00}) cannot be approximated by applying the Born approximation to $V_{\rm dd}$ (the Born approximation for $V_{\rm dd}$ gives $a_{00} = 0$) while the lowest non-vanishing scattering length for fermions (i.e., a_{11}) can be, away from resonance, approximated by the Born approximation for $V_{\rm dd}$ [32, 70]. The crosses and squares shown in Fig. 5.2(e) indicate the positions of F_1 and F_2 resonances, respectively, as predicted from the WKB phase of the lowest adiabatic potential curve

and of all other adiabatic potential curves. The WKB prediction for the positions of F_1 resonances is less accurate than that of B_1 resonances.

We find that the widths of B_1 and F_1 resonances are in general larger than the widths of B_2 and F_2 resonances, respectively. Furthermore, Fig. 5.2 shows that the widths within each of the resonance sequences increases with increasing E for fixed D_*/r_c and with increasing D_*/r_c for fixed E, and thus with increasing E/E_{D_*}.

To better understand the resonance structure in Fig. 5.2, we determine the bound state energies of the two interacting dipoles in free space. The Schrödinger equation for the relative coordinate is solved using two-dimensional B-splines. The two-dipole system supports a new bound state at those D_*/r_c values where the scattering lengths a_{00} and a_{11} for two identical bosons and fermions, respectively, diverge. Solid lines in Figs. 5.4(a) and 5.4(b) show the bound state energy for two identical bosons in the vicinity of a B_1 and a B_2 resonance, respectively, while solid lines in Figs. 5.4(c) and 5.4(d) show the bound state energy for two identical fermions in the vicinity of a F_1 and a F_2 resonance, respectively.

The two-body energy E_b of weakly-bound s-wave interacting systems is well described by the s-wave scattering length a_{00}, $E_b = -\hbar^2/(2\mu[a_{00}(E)]^2)$ [see Eq. (3.16)]. To test if this simple zero range pseudopotential expression holds for dipolar systems, we analytically continue the scattering lengths for $V_{\text{model}}(\vec{r})$ to negative energies. We obtain stable $a_{00}(E)$ and $a_{11}(E)$ for negative scattering energies by matching the coupled channel solutions to the free-space solutions at relatively small r values ($r_0 \approx |k|^{-1}$).

To illustrate the convergence of the scattering lengths for negative energies, crosses in Figs. 5.5(a) and (b) show the K-matrix elements K_{00}^{00} and K_{10}^{10}, respectively, as a function of r_0. The scattering energy E is about $-3.285\times10^{-6}E_{r_c}$ in both panels corresponding to $|k|^{-1} \approx 390 r_c$. Correspondingly, the r_0 chosen in Figs. 5.5(a) and (b) ranges from $0.1414|k|^{-1}$ to $1.98|k|^{-1}$. The size of a bound state is approximately given by $|k|^{-1}$. If

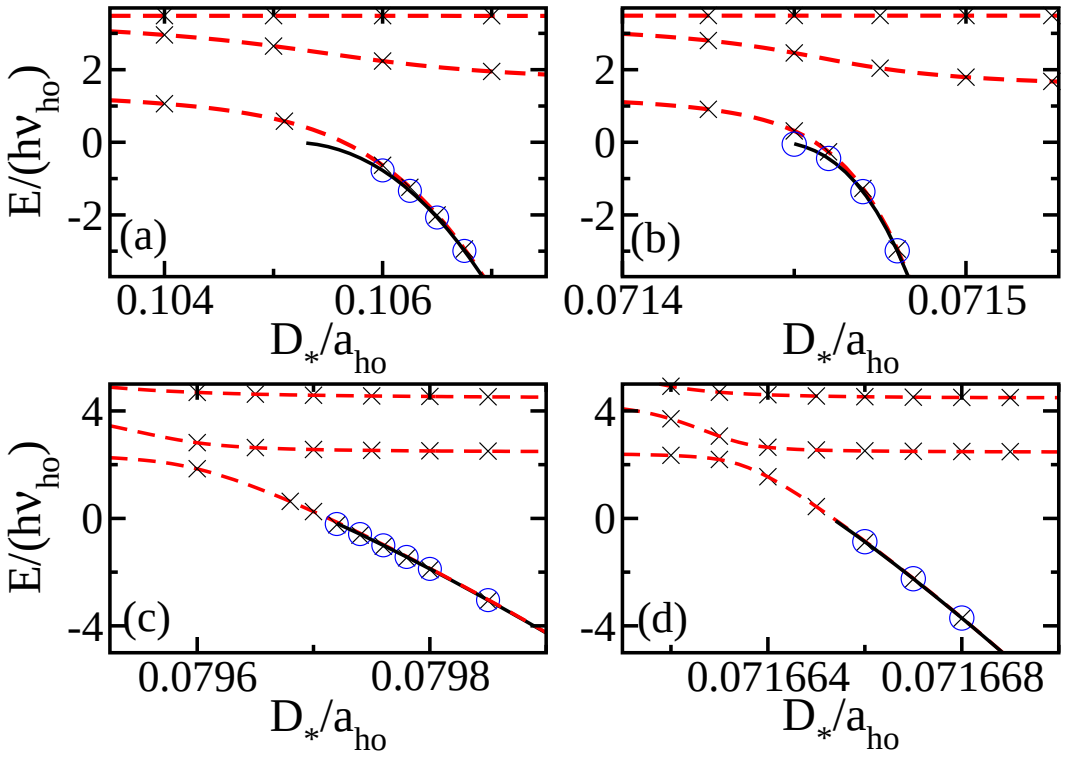

Figure 5.4: (Color online) Eigenenergies for two identical bosons in the vicinity of (a) a B_1 resonance and (b) a B_2 resonance, and for two identical fermions in the vicinity of (c) a F_1 resonance and (d) a F_2 resonance. Solid lines and circles show the bound state energies for two dipoles in free space interacting through $V_{\text{model}}(\vec{r})$ and $V_{\text{pp, reg}}$, respectively. Dashed lines and crosses show the bound state energies for two dipoles under external harmonic confinement interacting through $V_{\text{model}}(\vec{r})$ and $V_{\text{pp, reg}}$, respectively. The oscillator length a_{ho} is given by $\sqrt{\hbar/(\mu\omega_{\text{ho}})}$, and the hard core radius r_c of $V_{\text{model}}(\vec{r})$ is 0.00306 a_{ho}. This figure is taken from Ref. [71].

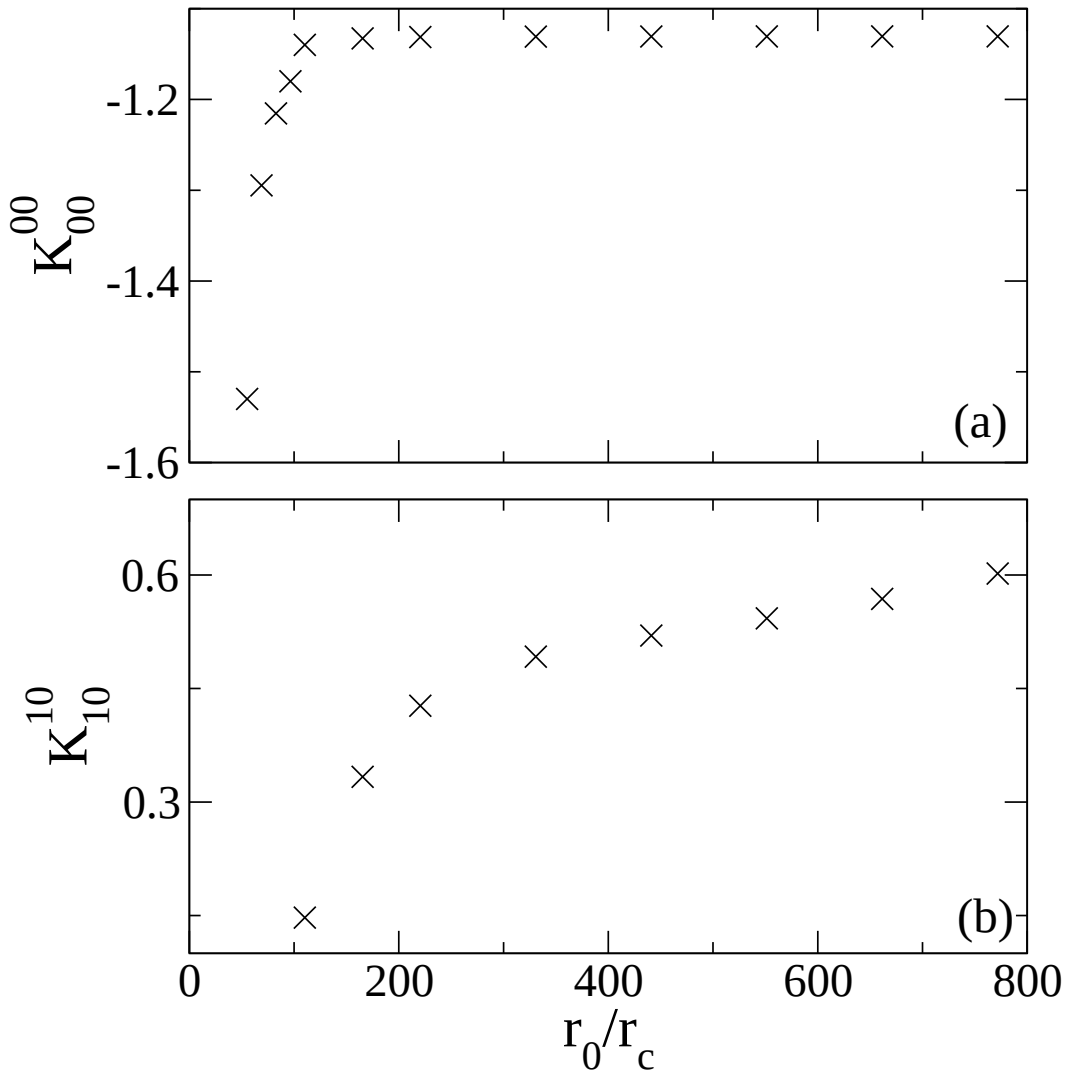

Figure 5.5: Panels (a) and (b) show the K-matrix elements K_{00}^{00} and K_{10}^{10}, respectively, as a function of r_0. In (a), the parameters are $D_* = 9.7329 r_c$ and $E = -3.285 \times 10^{-6} E_{r_c}$. In (b), the parameters are $D_* = 26.038 r_c$ and $E = -3.285 \times 10^{-6} E_{r_c}$. Panels (a) and (b) have the same x-axis label and scale.

r_0 is much larger than $|k|^{-1}$, then the exponentially decaying part of the wavefunction is small compared to the exponentially growing part. In this case the exponentially increasing and decreasing functions become "numerically" linearly dependent, which prohibits the reliable extraction of the phase shift. On the other hand, r_0 must be large enough for most of the phase to be accumulated. This gives a small window of r_0 values for which the K-matrix elements are converged at negative energies.

The bound state energies for two identical bosons in free space, determined self-consistently [107, 106] from $E_b = -\hbar^2/(2\mu[a_{00}(E_b)]^2)$, are shown by circles in Figs. 5.4(a) and 5.4(b). Similarly, we determine the bound state energies for two identical fermions in free space by solving the equation $E_b = -\hbar^2/(2\mu[a_{11}(E_b)]^2)$ [65, 64] self-consistently [circles in Figs. 5.4(c) and 5.4(d)]. Somewhat surprisingly, the bound state energies in the vicinity of all four resonance types are very well described by a single-channel expression.

In addition to the free-space system, we consider the trapped system. Dashed lines in Fig. 5.4 show the energies for two dipoles interacting through $V_{\text{model}}(\vec{r})$ under spherically symmetric external harmonic confinement $V_{\text{trap}}(r)$, $V_{\text{trap}}(r) = \mu\omega_{\text{ho}}^2 r^2/2$. Near resonance, the lowest state with positive energy changes rapidly and turns into a negative energy state with molecular-like character. The energy of this "diving" state is slightly higher than the energy of the free-space system (the trap pushes the energy up).

Figures 5.6(a) and 5.6(b) show the scaled eigenfunctions $r\psi(r,\theta)$ for two identical bosons with $E \approx -0.88\hbar\omega_{\text{ho}}$ as a function of r for different θ near a B_1 and a B_2 resonance, respectively. Similarly, Figs. 5.6(c) and 5.6(d) show the scaled eigenfunctions for two identical fermions with $E \approx -0.88\hbar\omega_{\text{ho}}$ near a F_1 and a F_2 resonance, respectively. Although calculated for the simple model potential $V_{\text{model}}(\vec{r})$, the wavefunctions for $r > r_c$ are expected to share some key features with those obtained for more realistic interactions between polar molecules. In all panels, the wavefunction cut for

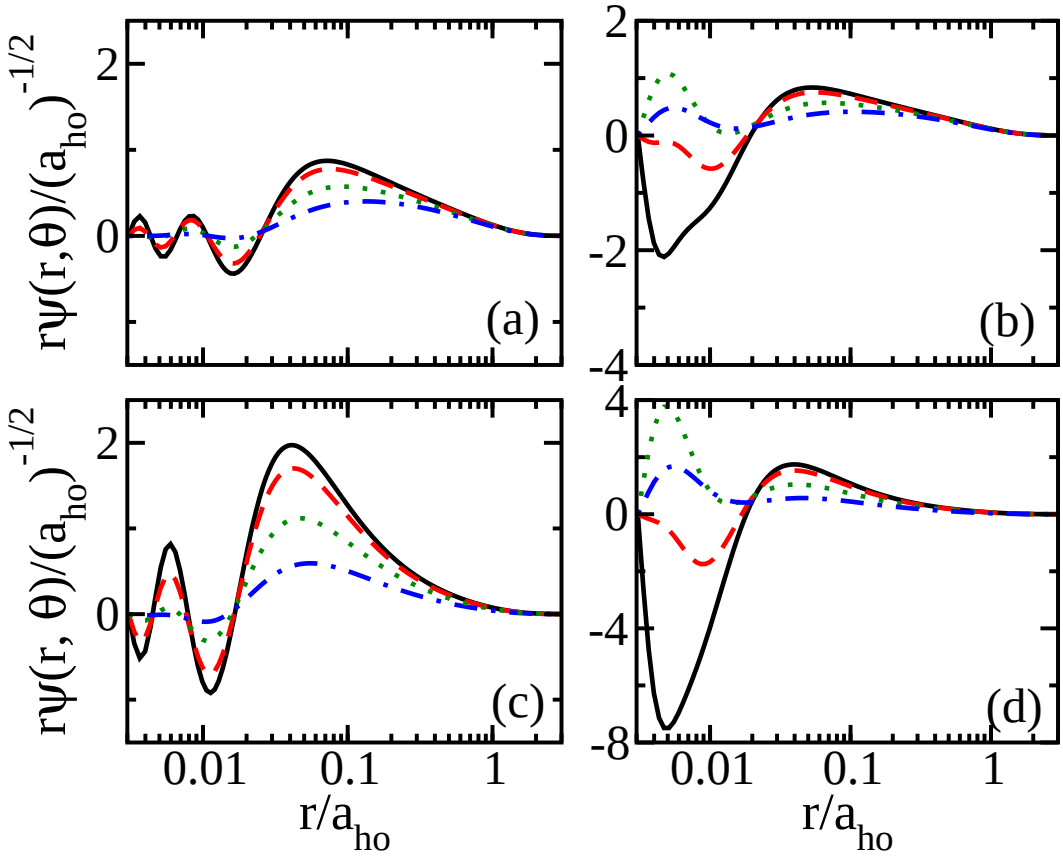

Figure 5.6: Eigenfunctions for two identical bosons in the vicinity of (a) a B_1 resonance ($D_* = 0.1061 a_{\rm ho}$) and (b) a B_2 resonance ($D_* = 0.07147 a_{\rm ho}$), and for two identical fermions in the vicinity of (c) a F_1 resonance ($D_* = 0.07976 a_{\rm ho}$) and (d) a F_2 resonance ($D_* = 0.07167 a_{\rm ho}$) in a spherical harmonic trap interacting via $V_{\rm model}(\vec{r})$ for $\theta = 0^\circ$ (solid line), $\theta \approx 18.2^\circ$ (dashed line), $\theta \approx 36.4^\circ$ (dotted line) and $\theta \approx 54.6^\circ$ (dash-dotted line). In all panels, r_c equals 0.00306 $a_{\rm ho}$. Note the log scale for r and the different ranges of the y-axis. This figure is taken from Ref. [71].

$\theta = 0^\circ$ has the largest amplitude, reflecting the fact that the dipole-dipole potential is most attractive for $\theta = 0^\circ$. Interestingly, the nodal structure of the wavefunction for two identical bosons near the B_1 resonance [Fig. 5.6(a)] has a similar structure to that of the wavefunction of two identical fermions near the F_1 resonance [Fig. 5.6(c)]: Both nodal surfaces show approximately spherical symmetry. On the other hand, the nodal structure of the wavefunction for two identical bosons near the B_2 resonance [Fig. 5.6(b)] has a similar structure to that of the wavefunction for two identical fermions near the F_2 resonance [Fig. 5.6(d)]: The nodal surfaces depend on both r and θ.

To quantify the higher partial wave contributions, we project the wavefunctions shown in Fig. 5.6 onto spherical harmonics. The projection p_l onto the l^{th} spherical harmonic Y_{l0} is given by

$$p_l = \int_{r_c}^{\infty} \left| \int_0^{2\pi} \int_0^{\pi} Y_{l0}(\theta,\phi)\psi(r,\theta)\sin\theta\, d\theta\, d\phi \right|^2 r^2 dr. \tag{5.14}$$

The s-wave contribution p_0 of the boson states near the B_1 and B_2 resonances is about 95%, while the p-wave contribution p_1 of the fermion states near the F_1 and F_2 resonances is about 95 and 80%, respectively. The gas-like states near resonance, in contrast, are dominated by a single partial wave (for bosons, e.g., the s-wave contribution p_0 of the energetically lowest-lying gas-like state is about 99% while the d-wave contribution p_2 of the energetically next higher-lying state is about 99%).

5.3 Dipole-dipole interaction: Zero range pseudopotential

This section introduces a zero range pseudopotential that reproduces the wavefunction corresponding to the realistic interaction potential for $r > r_0$, and then treats two aligned dipoles under harmonic confinement.

5.3.1 Introduction of the pseudopotential

Within the mean-field Gross-Pitaevskii formalism, the interaction between two identical bosonic dipoles, aligned along the space-fixed $\hat{z}$-axis by an external field, has been successfully modeled by the pseudopotential $V_{\rm pp}(\vec{r})$ [118],

$$V_{\rm pp}(\vec{r}) = \frac{2\pi\hbar^2}{\mu} a_{00}\delta(\vec{r}) + V_{\rm dd}(\vec{r}). \tag{5.15}$$

The s-wave scattering length a_{00} depends on both the short- and long-range parts of the true interaction potential. The second term on the right hand side of Eq. (5.15) couples angular momentum states with $l = l'$ ($l > 0$) and $|l - l'| = 2$ (any l, l'). For identical fermions, s-wave scattering is absent and the interaction is described, assuming the long-range dipole-dipole interaction is dominant, by the second term on the right hand side of Eq. (5.15). Our goal is to treat two aligned dipoles interacting through a pseudopotential.

The pseudopotential $V_{\rm pp}(\vec{r})$ cannot be used directly in Eq. (3.11) since both parts of the pseudopotential lead to divergences. The divergence of the δ-function potential arises from the singular $1/r$ behavior at small r of the spherical Neumann function $n_0(r)$, and can be cured by introducing the regularization operator $\frac{\partial}{\partial r} r$ [59]. Curing the

divergence of the long-ranged $1/r^3$ term of $V_{\rm pp}$ is more involved, since it couples an infinite number of angular momentum states, each of which gives rise to a singularity in the $r \to 0$ limit [1]. The nature of each of these singularities depends on the quantum numbers l and l' coupled by the pseudopotential, and hence has to be cured separately for each l and l' combination to allow an analytical solution of the two-dipole Schrödinger equation to be obtained.

In this work, we follow Derevianko [68, 69] and cure the divergences by replacing $V_{\rm pp}(\vec{r})$ with a regularized zero-range potential $V_{\rm pp,\,reg}(\vec{r})$, which contains *infinitely* many terms,

$$V_{\rm pp,\,reg}(\vec{r}) = \sum_{l,l'} V_{l\,l'}(\vec{r}). \tag{5.16}$$

The sum in Eq. (5.16) runs over l and l' even for identical bosons, and over l and l' odd for identical fermions. For non identical particles the sum is over all l and l'. However, the sum over even l and l' can be treated separately from the sum over odd l and l' as there is no coupling between states with even and odd angular momentum quantum numbers. This is because the interaction potential between two aligned dipoles is parity conserving.

For $l \neq l'$, $V_{ll'}$ and $V_{l'l}$ are different and both terms have to be included in the sum. In Sec. 5.3.2, we apply the pseudopotential to systems under spherically symmetric external confinement. For these systems, the projection quantum number m is a good quantum number, i.e., the energy spectrum for two interacting dipoles under spherically symmetric confinement can be solved separately for each allowed m value. Con-

[1] The divergence of the $1/r^3$ term arises if the repulsive short-range potential, which exists for realistic atom-atom and molecule-molecule potentials, is removed and the long-range dipolar interaction is taken to extend to $r = 0$. In numerical calculations this divergence can be cured, e.g., by introducing a small r cutoff.

sequently, a separate pseudopotential can be constructed for each m value. In the following, we restrict ourselves to systems with vanishing projection quantum number m; the generalization of the pseudopotential to general m is discussed at the end of this section. The $V_{ll'}$ are defined through their action on an arbitrary $\vec{r}$-dependent function $\Phi(\vec{r})$ [68, 69],

$$V_{ll'}(\vec{r})\Phi(\vec{r}) = g_{ll'}(k)\frac{\delta(r)}{r^{l'+2}}Y_{l'0}(\theta,\phi)\left[\frac{\partial^{2l+1}}{\partial r^{2l+1}}r^{l+1}\int Y_{l0}(\theta,\phi)\Phi(\vec{r})d\Omega\right]_{r\to 0} \tag{5.17}$$

with

$$g_{ll'}(k) = -\frac{\hbar^2}{2\mu}\frac{K_{l0}^{l'0}(k)}{k^{l+l'+1}}\frac{(2l+1)!!(2l'+1)!!}{(2l+1)!}. \tag{5.18}$$

Since we are restricting ourselves to $m=0$, the $V_{ll'}$ are written in terms of the spherical harmonics Y_{lm} with $m=0$. When applying the above pseudopotential we treat a large number of terms in Eq. (5.16), and do not terminate the sum after the first three terms as done in Refs. [68, 69, 122]. We note that the non-Hermiticity of $V_{\text{pp, reg}}$ does not lead to problems when determining the energy spectrum; however, great care has to be taken when calculating, e.g., structural expectation values [123].

To understand the functional form of the zero-range pseudopotential defined in Eqs. (5.16) through (5.18), let us first consider the piece of Eq. (5.17) in square brackets. If we decompose the incoming wave $\Phi(\vec{r})$ into partial waves,

$$\Phi(\vec{r}) = \sum_{n_i,l_i,m_i} c_{n_i l_i m_i} Q_{n_i l_i}(r) Y_{l_i m_i}(\theta,\phi), \tag{5.19}$$

where the $c_{n_i l_i m_i}$ denote expansion coefficients and the $Q_{n_i l_i}$ radial basis functions, the spherical harmonic Y_{l0} in the integrand of $V_{ll'}$ acts as a projector or filter. After the

integration over the angles, only those components of $\Phi(\vec{r})$ that have $l_i = l$ and $m_i = 0$ survive. The operator $\frac{\partial^{2l+1}}{\partial r^{2l+1}} r^{l+1}$ in Eq. (5.17) is designed to then first cure the r^{-l-1} divergences of the $Q_{n_i l}$, which arise in the $r \to 0$ limit, and to then second "extract" the coefficients of the regular part of the $Q_{n_i l}(r)$ that go as r^l [59]. Alltogether, this shows that the square bracket in Eq. (5.17) reduces to a constant when the $r \to 0$ limit is taken. To understand the remaining pieces of the pseudopotential, we multiply Eq. (5.17) from the left with $Q^*_{n_o l_o} Y^*_{l_o m_o}$ and integrate over all space. The spherical harmonic $Y_{l'0}$ in Eq. (5.17) then ensures that the integral is only non-zero when $l' = l_o$ and $m_o = 0$. When performing the radial integration, the $\delta(r)/r^{l'}$ term ensures that the coefficients of the regular part of the $Q_{n_o l_o}$ that go as r^{l_o} are being extracted (note that the remaining $1/r^2$ term cancels the r^2 in the volume element).

Alltogether, the analysis outlined in the previous paragraph shows that the functional form of $V_{ll'}$ ensures that the divergences of the radial parts of the incoming and outgoing wave is cured in the $r \to 0$ limit and that the l^{th} component of the incoming wave is scattered into the l'^{th} partial wave. The sum over all l and l' values in Eq. (5.16) guarantees that any state with quantum number l can be coupled to any state with quantum number l', provided the corresponding K-matrix element $K_{l0}^{l'0}(k)$ is non-zero. We note that this pseudopotential can not only be used to model dipole-dipole scattering but also to model any interaction potential whose angular dependence is given by $Y_{00}(\theta, \phi)$ or $Y_{20}(\theta, \phi)$, irrespective of its r dependence. The only requirement is that the potential is characterized by well behaved K-matrix elements. Importantly, the regularized pseudopotential given by Eqs. (5.16) through (5.18) is only appropriate if the external confining potential in Eq. (3.12) has spherical symmetry [99]. Generalizations of the above zero-range pseudopotential, aimed at treating interacting dipoles under elongated confinement, require the regularization scheme to be modified to additionally cure divergences of cylindrically symmetric wavefunctions. These extensions are

discussed in Sec. 5.4.

One can show readily that the K-matrix elements $K_{l0}^{l'0}$ of $V_{\text{pp, reg}}$, calculated in the first Born approximation, with $a_{ll'}$ given by Eqs. (5.11) and (5.12) coincide with the K-matrix elements $K_{l0}^{l'0}$ of V_{pp}. This provides a simple check of the zero-range pseudopotential construction and proves that the prefactors of $V_{ll'}$ are correct. In turn, this suggests that the applicability regimes of V_{pp} and $V_{\text{pp, reg}}$ are comparable, if the generalized scattering lengths $a_{ll'}$ used to quantify the scattering strengths of $V_{ll'}$ are approximated by Eqs. (5.11) and (5.12). The applicability regime of $V_{\text{pp, reg}}$ may, however, be larger than that of V_{pp} if the full energy-dependent K-matrix of a realistic potential is used instead (see, e. g., Fig. 5.9).

To generalize the zero-range pseudopotential defined in Eqs. (5.16) through (5.18) for projection quantum numbers $m = 0$ to any m, only a few changes have to be made. In Eq. (5.17), the spherical harmonics Y_{l0} have to be replaced by Y_{lm}, and the $K_{l0}^{l'0}$ have to be replaced by $K_{lm}^{l'm'}$. Correspondingly, Eqs. (5.11) and (5.12) become m-dependent.

5.3.2 Derivation of the eigenequation for spherically harmonic confinement

To determine the eigenenergies of two aligned dipoles with $m = 0$ under spherical harmonic confinement interacting through the zero-range potential $V_{\text{pp, reg}}$, we expand the eigenfunctions $\Psi(\vec{r})$ in terms of the orthonormal harmonic oscillator eigenfunctions $R_{n_i l_i} Y_{l_i 0}$,

$$\Psi(\vec{r}) = \sum_{n_i, l_i} c_{n_i l_i} R_{n_i l_i}(r) Y_{l_i 0}(\theta, \phi). \tag{5.20}$$

In contrast to Eq. (3.23), Eq. (5.20) contains a sum over the angular momentum quantum number. The pseudopotential $V_{\mathrm{pp,\,reg}}$ enforces the proper boundary condition of $\Psi(\vec{r})$ at $r=0$, and thus determines the expansion coefficients $c_{n_i l_i}$. To introduce the key ideas we first consider s-wave interacting particles [60], for which the pseudopotential reduces to a single term, and then consider the general case, in which the pseudopotential contains infinitely many terms.

Including only the term with l and $l'=0$ in Eq. (5.16), the Schrödinger equation [Eq. (3.11)] becomes

$$\sum_{n_i,l_i} c_{n_i l_i}(E_{n_i l_i}-E+V_{00})R_{n_i l_i}(r)Y_{l_i 0}(\theta,\phi)=0, \tag{5.21}$$

where the $E_{n_i l_i}$ denote the eigenenergies of the non-interacting harmonic oscillator,

$$E_{n_i l_i}=\left(2n_i+l_i+\frac{3}{2}\right)\hbar\omega_{\mathrm{ho}}. \tag{5.22}$$

In what follows, it is convenient to express the energy E of the interacting system in terms of a non-integer quantum number ν,

$$E=\left(2\nu+\frac{3}{2}\right)\hbar\omega_{\mathrm{ho}}. \tag{5.23}$$

Multiplying Eq. (5.21) from the left with $R^*_{n_o l_o}Y^*_{l_o 0}$ with $l_o>0$ and integrating over all space, we find that the $c_{n_i l_i}$ with $l_i>0$ vanish. This can be understood readily by realizing that the s-wave pseudopotential V_{00} only couples states with $l=l'=0$ (see Sec. 5.3.1). To determine the expansion coefficients $c_{n_i 0}$, we multiply Eq. (5.21) from the left with $R^*_{n_o 0}Y^*_{00}$ and integrate over all space. This results in

$$c_{n_o 0}(2n_o-2\nu)\hbar\omega_{\mathrm{ho}}+R^*_{n_o 0}(0)g_{00}B_0=0, \tag{5.24}$$

where B_0 denotes the result of the square bracket in Eq. (5.17),

$$B_0 = \left[\frac{\partial}{\partial r} \left(r \sum_{n_i=0}^{\infty} c_{n_i 0} R_{n_i 0}(r) \right) \right]_{r \to 0} . \tag{5.25}$$

Note that B_0 is constant and independent of n_i. In Eq. (5.24), the r-independent term $R^*_{n_o 0}(0)$ arises from the radial integration over the δ-function of the pseudopotential. If we solve Eq. (5.24) for $c_{n_o 0}$ and plug the result into Eq. (5.25), the unknown constant B_0 cancels and we obtain an implicit eigenequation for ν,

$$1 = g_{00}(k) \left[\frac{\partial}{\partial r} \left(r \sum_{n_i=0}^{\infty} \frac{R^*_{n_i 0}(0) R_{n_i 0}(r)}{(2\nu - 2n_i)\hbar\omega_{\mathrm{ho}}} \right) \right]_{r \to 0} . \tag{5.26}$$

Using Eqs. (A.1) and (A.6) from Appendix A to simplify the term in square brackets, we obtain the well-known implicit eigenequation for two particles interacting through the s-wave pseudopotential under spherical harmonic confinement [60],

$$\frac{\Gamma\left(\frac{-E}{2\hbar\omega_{\mathrm{ho}}} + \frac{1}{4}\right)}{2\Gamma\left(\frac{-E}{2\hbar\omega_{\mathrm{ho}}} + \frac{3}{4}\right)} - \frac{a_{00}(k)}{a_{\mathrm{ho}}} = 0. \tag{5.27}$$

The derivation of the implicit eigenequation for two dipoles under external harmonic confinement interacting through the pseudopotential with infinitely many terms proceeds analogously to that outlined above for the s-wave system. The key difference is that each $V_{ll'}$ term in Eq. (5.17) with $l \neq l'$ couples states with different angular momenta, resulting in a set of coupled equations for the expansion coefficients $c_{n_i l_i}$. However, since $V_{\mathrm{pp,\,reg}}$ for dipolar systems couples only angular momentum states with $|l - l'| \leq 2$ [see, e.g., the discussion at the beginning of Sec. 5.3.1 and around Eqs. (5.11) and (5.12)], the coupled equations can, as we outline in the following, be solved analyt-

ically by including successively more terms in $V_{\text{pp, reg}}$.

To start with, we plug the expansion given in Eq. (5.20) into Eq. (3.11), where the interaction potential $V_{\text{int}}(\vec{r})$ is now taken to be the pseudopotential $V_{\text{pp, reg}}(\vec{r})$ with infinitely many terms. To obtain the general equation for the expansion coefficients $c_{n_i l_i}$, we multiply as before from the left with $R^*_{n_o l_o} Y^*_{l_o 0}$ and integrate over all space,

$$\begin{aligned} c_{n_o l_o}(2n_o + l_o - 2\nu)\hbar\omega_{\text{ho}} + \left[\frac{R^*_{n_o l_o}(r)}{r^{l_o}}\right]_{r\to 0} \times \\ \left[g_{l_o-2,l_o} B_{l_o-2} + g_{l_o l_o} B_{l_o} + g_{l_o+2,l_o} B_{l_o+2}\right] = 0. \end{aligned} \tag{5.28}$$

Here, the B_{l_o-2}, B_{l_o} and B_{l_o+2} denote constants that are independent of n_i,

$$B_{l_o} = \left[\frac{\partial^{2l_o+1}}{\partial r^{2l_o+1}}\left\{r^{l_o+1}\left(\sum_{n_i=0}^{\infty} c_{n_i l_o} R_{n_i l_o}(r)\right)\right\}\right]_{r\to 0}. \tag{5.29}$$

The three terms in the square bracket in the second line of Eq. (5.28) arise because the $V_{l'-2,l'}$, $V_{l'l'}$ and $V_{l'+2,l'}$ terms in the pseudopotential $V_{\text{pp, reg}}$ couple the state $R^*_{n_o l_o} Y^*_{l_o 0}$, for $l' = l_o$, with three components of the expansion for Ψ, Eq. (5.20). Importantly, the constants B_{l_o-2}, B_{l_o} and B_{l_o+2}, defined in Eq. (5.29), depend on the quantum numbers l_o-2, l_o and l_o+2, respectively, which implies that Eq. (5.28) defines a set of infinitely many coupled equations that determine, together with Eq. (5.29), the expansion coefficients $c_{n_i l_i}$. Notice that Eqs. (5.28) and (5.29) coincide with Eqs. (5.24) and (5.25) if we set $l_o = 0$ and $g_{ll'}(k) = 0$ if l or $l' > 0$.

We now illustrate how Eqs. (5.28) and (5.29) can be solved for identical bosons, i.e., in the case where l and l' are even (the derivation for identical fermions proceeds analogously). Our strategy is to solve these equations by including successively more terms in the coupled equations, or equivalently, in the pseudopotential. As discussed above, if K^{00}_{00} is the only non-zero K-matrix element, the eigenenergies are given by Eq. (5.27).

Next, we also allow for non-zero K_{20}^{00}, K_{00}^{20} and K_{20}^{20}, i.e., we consider l and $l' \leq 2$ in Eq. (5.16). In this case, the coefficients $c_{n_i 0}$ and $c_{n_i 2}$ are non-zero and coupled, but all $c_{n_i l_i}$ with $l_i > 2$ are zero. Using the expressions for B_0 and B_2 given in Eq. (5.29), we decouple the equations. Finally, using Eqs. (A.1) and (A.6) from Appendix A, the eigenequation can be compactly written as

$$t_0 + \frac{q_2}{t_2} = 0, \tag{5.30}$$

where

$$t_l = \frac{\Gamma(\frac{-E}{2\hbar\omega_{\rm ho}} + \frac{1}{4} - \frac{l}{2})}{2^{2l+1}\Gamma(\frac{-E}{2\hbar\omega_{\rm ho}} + \frac{3}{4} + \frac{l}{2})} - (-1)^l \frac{K_{l0}^{l0}(k)}{k^{2l+1} a_{\rm ho}^{2l+1}} \tag{5.31}$$

and

$$q_l = -\frac{\left(K_{(l-2)0}^{l0}(k)\right)^2}{k^{4l-2} a_{\rm ho}^{4l-2}}. \tag{5.32}$$

Equation (5.30) can be understood as follows. If only $K_{00}^{00}(k)$ is non-zero, it reduces to $t_0 = 0$, in agreement with Eq. (5.27). If only $K_{00}^{00}(k)$, $K_{00}^{20}(k)$ and $K_{20}^{00}(k)$ are non-zero, Eq. (5.30) remains valid if $K_{20}^{20}(k)$ in t_2 is set to zero. This shows that the term q_2 and the first term on the right hand side of t_2 arise due to the coupling between states with angular momenta 0 and 2. The second term of t_2, in contrast, arises due to a non-zero K_{20}^{20}. Finally, for non-zero K_{00}^{00} and K_{20}^{20} but vanishing K_{00}^{20} and K_{20}^{00}, Eq. (5.30) reduces to $t_0 t_2 = 0$. In this case, we recover the eigenequations $t_0 = 0$ for s-wave interacting particles [60] and $t_2 = 0$ for d-wave interacting particles [65].

We now consider l and l' values with up to $l_{\rm max} = 4$ in Eq. (5.16), i.e., we additionally allow for non-zero $K_{20}^{40}(k)$, $K_{40}^{20}(k)$ and $K_{40}^{40}(k)$, and discuss how the solution changes

compared to the $l_{\max}=2$ case. The equation for the expansion coefficients $c_{n_i 0}$ remains unchanged while that for $c_{n_i 2}$ is modified. Furthermore, the expansion coefficients $c_{n_i 4}$ are no longer zero. Consequently, we have three coupled equations, which can be decoupled, resulting in the following implicit eigenequation, $t_0 + q_2/(t_2 + q_4/t_4) = 0$. In analogy to the $l_{\max}=2$ case, the q_4 term and the first part on the right hand side of the t_4 term arise due to the "off-diagonal" K-matrix elements $K_{20}^{40}(k)$ and $K_{40}^{20}(k)$, and the second term of t_4 arises due to the "diagonal" K-matrix element $K_{40}^{40}(k)$.

Next, let us assume that we have found the implicit eigenequation for the case where we include terms in Eq. (5.16) with l and l' up to $l_{\max}-2$. If we now include terms with l and l' up to $l_{\max}$, only the equations for the expansion coefficients $c_{n_o l_o}$ with $l_o = l_{\max}-2$ and $l_{\max}$ change; those for the expansion coefficients $c_{n_o l_o}$ with $l_o \leq l_{\max}-4$ remain unchanged. This allows the $(l_{\max}/2)+1$ coupled equations for the expansion coefficients to be decoupled analytically using the results already determined for the case where l and l' go up to $l_{\max}-2$. Following this procedure, we find the following implicit eigenequation

$$T_{l_{\max}} = 0, \tag{5.33}$$

where $T_{l_{\max}}$ itself can be written in a continued fraction type form. For identical bosons we find,

$$T_{l_{\max}} = t_0 + \cfrac{q_2}{t_2 + \cfrac{q_4}{t_4 + \cdots + \cfrac{q_{l_{\max}}}{t_{l_{\max}}}}}. \tag{5.34}$$

Taking $l_{\max} \to \infty$ gives the eigenequation for two identical bosons under spherical harmonic confinement interacting through $V_{\text{pp, reg}}$ with infinitely many terms. For two identical fermions, Eqs. (5.31) through (5.34) remain valid if the subscripts $0, 2, \cdots$ in

Eq. (5.34) are replaced by $1,3,\cdots$. It is important to note that Eq. (5.34) is valid as long as the denominators $D_{l,l_{\max}} \neq 0$ for $l = 2,4,6,\ldots,l_{\max}$, where

$$D_{l,l_{\max}} = t_l + \frac{q_{l+2}}{t_{l+2} + \frac{q_{l+4}}{t_{l+4}+\cdots+\frac{q_{l_{\max}}}{t_{l_{\max}}}}}. \tag{5.35}$$

For $D_{l,l_{\max}} = 0$ extra unphysical roots arise, which are discussed in more detail in Sec. 5.4.4.

The derived eigenequation reproduces the eigenenergies in the known limits. For the non-interacting case (all $K_{l0}^{l'0} = 0$), the eigenenergies coincide with the eigenenergies of the harmonic oscillator, i.e., $E_{nl} = (2n + l + 3/2)\hbar\omega_{\rm ho}$, where $n = 0,1,2,\cdots$ and $l = 0,2,4,\cdots$ (in the case of identical bosons) and $l = 1,3,\cdots$ (in the case of identical fermions). The kth levels, with energy $(2k+3/2)\hbar\omega_{\rm ho}$ for bosons and $(2k+5/2)\hbar\omega_{\rm ho}$ for fermions, has a degeneracy of $k+1$, $k = 0,1,\cdots$. Non-vanishing $K_{l0}^{l'0}$ lead to a splitting of degenerate energy levels but leave the number of energy levels unchanged. If K_{l0}^{l0} is the only non-zero K-matrix element, the eigenequation reduces to that obtained for spherically symmetric pseudopotentials with partial wave l [see Eq. (3.50) and Ref. [65]].

5.3.3 Energy spectrum of the two dipole system under spherical harmonic confinement

This section analyzes the implicit eigenequation, Eq. (5.33), for the zero-range pseudopotential with $m = 0$ and compares the resulting energy spectrum with that obtained for the shape-dependent model potential $V_{\rm model}(\vec{r})$. The implicit eigenequation, Eq. (5.33), can be solved readily numerically by finding its roots in different energy regions.

Lines in Figs. 5.7(a) and (b) show the eigenenergies obtained by solving Eq. (5.33) for two identical bosons and two identical fermions, respectively, interacting through

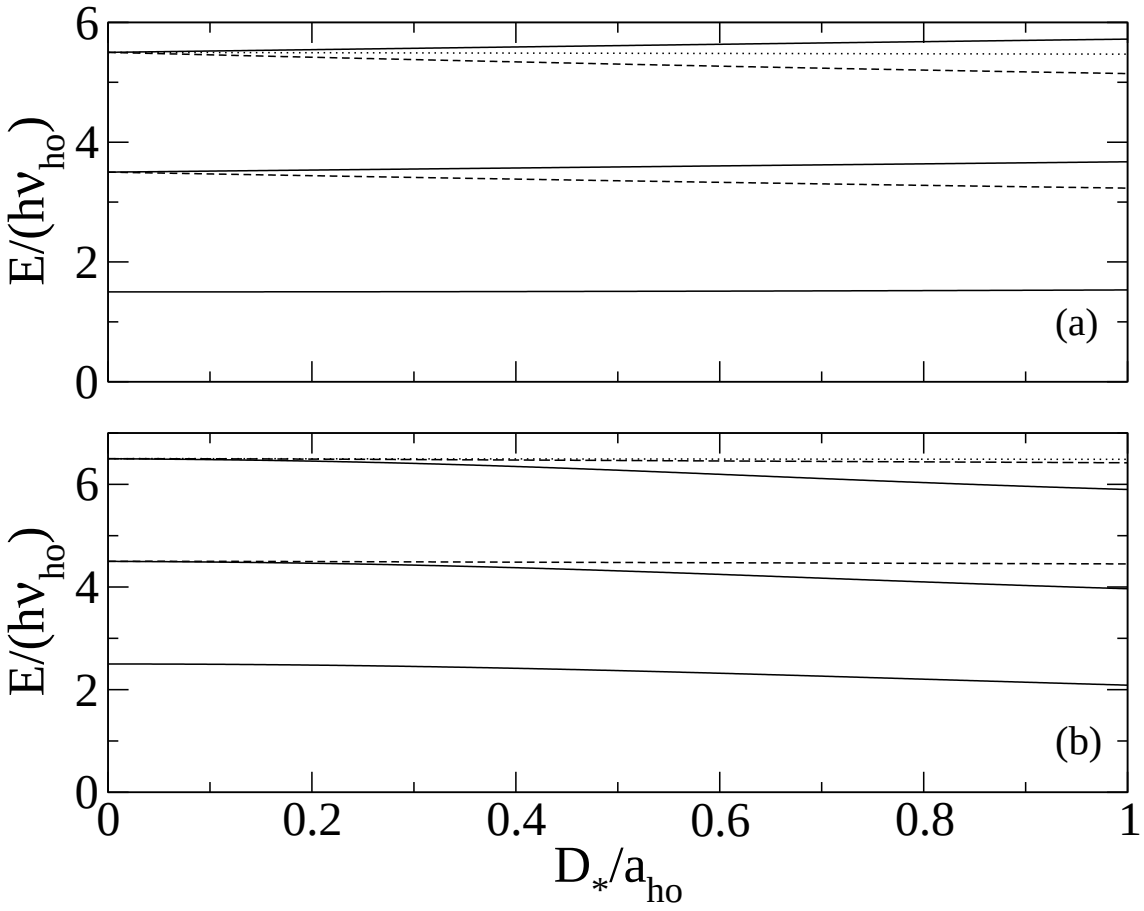

Figure 5.7: Relative eigenenergies E for (a) two identical bosonic dipoles and (b) two identical fermionic dipoles interacting through $V_{\text{pp, reg}}$ [using $a_{00} = 0$ in (a)] under spherical harmonic confinement as a function of D_*/a_{ho}. The line style indicates the approximate quantum number of the corresponding eigenstates. In (a), a solid line refers to $l \approx 0$, a dashed line to $l \approx 2$, and a dotted line to $l \approx 4$; in (b), a solid line refers to $l \approx 1$, a dashed line to $l \approx 3$, and a dotted line to $l \approx 5$.

$V_{\mathrm{pp,reg}}(\vec{r})$ under external spherically symmetric harmonic confinement as a function of the dipole length D_*. In both panels, we assume that the interaction between the two dipoles is purely dipolar, i.e., in Fig. 5.7(a) we set $a_{00} = 0$. The other scattering lengths $a_{ll'}$ are evaluated in the Born approximation [see Eqs. (5.11) and (5.12)]. Interestingly, for identical bosons, the lowest gas-like level, which starts at $E = 1.5\hbar\omega_{\mathrm{ho}}$ for $D_* = 0$, increases with increasing D_*. For identical fermions, in contrast, the lowest gas-like state decreases with increasing D_*.

In addition to obtaining the eigenenergies themselves, the pseudopotential treatment allows the spectrum to be classified in terms of angular momentum quantum numbers. To this end, we solve the implicit eigenequation, Eq. (5.33), for increasing l_{max}, and monitor how the energy levels shift as additional angular momenta are included in $V_{\mathrm{pp,\,reg}}$. Since a level with approximate quantum number l changes only little as larger angular momentum values are included in the pseudopotential, this analysis reveals the approximate quantum number of each energy level. In Fig. 5.7(a), the eigenfunctions of energies shown by solid, dashed and dotted lines have approximate quantum numbers $l = 0$, 2 and 4, respectively. In Fig. 5.7(b), the eigenfunctions of energies shown by solid, dashed and dotted lines have approximate quantum numbers $l = 1$, 3 and 5, respectively. We find that the lowest excitation frequency between states with approximate quantum number $l = 0$ [$l = 1$], increases [decreases] for identical bosons [fermions] with increasing D_*. These predictions can be verified directly experimentally.

To assess the accuracy of the developed zero-range pseudopotential treatment, we consider two interacting bosons with non-vanishing s-wave scattering length a_{00}. We imagine that the dipole moment of two identical polarized bosonic polar molecules is tuned by an external electric field. As the dipole moment d is tuned, the s-wave scattering length a_{00}, which depends on the short-range and the long-range physics of the

"true" interaction potential, changes. The other scattering lengths are, as before, approximated by the expressions given in Eqs. (5.11) and (5.12). Solid lines in Fig. 5.8(a) and (b) show the eigenenergies obtained for V_{model} as a function of D_*. Crosses show the eigenenergies obtained for $V_{\text{pp, reg}}$ using a value of $l_{\max}$ that results in converged eigenenergies. The overview spectrum shown in Fig. 5.8(a) shows that one of the energy levels dives down to negative energies close to that D_* value at which the two-body potential V_{model} supports a new bound state. The blow-up, Fig. 5.8(b), around $E \approx 5.5\hbar\omega_{\text{ho}}$ shows excellent agreement between the energies obtained using $V_{\text{pp, reg}}$ (crosses) and those obtained using V_{model} (solid lines); the maximum deviation for the energy range shown is 0.05 %.

As before, we can assign approximate quantum numbers to each energy level. For $D_* \ll a_{\text{ho}}$, the three energy levels around $E \approx 5.5\hbar\omega_{\text{ho}}$ have, from bottom to top, approximate quantum numbers $l = 2$, 4 and 0. After two closely spaced avoided crossings around $D_* \approx 0.025 a_{\text{ho}}$, the assignment changes to $l = 0$, 2 and 4 (again, from bottom to top). If the maximum angular momentum $l_{\max}$ of the pseudopotential is set to 2, the energy level with approximate quantum number $l = 4$ would be absent entirely. This illustrates that a complete and accurate description of the energy spectrum requires the use of a zero-range pseudopotential with infinitely many terms. The energy of a state with approximate quantum number l requires $l_{\max}$ to be at least l for the correct degeneracy be obtained and at least $l+2$ for a quantitative description.

The sequence of avoided crossings at $D_* \approx 0.025 a_{\text{ho}}$ suggests an interesting experiment. Assume that the system is initially, at small electric field (i.e., small D_*/a_{ho}), prepared in the excited state with angular momentum $l \approx 0$ and $E \approx 5.52\hbar\omega_{\text{ho}}$. The electric field is then slowly swept across the first broad avoided crossing at $D_* \approx 0.019 a_{\text{ho}}$ to transfer the population from the state with $l \approx 0$ to the state with $l \approx 2$. We then suggest to sweep quickly across the second narrower avoided crossing at $D_* \approx 0.028 a_{\text{ho}}$

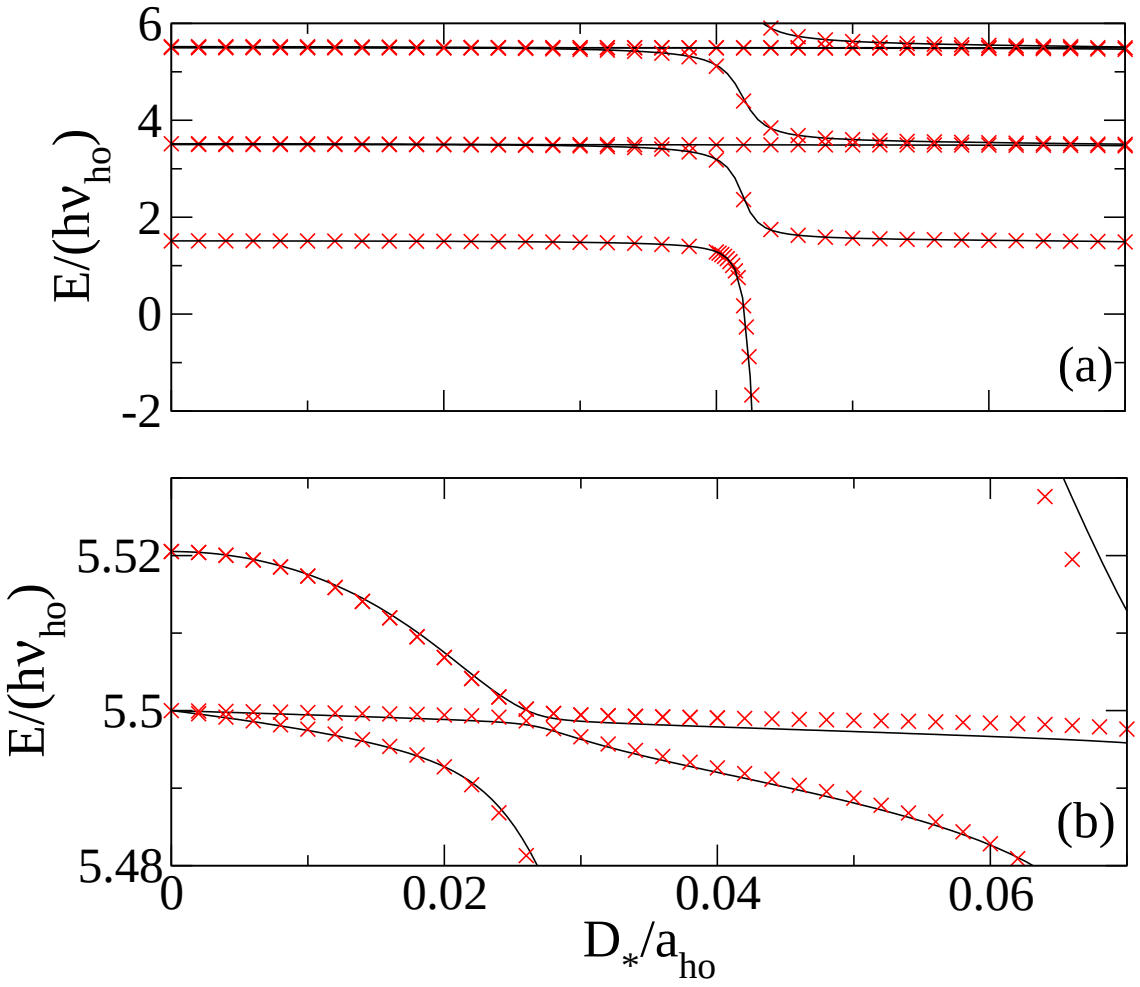

Figure 5.8: Panel (a) shows the relative energies E for two aligned identical bosonic dipoles under external spherical harmonic confinement as a function of D_*/a_{ho}. Solid lines show the numerically determined energies obtained using V_{model} with $r_c = 0.0097 a_{\mathrm{ho}}$. Crosses show the energies obtained using $V_{\mathrm{pp,\,reg}}$ with essentially infinitely many terms, and a_{00} calculated for V_{model}. The other scattering lengths are, as before, approximated by the expressions given in Eqs. (5.11) and (5.12). Panel (b) shows a blow-up of the energy region around $E \approx 5.5\hbar\omega_{\mathrm{ho}}$. Note that the horizontal axis in (a) and (b) are identical. This figure is taken from Ref. [70].

(the ramp speed must be chosen so minimize population transfer from the state with $l \approx 2$ to the state with $l \approx 4$). As in the case of s-wave scattering only [96], the time-dependent field sequence has to be optimized to obtain maximal population transfer. The proposed scheme promises to provide an efficient means for the transfer of population between states with different angular momenta and for quantum state engineering.

Figure 5.8 illustrates that the pseudopotential treatment reproduces the eigenenergies of the shape-dependent model potential $V_{\rm model}$. To further assess the validity of the pseudopotential treatment, we now consider two interacting bosonic dipoles for which the dipolar interaction is dominant, i.e., we consider $a_{00} = 0$. For $V_{\rm model}$ with $r_c = 0.0031 a_{\rm ho}$, we determine a set of D_* values at which $a_{00} = 0$. Note that the number of bound states with approximate quantum number $l = 0$ increases by one for each successively larger D_*. Crosses in Figs. 5.9(a)-(c) show the eigenenergies for $V_{\rm model}$ with $a_{00} = 0$ as a function of D_* in the energy ranges around 1.5, 3.5 and $5.5\hbar\omega_{\rm ho}$. For comparison, lines show the eigenenergies obtained for the regularized pseudopotential with $a_{00} = 0$. As in Fig. 5.7, the linestyle indicates the approximate quantum number of the energy levels (solid line: $l \approx 0$; dashed line: $l \approx 2$; and dotted line: $l \approx 4$). The agreement between the energies obtained for the pseudopotential with $a_{ll'}$ given by Eqs. (5.11) and (5.12) and for the model potential for small D_* is very good, thus validating the applicability of the pseudopotential treatment. The agreement becomes less good, however, as D_* increases. This can be explained readily by realizing that the dipole length D_* approaches the harmonic oscillator length $a_{\rm ho}$.

In general, the description of confined particles interacting through zero-range pseudopotentials is justified if the characteristic lengths of the two-body potential are smaller than the characteristic length of the confining potential. For example, in the case of s-wave interactions only, the van der Waals length has to be smaller than the oscillator

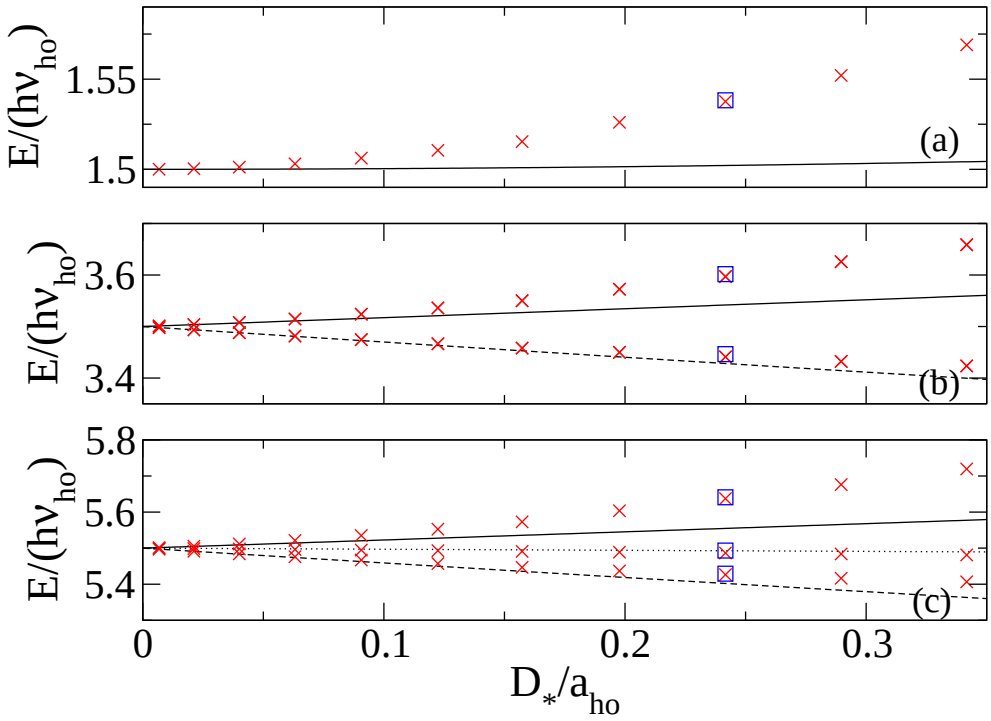

Figure 5.9: Crosses show the relative eigenenergies E as a function of $D_*/a_{\rm ho}$ for two identical bosons with $a_{00} = 0$ interacting through $V_{\rm model}$ with $r_c = 0.0031 a_{\rm ho}$ in three different energy regions. Lines show E for two identical bosons with $a_{00} = 0$ interacting through $V_{\rm pp,reg}$ with $a_{ll'}$ given by Eqs. (5.11) and (5.12). As in Fig. 5.7(a) solid, dashed and dotted lines show the energies of levels characterized by approximate quantum numbers $l \approx 0$, 2 and 4. The agreement between the crosses and the lines is good at small $D_*/a_{\rm ho}$ but less good at larger $D_*/a_{\rm ho}$. Squares show the eigenenergies obtained for the energy-dependent pseudopotential at $D_* = 0.242 a_{\rm ho}$; the agreement between the squares and the crosses is excellent, illustrating that usage of the energy-dependent K-matrix greatly enhances the applicability regime of $V_{\rm pp,\,reg}$. This figure is taken from Ref. [71].

length [106, 107]. The model potential V_{model} is characterized by a short-range length scale, the hardcore radius r_c, and the dipole length D_*; in Fig. 5.9, it is the relatively large value of D_*/a_{ho} that leads, eventually, to a break-down of the pseudopotential treatment. As in the case of spherical interactions, the break-down can be pushed to larger D_* values by using energy-dependent generalized scattering lengths $a_{ll'}(k)$ [see Eq. (5.9)] and by then solving the eigenequation, Eq. (5.33), self-consistently [106, 107].

Figure 5.10 shows three selected scattering lengths $a_{ll'}(k)$ for the model potential V_{model} with $D_* = 78.9b$ as a function of energy. This two-body potential supports eight bound states with projection quantum number $m = 0$ and approximate angular momentum quantum number $l = 0$. Both energy and length in Fig. 5.10 are expressed in oscillator units to allow for direct comparison with the data shown in Fig. 5.9. The scattering length $a_{00}(k)$, shown by a solid line in Fig. 5.10, is zero at zero energy and increases with increasing energy. Both $a_{20}(k)$ (dashed line) and $a_{22}(k)$ (dash-dotted line) are negative and their zero-energy values coincide with those calculated in the Born approximation (horizontal dotted lines).

Using these energy-dependent $a_{ll'}(k)$ to parametrize the strengths of the pseudopotential and solving the eigenequation, Eq. (5.33), self-consistently, we obtain the squares in Fig. 5.9. The energies for $V_{\text{pp, reg}}$ with $a_{ll'}(k)$ (squares) are in much better agreement with the energies obtained for the model potential (crosses) than the energies obtained using $a_{ll'}$ [Eq. 5.10 for $l = l' = 0$ and Eqs. (5.11) and (5.12) otherwise] to parametrize the pseudopotential (lines). This suggests that the applicability regime of the regularized zero-range pseudopotential can be extended significantly by introducing energy-dependent scattering lengths.

The self-consistent solutions (crosses) for non-zero a_{00} were already shown in Fig. 5.4. These were obtained by solving Eq. (5.34) using the coupled channel energy dependent scattering lengths $a_{ll'}(k)$ as input parameters. Hence these eigenenergies and those

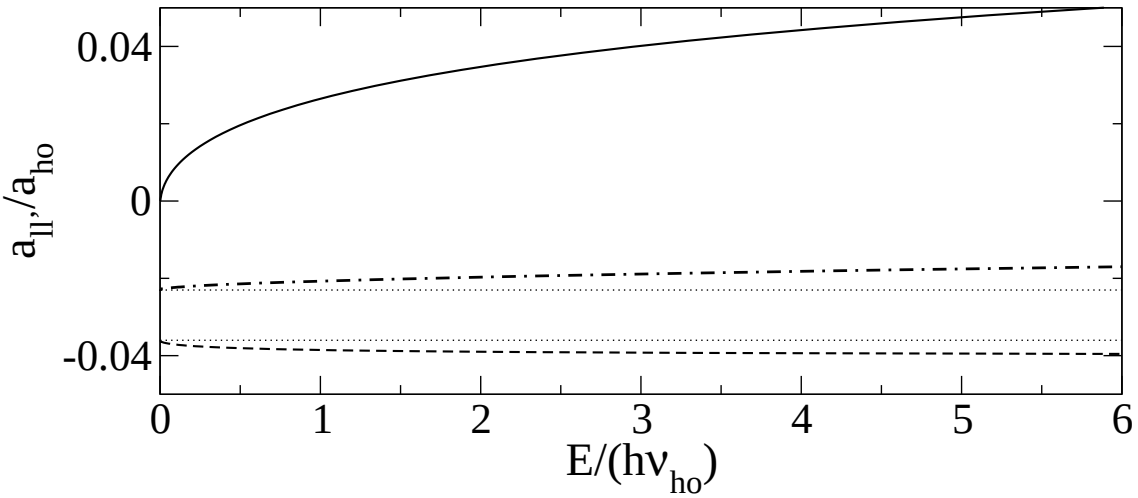

Figure 5.10: Energy-dependent scattering lengths $a_{00}(k)$ (solid line), $a_{20}(k)$ (dashed line) and $a_{22}(k)$ (dash-dotted line) for the model potential V_{model} with $D_* = 78.9b$ as a function of the relative energy E. In oscillator units, V_{model} is characterized by $r_c = 0.0031a_{\text{ho}}$ and $D_* = 0.242a_{\text{ho}}$. For comparison, horizontal dotted lines show the energy-independent scattering lengths a_{22}, Eq. (5.11), and a_{20}, Eq. (5.12), calculated in the first Born approximation. This figure is taken from Ref. [71].

obtained for V_{model} (dashed lines) show excellent agreement even for fairly large values of D_*/a_{ho}.

We now use $V_{\text{pp, reg}}$ to obtain the bound states of the system. For small $|E|$, the eigenequation for the zero range pseudopotential results in an unphysical eigenenergy [not shown in Figs. 5.4(a)-(d) but discussed in more detail in Sec. 5.4.4]. For two identical bosons, e.g., the eigenequation for $V_{\text{pp, reg}}$ permits a solution with $E \approx 0.05\hbar\omega_{\text{ho}}$, which is absent in the eigenspectrum of two identical bosons under external harmonic confinement interacting through $V_{\text{model}}(\vec{r})$. Importantly, if we restrict the zero range pseudopotential to the V_{00} and V_{11} terms for two identical bosons and fermions, respectively, the eigenspectra for $V_{\text{pp, reg}}$ and $V_{\text{model}}(\vec{r})$ agree very well for $E \lesssim 0.5\hbar\omega_{\text{ho}}$ (two identical bosons) and $E \lesssim 1.5\hbar\omega_{\text{ho}}$ (two identical fermions), and the unphysical eigenenergies are absent. This shows (i) that the scattering lengths a_{00} (identical bosons) and a_{11} (identical fermions) are dominant in this regime, and (ii) that the unphysical eigenenergies are due to the higher partial wave contributions of $V_{\text{pp, reg}}$. The latter can be understood as follows: The coupling strengths $g_{ll'}(k)$ for two interacting dipoles are proportional to $a_{ll'}(k)/k^{l+l'}$, and—since the $a_{ll'}(k)$ are defined so that they approach a constant in the $k \to 0$ limit—diverge as k goes to zero for $l + l' > 0$. A detailed analysis of the eigenequation for $V_{\text{pp, reg}}$ shows that these divergences give rise to the unphysical eigenenergies for small $|k|$. No unphysical eigenenergies arise for larger $|k|$; in this regime, the $1/k^{l+l'}$ factor in $g_{ll'}(k)$ can be thought of as a simple "rescaling". Furthermore, the unphysical eigenenergies do not arise if the phase shifts are obtained for a short-range model potential whose scattering lengths are defined by $-\tan\delta_{ll'}(k)/k^{l+l'+1}$. Although the zero range pseudopotential reproduces the eigenenergies well, we note that the single-parameter description fails to describe the higher partial wave admixtures discussed in the context of Fig. 5.6.

5.4 Pseudopotential treatment under cylindrically symmetric confinement

5.4.1 Derivation of the pseudopotential

The goal in this section is to determine a pseudopotential that reproduces the K-matrix of the true interaction potential for any positive scattering energy E and that can be applied to two interacting particles under external harmonic confinement of either spherical or cylindrical symmetry. Although the pseudopotential is derived by considering the relative Hamiltonian in Eq. (3.11) without an external confinement, it turns out that its functional form needs to be chosen to "match" the symmetry of the Hamiltonian that it is used in later on. We assume that the true interaction potential asymptotically approaches a constant, but that coupling between different partial waves can occur at shorter interparticle distances. These assumptions allow, e. g., for a treatment of interacting dipoles but exclude the treatment of Feshbach resonances in a single partial wave. The multi-channel pseudopotential $V_{\mathrm{ps}}(\vec{r})$ can be written as

$$V_{\mathrm{ps}}(\vec{r}) = \sum_{l=0}^{\infty} \sum_{m=-l}^{m=l} \sum_{l'=0}^{\infty} \sum_{m'=-l'}^{m'=l'} V_{l\,m}^{l'm'}(\vec{r}), \tag{5.36}$$

where l and m denote the angular momentum and projection quantum numbers of the incoming wave, and l' and m' those of the outgoing wave. $V_{l\,m}^{l'm'}$ couples the incoming partial wave labeled by $(l\,m)$ and the outgoing partial wave labeled by $(l'm')$, and is

defined by its action on $\vec{r}$ dependent functions χ and ξ [68, 69],

$$\langle\xi(\vec{r})|V_{lm}^{l'm'}(\vec{r})|\chi(\vec{r})\rangle = g_{lm}^{l'm'}(k)\times$$
$$\left(\int \frac{\delta(r)}{r^{l'+2}} Y_{l'm'}(\theta,\phi)\xi^*(\vec{r})r^2 dr d\Omega\right)\left[\frac{\partial^{2l+1}}{\partial r^{2l+1}}\left(r^{l+1}\int Y_{lm}(\theta,\phi)\chi(\vec{r})d\Omega\right)\right]_{r\to 0}, \quad (5.37)$$

where r, θ and ϕ denote the spherical coordinates of the relative vector $\vec{r}$. The coupling strengths $g_{lm}^{l'm'}(k)$ are given by

$$g_{lm}^{l'm'}(k) = -\frac{\hbar^2}{2\mu}\frac{K_{lm}^{l'm'}(k)}{k^{l+l'+1}}\frac{((2l+1)!!)((2l'+1)!!)}{(2l+1)!}. \quad (5.38)$$

For $m = m' = 0$, Eq. (5.38) reduced to Eq. (5.18). Since the $g_{lm}^{l'm'}(k)$ are written in terms of the K-matrix elements, the pseudopotential in Eq. (5.37) can be applied to any single threshold interaction potential with well defined K-matrix elements. In Eq. (5.37), the spherical harmonic $Y_{lm}(\theta,\phi)$ together with the integration over the angles extracts the (lm) component of the incoming wavefunction $\chi(\vec{r})$, while $Y_{l'm'}(\theta,\phi)$ together with the angular integration extracts the $(l'm')$ component of the outgoing wavefunction $\xi(\vec{r})$. For the derivation to follow, it will be useful to write Eq. (5.37) in a slightly modified form,

$$\langle\xi(\vec{r})|V_{lm}^{l'm'}(\vec{r})|\chi(\vec{r})\rangle = g_{lm}^{l'm'}(k)\times$$
$$\left[\int \frac{Y_{l'm'}(\theta,\phi)}{l'!}\left(\frac{\partial^{l'}\xi^*(\vec{r})}{\partial r^{l'}}\right)_{r\to 0} d\Omega\right]\left[\int Y_{lm}(\theta,\phi)\left(\frac{\partial^{2l+1}}{\partial r^{2l+1}}\left(r^{l+1}\chi(\vec{r})\right)\right)_{r\to 0} d\Omega\right]. \quad (5.39)$$

In determining Eq. (5.39), we used the identity $\frac{\delta(r)}{r^{l'}} = (-1)^{l'}\frac{\delta^{(l')}(r)}{l'!}$, where $\delta^{(l')}(r) = \frac{\partial^{l'}}{\partial r^{l'}}\delta(r)$, and performed the integration over r.

The pseudopotential defined through Eqs. (5.36) and (5.37) can be conveniently used to model the interaction potential $V_{\rm int}(\vec{r})$ if the external potential $V_{\rm ext}$ depends only

on r and not on the angles θ and ϕ. However, if V_{ext} does not possess spherical symmetry and if the state of interest is expanded in terms of a set of basis functions that have the same symmetry as V_{ext}, then usage of V_{ps} may lead to divergences. In the following, we rewrite the $V_{lm}^{l'm'}$ in Eq. (5.37) so that they can be used conveniently when the external potential is cylindrically symmetric, i. e., when $V_{\text{ext}} = V_{\text{ext}}(\rho, z)$, where ρ and z denote cylindrical coordinates defined through $\rho^2 = r^2 - z^2$ and $z = r\cos\theta$.

To rewrite Eq. (5.39) in cylindrical coordinates, we follow the procedure illustrated in Ref. [99, 124]: We first work in cartesian coordinates and then switch to cylindrical coordinates. To evaluate the $r \to 0$ limit of $\left(\frac{\partial^{l'}\xi^*(\vec{r})}{\partial r^{l'}}\right)$ in Eq. (5.39), we Taylor expand $\xi^*(\vec{r})$ in cartesian coordinates,

$$\xi^*(\vec{r}) = \sum_{j=0}^{\infty} \frac{r^j}{j!} \left[\sum_{q_1}\sum_{q_2}\ldots\sum_{q_j} (n_{q_1} n_{q_2}\ldots n_{q_j}) \left(\frac{\partial^j \xi^*(\vec{r})}{\partial q_1 \partial q_2 \ldots \partial q_j} \right) \right]_{x,y,z\to 0}, \tag{5.40}$$

where q_i is x, y or z and $n_{q_i} = \hat{r}\cdot\hat{q}_i$ ($\hat{q}_i$ denotes the unit vector in the q_i-direction). Using Eq. (5.40), we find

$$\left(\frac{\partial^{l'}\xi^*(\vec{r})}{\partial r^{l'}}\right)_{r\to 0} = \left[\sum_{q_1}\sum_{q_2}\ldots\sum_{q_{l'}} (n_{q_1} n_{q_2}\ldots n_{q_{l'}}) \left(\frac{\partial^{l'}\xi^*(\vec{r})}{\partial q_1 \partial q_2 \ldots \partial q_{l'}} \right) \right]_{x,y,z\to 0}. \tag{5.41}$$

To evaluate the second term in round brackets on the right hand side of Eq. (5.39), we use

$$\left[\frac{\partial^{2l+1}}{\partial r^{2l+1}} \left(r^{l+1}\chi(\vec{r}) \right) \right]_{r\to 0} = \left[\frac{\partial^l}{\partial r^l} \left(\frac{r^l}{l!} \frac{\partial^{2l+1}}{\partial r^{2l+1}} \left(r^{l+1}\chi(\vec{r}) \right) \right) \right]_{r\to 0}, \tag{5.42}$$

and Taylor expand $\frac{r^l}{l!}\frac{\partial^{2l+1}}{\partial r^{2l+1}}(r^{l+1}\chi(\vec{r}))$. Applying the partial differential operator $\frac{\partial^l}{\partial r^l}$ to the Taylor expanded expression and taking the $r \to 0$ limit, we find

$$\left(\frac{\partial^{2l+1}}{\partial r^{2l+1}}\left(r^{l+1}\chi(\vec{r})\right)\right)_{r\to 0} = \left[\sum_{q_1}\sum_{q_2}...\sum_{q_l}(n_{q_1}n_{q_2}...n_{q_l})\left(\frac{\partial^l\left(\frac{r^l}{l!}\frac{\partial^{2l+1}}{\partial r^{2l+1}}\left(r^{l+1}\chi(\vec{r})\right)\right)}{\partial q_1\partial q_2...\partial q_l}\right)\right]_{x,y,z\to 0}. \tag{5.43}$$

If we plug Eqs. (5.41) and (5.43) into Eq. (5.39), we obtain an expression for $\langle\xi(\vec{r})|V_{lm}^{l'm'}(\vec{r})|\Phi(\vec{r})\rangle$ in cartesian coordinates. Up to here, our treatment is general and can be used as a starting point for rewriting Eq. (5.39) in any coordinate system. We now adopt cylindrical coordinates and assume that both ξ and χ are cylindrically symmetric functions, i. e., $\xi(\vec{r})=\xi(\rho,z)$ and $\chi(\vec{r})=\chi(\rho,z)$. Furthermore, the cylindrical symmetry conserves the projection quantum number, and we specialize to the $m=m'=0$ case. To simplify the notation, we replace $V_{lm}^{l'm'}$ by $V_{ll'}$ and $g_{lm}^{l'm'}$ by $g_{ll'}$,

$$V_{\rm ps}^0(\vec{r})=\sum_{l=0}^{\infty}\sum_{l'=0}^{\infty}V_{ll'}(\vec{r}). \tag{5.44}$$

The approach outlined can be generalized to other m values (see, e. g., Refs. [99, 125]). Performing the angular integrals in Eq. (5.39) and rearranging the terms, we obtain

$$\langle\xi(\rho,z)|V_{ll'}(\vec{r})|\chi(\rho,z)\rangle = h_{ll'}(k)\left[\overline{Y}_{l'0}(\vec{\nabla})\xi^*(\rho,z)\right]_{\rho,z\to 0}\left[\overline{Y}_{l0}(\vec{\nabla})\left(r^l\frac{\partial^{2l+1}}{\partial r^{2l+1}}\left(r^{l+1}\chi(\rho,z)\right)\right)\right]_{\rho,z\to 0}, \tag{5.45}$$

where

$$h_{ll'}(k)=g_{ll'}(k)\beta(l)\beta(l') \tag{5.46}$$

and

$$\beta(l)=\frac{(-1)^l 2\pi}{2^{[[\frac{l}{2}]]-1}3^{[[\frac{l}{2}]]}}\times \\ \frac{(2[[\frac{l}{2}]])!!\Xi(l)}{(([[l/2]])!)^2(2[[\frac{l}{2}]]-1)!!(2l+1)}\left(\prod_{i=1}^{[[l/2]]}\langle 2i-2,2,0,0|2i,0\rangle^2\right). \tag{5.47}$$

In Eq. (5.47), $\langle l_1,l_2,m_1,m_2|l,m\rangle$ is a Clebsch Gordan coefficient and $[[x]]$ indicates the greatest integer less than or equal to x. Further, we defined

$$\Xi(l)=\begin{cases}1 & \text{for} \quad l\in\text{even}\\ \frac{1}{2l-1} & \text{for} \quad l\in\text{odd.}\end{cases} \tag{5.48}$$

In Eq. (5.45), we introduced the differential operator $\overline{Y}_{l0}(\vec{\nabla})$,

$$\overline{Y}_{l0}(\vec{\nabla})=\sum_{p=0}^{[[l/2]]}A_{pl}(\nabla^2)^p\left(\frac{\partial}{\partial z}\right)^{l-2p}, \tag{5.49}$$

where A_{pl} is the coefficient of $(\cos\theta)^{l-2p}$ in the spherical harmonic $Y_{l0}(\hat{r})$. For example, the $Y_{40}(\hat{r})$ spherical harmonic can be written as $A_{24}+A_{14}\cos^2\theta+A_{04}\cos^4\theta$, where $A_{24}=\frac{9}{16\sqrt{\pi}}$, $A_{14}=-\frac{90}{16\sqrt{\pi}}$ and $A_{04}=\frac{105}{16\sqrt{\pi}}$. Noting that $\hat{z}\cdot\hat{r}=\cos\theta$, the $Y_{40}(\hat{r})$ can alternatively be written as $A_{24}(\hat{r}\cdot\hat{r})^2+A_{14}(\hat{r}\cdot\hat{r})(\hat{z}\cdot\hat{r})^2+A_{04}(\hat{z}\cdot\hat{r})^4$. This expression motivates us to label the operator defined in Eq. (5.49) by $\overline{Y}_{l0}(\vec{\nabla})$: Keeping the order of $\hat{r}$ and $\hat{z}$ unchanged but replacing $\hat{r}$ by $\vec{\nabla}$, the $Y_{4,0}(\hat{r})$ becomes $A_{24}(\vec{\nabla}\cdot\vec{\nabla})^2+A_{14}(\vec{\nabla}\cdot\vec{\nabla})(\hat{z}\cdot\vec{\nabla})^2+A_{04}(\hat{z}\cdot\vec{\nabla})^4$, which is just $\overline{Y}_{40}(\vec{\nabla})$. Writing the Laplacian operator in Eq. (5.49) in cylindrical coordinates and

expanding in a binomial series, the $\overline{Y}_{l0}(\vec{\nabla})$ can be alternatively written as

$$\overline{Y}_{l0}(\vec{\nabla}) = \sum_{p=0}^{[[l/2]]} \sum_{q=0}^{p} A_{pl} \frac{p!}{q!(p-q)!} \left(\frac{\partial^2}{\partial \rho^2} + \frac{1}{\rho} \frac{\partial}{\partial \rho} \right)^{p-q} \frac{\partial^{l-2p+2q}}{\partial z^{l-2p+2q}}. \tag{5.50}$$

Here, we omitted derivatives with respect to the azimuthal angle ϕ, since the $\overline{Y}_{l0}(\vec{\nabla})$ act, by construction, on wavefunctions that only depend on ρ and z.

The pseudopotential $V_{ll'}$ in Eq. (5.45) is defined through its action on the functions ξ and χ. Alternatively, we can interpret the $V_{ll'}$ as differential operators given by

$$V_{ll'}(\vec{r}) = h_{ll'}(k) \overline{Y}^{\dagger}_{l'0}(\vec{\nabla}) \frac{\delta(\rho)\delta(z)}{2\pi\rho} \overline{Y}_{l0}(\vec{\nabla}) r^l \frac{\partial^{2l+1}}{\partial r^{2l+1}} r^{l+1}. \tag{5.51}$$

Following Eq. (5.45), the operator $\overline{Y}^{\dagger}_{l'0}$ acts to the left and all other differential operators act to the right.

5.4.2 Derivation of the eigenequation for cylindrically harmonic confinement

This section determines the eigenequation [see Eq. (5.71) below] for two particles interacting through $V^0_{\rm ps}(\vec{r})$ under external cylindrically symmetric harmonic confinement. The confining potential in the relative coordinate is given by

$$V_{\rm ext}(\rho, z) = \frac{1}{2} \mu \omega_z^2 (\eta^2 \rho^2 + z^2), \tag{5.52}$$

where we have defined the aspect ratio η as the ratio between the radial and longitudinal angular frequencies, $\eta = \omega_\rho / \omega_z$. The relative Hamiltonian $H_{\rm rel}$ can be written

as

$$H = H_{\rm osc} + V_{\rm ps}^0(\vec{r}), \tag{5.53}$$

where

$$H_{\rm osc} = -\frac{\hbar^2}{2\mu}\nabla_{\vec{r}}^2 + V_{\rm ext}(\rho, z). \tag{5.54}$$

In the following, we expand the eigenfunctions Ψ of H in terms of the eigenfunctions $\Phi_{n\alpha}$ of $H_{\rm osc}$,

$$H_{\rm osc}\Phi_{n\alpha}(\rho, z) = E_{n\alpha}\Phi_{n\alpha}(\rho, z), \tag{5.55}$$

where

$$E_{n\alpha} = [\eta(2n+1) + (\alpha + 1/2)]\hbar\omega_z. \tag{5.56}$$

The quantum number n takes integer values, $n = 0, 1, 2...$, while the quantum number α takes even integer values ($\alpha = 0, 2, 4, ...$) for even l and odd integer values ($\alpha = 1, 3, 5, ..$) for odd l. If the aspect ratio η equals $1/m$, where m is an integer, the m energetically lowest-lying energy levels are non degenerate, the next m energy levels have a degeneracy of two, the next m energy levels have a degeneracy of three and so on. We write the oscillator functions $\Phi_{n,\alpha}$ as a product of the oscillator functions $R_n(\rho)$ and $\Theta_\alpha(z)$ in ρ and z, respectively,

$$\Phi_{n\alpha}(\rho, z) = R_n(\rho)\Theta_\alpha(z), \tag{5.57}$$

where

$$R_n(\rho) = \frac{1}{a_z}\sqrt{\frac{\eta}{\pi}}\exp\left(-\frac{\eta\rho^2}{2a_z^2}\right) L_n^{(0)}(\eta(\rho/a_z)^2) \tag{5.58}$$

and

$$\Theta_\alpha(z) = \frac{1}{\sqrt{a_z}\pi^{1/4}\sqrt{2^\alpha \alpha!}}\exp\left(-\frac{z^2}{2a_z^2}\right) H_\alpha(z/a_z). \tag{5.59}$$

Throughout, lengths are measured in units of the oscillator length a_z,

$$a_z = \sqrt{\hbar/(\mu\omega_z)}. \tag{5.60}$$

In Eqs. (5.58) and (5.59), the $L_n^{(0)}$ and H_α denote associated Laguerre and Hermite polynomials, respectively.

The eigenfunctions Ψ of the full relative Hamiltonian are expanded in terms of the complete orthonormal set $\Phi_{n\alpha}(\rho,z)$,

$$\Psi(\rho,z) = \sum_{n=0}^{\infty}\sum_{\alpha=0}^{\infty} c_{n\alpha}\Phi_{n\alpha}(\rho,z), \tag{5.61}$$

where the $c_{n\alpha}$ denote expansion coefficients. Plugging Eq. (5.61) into $H_{\rm rel}\Psi(\rho,z) = E\Psi(\rho,z)$, multiplying from the left with $\Phi^*_{n',\alpha'}(\rho,z)$, integrating over all space and using orthonormality of the $\Phi_{n\alpha}(\rho,z)$, we get

$$c_{n',\alpha'} = \frac{\langle\Phi_{n',\alpha'}(\rho,z)|\sum_{l,l'} V_{ll'}(\vec{r})|\sum_{n,\alpha} c_{n\alpha}\Phi_{n\alpha}(\rho,z)\rangle}{E - E_{n',\alpha'}}. \tag{5.62}$$

Importantly, the right hand side of Eq. (5.62) is independent of n and α since both these indices are being summed over. Thus, Eq. (5.62) determines the expansion coefficients $c_{n',\alpha'}$. To evaluate the right hand side of Eq. (5.62) and to eventually arrive at an implicit eigenequation for E, we plug Eq. (5.51) into Eq. (5.62), and, using the properties of δ-functions, perform the integration over all space. This yields

$$c_{n',\alpha'} = \frac{\sum_{l,l'} h_{ll'}(k)\left[\overline{Y}^{\dagger}_{l'0}(\vec{\nabla})\Phi_{n',\alpha'}(\rho,z)\right]_{\rho,z\to 0} C_l}{E - E_{n',\alpha'}}, \tag{5.63}$$

where

$$C_l = \left[\sum_{n,\alpha} c_{n\alpha} \hat{O}_l \Phi_{n\alpha}(\rho, z) \right]_{\rho,z\to 0} \tag{5.64}$$

and

$$\hat{O}_l = \overline{Y}_{l0}(\vec{\nabla}) r^l \frac{\partial^{2l+1}}{\partial r^{2l+1}} r^{l+1}. \tag{5.65}$$

Plugging Eq. (5.63) into Eq. (5.64), we find an equation for C_λ,

$$C_\lambda = \left[\hat{O}_\lambda \left(\sum_{n,\alpha} \frac{\sum_{l,l'} h_{ll'}(k) \left[\overline{Y}^\dagger_{l'0}(\vec{\nabla}) \Phi_{n\alpha}(\rho, z) \right]_{\rho,z\to 0} C_l}{E - E_{n\alpha}} \Phi_{n\alpha}(\rho, z) \right) \right]_{\rho,z\to 0}. \tag{5.66}$$

We now exchange the sums in Eq. (5.66) and collect the n and α dependent terms in S_l,

$$C_\lambda = \left[\hat{O}_\lambda \left(\sum_{l,l'} h_{ll'}(k) S_{l'}(\rho, z) C_l \right) \right]_{\rho,z\to 0}, \tag{5.67}$$

where

$$S_l(\rho, z) = \left(\sum_{n,\alpha} \frac{\left[\overline{Y}^\dagger_{l0}(\vec{\nabla}) \Phi_{n\alpha}(\rho, z) \right]_{\rho,z\to 0}}{E - E_{n\alpha}} \Phi_{n\alpha}(\rho, z) \right). \tag{5.68}$$

Bringing all terms of Eq. (5.67) to one side and defining

$$M_{\lambda l} = \sum_{l'} h_{ll'}(k) \left[\hat{O}_\lambda S_{l'}(\rho, z) \right]_{\rho,z\to 0} - \delta_{\lambda,l}, \tag{5.69}$$

Eq. (5.67) becomes

$$\sum_l M_{\lambda l} C_l = 0. \tag{5.70}$$

The eigenenergies E of the relative Hamiltonian H can thus be obtained by solving the determinantal equation

$$\det(\boldsymbol{M}) = 0, \tag{5.71}$$

where the matrix elements of $\boldsymbol{M}$ are given by Eq. (5.69). The evaluation of the matrix elements $M_{\lambda l}$ requires acting with $\hat{O}_\lambda$ on $S_{l'}$, and then taking the $\rho, z \to 0$ limits. Before detailing how the expression $[\hat{O}_\lambda S_{l'}]_{\rho,z\to 0}$ can be simplified, we discuss a number of properties of Eq. (5.71).

Since the pseudopotential $V_{\rm ps}^0$ that describes the interaction between the particles contains infinitely many terms, the matrix $\boldsymbol{M}$ has infinite dimensions. In practice, we reduce the size of the matrix $\boldsymbol{M}$ to a manageable size. This can either be achieved by truncating the pseudopotential itself or by setting certain coupling constants $g_{ll'}$ to zero. For example, if we consider only the $l = 0$ term in the pseudopotential, the eigenequation $\det(\boldsymbol{M}) = 0$ [see Eqs. (5.81)-(5.83) below] reduces to those derived in Ref. [60] and Refs. [110, 126] for spherically and cylindrically symmetric traps, respectively. Similarly, if we only allow for a non-zero $g_{1,1}$, we recover the p-wave eigenequations derived in Refs. [64, 99, 124] for the $m = 0$ case, and so on. If we consider an interaction potential that couples different partial waves, such as the dipole-dipole potential, then the matrix $\boldsymbol{M}$ contains non-vanishing off-diagonal elements. If the true or model potential conserves parity, then even (odd) incoming partial waves are scattered into even (odd) outgoing partial waves. In this case, all coupling strengths $g_{ll'}$ with l even and l' odd (and l odd and l' even) vanish, and the matrix $\boldsymbol{M}$ is block diagonal: The first block corresponds to even l and l', and the second block to odd l and l'; the

eigenvalues of these blocks can be determined separately. If $g_{ll'}=0$ for $|l-l'|>2$, the resulting determinantal equation for $\eta=1$ can be rewritten in a continued fraction type form and coincides with that obtained in Eq. (5.33). For $\eta\neq 1$, however, an eigenequation that accounts for the coupling between different channels has not been obtained previously.

We now first simplify $S_l(\rho,z)$ and then evaluate the action of $\hat{O}_\lambda$ on S_l. Using Eq. (5.56), we write the denominator on the right hand side of Eq. (5.68) as

$$\frac{1}{E-E_{n\alpha}}=-\frac{1}{\hbar\omega_z}\int_0^\infty e^{(\frac{E}{\hbar\omega_z}-\eta-1/2)t-2\eta nt-\alpha t}\,dt. \tag{5.72}$$

This yields

$$S_l(\rho,z)=\frac{-1}{\hbar\omega_z}\int_0^\infty\sum_{n,\alpha}\left[\overline{Y}^\dagger_{l0}(\vec{\nabla})\Phi_{n\alpha}(\rho,z)\right]_{\rho,z\to 0}\Phi_{n\alpha}(\rho,z)e^{(\frac{E}{\hbar\omega_z}-\eta-1/2)t-2\eta nt-\alpha t}\,dt. \tag{5.73}$$

Equation (5.72) is valid only if the exponent in the integrand is negative. Since n and α take values starting from zero, Eq. (5.72) and the equations that follow from it are valid only for $\frac{E}{\hbar\omega_z}<\eta+\frac{1}{2}$. Plugging Eqs. (5.50) and (5.57) into Eq. (5.73), we obtain

$$\begin{aligned}S_l(\rho,z)=\frac{-1}{\hbar\omega_z}\sum_{p=0}^{[[l/2]]}\sum_{q=0}^{p}A_{p,l}\frac{p!}{(p-q)!q!}\\ \int_0^\infty\left\{\sum_{n=0}^\infty\left[\left(\frac{\partial^2}{\partial\rho^2}+\frac{1}{\rho}\frac{\partial}{\partial\rho}\right)^{p-q}R_n(\rho)\right]_{\rho\to 0}R_n(\rho)e^{-2\eta nt}\right\}\\ \left\{\sum_{\alpha=0}^\infty\left[\frac{\partial^{\,l-2p+2q}}{\partial z^{\,l-2p+2q}}\Theta_\alpha(z)\right]_{z\to 0}\Theta_\alpha(z)e^{-\alpha t}\right\}e^{(\frac{E}{\hbar\omega_z}-\eta-1/2)t}\,dt.\end{aligned} \tag{5.74}$$

The infinite sum over n can be evaluated using Eqs. (5.58) and (16) from Ref. [110],

$$\sum_{n=0}^{\infty}\left[\left(\frac{\partial^2}{\partial\rho^2}+\frac{1}{\rho}\frac{\partial}{\partial\rho}\right)^{p-q}R_n(\rho)\right]_{\rho\to 0}R_n(\rho)e^{-2\eta nt}=$$
$$-\frac{(-\eta)^{p-q+1}}{\pi a_z^{2p-2q+2}}((2p-2q)!!)^2\sum_{i=0}^{p-q}\frac{1}{i!(p-q-i)!2^{p-q-i}}\hat{D}_i\left(\frac{\exp\left(-\frac{\eta\rho^2}{2a_z^2}\frac{1+\exp(-2\eta t)}{1-\exp(-2\eta t)}\right)}{1-\exp(-2\eta t)}\right), \quad (5.75)$$

where $\hat{D}_i=\prod_{j=0}^{i-1}(\frac{-1}{2\eta}\frac{d}{dt}-j)$. Similarly, the infinite sum over α can be performed using Eqs. (5.59) and (18) from Ref. [110],

$$\sum_{\alpha=0}^{\infty}\left[\frac{\partial^{l-2p+2q}}{\partial z^{l-2p+2q}}\Theta_\alpha(z)\right]_{z\to 0}\Theta_\alpha(z)e^{-\alpha t}=\frac{1}{a_z\sqrt{\pi}}\exp\left(-\frac{z^2}{2a_z^2}\right)\times$$
$$\left[\frac{\partial^{l-2p+2q}}{\partial x^{l-2p+2q}}\left(\frac{1}{\sqrt{1-e^{-2t}}}\exp\left(\frac{-x^2}{2a_z^2}+\frac{-(x^2+y^2)e^{-2t}+2xye^{-t}}{a_z^2(1-e^{-2t})}\right)\right)\right]_{x=0,y=z}. \quad (5.76)$$

Plugging Eqs. (5.75) and (5.76) into Eq. (5.74), we find

$$S_l(\rho,z)=\frac{1}{\hbar\omega_z}\sum_{p=0}^{[[l/2]]}\sum_{q=0}^{p}A_{p,l}\frac{p!}{(p-q)!q!}\frac{(-\eta)^{p-q+1}}{a_z^{2p-2q+3}\pi^{3/2}}((2p-2q)!!)^2\exp\left(-\frac{z^2}{2a_z^2}\right)\times$$
$$\int_0^{\infty}\left[\frac{\partial^{l-2p+2q}}{\partial x^{l-2p+2q}}\left(\frac{\exp\left(\frac{-x^2}{2a_z^2}+\frac{-(x^2+y^2)e^{-2t}+2xye^{-t}}{a_z^2(1-e^{-2t})}\right)}{\sqrt{1-e^{-2t}}}\right)\right]_{x=0,y=z}\sum_{i=0}^{p-q}\frac{\hat{D}_i\left(\frac{\exp\left(-\frac{\eta\rho^2}{2a_z^2}(\frac{1+e^{-2\eta t}}{1-e^{-2\eta t}})\right)}{1-e^{-2\eta t}}\right)}{i!(p-q-i)!2^{p-q-i}}dt. \quad (5.77)$$

The quantity $[\hat{O}_\lambda S_l]_{\rho,z\to 0}$ can now be evaluated by expanding the integrand in Eq. (5.77) in powers of ρ and z. This yields

$$S_l(\rho,z)=\frac{1}{\hbar\omega a_z^{l+3}}\sum_{i=0}^{\infty}\sum_{j}\sum_{u=1}^{u_{ij}^l} I_{iju}^l\left(\frac{\rho}{a_z}\right)^{2i}\left(\frac{z}{a_z}\right)^{j}, \tag{5.78}$$

where

$$u_{ij}^l = \left(\sum_{\alpha=0}^{[[\frac{l+2}{4}]]}([[l/2]]+1-2\alpha)^2\right)\left([[(2i+j)/2]]+1+i[[j/2]]\right) \tag{5.79}$$

and

$$I_{iju}^l=\frac{B_{iju}^l}{2}\int_0^{\infty}\frac{e^{(\frac{E}{2\hbar\omega_z}-a_{iju}^l\eta-b_{iju}^l)t}}{(1-e^{-\eta t})^{f_{iju}^l}(1-e^{-t})^{d_{iju}^l}}dt. \tag{5.80}$$

In Eq. (5.78), j takes the values $0,2,4...$ if l is even and the values $1,3,5...$ if l is odd. The quantities a_{iju}^l, b_{iju}^l, f_{iju}^l and d_{iju}^l in Eq. (5.80) are η-independent constants of the form $n+1/2$, $n+1/4$, n and $n+1/2$, where n can take the values $0,1,2....$ The B_{iju}^l are real numbers that depend on η. We have not been able to find simple analytical expressions for these coefficients. In practice, we perform the Taylor expansion of Eq. (5.77) in Mathematica and tabulate the values of a_{iju}^l, b_{iju}^l, f_{iju}^l, d_{iju}^l and B_{iju}^l for all possible i, j and u (and in case of B_{iju}^l, separately for each η).

The action of the operator $\hat{O}_\lambda$ on S_l can now be evaluated readily. For $\rho,z\to 0$, we obtain

$$[\hat{O}_\lambda S_l(\rho,z)]_{\rho,z\to 0} = \sum_{p=0}^{[[\frac{\lambda}{2}]]}\sum_{q=0}^{p} A_{p,\lambda}\frac{p![(2\lambda+1)!((2p-2q)!!)^2(\lambda-2p+2q)!]}{\hbar\omega a_z^{\lambda+l+3}q!(p-q)!}J^l_{p-q,\lambda-2p+2q},$$

(5.81)

where

$$J^l_{i,j} = \sum_{u=1}^{u^l_{ij}} I^l_{iju}. \tag{5.82}$$

The prefactors in the square bracket on the right hand side of Eq. (5.81) can be understood as follows: The $(2\lambda+1)!$ term comes from the r-dependent part of $\hat{O}_\lambda$ acting on the $\rho^{2p-2q}z^{\lambda-2p+2q}$ term of S_l, the $((2p-2q)!!)^2$ term comes from the ρ-dependent part of $\overline{Y}_{\lambda,0}(\vec{\nabla})$ acting on the ρ^{2p-2q} term of S_l, and the $(\lambda-2p+2q)!$ term comes from the z-dependent part of $\overline{Y}_{\lambda,0}(\vec{\nabla})$ acting on the $z^{\lambda-2p+2q}$ term of S_l. The evaluation of the quantity $[\hat{O}_\lambda S_l]_{\rho,z\to 0}$ requires knowing the energy-dependent integrals I^l_{iju}. Unfortunately, no general expressions for I^l_{iju} are known. However, if the angular trapping frequencies are integer multiples of each other, then the integral I^l_{iju} has a closed form [110]. For pancake shaped traps with $\eta = 1/m$, where m denotes an integer, we find

$$I^l_{iju} = \sum_{s_1=0}^{m-1}\sum_{s_2=0}^{m-1}....\sum_{s_{f^l_{iju}}=0}^{m-1}\frac{B^l_{iju}}{2}\frac{\Gamma\left(\frac{s_1+s_2+....+s_{f^l_{iju}}}{m}+\frac{a^l_{iju}}{m}+b^l_{iju}-\frac{E}{2\hbar\omega_z}\right)\Gamma\left(1-f^l_{iju}-d^l_{iju}\right)}{\Gamma\left(\frac{s_1+s_2+....+s_{f^l_{iju}}}{m}+\frac{a^l_{iju}}{m}+b^l_{iju}-\frac{E}{2\hbar\omega_z}+1-f^l_{iju}-d^l_{iju}\right)}.$$

(5.83)

The expression for I^l_{iju} contains f^l_{iju} sums (recall, f^l_{iju} is an integer). For a given i, j, l and m, the right hand side of Eq. (5.83) contains $m^{f^l_{iju}}$ terms. This number can be quite large for anisotropic traps. The largest f^l_{iju} value for a fixed l is given by $l+1$,

resulting, e. g., in 10^7 terms for $l=6$ and $m=10$. In practical evaluations we reduce the number of terms by realizing that the quantity $s_1+s_2+....+s_{f^l_{iju}}$ can take only values from 0 to $f^l_{iju}(m-1)$. Knowing the frequency with which each term occurs, Eq. (5.83) can be rewritten as a sum of $f^l_{iju}(m-1)$ terms, thereby reducing the computational efforts needed to evaluate the matrix elements $M_{\lambda,l}$ drastically, especially for large m and l.

The above derivation is valid if $\frac{E}{\hbar\omega_z} < \eta+\frac{1}{2}$. For $\frac{E}{\hbar\omega_z} > \eta+\frac{1}{2}$, Eq. (5.83) can be analytically continued so that the entire energy spectrum can be obtained if $\eta = 1/m$.

5.4.3 Application of the eigenequation to short range potentials

The pseudopotential in Eq. (5.44) was originally designed to treat dipole-dipole interactions. However, due to the long range nature of these interactions we encounter some problems in applying Eq. (5.71), which are elaborated on in Sec. 5.4.4. Similar problems are not expected to arise for short range potentials. Consequently, as a first test we apply Eq. (5.71) it to two particles interacting via an attractive short range anisotropic potential $V_{\rm int}(\vec{r})$,

$$V_{\rm int}(\vec{r}) = -d\exp\left(-\frac{r^2}{2r_0^2}\right)Y_{20}(\theta,\phi), \tag{5.84}$$

where $d>0$. In this case, the energy dependent generalized scattering lengths $a_{ll'}(k)$ are determined by [112]

$$a_{ll'}(k) = -\frac{K^{l'0}_{l0}(k)}{k^{l+l'+1}} \tag{5.85}$$

and the energy independent scattering lengths $a_{ll'}$ [$a_{ll'}=\lim_{k\to 0} a_{ll'}(k)$] are constant. Note that these generalized scattering lengths have a different threshold behavior from those for the dipole-dipole interaction defined in Eqs. (5.9) and (5.10).

First, we test the diagonal elements of $\boldsymbol{M}$. We confirmed that the diagonal elements

corresponding to $l = 0$ and $l = 1$ are correct by comparing with the eigenequations in Refs. [110, 126, 64, 99, 124]. Furthermore, we have checked that diagonal element corresponding to $l = 2$ is correct by comparing the eigenenergies with those obtained numerically for a short range shape dependent d-wave potential. Hence we believe that the diagonal terms of the $\boldsymbol{M}$-matrix are correct.

Second, we test the off diagonal elements of the $\boldsymbol{M}$-matrix. To do this, we compare the eigenenergies obtained numerically for the interaction potential in Eq. (5.84) with those obtained semi-analytically from Eq. (5.71) by using in the K-matrix elements obtained for the potential in Eq. (5.84). For the range of d values considered, the only non-negligible scattering lengths are $a_{00}(k)$ and $a_{22}(k)$ and the eigenenergies obtained using Eq. (5.71) are converged for $l_{\max} = 2$. This implies that the eigenenergies are only sensitive to M_{00}, M_{20}, M_{02} and M_{22} matrix elements and that this example therefore only allows us to test for these matrix elements. Another restriction of this test is that the elements M_{20} and M_{02} only contribute significantly near a d-wave resonance.

To determine the eigenenergies for the pseudopotential [Eq. (5.44)], we use the K-matrix elements obtained for V_{int} [Eq. (5.84)] with $r_0 = 0.01 a_z$. Solid lines in Fig. 5.11 show the eigenenergies for two particles interacting via the potential in Eq. (5.84) under cylindrically symmetric harmonic confinement with $\eta = 1/2$ as a function of d. Crosses show the energies obtained from Eq. (5.71) with the K-matrix elements calculated for the potential in Eq. (5.84). Figure 5.11(a) shows an overview of the eigenspectrum while Figs. 5.11(b) and (c) show the blow ups of the levels near $3\hbar\omega_z$ and $1\hbar\omega_z$, respectively. The two lowest energy levels are non degenerate. For the lowest level this can be seen from Fig. 5.11(c). The $3\hbar\omega_z$ level is two fold degenerate for non-interacting particles [see discussion following Eq. (5.56)]. Figure 5.11(b) shows that the degeneracy is broken due to the interaction potential, resulting in two closely spaced eigenenergies.

To see how the eigenspectrum changes with decreasing aspect ratio, Fig. 5.12 shows

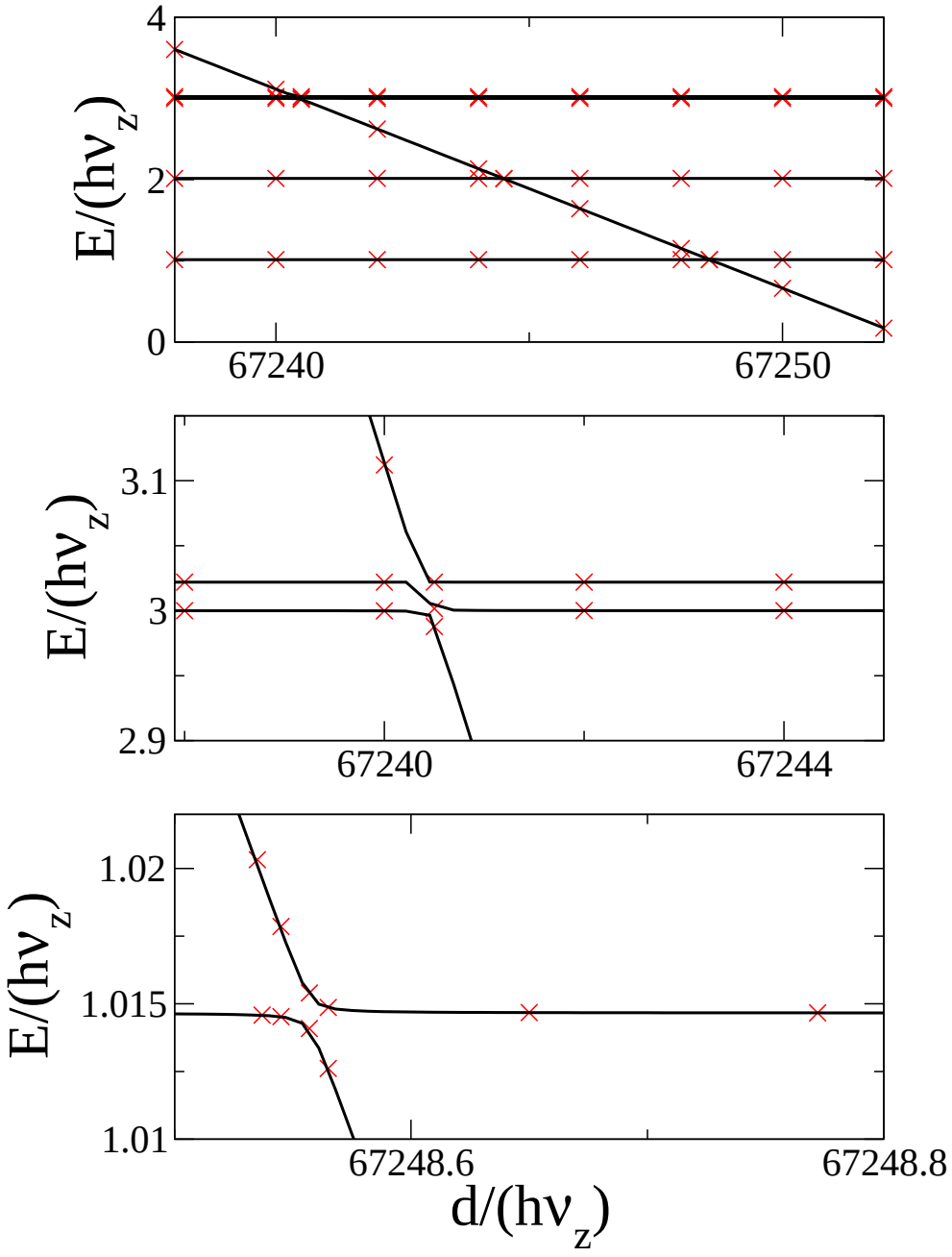

Figure 5.11: Energy spectrum for two particles under cylindrically symmetric external confinement with $\eta = 1/2$ as a function of d. (a) Solid lines show the energies calculated numerically for the interaction potential given in Eq. (5.84) with $r_0 = 0.01 a_z$, while crosses show the energies obtained from Eq. (5.71). (b) Blow up of the energy levels near $3\hbar\omega_z$. (c) Blow up of the energy level near $1\hbar\omega_z$. The eigenenergies for the interaction potential in Eq. (5.84) are provided by D. Blume.

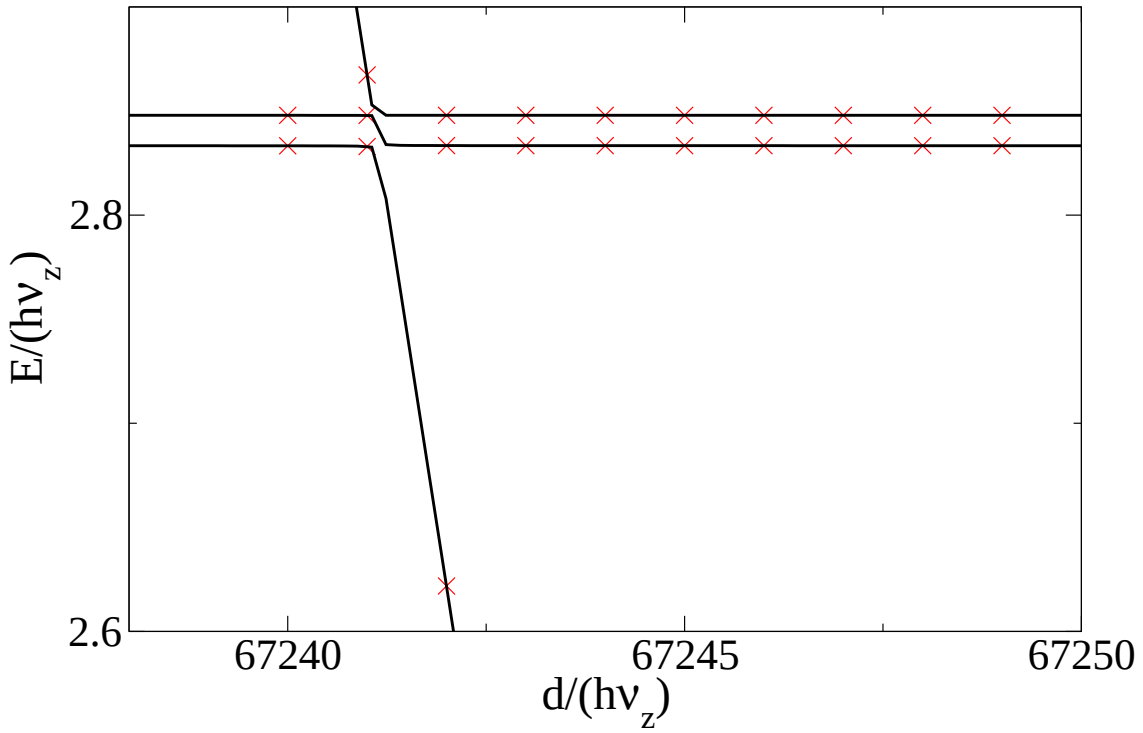

Figure 5.12: Energy spectrum for two particles under cylindrically symmetric external confinement with $\eta = 1/3$ as a function of d. Solid lines show the energies calculated numerically for the interaction potential given in Eq. (5.84) with $r_0 = 0.01 a_z$, while crosses show the energies obtained from Eq. (5.71). The eigenenergies for the interaction potential in Eq. (5.84) are provided by D. Blume.

the eigenenergy of the fourth level for two particles interacting through the same potentials as in Fig. 5.11 under cylindrically symmetric harmonic confinement with $\eta = 1/3$. Figure 5.12 shows that the lowest three levels are non degenerate and that there are two nearly degenerate levels around $\approx 2.833\hbar\omega_z$ [see discussion following Eq. (5.56)].

The good agreement between the two sets of eigenenergies in the above examples indicates that Eq. (5.71) reproduces the degeneracy correctly and that the matrix elements M_{20} and M_{02} are correct when a_{20} is negligible. We have not been able to test the validity of M_{20} and M_{02} for non-negligible a_{20} with the model potential given in Eq. (5.84).

For any anisotropic short range interaction potential it is hard to obtain a large coupling between the different partial waves and so it is difficult to use a short range potential to extensively test the working of Eq. (5.71), i. e., to test the matrix elements $M_{24}, M_{42}, M_{44}, \ldots$. If a short range potential with more non-negligible scattering lengths could be constructed, we believe the Eq. (5.71) should give the correct eigenenergies if all relevant channels are included. However, we have not been able to test this using the model potential given in Eq. (5.84).

The coupling between the different channels is larger for long ranged anisotropic potentials like the dipole-dipole interaction potential. In the next section we use Eq. (5.71) to obtain the eigenenergies of two aligned dipoles.

5.4.4 Application of the eigenequation to dipole-dipole potential

We have derived the eigenequation for two aligned dipoles under spherically symmetric harmonic confinement in two different ways. Section 5.3.2 obtains the eigenequation in the form of a continued fraction. Section 5.4.2 obtains the eigenequation for two aligned dipoles in the form of a matrix. Although we have obtained the eigenequations

for $l_{\max} = \infty$, in the following illustration we restrict ourselves $l_{\max} = 2$. The key points remain valid for larger $l_{\max}$ values. For even l and $l, l' \leq l_{\max} = 2$, the eigenequation for $\eta = 1$ can be written as

$$t_0 t_2 + q_2 = 0 \tag{5.86}$$

or, in terms of T_2, as

$$t_2 T_2 = 0. \tag{5.87}$$

The above equation implies that either $T_2 = 0$ and $t_2 \neq \infty$ or $t_2 = 0$ and $T_2 \neq \infty$.

In deriving Eq. (5.34), we required that $D_{2,2} = t_2 \neq 0$. Consequently, the latter case does not need to be considered. We note, however, that while the $t_2 \neq 0$ condition arises naturally in the derivation of the continued fraction, it does not appear to arise naturally in the derivation of the eigenequation written as a matrix. This does, as we show below, give rise to problems for $\eta = 1/m$ $(m > 1)$ that we do not know how to resolve at the moment.

The former condition ($T_2 = 0$ and $t_2 \neq \infty$) determines the eigenspectrum and is discussed in Sec. 5.3.3. In those applications, we restricted ourselves to $E \geq 1\hbar\omega_{\rm ho}$. Now we show that the eigenequation $T_2 = 0$, if applied to two aligned dipoles, has an additional root as was already mentioned in Sec. 5.3.3. We will show that this root is unphysical and has to be eliminated. The dashed dotted curve in Fig. 5.13(b) [and its inset] shows T_2 as a function of energy. The unphysical root occurs where T_2 crosses zero at $E \approx 0.062\hbar\omega_{\rm ho}$. This root is unphysical as it is not seen in the full energy spectrum obtained numerically for $V_{\rm model}$. We now investigate the origin of this unphysical root. The left hand side of Eq. (5.30) has an expression for T_2, which contains two terms. For T_2 to have a root, these terms must be equal in magnitude and be opposite in sign. In the energy regime where the unphysical root arises, t_0 is much greater than q_2. Consequently, t_2 needs to be small in this regime for the equation $T_2 = 0$ to have a root.

Figure 5.13(b) shows that

$$t_2 = \frac{\Gamma(\frac{-E}{2\hbar\omega} - \frac{3}{4})}{2^5\Gamma(\frac{-E}{2\hbar\omega} + \frac{7}{4})} - \frac{K_{20}^{20}}{k^5 a_{\rm ho}^{2l+1}}, \tag{5.88}$$

assumes a very small value for $E \approx 0.06\hbar\omega_{\rm ho}$. The solid curves in Fig. 5.13 show the first term on the right hand side of Eq. (5.88) as a function of energy. The dotted curve in Fig. 5.13 shows the second term on the right hand side of Eq. (5.88) as a function of energy obtained for $V_{\rm int}(\vec{r}) = V_{\rm model}(\vec{r})$ with $D_* = 0.0306 a_{\rm ho}$ and $r_c = 0.00306 a_{\rm ho}$. The solid and dotted curves are nearly equal to each other for $E \approx 0.06\hbar\omega_{\rm ho}$ and hence t_2 assumes a small value here. t_2 assumes a small value because $-\frac{K_{20}^{20}}{k^5}$ diverges as $k \to 0$ for the dipole-dipole interaction potential [see Fig. 5.13(a)]. The unphysical root can be eliminated by the procedure discussed in Sec. 5.3.3. For comparison, the dashed curve in Fig. 5.13(a) shows that $a_{22}(k)$ approaches a constant as $k \to 0$ for the short range anisotropic potential in Eq. (5.84) with $d = 60000\hbar\omega_{\rm ho}$ and $r_0 = 0.01 a_{\rm ho}$. Since the solid and dashed curves are not nearly equal to each other anywhere in the energy range $0 < E < 0.5\hbar\omega$, t_2 is not small in this range and $T_2 = 0$ has no root in this energy range.

For $\eta = 1$, the eigenequation with $l_{\rm max} = 2$ can be factored into two pieces yielding the conditions that either $T_2 = 0$ and $t_2 \neq \infty$ or $t_2 = 0$ and $T_2 \neq \infty$. For larger $l_{\rm max}$, an analogous though more complicated factorization holds. For $\eta < 1$, the eigenequation is more complicated and we have not been able to factorize the eigenequation in a manner that would separate out the unphysical roots. In fact, we believe that the additional coupling induced by the non-spherical confinement leads to a coupling of the physical and unphysical roots if the derived eigenequation is applied to dipole-dipole potentials. Importantly, the unphysical roots are not present for applications to short range potentials.

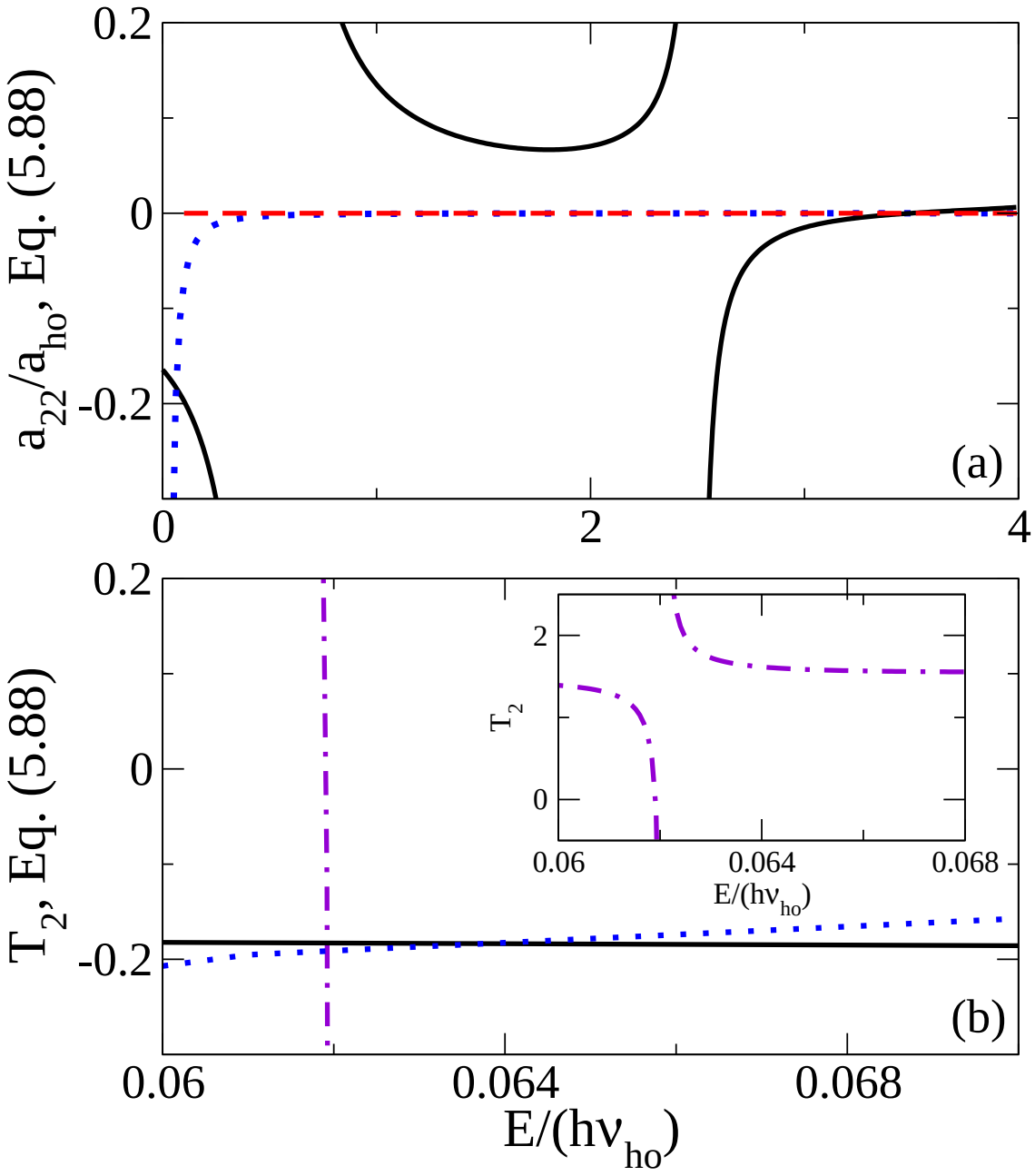

Figure 5.13: Solid curves show the first term on the right hand side of Eq. (5.88) as a function of energy. Dotted curves show the negative of the second term on the right hand side of Eq. (5.88) as a function of energy for $V_{\rm int} = V_{\rm model}$. (a) Dashed curves show the negative of the second term on the right hand side of Eq. (5.88) as a function of energy for $V_{\rm int}$ given by Eq. (5.84). (b) The dashed dotted curve shows T_2 [see Eq. (5.33)] as a function of energy. The parameters used are $D_* = 0.0306 a_{\rm ho}$ and $r_c = 0.00306 a_{\rm ho}$ for $V_{\rm model}$ and $d = 60000\hbar\omega_{\rm ho}$ and $r_0 = 0.01 a_{\rm ho}$ in the potential in Eq. (5.84). The inset of panel (b) shows T_2 as a function of energy on a larger y-scale.

5.5 Conclusions

This chapter pushes the pseudopotential treatment to regimes where it has never been used before. It treats anisotropic two body interactions in three dimensions. It obtains an eigenequation for two particles interacting through a cylindrically symmetric potential under cylindrically symmetric harmonic confinement in terms of K-matrix elements. For short range potentials, the threshold behavior of the scattering length is $1/(k^{l+l'+1})$ and the eigenequation works as expected. For the short range potentials considered, however, the coupling between channels is significant only over a tiny region and the effects of channel coupling are generally small. For long ranged potentials like the dipole-dipole interaction potential the coupling is more significant. This chapter develops a pseudopotential treatment for two aligned dipoles under spherically harmonic confinement, which works well with the caveat of an extra unphysical root. The chapter also identifies a simple procedure to eliminate this unphysical root. The applicability of the pseudopotential to two aligned dipoles under cylindrically symmetric harmonic confinement breaks down, since the threshold behavior of the scattering lengths is $1/k$. The chapter also explores the scattering properties of two aligned dipoles using a shape dependent model potential.

Chapter 6

Summary and outlook

This thesis treats different two body interactions under various conditions. The key results obtained and ideas developed are:

- We develop a zero range treatment for two particles interacting via a short range potential in strictly one dimension and obtain the eigenenergies of the system under harmonic confinement. We demonstate that our model is consistent with Fermi-Bose duality predicted and observed in one dimensional systems.

- We also use zero range pseudopotentials to model interactions in low dimensional systems. We analytically obtain the eigenequation of two particles interacting through a strictly two dimensional short range circularly symmetric pseudopotential under harmonic confinement for any partial wave. We also develop a coupled zero range two channel model to characterize a two dimensional Feshbach resonance.

- We analytically obtain the general eigenequation for two particles interacting through cylindrically symmetric potentials under cylindrically symmetric external harmonic confinement in three dimensions using a zero range pseudopotential. This

eigenequation has been applied to spherically symmetric short range interactions for any partial wave. It has also been applied to cylindrically symmetric short range interactions. It has been applied to two aligned dipoles under spherically symmetric harmonic confinement (cylindrical symmetry with $\eta = 1$) with the caveat of an extra unphysical root. The eigenequation breaks down due to the long range nature of the interaction when applied to two aligned dipoles under cylindrically symmetric harmonic confinement ($\eta < 1$).

- We use a shape dependent model potential to study scattering between two aligned dipoles. We observe two categories of resonances labeled B1 and B2 in the even parity case and F1 and F2 in the odd parity case. We examine the eigenspectrum of two aligned dipoles under spherically symmetric harmonic confinement near each type of resonance. We also obtain the eigenfunctions near each type of resonance and calculate the contribution of each partial wave to the eigenfunctions. We find that near B1 and B2 type resonances the major contribution to the lowest lying state is s-wave and near F1 and F2 type resonances the major contribution to the lowest lying state is p-wave.

In future research, it would be interesting to consider interactions between dipoles that are not aligned. This would be useful in analyzing a two dipole system in the presence of a weak external field. The broken azimuthal symmetry would lead to a coupling between the different m quantum numbers. The procedure to obtain the eigenenergies of two non-aligned dipoles under spherically symmetric harmonic confinement would be quite similar to that outlined in Sec. 5.3.2. It would be interesting to see if the zero range treatment would work in spite of the long range nature of the interaction.

It would also be interesting to see if the weakly bound states (“molecules”) formed across type 1 (B1 and F1) and type 2 (B2 and F2) resonances differ in their scattering

properties, and to analyze their partial wave composition in more detail.

Treating long ranged anisotropic interactions in lower dimensions using zero range pseudopotentials would also be of interest. Results obtained here may provide insights into systems of dipolar gases loaded into low dimensional optical lattices.

Appendix A

Evaluating an infinite sum

In this Appendix, we evaluate the infinite sum C_l,

$$C_l = \left[\frac{\partial^{2l+1}}{\partial r^{2l+1}} \left\{ r^{l+1} \sum_{n=0}^{\infty} \frac{\left[\frac{R^*_{nl}(r)}{r^l} \right]_{r\to 0} R_{nl}(r)}{2\left(\nu - n - \frac{l}{2}\right)\hbar\omega} \right\} \right]_{r\to 0} . \tag{A.1}$$

Writing the radial harmonic oscillator functions $R_{nl}(r)$ in terms of the Laguerre polynomials $L_n^{(l+1/2)}$,

$$R_{nl}(r) = \sqrt{\frac{2^{l+2}}{(2l+1)!!\pi^{1/2} L_n^{(l+1/2)}(0) a_{ho}^3}} \times \exp\left(-\frac{r^2}{2a_{ho}^2}\right) \left(\frac{r}{a_{ho}}\right)^l L_n^{(l+1/2)}(r^2/a_{ho}^2), \tag{A.2}$$

we find

$$\left[\frac{R_{nl}(r)}{r^l}\right]_{r\to 0} = \sqrt{\frac{2^{l+2} L_n^{(l+1/2)}(0)}{(2l+1)!!\pi^{1/2} a_{ho}^{2l+3}}}. \tag{A.3}$$

Using Eqs. (A.2) and (A.3), the C_l can be rewritten as

$$C_l = \frac{2^{l+1}}{(2l+1)!!\pi^{1/2}a_{ho}^{2l+3}} \times \left[\frac{\partial^{2l+1}}{\partial r^{2l+1}}\left(\exp\left(\frac{-r^2}{2a_{ho}^2}\right) r^{2l+1}\sum_{n=0}^{\infty}\frac{L_n^{(l+1/2)}\left((\frac{r}{a_{ho}})^2\right)}{\left(\nu-n-\frac{l}{2}\right)\hbar\omega}\right)\right]_{r\to 0}. \tag{A.4}$$

We evaluate the infinite sum in Eq. (A.4) using the properties of the generating function [83],

$$\sum_{n=0}^{\infty}\frac{L_n^{(l+1/2)}((r/a_{ho})^2)}{\nu-n-\frac{l}{2}} = -\Gamma(-\nu+l/2)U(-\nu+l/2,l+3/2,(r/a_{ho})^2). \tag{A.5}$$

Using Eq. (A.5) together with the small r behavior of the hypergeometric function U [83], the expression for the C_l reduces to

$$C_l = \frac{(-1)^l 2^{2l+2}(2l)!!}{(2l+1)!!}\frac{\Gamma\left(-\nu+\frac{l}{2}\right)}{\Gamma\left(-\nu-\frac{l+1}{2}\right)}\frac{1}{\hbar\omega a_{ho}^{2l+3}}. \tag{A.6}$$

Appendix B

Three dimensional square well potential

The generalized energy dependent p-wave scattering length $a_1(k)$ for the single channel square well interaction potential $V_{\text{sq well}}(r)$ is given by

$$a_1(k) = V_p(k) = \frac{j_1(kr_0)\left(\frac{\partial j_1(\sqrt{2\mu(E+V_0)/\hbar^2}r)}{\partial r}\right)_{r=r_0} - j_1(\sqrt{2\mu(E+V_0)/\hbar^2}r_0)\left(\frac{\partial j_1(kr)}{\partial r}\right)_{r=r_0}}{k^3\left(j_1(\sqrt{2\mu(E+V_0)/\hbar^2}r_0)\left(\frac{\partial n_1(kr)}{\partial r}\right)_{r=r_0} - n_1(kr_0)\left(\frac{\partial j_1(\sqrt{2\mu(E+V_0)/\hbar^2}r)}{\partial r}\right)_{r=r_0}\right)}. \tag{B.1}$$

The energy independent $\boldsymbol{R}$ matrix elements for the coupled two channel square well potential [Eq. (3.63)] are given by

$$R_{11} = \frac{V_{12}^2}{\sqrt{2}}\left(\frac{2\sqrt{V_1+V_2-\varepsilon-\sqrt{D^2+4V_{12}^2}}\cot\Omega}{4V_{12}^2+D\left(D+\sqrt{D^2+4V_{12}^2}\right)} + \frac{\sqrt{V_1+V_2-\varepsilon-\sqrt{D^2+4V_{12}^2}}\cot\Omega}{V_{12}^2+\frac{1}{4}\left(D-\sqrt{D^2+4V_{12}^2}\right)^2}\right), \tag{B.2}$$

$$R_{12} = \frac{V_{12}\left(\sqrt{V_1+V_2-\varepsilon-\sqrt{D^2+4V_{12}^2}}\cot\Omega - \sqrt{V_1+V_2-\varepsilon+\sqrt{D^2+4V_{12}^2}}\cot\Omega\right)}{\sqrt{2(D^2+4V_{12}^2)}} \tag{B.3}$$

and

$$R_{22} = \frac{\left(4V_{12}^2 + D\left(D + \sqrt{D^2 + 4V_{12}^2}\right)\right)\sqrt{V_1 + V_2 - \varepsilon - \sqrt{D^2 + 4V_{12}^2}}\cot\Omega}{2\sqrt{2}\left(D^2 + 4V_{12}^2\right)} - \frac{\left(-4V_{12}^2 + D\left(D + \sqrt{D^2 + 4V_{12}^2}\right)\right)\sqrt{V_1 + V_2 - \varepsilon + \sqrt{D^2 + 4V_{12}^2}}\cot\Omega}{2\sqrt{2}\left(D^2 + 4V_{12}^2\right)}, \tag{B.4}$$

where

$$D = \varepsilon + V_1 - V_2 \tag{B.5}$$

and

$$\Omega = \frac{r_0\sqrt{V_1 + V_2 - \varepsilon + \sqrt{D^2 + 4V_{12}^2}}}{\sqrt{2}}. \tag{B.6}$$

Appendix C

Two dimensional square well potential

The generalized energy dependent scattering length of the square well interaction potential for all $m > 0$ is given by

$$a_m(k) = \frac{2^{2m}\Gamma(m)\Gamma(m+1)}{\pi k^{2m}} \times \frac{J_m(k\rho_0)\left(\frac{\partial J_m(\sqrt{2\mu(E+V_0)/\hbar^2}\rho)}{\partial\rho}\right)_{\rho=\rho_0} - J_m(\sqrt{2\mu(E+V_0)/\hbar^2}\rho_0)\left(\frac{\partial J_m(k\rho)}{\partial\rho}\right)_{\rho=\rho_0}}{\left(J_m(\sqrt{2\mu(E+V_0)/\hbar^2}\rho_0)\left(\frac{\partial N_m(k\rho)}{\partial\rho}\right)_{\rho=\rho_0} - N_m(k\rho_0)\left(\frac{\partial J_m(\sqrt{2\mu(E+V_0)/\hbar^2}\rho)}{\partial\rho}\right)_{\rho=\rho_0}\right)}. \quad \text{(C.1)}$$

Bibliography

[1] C. J. Pethick and H. Smith. *Bose-Einstein Condensation in Dilute Gases*. Cambridge University Press, 2002.

[2] F. Dalfovo, S. Giorgini, L. P. Pitaevskii, and S. Stringari. "Theory of Bose-Einstein condensation in trapped gases". In: *Reviews of Modern Physics* 71 (1999), p. 463.

[3] S. Giorgini, L. P. Pitaevskii, and S. Stringari. "Theory of ultracold atomic Fermi gases". In: *Reviews of Modern Physics* 80 (2008), p. 1215.

[4] A. J. Leggett. "Bose-Einstein condensation in the alkali gases: Some fundamental concepts". In: *Reviews of Modern Physics* 73 (2001), p. 307.

[5] H. B. Callen. *Thermodynamics and an Introduction to Thermostatistics*. 2nd ed. John Wiley and Sons, 1985.

[6] M. H. Anderson, J. R. Ensher, M. R. Matthews, C. E. Wieman, and E. A. Cornell. "Observation of Bose-Einstein Condensation in a Dilute Atomic Vapor". In: *Science* 269 (1995), p. 198.

[7] K. B. Davis, M. O. Mewes, M. R. Andrews, N. J. van Druten, D. S. Durfee, D. M. Kurn, and W. Ketterle. "Bose-Einstein Condensation in a Gas of Sodium Atoms". In: *Physical Review Letters* 75 (1995), p. 3969.

[8] B. DeMarco and D. S. Jin. "Onset of Fermi Degeneracy in a Trapped Atomic Gas". In: *Science* 285 (2002), p. 1703.

[9] I. Bloch, J. Dalibard, and W. Zwerger. “Many-body physics with ultracold gases”. In: *Reviews of Modern Physics* 80, 885 (2008), p. 885.

[10] M. Greiner, O. Mandel, T. Esslinger, T. W. Hansch, and I. Bloch. “Quantum phase transition from a superfluid to a Mott insulator in a gas of ultracold atoms”. In: *Nature* 415 (2002), p. 39.

[11] T. Stöferle, H. Moritz, C. Schori, M. Köhl, and T. Esslinger. “Transition from a Strongly Interacting 1D Superfluid to a Mott Insulator”. In: *Physical Review Letters* 92 (2004), p. 130403.

[12] M. Greiner, I. Bloch1, O. Mandel1, T. W. Hänsch, and T. Esslinger. “Bose-Einstein condensates in 1D- and 2D optical lattices”. In: *Applied Physics B* 73 (2001), p. 769.

[13] D. Jaksch, C. Bruder, J. I. Cirac, C. W. Gardiner, and P. Zoller. “Cold Bosonic Atoms in Optical Lattices”. In: *Physical Review Letters* 81 (1998), p. 3108.

[14] T. Stöferle, H. Moritz, K. Günter, M. Köhl, and T. Esslinger. “Molecules of Fermionic Atoms in an Optical Lattice”. In: *Physical Review Letters* 96 (2006), p. 030401.

[15] G. Modugno, G. Ferrari, G. Roati, R. J. Brecha, A. Simoni, and M. Inguscio. “Bose-Einstein Condensation of Potassium Atoms by Sympathetic Cooling”. In: *Science* 294 (2001), p. 1320.

[16] C. C. Bradley, C. A. Sackett, J. J. Tollett, and R. G. Hulet. “Evidence of Bose-Einstein Condensation in an Atomic Gas with Attractive Interactions”. In: *Physical Review Letters* 75 (1995), p. 1687.

[17] C. C. Bradley, C. A. Sackett, J. J. Tollett, and R. G. Hulet. “Evidence of Bose-Einstein Condensation in an Atomic Gas with Attractive Interactions [Phys. Rev. Lett. 75, 1687 (1995)]”. In: *Physical Review Letters* 79 (1997), p. 1170.

[18] T. Weber, J. Herbig, M. Mark, H.-C. Nägerl, and R. Grimm. “Bose-Einstein Condensation of Cesium”. In: *Science* 299 (2003), p. 232.

[19] A. Griesmaier, J. Werner, S. Hensler, J. Stuhler, and T. Pfau. “Bose-Einstein Condensation of Chromium”. In: *Physical Review Letters* 94 (2005), p. 160401.

[20] J. Stuhler, A. Griesmaier, T. Koch, M. Fattori, T. Pfau, S. Giovanazzi, P. Pedri, and L. Santos. “Observation of Dipole-Dipole Interaction in a Degenerate Quantum Gas”. In: *Physical Review Letters* 95 (2005), p. 150406.

[21] J. D. Weinstein, R. deCarvalho, and T. Guillet. “Magnetic trapping of calcium monohydride molecules at millikelvin temperatures”. In: *Nature* 395 (1998), p. 148.

[22] H. L. Bethlem, G. Berden, and G. Meijer. “Decelerating Neutral Dipolar Molecules”. In: *Physical Review Letters* 83 (1999), p. 1558.

[23] B. C. Sawyer, B. L. Lev, E. R. Hudson, B. K. Stuhl, M. Lara, J. L. Bohn, and J. Ye. “Magnetoelectrostatic Trapping of Ground State OH Molecules”. In: *Physical Review Letters* 98 (2007), p. 253002.

[24] J. G. Danzl, E. Haller, M. Gustavsson, M. J. Mark, R. Hart, N. Bouloufa, O. Dulieu, H. Ritsch, and H.-C. Nägerl. “Quantum Gas of Deeply Bound Ground State Molecules”. In: *Science* 321 (2008), p. 1062.

[25] K.-K. Ni, S. Ospelkaus, M. H. G. de Miranda, A. Pe’er, B. Neyenhuis, J. J. Zirbel, S. Kotochigova, P. S. Julienne, D. S. Jin, and J. Ye. “A High Phase-Space-Density Gas of Polar Molecules”. In: *Science* 322 (2008), p. 231.

[26] S. Ospelkaus, K.-K. Ni, M. H. G. de Miranda, B. Neyenhuis, D. Wang, S. Kotochigova, P. S. Julienne, D. S. Jin, and J. Ye. “Ultracold polar molecules near quantum degeneracy”. In: *arXiv:0811.4618v1* (2008).

[27] B. Deb and L. You. “Low-energy atomic collision with dipole interactions”. In: *Physical Review A* 64.2 (2001), p. 022717.

[28] D. DeMille. “Quantum Computation with Trapped Polar Molecules”. In: *Physical Review Letters* 88 (2002), p. 067901.

[29] M. G. Kozlov and D. DeMille. “Enhancement of the Electric Dipole Moment of the Electron in PbO”. In: *Physical Review Letters* 89 (2002), p. 133001.

[30] M. A. Baranov. “Theoretical progress in many-body physics with ultracold dipolar gases”. In: *Physics Reports* 464 (2008), p. 71.

[31] L. Santos, G. V. Shlyapnikov, P. Zoller, and M. Lewenstein. “Bose-Einstein Condensation in Trapped Dipolar Gases”. In: *Physical Review Letters* 85 (2000), p. 1791.

[32] S. Yi and L. You. “Trapped condensates of atoms with dipole interactions”. In: *Physical Review A* 63 (2001), p. 053607.

[33] S. Ronen, D. C. E. Bortolotti, and J. L. Bohn. “Radial and Angular Rotons in Trapped Dipolar Gases”. In: *Physical Review Letters* 98 (2007), p. 030406.

[34] A. Robert, O. Sirjean, A. Browaeys, J. Poupard, S. Nowak, D. Boiron, C. I. Westbrook, and A. Aspect. “A Bose-Einstein Condensate of Metastable Atoms”. In: *Science* 292 (2001), p. 461.

[35] Y. Takasu, K. Maki, K. Komori, T. Takano, K. Honda, M. Kumakura, T. Yabuzaki, and Y. Takahashi. “Spin-Singlet Bose-Einstein Condensation of Two-Electron Atoms”. In: *Physical Review Letters* 91 (2003), p. 040404.

[36] Ch. 5 of Ref. 39.

[37] A. J. Moerdijk, B. J. Verhaar, and A. Axelsson. “Resonances in ultracold collisions of ^{6}Li, ^{7}Li, and ^{23}Na”. In: *Physical Review A* 51 (1995), p. 4852.

[38] B. H. Bransden and C. J. Joachain. *Physics of Atoms and Molecules*. 2nd ed. Pearson Education Limited, 2003.

[39] J. Weiner, V. S. Bagnato, S. Zilio, and P. S. Julienne. “Experiments and theory in cold and ultracold collisions”. In: *Review of Modern Physics* 71 (1999), p. 1.

[40] T. Köhler, K. Góral, and P. S. Julienne. “Production of cold molecules via magnetically tunable Feshbach resonances”. In: *Reviews of Modern Physics* 78 (2006), p. 1311.

[41] Ch. 10 of Ref. 39.

[42] D. C. E. Bortolotti. “Feshbach Resonances in Ultracold Bose-Fermi Mixtures”. PhD thesis. University of Colorado, Boulder, 2007.

[43] J. Burke. “Theoretical Investigation of Cold Alkali Atom Collisions”. PhD thesis. University of Colorado, Boulder, 1999.

[44] M. Krauss and W. J. Stevens. “Effective core potentials and accurate energy curves for Cs[sub 2] and other alkali diatomics”. In: *The Journal of Chemical Physics* 93 (1990), p. 4236.

[45] P. Courteille, R. S. Freeland, D. J. Heinzen, F. A. van Abeelen, and B. J. Verhaar. “Observation of a Feshbach Resonance in Cold Atom Scattering”. In: *Physical Review Letters* 81 (1998), p. 69.

[46] J. L. Roberts, N. R. Claussen, J. P. Burke, C. H. Greene, E. A. Cornell, and C. E. Wieman. “Resonant Magnetic Field Control of Elastic Scattering in Cold ^{85}Rb”. In: *Physical Review Letters* 81 (1998), p. 5109.

[47] R. A. Duine and H. T. C. Stoof. “Atom-molecule coherence in Bose gases”. In: *Physics Reports* 396 (2004), p. 115.

[48] S. J. J. M. F. Kokkelmans, J. N. Milstein, M. L. Chiofalo, R. Walser, and M. J. Holland. “Resonance superfluidity: Renormalization of resonance scattering theory”. In: *Physical Review A* 65 (2002), p. 053617.

[49] C. Ticknor, C. A. Regal, D. S. Jin, and J. L. Bohn. “Multiplet structure of Feshbach resonances in nonzero partial waves”. In: *Physical Review A* 69 (2004), p. 042712.

[50] C. C-Tannoudji, B. Diu, and F. Laloe. *Quantum Mechanics*. 2nd edition. Vol. 2. p. 1120-1121. Wiley-Interscience, 1977.

[51] W. Petrich, M. H. Anderson, J. R. Ensher, and E. A. Cornell. “Stable, Tightly Confining Magnetic Trap for Evaporative Cooling of Neutral Atoms”. In: *Physical Review Letters* 74 (1995), p. 3352.

[52] D. E. Pritchard. “Cooling Neutral Atoms in a Magnetic Trap for Precision Spectroscopy”. In: *Physical Review Letters* 51 (1983), p. 1336.

[53] A. Görlitz, J. M. Vogels, A. E. Leanhardt, C. Raman, T. L. Gustavson, J. R. Abo-Shaeer, A. P. Chikkatur, S. Gupta, S. Inouye, T. Rosenband, and W. Ketterle. “Realization of Bose-Einstein Condensates in Lower Dimensions”. In: *Physical Review Letters* 87 (2001), p. 130402.

[54] H. Moritz, T. Stöferle, K. Günter, M. Köhl, and T. Esslinger. “Confinement Induced Molecules in a 1D Fermi Gas”. In: *Physical Review Letters* 94 (2005), p. 210401.

[55] K. Mølmer. “Bose Condensates and Fermi Gases at Zero Temperature”. In: *Physical Review Letters* 80 (1998), p. 1804.

[56] T. Stöferle, H. Moritz, C. Schori, M. Köhl, and T. Esslinger. “Transition from a Strongly Interacting 1D Superfluid to a Mott Insulator”. In: *Physical Review Letters* 92 (2004), p. 130403.

[57] I. B. Spielman, W. D. Phillips, and J. V. Porto. “Mott-Insulator Transition in a Two-Dimensional Atomic Bose Gas”. In: *Physical Review Letters* 98 (2007), p. 080404.

[58] E. Fermi. In: *Nuovo Cimento* 11 (1934), p. 157.

[59] K. Huang and C. N. Yang. “Quantum-Mechanical Many-Body Problem with Hard-Sphere Interaction”. In: *Physical Review* 105 (1957), p. 767.

[60] T. Busch, B.-G. Englert, K. Rzażewski, and M. Wilkens. “Two Cold Atoms in a Harmonic Trap”. In: *Foundations of Physics* 28 (1998), p. 549.

[61] E. P. Gross. In: *Nuovo Cimento* 20 (1963), p. 454.

[62] E. P. Gross. “Hydrodynamics of a Superfluid Condensate”. In: *Journal of Mathematical Physics* 4 (1963), p. 195.

[63] L. P. Pitaevskii. “Vortex lines in an imperfect Bose gas”. In: *Soviet Physics Journal of Experimental and Theoretical Physics* 13 (1961), p. 451.

[64] K. Kanjilal and D. Blume. “Nondivergent pseudopotential treatment of spin-polarized fermions under one- and three-dimensional harmonic confinement”. In: *Physical Review A* 70 (2004), p. 042709.

[65] R. Stock, A. Silberfarb, E. L. Bolda, and I. H. Deutsch. “Generalized Pseudopotentials for Higher Partial Wave Scattering”. In: *Physical Review Letters* 94 (2005), p. 023202.

[66] N. P. Mehta, S. T. Rittenhouse, J. P. D’Incao, and C. H. Greene. “Hyperspherical approach to the four-body problem”. In: *arXiv:0706.1296v1 [cond-mat.other]* (2007).

[67] K. Kanjilal and D. Blume. “Coupled-channel pseudopotential description of the Feshbach resonance in two dimensions”. In: *Physical Review A* 73 (2006), 060701(R).

[68] A. Derevianko. “Anisotropic pseudopotential for polarized dilute quantum gases”. In: *Physical Review A* 67 (2003), p. 033607.

[69] A. Derevianko. “Erratum: anisotropic pseudopotential for polarized dilute quantum gases [Phys. Rev. A 67 033607 (2003)]”. In: *Physical Review A* 72 (2005), p. 039901.

[70] K. Kanjilal, J. L. Bohn, and D. Blume. “Pseudopotential treatment of two aligned dipoles under external harmonic confinement”. In: *Physical Review A* 75 (2007), p. 052705.

[71] K. Kanjilal and D. Blume. “Low-energy resonances and bound states of aligned bosonic and fermionic dipoles”. In: *Physical Review A* 78 (2008), 040703(R).

[72] J. J. Sakurai. *Modern Quantum Mechanics*. Revised. page 448, entry A.2.8. New York: Addison-Wesley publishing Company, Inc., 1994.

[73] T. Cheon and T. Shigehara. “Realizing discontinuous wave functions with renormalized short-range potentials”. In: *Physics Letters A* 243 (1998), p. 111.

[74] T. Cheon and T. Shigehara. “Fermion-Boson Duality of One-Dimensional Quantum Particles with Generalized Contact Interactions”. In: *Physical Review Letters* 82 (1999), p. 2536.

[75] B. E. Granger and D. Blume. “Tuning the Interactions of Spin-Polarized Fermions Using Quasi-One-Dimensional Confinement”. In: *Physical Review Letters* 92 (2004), p. 133202.

[76] M. D. Girardeau and M. Olshanii. “Theory of spinor Fermi and Bose gases in tight atom waveguides”. In: *Physical Review A* 70 (2004), p. 023608.

[77] H. Grosse, E. Langmann, and C. Paufler. “Exact solution of a 1D quantum many-body system with momentum-dependent interactions”. In: *Journal of Physics A* 37 (2004), p. 4579.

[78] M. Girardeau. “Relationship between Systems of Impenetrable Bosons and Fermions in One Dimension”. In: *Journal of Mathematical Physics* 1 (1960), p. 516.

[79] M. D. Girardeau, E. M. Wright, and J. M. Triscari. “Ground-state properties of a one-dimensional system of hard-core bosons in a harmonic trap”. In: *Physical Review A* 63 (2001), p. 033601.

[80] M. Olshanii. “Atomic Scattering in the Presence of an External Confinement and a Gas of Impenetrable Bosons”. In: *Physical Review Letters* 81 (1998), p. 938.

[81] S. A. Bender, K. D. Erker, and B. E. Granger. “Exponentially Decaying Correlations in a Gas of Strongly Interacting Spin-Polarized 1D Fermions with Zero-Range Interactions”. In: *Physical Review Letters* 95 (2005), p. 230404.

[82] M. Abramowitz and I. A. Stegun. *Handbook of Mathematical Functions with Formulas, Graphs, and Mathematical Tables*. Ninth Dover printing, tenth GPO printing. New York: Dover, 1964.

[83] Eqs. (13.1.20) and (13.1.3) of Ref. 82.

[84] M. D. Girardeau, H. Nguyen, and M. Olshanii. “Effective interactions, Fermi-bose duality, and ground states of ultracold atomic vapors in tight de Broglie waveguides”. In: *Optics Communications* 243 (2004), p. 3.

[85] Ch. 12 of Ref. 39.

[86] A. Omont. “On the theory of collisions of atoms in rydberg states with neutral particles”. In: *Journal de Physique* 38 (1977), p. 1343.

[87] E. L. Hamilton, C. H. Greene, and H. R. Sadeghpour. “Shape-resonance-induced long-range molecular Rydberg states”. In: *Journal of Physics B* 35 (2002), p. L199.

[88] R. Roth and H. Feldmeier. “Effective s- and p-wave contact interactions in trapped degenerate Fermi gases”. In: *Physical Review A* 64 (2001), p. 043603.

[89] E. L. Hamilton. “Photoionization, Photodissociation, and Long-Range Bond Formation in Molecular Rydberg States”. PhD thesis. Univeristy of Colorado, Boulder, 2003.

[90] Y. N. Demkov and G. F. Drukarev. “Loosely bound particle with nonzero orbital angular momentum in an electric or magnetic field”. In: *Soviet Physics Journal of Theoretical and Experimental Physics* 54 (1981), p. 650.

[91] M. V. Frolov, N. L. Manakov, E. A. Pronin, and A. F. Starace. “Model-Independent Quantum Approach for Intense Laser Detachment of a Weakly Bound Electron”. In: *Physical Review Letters* 91 (2003), p. 053003.

[92] S. P. Andreev, B. M. Karnakov, V. D. Mur, and V. A. Polunin. “Spectrum of weakly bound states of a particle in external electric fields”. In: *Soviet Physics Journal of Theoretical and Experimental Physics* 59 (1984), p. 506.

[93] S. P. Andreev, B. M. Karnakov, and V. D. Mur. “Energy spectrum of a particle in potentials with strongly differing ranges”. In: *Theoretical and Mathematical Physics* 64 (1985), p. 838.

[94] A. S. Baltenkov. “The application of general zero-range potentials to multi-center problems”. In: *Theoretical and Mathematical Physics* 268 (2000), p. 92.

[95] C. H. Greene. See http://lumberjack.colorado.edu/Feshbach/.

[96] J. W. Dunn, D. Blume, B. Borca, B. E. Granger, and C. H. Greene. “Feshbach resonance cooling of trapped atom pairs”. In: *Physical Review A* 71 (2005), p. 033402.

[97] D. S. Petrov, M. Holzmann, and G. V. Shlyapnikov. “Bose-Einstein Condensation in Quasi-2D Trapped Gases”. In: *Physical Review Letters* 84.12 (2000), p. 2551.

[98] D. Rychtarik, B. Engeser, H.-C. Nägerl, and R. Grimm. “Two-Dimensional Bose-Einstein Condensate in an Optical Surface Trap”. In: *Physical Review Letters* 92 (2004), p. 173003.

[99] Z. Idziaszek and T. Calarco. “Pseudopotential Method for Higher Partial Wave Scattering”. In: *Physical Review Letters* 96 (2006), p. 013201.

[100] K. Günter, T. Stöferle, H. Moritz, M. Köhl, and T. Esslinger. “p-Wave Interactions in Low-Dimensional Fermionic Gases”. In: *Physical Review Letters* 95 (2005), p. 230401.

[101] G. B. Partridge, K. E. Strecker, R. I. Kamar, M. W. Jack, and R. G. Hulet. “Molecular Probe of Pairing in the BEC-BCS Crossover”. In: *Physical Review Letters* 95 (2005), p. 020404.

[102] B. J. Verhaar, J. P. H. W. van den Eijnde, M. A. J. Voermans, and M. M. J. Schaffrath. “Scattering length and effective range in two dimensions: application to adsorbed hydrogen atoms”. In: *Journal of Physics A* 17 (1984), p. 595.

[103] M. Olshanii and L. Pricoupenko. “Rigorous Approach to the Problem of Ultraviolet Divergencies in Dilute Bose Gases”. In: *Physical Review Letters* 88 (2001), p. 010402.

[104] K. Wódkiewicz. “Fermi pseudopotential in arbitrary dimensions”. In: *Physical Review A* 43 (1991), p. 68.

[105] A. S. Jensen, K. Riisager, D. V. Fedorov, and E. Garrido. “Structure and reactions of quantum halos”. In: *Review of Modern Physics* 76 (2004), p. 215.

[106] E. L. Bolda, E. Tiesinga, and P. S. Julienne. “Effective-scattering-length model of ultracold atomic collisions and Feshbach resonances in tight harmonic traps”. In: *Physical Review A* 66 (2002), p. 013403.

[107] D. Blume and C. H. Greene. “Fermi pseudopotential approximation: Two particles under external confinement”. In: *Physical Review A* 65 (2002), p. 043613.

[108] D. S. Petrov and G. V. Shlyapnikov. “Interatomic collisions in a tightly confined Bose gas”. In: *Physical Review A* 64 (2001), p. 012706.

[109] L. Pricoupenko and M. Olshanii. “Stability of two-dimensional Bose gases in the resonant regime”. In: *Journal of Physics B* 40 (2007), p. 2065.

[110] Z. Idziaszek and T. Calarco. “Analytical solutions for the dynamics of two trapped interacting ultracold atoms”. In: *Physical Review A* 74 (2006), p. 022712.

[111] M. G. Moore. “Pseudopotential Analog for Zero-Range Photoassociation and Feshbach Resonance”. In: *Physical Review Letters* 96 (2006), p. 100401.

[112] R. G. Newton. *Scattering theory of waves and particles*. 2nd ed. Dover Publications Inc., New York, 1982.

[113] N. F. Mott and H. S. W. Massey. *Theory of Atomic Collisions*. 3rd ed. Oxford University Press, London, 1965.

[114] C. Ticknor and J. L. Bohn. “Long-range scattering resonances in strong-field-seeking states of polar molecules”. In: *Physical Review A* 72 (2005), p. 032717.

[115] S. Ronen, D. C. E. Bortolotti, D. Blume, and J. L. Bohn. “Dipolar Bose-Einstein condensates with dipole-dependent scattering length”. In: *Physical Review A* 74 (2006), p. 033611.

[116] D. C. E. Bortolotti, S. Ronen, J. L. Bohn, and D. Blume. “Scattering Length Instability in Dipolar Bose-Einstein Condensates”. In: *Physical Review Letters* 97 (2006), p. 160402.

[117] B. R. Johnson. “The multichannel log-derivative method for scattering calculations”. In: *Journal of Computational Physics* 13 (1973), pp. 445 –449.

[118] S. Yi and L. You. “Trapped atomic condensates with anisotropic interactions”. In: *Physical Review A* 61 (2000), p. 041604.

[119] V. Roudnev and M. Cavagnero. “Universal resonant ultracold molecular scattering”. In: *Physical Review A* 79 (2009), p. 014701.

[120] V. Roudnev and M. Cavagnero. “Resonance phenomena in ultracold dipole-dipole scattering”. In: *Journal of Physics B* 42 (2009), p. 044017.

[121] C. Ticknor. “Collisional Control of Ground State Polar Molecules and Universal Dipolar Scattering”. In: *Physical Review Letters* 100 (2008), p. 133202.

[122] S. Yi and L. You. “Calibrating Dipolar Interaction in an Atomic Condensate”. In: *Physical Review Letters* 92 (2004), p. 193201.

[123] I. Reichenbach, A. Silberfarb, R. Stock, and I. H. Deutsch. “Quasi-Hermitian pseudopotential for higher partial wave scattering”. In: *Physical Review A* 74 (2006), p. 042724.

[124] Z. Idziaszek. “Analytical solutions for two atoms in a harmonic trap: p-wave interactions”. In: *arXiv:0902.2167v1 [physics.atom-ph]* (2009).

[125] Andrei Derevianko. “Simplified contact pseudopotential for anisotropic interactions of polarized particles under harmonic confinement”. In: *arXiv:0807.3111v1 [quant-ph]* (2008).

[126] Z. Idziaszek and T. Calarco. “Two atoms in an anisotropic harmonic trap”. In: *Physical Review A* 71 (2005), p. 050701.